ProQuest LLC.
789 East Eisenhower Parkway
P.O. Box 1346
Ann Arbor, MI 48106 – 1346

This thesis is dedicated to my family

Hybrid Pulse Interval Modulation – Code-Division Multiple-Access for Optical Wireless Communications

Chun Kit SEE

A thesis submitted in partial fulfilment of the requirements of
Sheffield Hallam University
for the degree of Doctor of Philosophy

This thesis is accompanied by software (1 CD)

October 2003

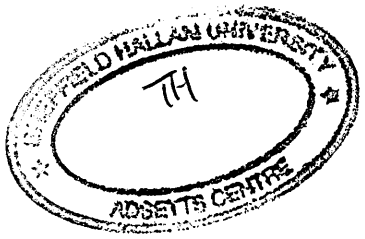
SHEFFIELD HALLAM UNIVERSITY
ADSETTS CENTRE

DECLARATION

No portion of the work referred to in this thesis has been submitted in support of an application for another degree or qualification to this, or any other university, other institute of learning, or industrial organisation.

Chun Kit SEE

October 2003

ABSTRACT

The work in this thesis investigates the properties of the IR diffuse wireless link with regard to: the use of sets of signature sequences with good message separation properties (hence providing low BER), the suitability of a *h*PIM-CDMA scheme for the IR diffuse wireless systems under the constraint of eye safety regulations (i.e. when all users are transmitting simultaneously), the quality of message separation due to multipath propagation. The suitability of current DS-CDMA systems using other modulation techniques are also investigated and compared with *h*PIM-CDMA for the performances in power efficiency, data throughput enhancement and error rate.

A new algorithm has also been proposed for generating large sets of $(n,3,1,1)$OOC practically with reduced computation time. The algorithm introduces five conditions that are well refined and help in speeding up the code construction process. Results for elapsed computation times for constructing the codes using the proposed algorithm are compared with theory and show a significant achievement. The models for *h*PIM-CDMA and *h*PPM-CDMA systems, which were based on passive devices only, were also studied. The technique used in *h*PIM-CDMA, which uses a variable and shorter symbol duration, to achieve higher data throughput is presented in detail.

An in-depth analysis of the BER performance was presented and results obtained show that a lower BER and higher data throughput can be achieved. A corrected BER expression for the *h*PPM-CDMA was presented and the justification for this detailed. The analyses also show that for DS-CDMA systems using certain sets of signature sequences, the BER performance cannot be approximated by a Gaussian function.

ACKNOWLEDGEMENTS

Very special thanks to Professor Z. Ghassemlooy, my director of studies, as he encouraged me to pursue this PhD study. During the course of this study, he has been providing me with precious advice, guidance and support.

Thanks also to Dr J. Holding, my second supervisor, for providing me with the technical help throughout this work. Two of the most valuable things I learned from him are English and programming in MATLAB technical language, which I will never forget.

Having a discussion with them was enjoyable for me as they made me laugh.

Sincere thanks also go to Dr R. McLaughlin and Dr R. Saatchi for helping me with mathematics from time to time and to the technical and secretarial staff in within the School of Engineering who assisted me during my studies.

I would also like to thank my colleagues and friends I met within the School of Engineering from the past and present, especially to Nelson Cheung, Ruixin Gao, Arul Selvan, Andrew Hayes, Adrian Als, and Bala Amavasai, for their helps and their friendship – making my life in the enclosed research laboratory pleasant.

Not forgetting to mention, my friends, Ted Kingdom, Raymond Parnell, James Lyon-Joyce, Robert Hoole, Ian Curry, Sophie Robinson, James Venables, colleagues at the Royal Mail HR centre, and also friends in Malaysia, especially Sin Kok Keong, for their constant support and encouragement over the last five years.

Finally, I would like to thank my parents and my brothers for their love and encouragement in completing this study.

TABLE OF CONTENT

GLOSSARY OF ABBREVIATIONS

Abbreviation	Description
AM	Amplitude modulation
BEF	Bit-rate-enhancement factor
BER	Bit-error-rate
CCD	Charge-couple-devices
CDMA	Code-division multiple-access
CD	Compact disc
CMOS	Complementary metal oxide semiconductor
CW	Codeword
DC	Direct current
DFE	Decision-feedback equaliser
DPPM	Differential pulse position modulation
DS	Direct-sequence
DSSS	Direct-sequence spread spectrum
EPS(*P*)	Extended prime-sequence (*P*)
ERD	Extended-relative-distance
FDMA	Frequency-division multiple-access
FH	Frequency-hopping
FHSS	Frequency-hopping spread spectrum
FM	Frequency modulation
FOV	Field of view
*h*PIM-CDMA	Hybrid pulse interval modulation – code-division multiple-access
*h*PPM-CDMA	Hybrid pulse position modulation – code-division multiple-access
IEEE	Institute of Electrical and Electronics Engineers
IID	Independent, identically distributed
IM/DD	Intensity modulation with direct detection
IR	Infrared
ISI	Inter-symbol interference
ISM	Industrial, scientific and medical
LED	Light-emitting diode
LOS	Line-of-sight
LPF	Low pass filter
MAI	Multiple-access-interference
MF	Matched filter
MPR	Modified prime codes
OFDM	Orthogonal frequency division multiplexing

OOC	Optical orthogonal codes
OOK	On-off keying
PC	Prime codes
PCM	Pulse code modulation
PDF	Probability density function
PER	Packet-error-rate
PHY	Physical
PIM	Pulse interval modulation
PLL	Phase-lock-loop
PM	Phase modulation
PN	Pseudonoise
PPM	Pulse position modulation
PS(P)	Prime-sequence (P)
QC	Quadratic congruence
QF	Quantisation feedback
QPS(P)	Quasi-prime sequence (P)
RD	Relative-distance
RF	Radio frequency
RMS	Root-mean-square
SER	Symbol-error-rate
SIR	Signal-to-interference ratio
SNR	Signal-to-noise ratio
SOOC	Strict optical orthogonal code
TC	Truncated Costas
TDMA	Time-division multiple-access
WDMA	Wavelength-division multiple-access
WLAN	Wireless local area network

GLOSSARY OF SYMBOLS

Abbreviation	Description
a	Number of program lines
A	Ampere
a_h	Constant related to RMS delay spread
b	Number of machine codes
$b_{Tx}(t)$; $b_{Tx}^{i}(t)$	Output signal of modulator; Output signal of modulator of the i^{th} transmitter
$b_{Rx}(t)$; $b_{Rx}^{i}(t)$	Input signal to demodulator; Input signal to demodulator of the i^{th} receiver
$B_{k\|Tx}$; $B_{k\|Tx}^{i}$	Binary data from information source; Binary data from information source of the i^{th} transmitter
$B_{k\|Rx}$; $B_{k\|Rx}^{i}$	Binary data to information processor; Binary data to the i^{th} information processor
$BEF_{\frac{Modulation\,1}{Modulation\,2}}$	Bit-rate-enhancement factor of 'Modulation 1' over 'Modulation 2'
BEF_{OP}	Optimum bit-rate-enhancement factor
c_{Com}	Computer clock frequency
c_L	Speed of light
$'code'$	Code name
$cw_{(i,j)}$	Element of ${}^{'code'}_{n}CW_{(i,j)}^{F\times w}$
C	Capacitance
${}^{'code'}_{n}CW_{(i,j)}^{F\times w}$	Codeword matrix
$d_{Rx}(t)$; $d_{Rx}^{i}(t)$	Photocurrent; Generated photocurrent by the photodiode of the i^{th} receiver
$d_{Tx}^{i}(t)$	Output signal of encoder of the i^{th} transmitter
$D_{L\|Spread}$	Maximum length of spread distance, measured between two correlated pulses of minimum spread distance and maximum spread distance, respectively
D_{RMS}	Channel RMS delay spread
$D_{RMS\|Modulation}$	Channel RMS delay spread of 'Modulation' signal
D_{Signal}	Spread distance of correlated signal pulse
D_{Spread}	Spread distance of a correlated pulse
$D_{Spread\|\min}$	Minimum spread distance of a correlated pulse

$D_{Spread\|\max}$	Maximum spread distance of a correlated pulse
D_T ; $D_{T\|Modulation}$	Normalised delay spread; Normalised delay spread of 'Modulation' signal
$D_{T\|\min}$	Minimum normalised delay spread with signal dispersion of $0.3T_c$ or less
$D_{T\|0.3}$	Normalised delay spread of $0.3T_c$ signal dispersion
$D_{Tx}(t)$; $D_{Tx}^{i}(t)$	Power of optical source or channel input signal; Optical signal transmitted by the i^{th} transmitter
$e_{Rx}^{i}(t)$	Output signal of multiplier of the i^{th} correlator receiver, or output signal of tap-delay structure of the i^{th} MF receiver
$erd_{(i,j)}$	Element of ${}^{'code'}_{n}ERD_{(i,j)}^{F\times w(w-1)}$
${}^{'code'}_{n}ERD_{(i,j)}^{F\times w(w-1)}$	Extended-relative-distance matrix
F	Number of system clients or users
$g(t)$	Square pulse
$g_b(t)$	A square pulse of T_b
$g_c(t)$	A square pulse of T_c
G_{OC} ; $G_{OC}^{I\|i}$	Optical gain of channel; optical channel gain of the signal from the I^{th} transmitter to the i^{th} receiver
$h(t)$; $h^{I\|i}(t)$	Effective channel impulse response – normalised; Effective channel impulse response of the signal from the I^{th} transmitter to the i^{th} receiver
$h_c(t,a_h)$	Channel impulse response for a given value a_h
H	Effective height of the ceiling above optical source and detector
i	Variable related to the numbering of client (or user) or the row index of matrix
I	Variable related to the numbering of client (or user) or the row index of matrix
j	Variable related to the column index of matrix
J	Variable related to the column index of matrix
k	Bit or symbol sequence number
K	Order of cascading codewords
l	Number of symbol sequence of one less than k
L	Number of symbols or order of PIM and PPM
L_a	Average PIM symbol length
m	Temporary variable
M	Total number of bits

n	Signature sequence length
$n(t)$	Shot noise
$\breve{n}$	A positive integer related to the code weight of $2^{\breve{n}}$ PS(P)
n_{mid}	Mid value of sequence length
p	Probability of success
P	Prime number
$P_{B.BER\|Modulation}$	Probability of bit-error-rate, obtained using Binomial function, of 'Modulation' scheme
$P_{B.E}$	Probability of error obtained using Binomial function
$P_{B.MAI\|Modulation}$	Probability of a false alarm occurring in a single chip, obtained using Binomial function, due to MAI (as a result of cross-correlation), of 'Modulation' scheme
$P_{B.Self\|Modulation}$	Probability of a false alarm occurring in a single chip, obtained using Binomial function, due to self interference (as a result of auto-correlation), of 'Modulation' scheme
$P_{CFA\|Modulation}$	Probability of a false alarm occurring in a single chip position of 'Modulation' scheme
$P_{G.E}$	Probability of error obtained using Gaussian function
$P_{G.BER\|Modulation}$	Probability of bit-error-rate, obtained using Gaussian function, of 'Modulation' scheme
$P_{NS\|Modulation}$	Probability of a new symbol will occur of 'Modulation' scheme
$P_{SER\|Modulation}$	Probability of symbol-error-rate of 'Modulation' scheme
$P_{SFA\|Modulation}$	Probability of a symbol, with γ slots, in error due false alarm of 'Modulation' scheme
$P_{1SFA\|Modulation}$	Probability of one symbol in error due to false alarm
$P_{2SFA\|Modulation}$	Probability of two consecutive symbols in error due to false alarm
$P_{\lambda_a\|Modulation}$	Probability of self-interference (due to auto-correlation) of 'Modulation' scheme
$P_{\lambda_c\|Modulation}$	Probability of one other user interference (due to cross-correlation) of 'Modulation' scheme
$PDF_{B.}$	Probability density function obtained using Binomial function
$PDF_{B.MAI\|Modulation}$	Probability density function due to MAI, obtained using Binomial function, of 'Modulation' scheme
$PDF_{G.}$	Probability density function obtained using Gaussian function

$PDF_{G.MAI\|Modulation}$	Probability density function due to MAI, obtained using Gaussian function, of 'Modulation' scheme
$PDF_{SI\|Modulation}$	Probability density function due to a single user interference of 'Modulation' scheme
$PDF^{i}_{SI\|Modulation}$	Probability density function due to the i^{th} user interference of 'Modulation' scheme
q	Probability of failure. The complement of p
$\breve{q}$	Order of cyclically shifting the frames of PS(P) codeword to the left
Q	Code weight of QPS(P)
$rd_{(i,j)}$	Element of ${}^{'code'}_{n}RD^{F\times w}_{(i,j)}$
R	Resistance
R_b ; $R_{b\|Modulation}$	Bit rate; Bit rate of 'Modulation' scheme
R_c	Chip rate
$R_{c\|0.3}$	Chip rate limited by $D_{T\|0.3}$
R_{Rx} ; R^{i}_{Rx}	Photodetector responsivity; Photodetector responsivity of the i^{th} receiver
R_s	Slot rate
R_{Tx} ; R^{i}_{Tx}	Optical source responsivity; Optical source responsivity of the i^{th} transmitter
${}^{'code'}_{n}RD^{F\times w}_{(i,j)}$	Relative-distance matrix
S	Seconds
ς	Sum
S^{i}_{k}	A decimal integer, corresponding to M bits of information being mapped, of the k^{th} symbol of the i^{th} data source
$s^{i}_{Rx}(t)$	Output signal (signature sequence) of code register of the i^{th} receiver
$s^{i}_{Tx}(t)$	Output signal (signature sequence) of code register of the i^{th} transmitter
t	Time
T_b	Bit duration
T_c	Chip duration
$T_{c\|0.3}$	Chip duration related to normalised delay spread of 0.3
T_{EP}	Effective pulse duration
T_s	Slot duration
$T_{S\|Modulation}$	Symbol duration of 'Modulation' signal
T	Time duration

$Total_{Arr}$	Total of possible arrangements of $erd_{(i,j)}$ values
$Total_{Com}$	Estimated total computing time
$u(t)$	Unit step function
V	Volt
V_b	Peak voltage of modulator output signal
V_d	Peak voltage of encoder output signal
V_P	Signal peak voltage
V_s	Peak voltage of code register output signal
v_{th}	Threshold level
V_T	Peak voltage of threshold detector output signal
w	Code weight of OOC
W	Watt
$W_{ave\|Modulation}$	Average optical power of 'Modulation' signal
$W_{ave\|Rx}$	Received average optical power
$W_{ave\|Tx}$	Average intensity or optical power of transmitted signal
W_{Eff} ; $W_{Eff\left\|\frac{Modulation1}{Modulation2}\right.}$	Power efficiency; Power efficiency of 'Modulation 1' over 'Modulation 2'
$W_{\max}$	Maximum optical transmit power
W_P	Peak optical power
x	Temporary variable
x_B	Integer random variable of Binomial function
x_G	Random variable, of real number, of Gaussian function
X	No of trials
X_k	Redundant chips of the k^{th} symbol
y	Temporary variable
Z	Temporary variable
z_{BEF}	Ratio of the sequence length over the information length, where the optimum *BEF* is achieved
z_{NS}	Ratio of the sequence length over the information length, where a symbol being divided into two (worst case) will occur. It also denotes the number of symbols that a false alarm must occur consecutively before a new symbol is generated
$\delta(x)$	Dirac delta function
γ	Information slots

$\bar{\gamma}$	Average information slots
μ	Mean
$\mu_{MAI\|OOK-CDMA}$	Mean of OOK-CDMA considering MAI only
σ	Standard deviation
$\sigma^2_{MAI\|OOK-CDMA}$	Variance of OOK-CDMA considering MAI only
$\tau^i_{d\|Tx}$	Transmission time delay of the i^{th} transmitter
$\tau^i_{d\|Rx}$	Receiving time delay of the i^{th} receiver
$\tau^i_{SP\|C}$	Centre time shift of dispersed signal pulse, where most power is concentrated, recovered at the i^{th} receiver
λ_a	Auto-correlation constraint
λ_c	Cross-correlation constraint
λ_1 and λ_2	Optical wavelength 1 and 2

LIST OF FIGURES

LIST OF TABLES

Chapter 1

INTRODUCTION

The study of infrared frequencies for short-range wireless communications has received extensive interest over the past decade. It started from the proposition and demonstration of the diffuse infrared (IR) radiation for wireless in-house data communication, which was first introduced by Gfeller and Bapst in 1979 [Gfeller79]. Since then there has been a number of research interests in IR frequency for wireless local-area-networks (WLANs) in place of the well-established radio frequency (RF) systems [Yen85, Barry93, Carruthers96b, Tanaka97, Yu02, Sidorovich02, Al-Ghamdi03, Giakos03]. The advantages of using IR frequency over RF for short-range wireless communications are as follow [Marsh96, Kahn97]:

- IR emitters and detectors capable of high-speed operation are available at low cost, are relatively simple to design circuits with and are physically small in size compared to their RF counterparts

- The RF spectrum is already extremely congested and bandwidth allocation is limited. Compared with IR frequency, which offers a huge unregulated bandwidth, allows manufacturers to design one product that can be used in any country worldwide, thus avoiding costly "market specific" designs and the need for licensing

- The fact that IR frequencies cannot penetrate the boundaries of the room from which they originate makes wireless infrared inherently secure. This gives an

additional advantage in that similar systems may be operated in adjacent rooms without interference

To improve the quality of transmission and reception of wireless IR communication systems, a number of modulation techniques have been introduced. Of all these techniques, On-Off Keying (OOK) is the simplest to implement, and has been used in a number of high-speed prototype systems [McCullagh94, Audeh96]. The use of a power efficient modulation scheme, such as Pulse Position Modulation (PPM), offers a decrease in the average power requirement compared with OOK [Kaluarachi96a] but at the cost of increased bandwidth. Pulse Interval Modulation (PIM) technique, being investigated at the Sheffield Hallam University over the past nine years, has been suggested as a possible alternative to PPM for optical wireless communication systems. Compared with PPM, PIM has a higher transmission capacity by virtue of its anisochronous nature, and requires no complex symbol synchronisation at the receiver [Ghassemlooy98a, Hayes98].

As in RF wireless systems, diffuse IR wireless systems can employ a multiple access scheme for channel reuse strategy. The Direct-Sequence Code-Division Multiple-Access (DS-CDMA) is one promising scheme, which operates in both the time and wavelength domains, can enhance the channel capacity when the wavelength resource is constrained. However, this is achieved at the cost of reduced data throughput. A DS-CDMA system employing OOK signal format, which is also known as OOK-CDMA, was first introduced for fibre optic systems by [Salehi89a, Salehi89c]. It utilises optical orthogonal codes (OOC) to form signature sequences for the purpose of message separation. OOC are sets of zero and one sequences with good auto- and cross-correlation properties, i.e., the auto-correlation of each sequence exhibits a "thumbtack" shape (a pulse of high amplitude at zero shift and pulses of low amplitudes at other shifts) and the cross-correlation between any two sequences produces pulses of low amplitudes throughout. The use of OOC enables a large number of asynchronous users to transmit information efficiently and reliably. The thumbtack shape of the auto-correlation facilitates the

detection of the desired signal, and the low cross-correlation reduces interference from unwanted signals in the network [Chung89].

Generally, a DS-CDMA system encoding is carried out by "spreading" individual bits to form a signature sequence with a higher bandwidth. However, the bandwidth of an IR diffuse wireless system is limited by characteristics of the channel (due to the room dimensions) the system operates in. Under such a bandwidth constraint, a DS-CDMA system's throughput is reduced, which is inversely proportional to the length of the signature sequence. For example, the throughput of OOK-CDMA system is lower than an OOK system under limited bandwidth. To improve a DS-CDMA system's throughput without increasing the bandwidth, hybrid PPM-CDMA (*h*PPM-CDMA) system (i.e. DS-CDMA system employing PPM technique) has been proposed to enhance the data rate based on the property of PPM technique to perform data compression [Elmirghani94]. In addition, it is found that the throughput can be further enhanced using a *h*PIM-CDMA system, where PIM technique offer better data compression. *h*PIM-CDMA system design is also simpler in that the signal is anisochronous and hence no symbol synchronisation is required compared with the OOK-CDMA and *h*PPM-CDMA systems.

Both *h*PIM-CDMA and *h*PPM-CDMA systems achieve data compression by transmitting a shorter symbol than OOK-CDMA. On the other hand, a symbol of shorter duration will affect the performance of both hybrid systems in terms of bit-error-rate (BER) and power efficiency as the signal power per symbol has been condensed. Moreover, the total signal power allowed to transmit to the channel is limited by the eye safety regulations where the signal power, in average, shall not exceed the critical level that can damage the retina of eye. These criterions impose challenges to the design of *h*PIM-CDMA, and *h*PPM-CDMA, for use in IR diffuse wireless systems. However, with careful design and employing OOC with good correlation properties, which is the main focus of this work, the *h*PIM-CDMA system performance can be improved and can be considered as a potential candidate for the IR diffuse wireless systems for achieving higher data throughput.

1.1 Research Objectives

In order to achieve the above mentioned, a number of research objectives have been identified as outlined below:

- Comprehensive literature survey of indoor optical wireless communication systems. Acquire an understanding of the IR diffuse channel characteristics and identify the constraints that it imposes. Review the various modulation techniques employed, such as the OOK, PPM and PIM, to improve systems performances under the constraints identified

- Review the multiple-access schemes that can be efficiently used in IR diffuse wireless systems and identify the advantages and disadvantages compared with the RF systems. Investigate the DS-CDMA systems employed in the electrical domain, the changes that are required to the system design when migrating to the optical domain

- Review the correlation properties of OOC for message separation. Perform a literature survey of the various proposed OOC for use in optical DS-CDMA systems. Develop a new algorithm that can be used to construct large sets of OOC with good correlation properties, that is practical to implement and requires minimal computation time

- Review the fundamental properties of a conventional optical wireless DS-CDMA system, which is the OOK-CDMA. Understand the system design and how the signature sequence encoding and decoding are carried out in the encoder and decoder, respectively. Examine the performance OOK-CDMA under the constraints imposed by an IR diffuse wireless system

- Perform a literature survey of optical wireless DS-CDMA systems over a range of modulation techniques. Investigate the hardware and configurations for designing the

proposed *h*PIM-CDMA system. Examine the performance of a *h*PIM-CDMA system under the constraints of an IR diffuse wireless channel and compare with OOK-CDMA and *h*PPM-CDMA systems

1.2 Organisation of Thesis

A general block diagram of an optical wireless DS-CDMA system is shown in figure 1.1. To present this work, the thesis is divided into 8 chapters and the contents of this thesis are summarised with reference to the system blocks in figure 1.1.

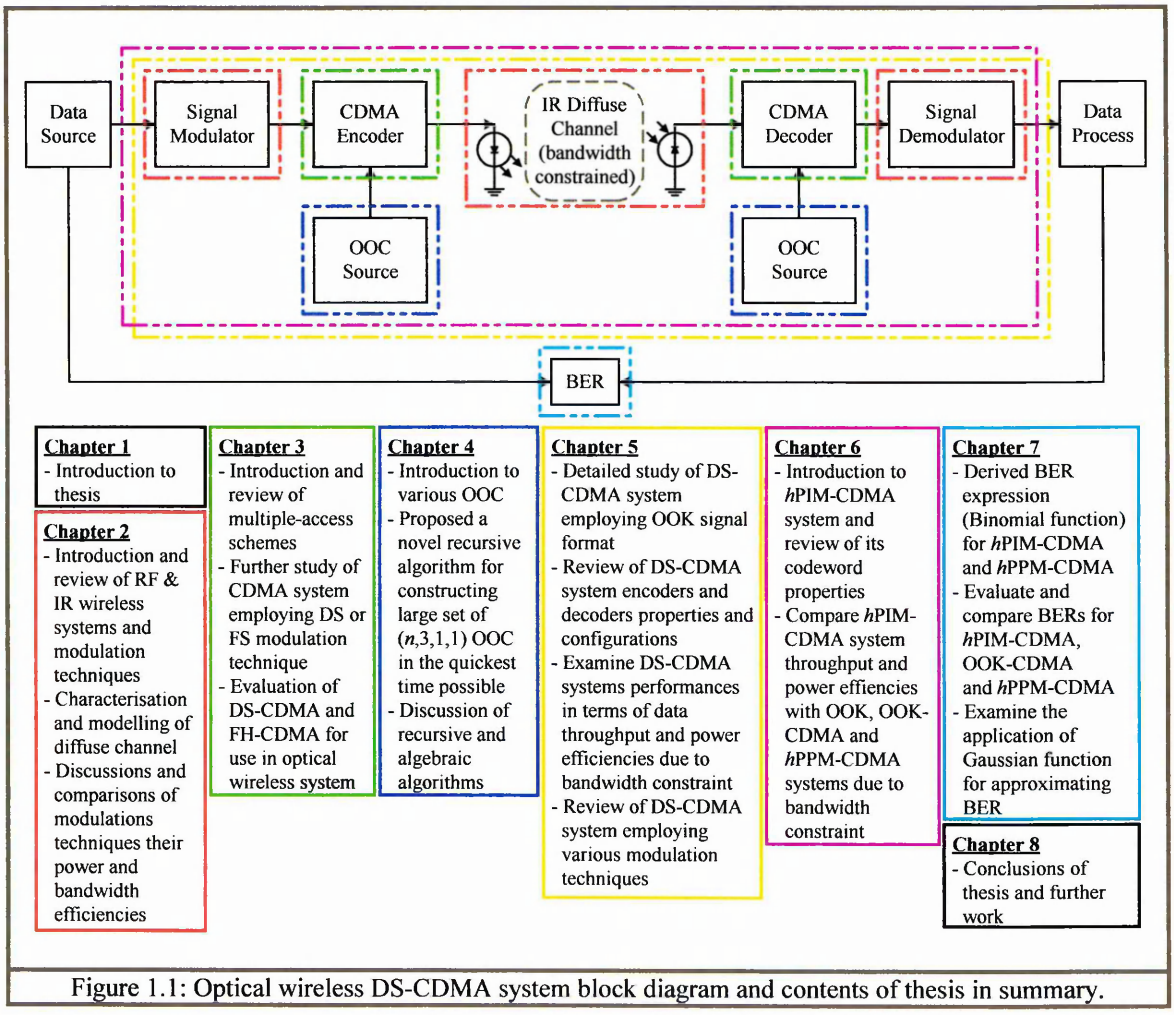

Figure 1.1: Optical wireless DS-CDMA system block diagram and contents of thesis in summary.

Following chapter 1, chapter 2 provides a review of the current RF and IR wireless communication systems. The chapter will begin with the introduction to RF wireless communication systems and identifies the advantages and disadvantages. IR wireless communication systems are then introduced and compared with the RF wireless systems. A

general introduction to indoor optical wireless links is presented concentrating on the most viable link for a multiple-access communication system – using a diffuse link. The properties of an indoor diffuse IR channel are described and methods of modelling and characterising the channel are reviewed. Next the OOK, PPM and PIM modulation techniques are discussed and compared in terms of their efficiency under the constraints of a diffuse link.

Chapter 3 presents an evaluation of multiple-access schemes for use in optical wireless communication systems. The chapter focuses on the CDMA scheme, which utilises both the time and wavelength domains, as a candidate for the IR diffuse wireless system to enhance the network channel capacity efficiently. Modulation techniques such as direct-sequence (DS) and frequency-hopping (FH) techniques suitable for the CDMA systems are compared and evaluated for use in optical wireless systems.

In chapter 4, various OOC that have been proposed to date are presented and the algorithms, which can be categorised as either a recursive or algebraic, used for generating the codewords are discuss. A new recursive algorithm for generating larger sets of OOC codewords in the quickest time possible is proposed and results presented. The reasons a new algorithm is needed are discussed and the proposed algorithm is used as an example to demonstrate why a recursive algorithm always requires longer time than an algebraic algorithm for generating a large set of codewords.

In chapter 5, the procedures for signal modulation and demodulation, and of signature sequence encoding and decoding for an optical DS-CDMA system employing OOK signal format, are presented. There are two configurations for implementing the encoder and decoder, based on active or passive devices. The properties of the two configurations are reviewed. Then the optical DS-CDMA systems performances, under the bandwidth constraint of an IR diffuse wireless channel, are examined in terms of data throughput and power efficiencies. DS-CDMA systems employing various other modulation techniques proposed so far are reviewed.

Chapter 6 presents the proposed *h*PIM-CDMA scheme together with the codeword properties and the encoder-decoder configurations of the system. The data throughput and power efficiency of *h*PIM-CDMA are compared with the OOK, OOK-CDMA and *h*PPM-CDMA systems.

A comprehensive BER analysis of *h*PIM-CDMA system is carried out in chapter 7. The analysis takes into account multiple-access-interference (MAI), self-interference and the hybrid nature of the *h*PIM-CDMA signal detection. Also presented in this chapter is the BER expression for the *h*PPM-CDMA system, which has not been previously reported. BER performances are compared for *h*PIM-CDMA, OOK-CDMA and *h*PPM-CDMA. The use of Gaussian distribution for DS-CDMA BER approximation is investigated. Usually, the assumption is made that the MAI is large in order to use the Gaussian approximation. However, it is found that the BER of an optical DS-CDMA system (either OOK-CDMA, *h*PIM-CDMA or *h*PPM-CDMA) employing certain groups of OOC is not close to a Gaussian approximation even when the MAI tends toward infinity. This is because there are two conditions that must be satisfied, which are discussed in this chapter.

Finally in chapter 8, concluding remarks and the summaries of the major contributions of this thesis are presented. The possible areas of future work are also discussed.

1.3 Original Contributions

1. Analysis of IR diffuse wireless channel characteristics and the effect of the normalised delay spread due to the change of signal modulation bandwidth (sections 2.3.2 and 2.3.3).

2. Derivation of new expressions for representing the properties of a set of codewords using a *standard matrix* format, for the ease and convenient of referencing (section 4.1.1). A novel recursive algorithm for obtaining $(n,3,1,1)$OOC is proposed and implemented using the MATLAB programming language (section 4.2.1). The algorithm is equipped with well-refined conditions that help with computer programming and provides short cuts to the searching process for a valid set of codewords. The written programs are included in the CD.

3. Proposed $(n,3\times \mathrm{K},\mathrm{K},\mathrm{K})$OOC that can be constructed using the $(n,3,1,1)$OOC obtained from the proposed algorithm (section 4.2.2).

4. Developed new expressions for obtaining the Prime Codes (PC) sequences using the representation of the *standard matrix* format (section 4.4). Investigated the disadvantage of the recursive algorithm compared with the algebraic algorithm – in the context of computation time required to generate a large set of codewords (section 4.6).

5. Developed mathematical models for the OOK-CDMA IR diffuse wireless systems employing active and passive devices for the encoder and decoder (sections 5.2, 5.3 and 5.4). Investigated the efficiency of active and passive devices when operating with unipolar signals. Investigated the upper bound of minimum normalised delay spread for an IR wireless DS-CDMA system. Developed an expression for a correlator receiver to obtain maximum correlation (section 5.6.1). Investigated the performances of OOK-CDMA systems in terms of data throughput enhancement and power efficiency (section

5.7). Derived mathematical models for a *h*PPM-CDMA system and examined the appropriate configuration for its encoder and decoder (section 5.9).

6. Derived mathematical models for *h*PIM-CDMA systems and examined the appropriate configuration for its encoder and decoder (sections 6.2). Investigated and compared the performances, in terms of data throughput enhancement and power efficiency, of *h*PIM-CDMA, OOK-CDMA, PPM-CDMA and *h*PPM-CDMA under the constraints of a IR diffuse wireless channel (section 6.3).

7. Developed a BER expression for the proposed *h*PIM-CDMA system and the *h*PPM-CDMA system (section 7.2). Demonstrated that the BER of *h*PIM-CDMA, OOK-CDMA and *h*PPM-CDMA employing $(n, w, 1, 1)$OOC can't be approximated using a Gaussian function (section 7.3).

1.4 List of Publications

The work of this PhD has so far led to the publications listed below:

- C.K. See, Z.F. Ghassemlooy, J.M. Holding and R. McLaughlin, "Comparison of Binomial and Gaussian Distributions for Evaluating Optical DS-CDMA System BER Performance," Proceedings of the Postgraduate Research Conference in Electronics, Photonics, Communications and Software Year 2003 (PREP 2003), University of Exeter (oral presentation) (14 – 16 April 2003), p13-14.

- Z. Ghassemlooy, C.K. See, J.M. Holding and C. Lu, "Bit-Error-Rate Analysis for Hybrid PIM-CDMA Optical Wireless Communication Systems," Microwave and Optical Technology Letters v31 n1 (5 October 2001), p40-44.

- C.K. See, Z. Ghassemlooy and J.H. Holding, "Bit-Error Rate Analysis for PIM-CDMA Optical Wireless Communication Systems," Proceeding of SPIE (oral presentation) v4214 (2001), p153-161.

- C.K. See, Z. Ghassemlooy and J.M. Holding, "Hybrid PIM-CDMA for Optical Wireless Networks," Proceeding of PGNET 2000, 1st Annual PostGraduate Symposium on the Convergence of Telecommunications, Networking and Broadcasting, John Moores University, Liverpool (oral presentation) (19 – 20 June 2000), p195-200.

Chapter 2

REVIEW OF OPTICAL WIRELESS SYSTEMS

2.1 Introduction

This chapter will discuss the difference between RF wireless and optical wireless communication systems. The discussion will concentrate in particular on the need for exploring and developing optical wireless communication systems, for their capacity and efficiency, as an additional communication technique. This is motivated as a result of the bandwidth for the RF wireless systems is currently congested, which is the prime factor.

Both wireless systems require a modulation technique to transfer information to the destination. Section 2.2 will presents the fundamental need for a modulation technique for the RF wireless communication system. The advantages and disadvantages of radio frequency, which serves as the electromagnetic information carrier, are presented. One of the distinct disadvantages is that the RF spectrum is already congested and allocations of sufficient bandwidths are extremely hard to obtain [Street97].

Communication between two devices could be in the range of short distance (i.e. less than 100 metres) or long distance. Short distance can be viewed as a communication between two terminal devices that requires wireless connection for the convenience of connection reconfiguration (i.e. ease of wiring problem) and short-range mobility – for example, a communication between two personal computer terminals within a room. Whereas, a long range communication involves high mobility and requires easy connection regardless of the communicators' location – for example, a mobile phone link. RF can pass through walls and can

travel long distances, whereas IR is a source of light and therefore does not pass through walls and stays confined within a room. RF may be more suitable for long-range and high mobility communications whereas IR could be used for short-range applications.

In section 2.3, the technique of using IR as an optical wireless communication carrier is presented. The difference between the modulations of RF and IR carriers, and their advantages and disadvantages are also discussed. Literature review of recent research and development in IR for indoor optical wireless communication systems and channel characteristics are presented. Section 2.4 will provide the comparison of OOK, PPM and PIM performances in a IR wireless system. Then it will discuss the motive behind study of the optical wireless communication and why PIM has been selected for this application. Summary is presented in section 2.5.

2.2 RF Wireless Communication Systems

Modulation is a process of converting information signals at a base-band frequency to a new frequency, where the signal now occupies a spectral range known as the pass-band that can be accommodated by the channel medium. The pass-band signal in most electrical communication systems is usually a coherent continuous-wave. Modulation techniques such as the amplitude modulation (AM), frequency modulation (FM) and phase modulation (PM) are commonly used in radio communication systems, as they can employ simple coherent detection devices, such as a local oscillator, for demodulation. Each of these modulations requires a carrier wave to transport information at the frequency at least ten times higher than the base-band frequency.

There are numerous RF wireless products available on the market today for WLANs. The majority of these products operate in the industrial, scientific and medical (ISM) band located at 2.4 GHz, which has the advantage of being license free in most countries [Hayes02]. However, the available bandwidth is limited to 83.5MHz, and must be shared with others such as ISM users, other WLAN vendor products, retail theft protection systems, and to tolerate radio interference from microwave ovens and elevator motors [Street97]. In theory, infinite numbers

of channels can exist by dividing the available bandwidth of 83.5 MHz with each channel having very narrow bandwidth, and with very narrow bandwidth separation. However, in practice, this is difficult to achieve due to limitation by the hardware capability.

Consequently, robust spread spectrum modulation techniques are required, which result in low data rates. As an example, the IEEE 802.11-1997 standard for WLANs physical (PHY) layer specifies that either the direct-sequence spread spectrum (DSSS) or the frequency-hopping spread spectrum (FHSS) be used (and or PPM for IR wireless system, this will be discussed later in section 2.3.3) [WWW2, IEEE97]. The data rate of the PHY layer is standardised to operate at either 1 Mbps or 2 Mbps at maximum. This was then improved upon in 1999 with the ratification of the IEEE 802.11b standard, which adds two higher data rates of 5.5 Mbps and 11Mbps to the DSSS standard [IEEE99]. Many of the products currently on the market today are either based on this standard, or the HomeRF standard, which also operates in the ISM band, and achieves a maximum data rate of 10 Mbps using FHSS. The next generation RF WLAN products operate in the so-called 5 GHz band that was allocated solely for use by WLAN products. This allows systems to be optimised in terms of data rate and efficiency, free from the constraints associated when coexisting with other products. There are currently two competing standards in this band, these being IEEE 802.11a and HiperLAN2, both of which provide maximum data rates of 54 Mbps. Another standard worth mentioning is Bluetooth, which is a short range point-to-multipoint standard for voice and data transfer, also operating in the ISM band. The data rate is a mere 723.2 kbps and can operate up to a range of 10 metres. Though these are a few disadvantages of Bluetooth technology, the rationale behind it is low cost, thus allowing it to be integrated into a variety of portable electronics devices, which may then communicate with each other via ad hoc wireless networks termed piconets [Hayes02]. An experiment has been carried out to compare the performance between the DSSS and Bluetooth systems and the results showed that the DSSS system performs better in the presence of interference [Punnoose01].

2.3 Optical Wireless Communication Systems

In an optical wireless system, the signal is transmitted over a channel at infrared frequencies using intensity modulation with direct detection (IM/DD). IM/DD is a simple process that takes place at the transmitter end and receiver front end, where an optical source such as an LED is used to convert an electrical current to an infrared intensity signal, and a photodiode is used to produce a photocurrent that is proportional to the infrared intensity that is incident upon it [Barry94]. At present, the IR spectrum is unregulated and the radiation does not produce visual interference, however it can harm the retina if the optical power is not carefully monitored. Infrared transmission eliminates the need for a radio carrier frequency as in the case of the electrical system discussed above, as the signal at base-band frequency can be directly modulated to IR frequency (pass-band) using the IM/DD technique [Kahn97, Shiu98a]. The use of radio carrier frequency in conjunction with IR can enable a multiple-access communication system, known as Orthogonal Frequency Division Multiplexing (OFDM) [You02].

One of the differences between an electrical (RF) signal and an optical (IR) signal is that an electrical signal can be bipolar and operates in both regions of positive and negative electric fields. Whereas an optical signal based on light intensity is always positive and unipolar. A schematic system block diagram of an IM/DD optical system is shown in figure 2.1. DC bias is included to ensure that the modulated signals are all positives prior to intensity modulation of the light source. At the receiver, the DC bias is removed from the detected signal before amplification and processing.

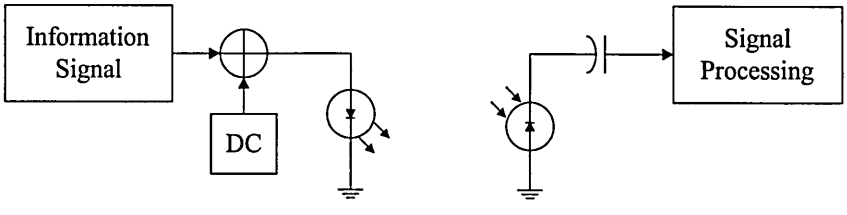

Figure 2.1: IM/DD base optical system block diagram.

Infrared is similar to visible light in that both are absorbed by opaque objects and do not pass through walls. In other words, an information signal carried by infrared is confined to the room in which it is originated. For this reason, the infrared frequency can be reused in the adjacent rooms with no regulation requirement, thus providing virtually unlimited transmission capacity [Kahn97]. Other comparisons between radio and infrared wireless systems, which have not been discussed above, are shown in table 2.1 [Ghassemlooy00, Barry94].

Property	Radio	Infrared	Implication for infrared
Bandwidth regulated?	Yes	No	Approval not required – world-wide compatibility
Passes through walls?	Yes	No	Inherently secure. Carrier reuse in adjacent rooms
Multipath fading	Yes	No	Simple link design
Multipath dispersion	Yes	Yes	Problematic at high data rates
Path loss	High	High	
Dominant noise	Other users	Background light	Short range
Average power proportional to	$\int \lvert D_{Tx}(t)\rvert^2 dt$	$\int D_{Tx}(t)dt$	$D_{Tx}(t)$ is the input signal with high peak-average ratio

Table 2.1: Comparison between RF and IR for indoor wireless communications.

Although an optical system has the advantage over an electrical system such as it does not interfere with audio, microwave and other radio frequencies, its radiation, if not carefully controlled, could damage the human eye. Therefore, there is a need for a modulation technique that offers both power and bandwidth efficiencies. The following subsections will address these two issues and will introduce the modulation techniques suitable for IR applications.

2.3.1 Optical wireless link configurations

There are a number of ways that an optical wireless system can be configured, as shown in figure 2.2 [Barry94]. The line of sight (LOS) configurations (top row) achieve higher power efficiency than the non-LOS, as most of the transmitter radiation travels in one path to the receiver. Especially, the directed LOS configuration (figure 2.2 (a)) achieves the highest power efficiency by utilising narrow beam transmitter and narrow field of view (FOV) receiver. The concentrated light that is directed from the transmitter to the receiver makes this an optimum

link with no multi-path propagation and ambient background light is largely rejected. Nevertheless, the data rate is limited by the power budget due to eye safety regulations [Smyth95]. All LOS communication links are susceptible to blocking in which their connections are terminated by opaque objects that stand in between the transmitter and receiver. This is a disadvantage of LOS configurations that limits their applications to point-to-point and point-to-multipoint communication, but not for multiple access or mobile communications [Kahn97].

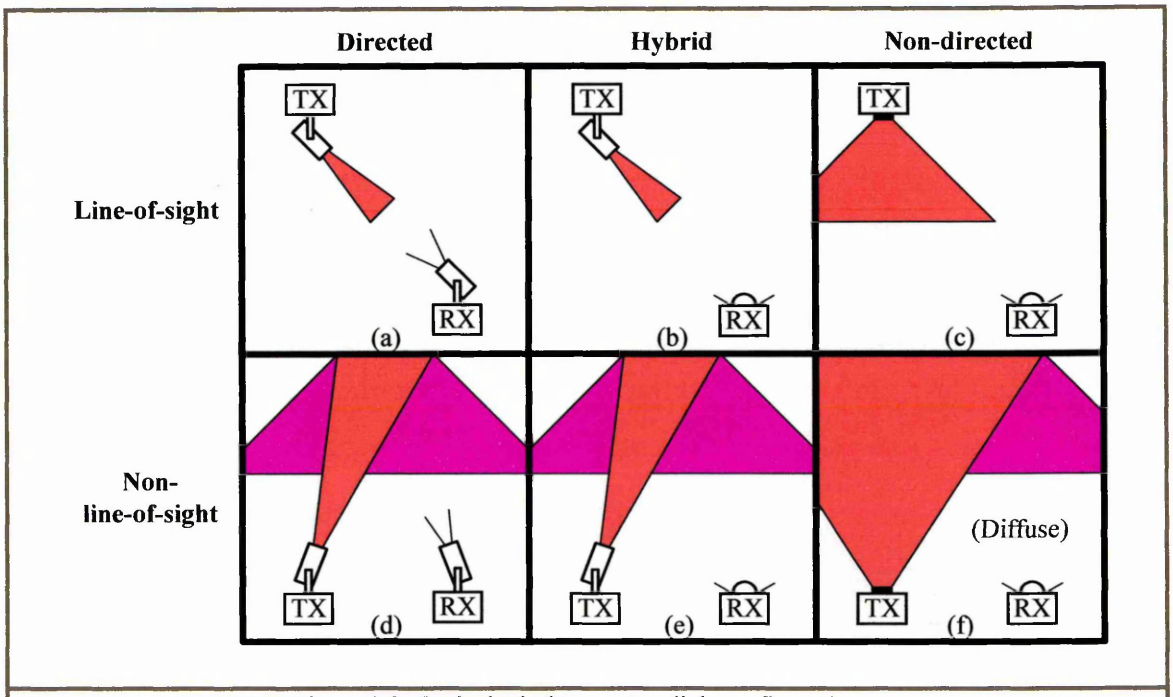

Figure 2.2: Optical wireless system link configurations.

The non-LOS configurations (figure 2.2 bottom row) rely on walls, room objects or ceiling to establish a link. The diffused infrared light, bearing the signal, will travel through many different paths and undergo one or more reflections before reaching the receiver FOV. The effect of such multi-path propagation maintains the communication linkage even when the LOS is blocked, but suffer from optical power loss. On the other hand, multiple reflections will affect the signal pulse being dispersed to the adjacent slot, causing inter-symbol interference (ISI). The severity of pulse dispersion depends on the room dimension and the transmission bandwidth [Gfeller79].

Fuller descriptions of each of the configurations shown in figure 2.2 have been presented in detail in [Barry94]. Here it was found that the diffuse system (figure 2.2 (f)), which is non-directed non-LOS, is the most convenient from the user's standpoint as the configuration does not require alignment between the transmitter and receiver, to maintain LOS allowing considerable mobility to communications. However it does suffer from multi-path propagation effects, however with careful design it has been experimentally proven that it has the capability to provide robustness and high-speed transmission [Marsh96]. The design involves using a large-area, wide FOV, narrow-band optical receiver to provide a high signal-to-noise ratio (SNR) in the presence of intense ambient illumination. It uses a high-pass filter to reduce the effect of fluorescent lights, and quantisation feedback (QF) to remove resulting baseline wander, with a decision-feedback equaliser (DFE) to mitigate ISI due to multi-path propagation [Marsh96, Lee98b, Lee98c]. From here on, this thesis will only consider the diffuse configuration.

2.3.1.1 diffuse system channel characteristics

A realistic infrared channel can be well characterised by two parameters, which are the optical path loss and the root-mean-square (RMS) delay spread. A diffuse channel can be modelled as a base-band linear system, with input power $D_{Tx}(t)$, output current $d_{Rx}(t)$, and an impulse response $h(t)$ which is fixed for a certain physical configuration of receiver, reflectors, and transmitter [Kahn95, Carruthers96a, Carruthers97], as shown in figure 2.3. The model is summarised as:

$$d_{Rx}(t) = R_{Rx} D_{Tx}(t) \otimes h(t) + n(t), \qquad (2.1)$$

where $\otimes$ denotes convolution, R_{Rx} is the receiver photo-detector responsivity with units (A/W) and $n(t)$ is channel noise with units (A) due to background radiation.

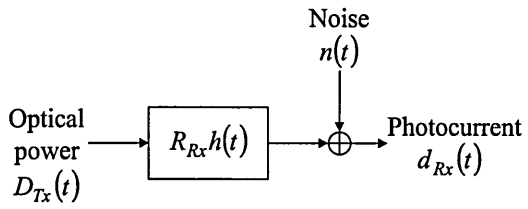

Figure 2.3: Diffuse link channel model.

To characterise a particular multi-path infrared channel, it is useful to determine the average transmitted optical power, given as:

$$W_{ave|Tx} = \lim_{T\to\infty} \frac{1}{2T} \int_{-T}^{T} D_{Tx}(t)dt, \tag{2.2}$$

which is required to achieve a certain BER for a particular modulation scheme [Carruthers96a]. (2.2) is the power constraint and it implies that for a given transmitted average optical power $W_{ave|Tx}$, the receiver SNR can be improved by transmitting a waveform $D_{Tx}(t)$ having a high peak-to-average ratio [Audeh94].

In [Carruthers97], the diffuse channel model definition is given as follows. Defining the optical gain G_{OC} for a channel with impulse response $h(t)$ to be $G_{OC} = \int_{-\infty}^{\infty} h(t)dt$, then the received average optical power is:

$$W_{ave|Rx} = G_{OC} W_{ave|Tx}. \tag{2.3}$$

The optical path loss can be written as:

$$\text{Optical path loss (optical dB)} = -10\log_{10} G_{OC}. \tag{2.4}$$

The transmitted optical signal after undergoing multiple reflections will cause pulse dispersion. The ceiling bounce model for multi-path dispersion is well represented by:

$$h_c(t, a_h) = \frac{6a_h^6}{(t + a_h)^7} u(t), \tag{2.5}$$

where $a_h = 2H/c_L$ and $u(t)$ is the unit step function. The variable H is the effective height of the ceiling above the transmitter and receiver, and c_L is the speed of light. The variable a_h is related to the RMS delay spread by:

$$D_{RMS}(h_c(t,a_h)) = \frac{a_h}{2}\sqrt{\frac{13}{11}}. \quad (2.6)$$

The normalised delay spread D_T is a dimensionless parameter defined as:

$$D_T = \frac{D_{RMS}}{T_{EP}}, \quad (2.7)$$

where T_{EP} is the effective pulse duration. This parameter can be used for investigating the diffuse system performance due to the severity of pulse dispersion.

In the following, it is assumed that $G_{OC} = 1$ when there is no power loss in channel. Thus the effective channel impulse response is defined as:

$$h(t) = \frac{h_c(t,a_h)}{\int_{-\infty}^{\infty} h_c(t,a_h)dt}, \quad (2.8)$$

so that $G_{OC} = \int_{-\infty}^{\infty} h(t)dt = 1$ [Carruthers96a].

2.3.2 Digital modulation techniques

To utilise a particular optical communication link, analogue signals are usually converted into digital signals before being intensity modulated by a light source. The unipolar characteristic of optical system makes it more suitable to transmit digital signals than analogue ones. A pulse of peak intensity W_P is transmitted to represent a '1' and no intensity for a '0'. There are several digital modulation techniques being proposed. In general, the choice of a modulation technique for a specific application is influenced by the characteristics of the message signal, the characteristics of the channel, the performance desired from the overall communication system, the use to be made of the transmitted data, and the cost factor, that is always important in practical applications [Tranter95]. The choice of a digital modulation technique for an indoor optical wireless communication is influenced by the eye safety regulations where the amount of optical shall not exceed the limit that will damage the human eye. The limit is defined as [Barry94]:

$$\lim_{T\to\infty}\frac{1}{2T}\int_{-T}^{T} D_{Tx}(t)dt \le W_{\max}, \qquad (2.9)$$

where $W_{\max}$ is the maximum allowable optical power transmitted for the duration of $2T$. Other influential issues include [Hayes02]:

- *Power efficiency* where power consumption is to be kept low while maintaining a desirable BER. Low power consumption will help to maintain a longer battery life for portable infrared devices.

- *Bandwidth efficiency* where the base-band bandwidth is limited by the multi-path propagation effect in a diffuse system.

Digital modulation techniques that have been investigated for use in optical wireless system are OOK, PPM and PIM [Hayes02]. All these modulation techniques will be studied throughout this thesis with the assumption that information from data source is in a binary format.

2.3.2.1 on-off keying

It is the simplest modulation technique to implement. The modulation is a process of converting the information bit '1' from data source to a pulse of constant amplitude V_P for the duration of one bit T_b. Whereas, the information bit '0' is basically converted to an off state of duration T_b. The data rate is $R_b = 1/T_b$. The system block diagram is shown in figure 2.4 (a). The waveforms observed at the input and output of the channel together with the channel impulse response is shown in figure 2.4 (b). As observed from figure 2.4 (b) and (c), the normalised delay spread for the OOK signal, denoted by $D_{T|OOK}$, represents the end point of the exponential tail of the dispersed signal decay to an insignificant value. The value of $D_{T|OOK}$ is obtained by choosing $D_{RMS} = 0.3\times10^{-6}$s, as an example, and the channel is assumed ideal with no noise $n(t)$.

Denoting the binary data as $B_{k|Tx}$, the information bit stream at the output of OOK modulator is represented by:

$$b_{Tx}(t) = V_P \sum_{k=0}^{\infty} B_{k|Tx}\, g(t - kT_b), \tag{2.10}$$

where k is an integer denoting the k^{th} bit information and $g(t)$ is a square pulse. The optical signal transmitted is given by:

$$D_{Tx}(t) = R_{Tx} b_{Tx}(t), \tag{2.11}$$

where R_{Tx} is the transmitter optical source responsivity of unit (W/A).

2.3.2.2 pulse position modulation

PPM is an orthogonal modulation technique that has been proposed to achieve power efficiency compare with OOK, but at the expense of increase bandwidth and system complexity. In PPM, each block of *M*-bits of information is mapped to one of L possible symbols. Each symbol is a fixed frame of duration LT_s, where the time slot $T_s = {}^{MT_b}\!/_{L}$ and $L = 2^M$.

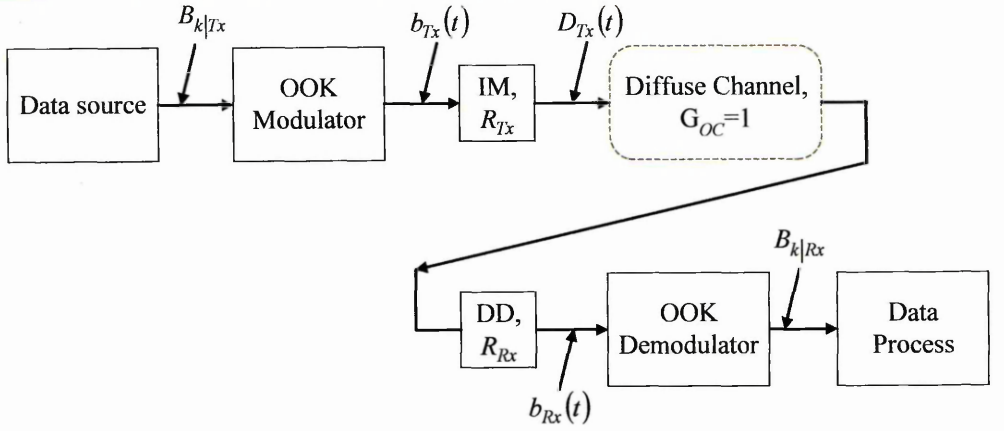

(a)

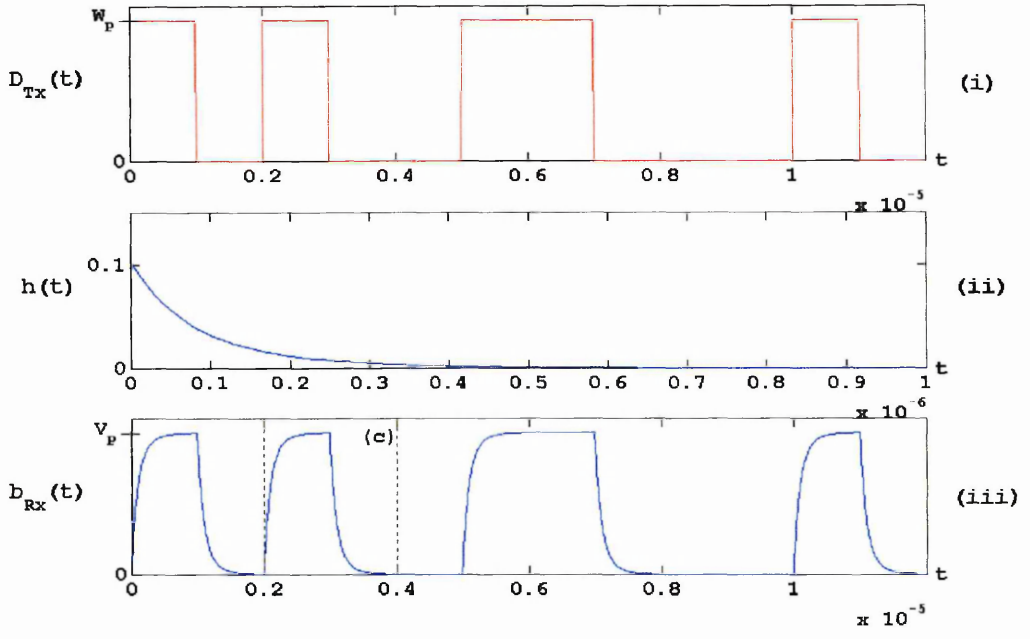

(b)

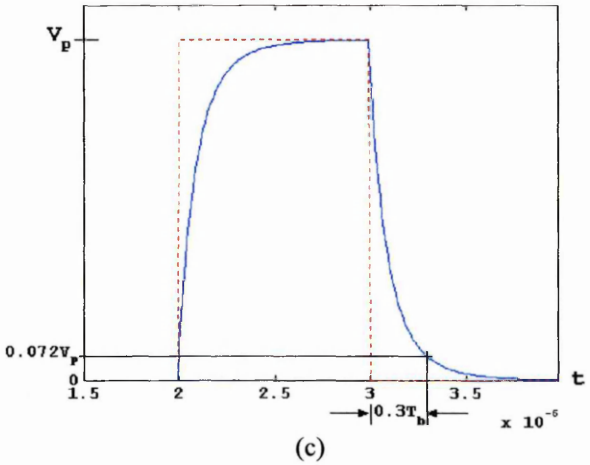

(c)

Figure 2.4: OOK diffuse system. (a) block diagram. (b) waveforms; (i) transmitter output, (ii) effective impulse response (using (2.8)), where $D_{RMS} = 0.3\times10^{-6}$ s, $R_b = 1$ Mb/s, $D_{1|OOK} = 0.3$ (using 2.7)), $G_{OC} = 1$ and $R_{Tx}R_{Rx} = 1$, and (iii) receiver input. (c) enlarged section of single pulse in (b) (iii).

Each symbol consists of a pulse of constant amplitude V_P and duration T_s. The position of a pulse within a symbol, displaced at an integer multiple of T_s from the symbol's origin, corresponds to the integer decimal value of the M-bits information. An example of a PPM symbol, mapping the 4-bits of information $B_{k|Tx} = \{1 \quad 0 \quad 1 \quad 0\}$, with a decimal value of 10, is shown in figure 2.5.

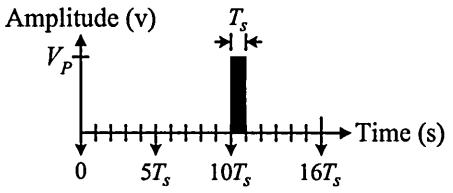

Figure 2.5: PPM symbol mapping 4-bits information $B_{k|Tx} = \{1 \quad 0 \quad 1 \quad 0\}$.

Generally, the notation L-PPM is used to indicate the order, and hence the example above is a 16-PPM. Using the same channel characteristics and data as in figure 2.4, the waveforms observed at the input and output of the channel together with the channel impulse response are shown in figure 2.6. Note that the PPM pulse width has been reduced as a result of increased bandwidth due to the increase of PPM mapping order L. As a result, the exponential tail of the dispersed signal shown in figure 2.6 (b), decay to an insignificant value at $1.2T_s$ durations away from the original pulse, further than the OOK shown in figure 2.4 (c). This is because the normalised delay spread $D_{T|PPM} = {}^{D_{RMS}}\!/_{T_s}$ for PPM is higher than the OOK.

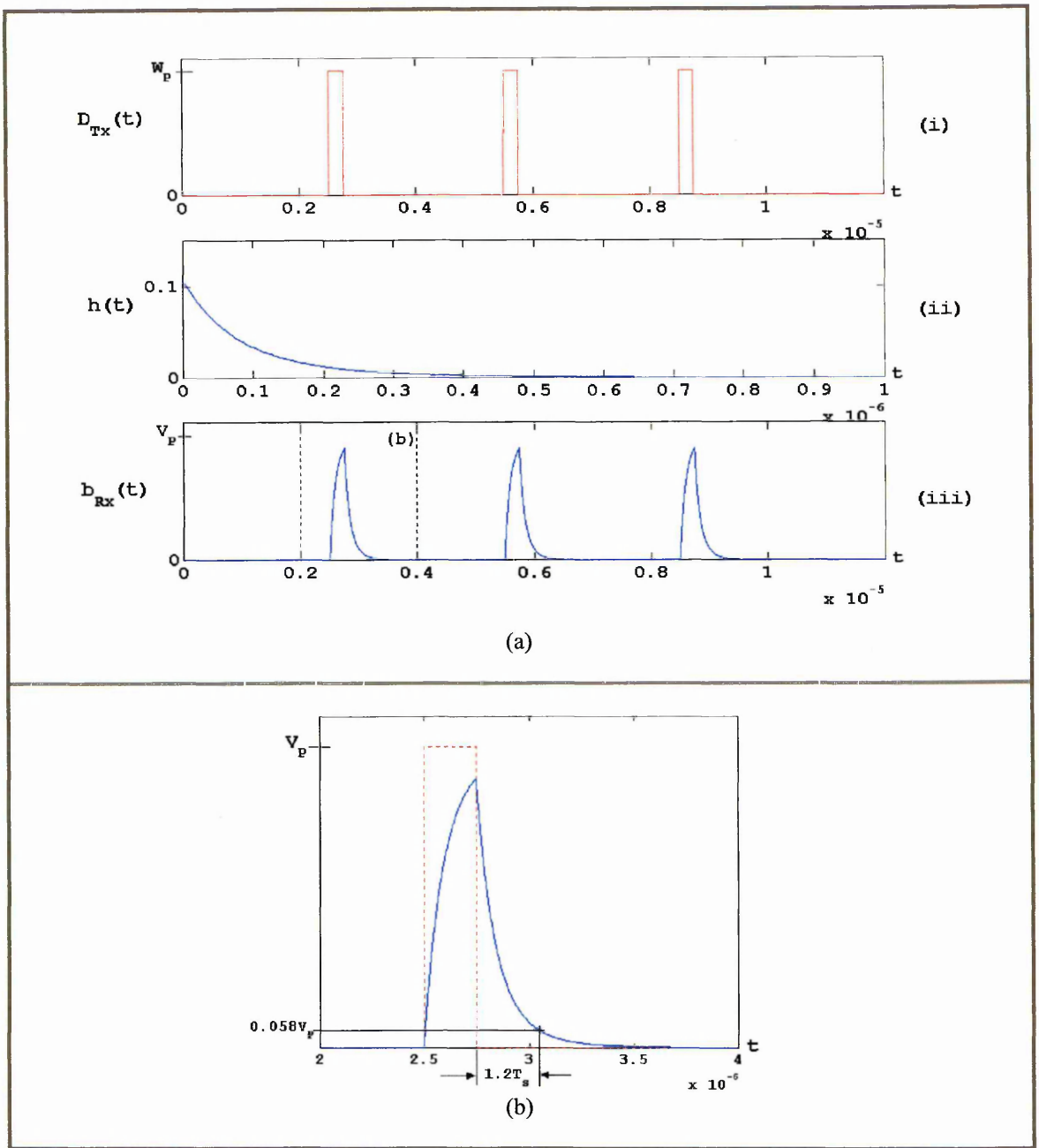

Figure 2.6: 16-PPM diffuse system. (a) waveforms, symbol duration is 4×10^{-6} s ; (i) transmitter output, (ii) effective impulse response, where $D_{RMS}=0.3\times10^{-6}$ s , $R_s=1/T_s=4$ Mb/s , $D_{T|PPM}=1.2$, $G_{OC}=1$ and $R_{Tx}R_{Rx}=1$, and (iii) receiver input. (b) enlarged section of single pulse in (a) (iii).

2.3.2.3 pulse interval modulation

As with the PPM, the name PIM implies that information bits modulate the interval between two pulses, where the interval length varies according to the integer decimal value being mapped. An example of a PIM symbol mapping the same 4-bits information as the above is shown in figure 2.7. The interval between the two pulses is of duration $10T_s$, which corresponds to decimal value 10.

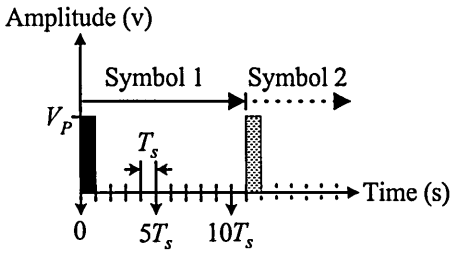

Figure 2.7: PIM symbol mapping 4-bits information $B_{k|Tx} = \{1 \quad 0 \quad 1 \quad 0\}$.

Each PIM symbol is composed of a pulse, occupying one T_s followed by a number of empty slots T_s. The PIM maximum symbol duration is equal to the PPM fixed symbol duration and the minimum symbol duration is $1T_s$, where the information is all '0's. Assuming that the information bits are independent and identically distributed (IID), then the average PIM symbol length $L_a = {(1+L)}/{2}$. PIM signal waveforms and channel response are shown in figure 2.8 using the same parameters as in figure 2.6. Note that PIM pulse width is the same as the PPM pulse width, and has the same severity of dispersion. As observed when comparing figures 2.8 with 2.6 (a), the PIM packet length when transmitting the same information as PPM is shorter. Hence PIM achieves a higher throughput than PPM and OOK.

Another proposed format of PPM known as the Differential PPM (DPPM) [Shiu98b, Shiu99] is similar to PIM. The only difference is the DPPM locates the information slots at the beginning of a symbol and only then a pulse at the end of the symbol. This difference does not affect both modulation schemes in term of BEF, BER and power efficiency performance. Therefore, only the PIM will be discussed.

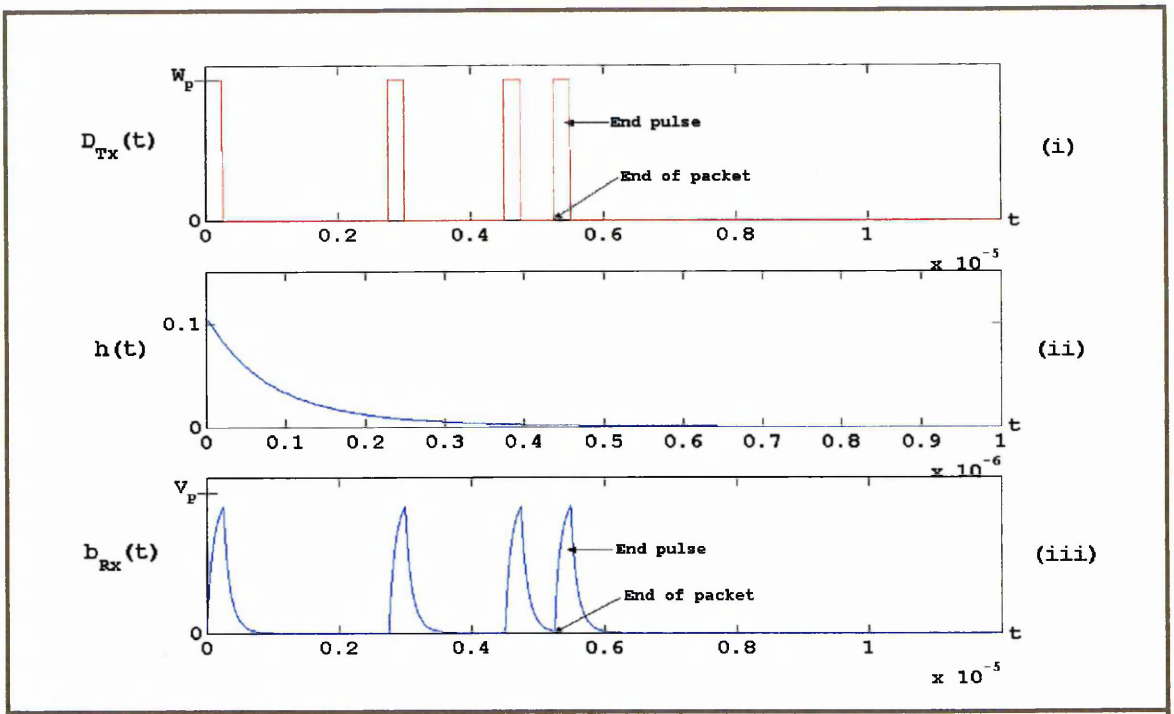

Figure 2.8: 16-PIM diffuse system signal waveforms, symbol duration is 4×10^{-6} s ; (i) transmitter output, (ii) effective impulse response, where $D_{RMS}=0.3\times10^{-6}$ s , $R_s=1/T_s=4$ Mb/s , $D_{T\mid PIM}=1.2$, $G_{OC}=1$ and $R_{Tx}R_{Rx}=1$, and (iii) receiver input.

2.3.3 Modulation techniques comparison

Being the simplest to implement, OOK modulation has been investigated extensively for use in diffuse system [Marsh94, Audeh95, Wong00]. A simple circuit implementation for an indoor optical wireless diffuse system employing OOK modulation can achieve a data rate of 50 Mbps , as reported in the experimental work by [Marsh94]. Simulation results have also shown that a data rate of up to 100 Mbps is possible [Audeh95]. However, in order to reduce power consumption and to conform to the eye safety regulations, PPM is a more suitable and effective technique for transmitting the same amount of information as OOK but with a much lower power.

Due to its improved power efficiency 16-PPM and 4-PPM have been adopted as the IEEE 802.11 standard for infrared physical layer with data rates of 1 Mbps and 2 Mbps , respectively [IEEE97, Hayes02]. Note that in both formats, the slot rate is the same, which implies that the effective pulse width T_{EP} is the same. Nevertheless, there is one significant disadvantage of PPM in that it requires a high degree of slot and symbol synchronisation at the demodulator.

PIM does achieve high throughput and alleviates the need for slot and symbol synchronisation. It offers improved power efficiency over OOK, but not PPM. Although PPM and PIM are power efficient, and PIM has high throughput, both schemes suffer from severe pulse dispersion as outlined below. Figure 2.9 (a) shows the comparison for power efficiency, W_{Eff}, against the number of bits, $M = \log_2 L$, being mapped. Also, the severity of dispersion D_T against M is shown in figure 2.9 (b).

For $M = 1$, PPM offers no power efficiency whereas PIM is lower by $\approx 1.25\,\text{dB}$. As M increases, the PPM power efficiency increases linearly at the rate of 3.01dB per bit mapping. On the other hand, PIM displays a non-linear characteristic; this is because of the variable symbol structure. Although PPM and PIM offer improved power efficiency at values of $M > 1$, compared with OOK, both suffer from pulse dispersion. Assume that the diffuse channel characteristic has a $D_{RMS} = 0.3 \times 10^{-6}\,\text{s}$ and the OOK data rate is $R_b = 1\,\text{Mbps}$, then the severity of delay spread for PPM and PIM as the M increase can be related to:

$$D_T = \frac{2^M D_{RMS} R_b}{M} = \frac{0.3 \times 2^M}{M}. \qquad (2.12)$$

Referring to figure 2.9 (b), the delay spread for both the PPM and PIM pulses are increased exponentially with M. In order to show a clear picture (for comparison) of the effect of dispersion on the signal pulse, a plot based on a constant slot duration of $T_s' = 1/R_b = 1 \times 10^{-6}\,\text{s}$ (in contrary to the T_s in figure 2.9 (b) that varies) but variable D_{RMS} (governed by (2.7)) is shown in figure 2.9 (c). As can be seen the signal pulse is severely dispersed and the signal peak amplitude reduced greatly as M is increased.

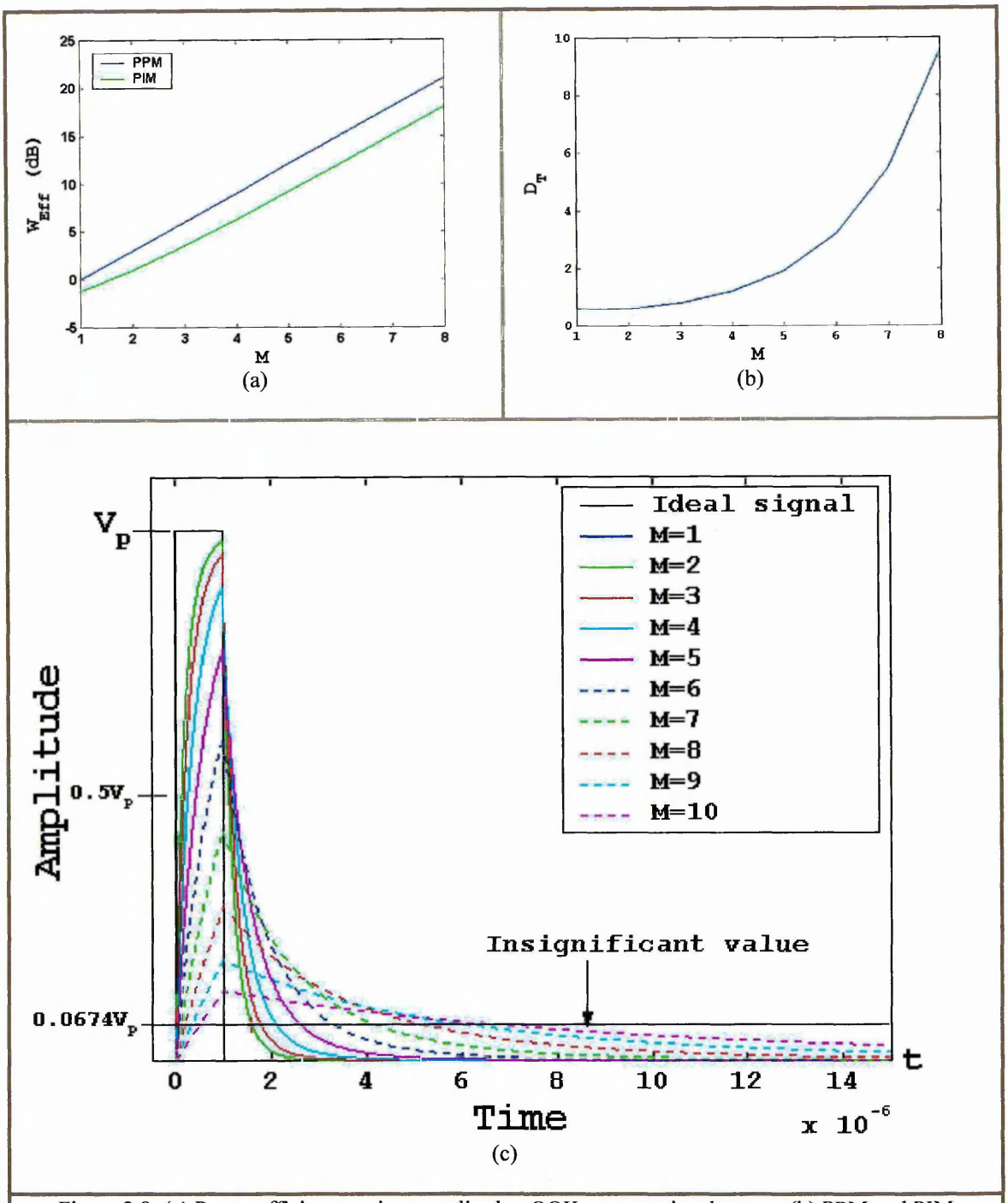

Figure 2.9: (a) Power efficiency ratio normalised to OOK average signal power. (b) PPM and PIM normalised delay spread. The change of pulse slot T_s is related to $T_s = MT_b/L$ with $R_b = 1$ Mbps, and the diffuse channel is characterised by $D_{RMS} = 0.3\times10^{-6}$ s. (c) Signals' dispersed shapes due to D_T in (b), where $T_s' = 1\times10^{-6}$ s and D_{RMS} varies as D_T varies.

2.4 Discussion

PPM has been shown to be the most power efficient modulation technique of all, and it is appropriate for use in optical wireless systems where eye safety regulations are a restriction. However, the order of L-PPM reaches a limit when the pulse delay spread becomes severe and

the signal becomes distorted. PIM also provides power efficiency and offers higher transmission throughput compared with OOK and PPM because of its variable symbol structure.

On average, PIM transmits $\log_2 L_a$ bits when OOK and PPM are transmitting M bits, where $\log_2 L_a < M$. The order of the data rate achievement compared with the OOK and PPM can be related to the bit-enhancement-factor (BEF) as:

$$BEF = \frac{M}{\log_2\left(\frac{2^M + 1}{2}\right)}. \tag{2.13}$$

BEF is a measure of the number of times a transmission speed is achieved [Elmirghani94]. Figure 2.10 shows the BEF against *M*, showing a linear increase. Therefore, PIM technique is chosen as a candidate to enhance the data throughput for a DS-CDMA system where bandwidth is limited – which will be discussed in chapter 6.

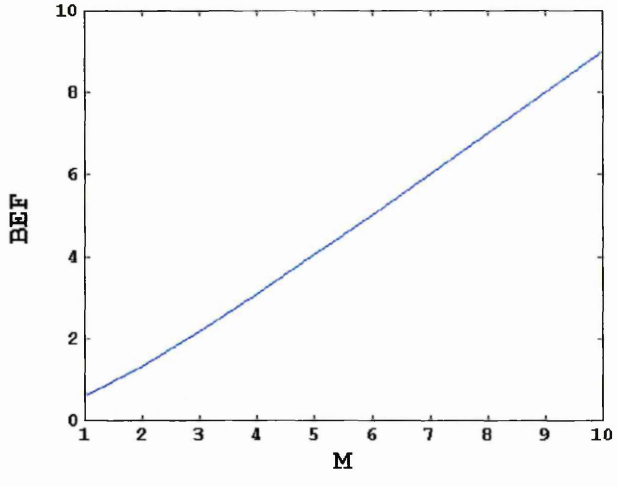

Figure 2.10: BEF performance of PIM over OOK and PPM.

2.5 Summary

Factors that govern the consideration of modulation techniques depend on the system performance requirement, such as eye safety regulations, background noise and multi-path propagation. The full comparison of the three modulation techniques, including analysis on baseline wander, power spectral density, power requirement and dispersion effect can be found

in [Hayes00, Hayes02]. Eye safety regulations are the dominant factors that limits the number of modulation techniques that could be used in optical wireless communication systems. It was shown that PIM achieved power efficiency and BEF compared with the OOK and PPM. Both PPM and PIM suffer from severe pulse dispersion, but employing equalisation techniques can result in improved performance [Marsh94, Marsh96].

Chapter 3

MULTIPLE-ACCESS SCHEMES

3.1 Introduction

In designing a WLAN network, where a wireless medium is shared by all network clients or users, it is essential to employ a multiple-access scheme [Marsh97]. A multiple-access scheme is a technique that separates the messages corresponding to different clients, so that they do not interfere with one another. Conventional schemes accomplish this by making the messages orthogonal in one domain so that can be easily handled with digital signal processing technologies.

There are a number of well-known optical multiple-access schemes, which employ time, wavelength (infrared) and time-and-wavelength domains for message separation. These are Wavelength-Division Multiple-Access (WDMA), Time-Division Multiple-Access (TDMA), and Code-Division Multiple-Access (CDMA). In WDMA and TDMA a fixed amount of wavelength and time, respectively, is allocated to accommodate the individual channels. Theoretically, an infinite number of possible channels can exist, although most of these are impractical due to the implementation difficulties [Liu00]. CDMA does not explicitly allocate a fixed amount of time to each channel but uses codes to spread the signals so that multiple channels can be transmitted concurrently. This is achieved at the expense of greater duration or bandwidth. Both WDMA and TDMA capacity is hard limited due to the number of channels determined by the total number of wavelength and time resources, where no more users can access the network once capacity is reached. Alternatively, the capacity of CDMA is soft limited as it allows flexible network capacity but at the cost of quality, the system BER depends

on the number of active users [Stok00]. The following sections will describe and compare all three multiple-access schemes, in particular CDMA.

3.1.1 Wavelength-division multiple-access

WDMA systems allocate the available optical bandwidth into distinct wavelengths that are simultaneously occupied by different clients' signals, to permit multiple-access communication links. A wavelength-time diagram is shown in figure 3.1(a) where three different information signals, indicated with different labels, simultaneously occupy the wavelength-time plane. A physical channel corresponds to a band of wavelength, where the wavelength at the centre of each band is the carrier. Each of the horizontal stripes represents one channel capable of providing a communication link that does not interfere with its neighbours. The total number of clients that can be transmitted is equal to the number of carriers allocated. In the electrical system, the equivalent of WDMA is known as Frequency-Division Multiple-Access (FDMA).

The problem with using WDMA in LANs is that a significant amount of dynamic coordination between communicating pairs or nodes is required. Though a control channel can be dedicated for pre-transmission coordination, this will waste the bandwidth that could otherwise be used for data transmission and introduces latency as communicating pairs attempt to negotiate a connection. On the one hand, the control channel can be avoided by assigning transmission rights in a predetermined fashion, or through contention-based protocols. However, in large networks with dynamic populations scheduling becomes difficult, and collision detection schemes waste bandwidth and can introduce significant latency [Stok00].

3.1.2 Time-division multiple-access

The complement of WDMA is TDMA, in which each signal uses only one carrier wavelength for a fraction of time, as shown in figure 3.1(b). To perform TDMA, a transmitter stores the source information that arrives in a time interval referred to as a TDMA frame. Each

transmitter and receiver pair only communicates for a fraction of the frame, one pair after another. Each pair occupies the same time slot within the frame for transmission. The time interval occupied by one signal stream is a slot. In TDMA, a physical channel corresponds to one time slot. When its time slot begins, a transmitter sends the stored information at an accelerated speed, so that all the information recorded in one frame is transmitted in a slot. The receiver records the signal arriving at a given slot and plays it back at the original slower rate. The playback interval is one frame and the received information, restored to the lower rate, emerges in a continuous stream with no gap. In principle, time-division techniques could be used for discrete analogue communications. In practice, however, they appear only in digital systems, where it is much simple to store binary signals arriving at the source rate, and then release them at the faster channel rate. The number of physical channels in a time division system is the number of slots per frame, which is the ratio of the frame duration to the slot duration. In figure 3.1(b), each frame has 3 slots corresponding to 3 carriers.

TDMA system requires each communicating pair to be in completely synchronised. Though a global synchronisation system can be employed, it does not guarantee transmission time matching between source and destination, resulting in time drift between the communication pair. Eventually, the receiver will drift ahead of or behind the transmitter by one entire TDMA frame's duration, resulting in reception of the wrong signal. Therefore, each frame needs an extra bit for synchronisation purposes, so that the transmitter and receiver pair can synchronise their clocks at regular intervals. There is a disadvantage of TDMA technique, where some channels may have nothing to transmit during the off-peak hours. The channels that dedicated to the idle pairs will still be reserved and hence time capacity is wasted [Matloff01].

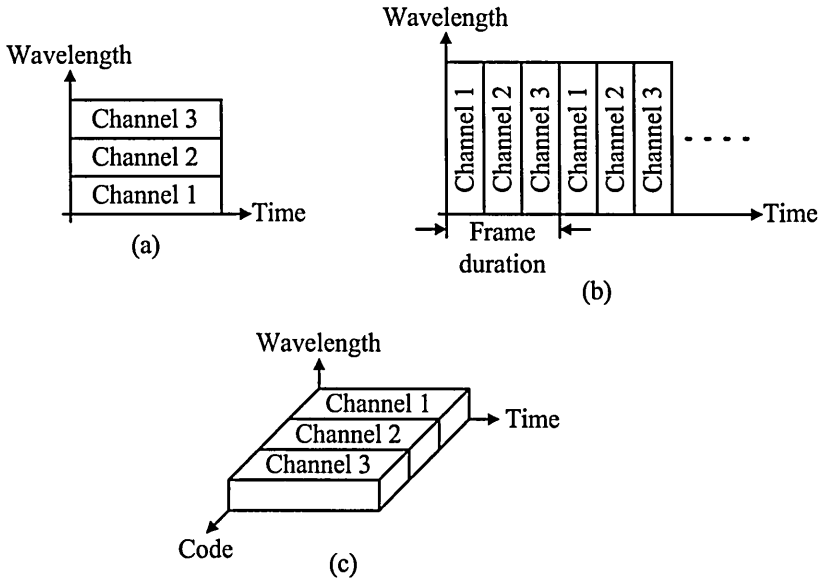

Figure 3.1: Multiple access schemes. (a) WDMA, (b) TDMA and (c) DS-CDMA.

3.2 Code-Division Multiple-Access

CDMA is based on spread-spectrum techniques. It spreads the message signal to a relatively wide bandwidth by using a unique code, in order to reduce interference, enhance system processing, and support for multiple-access communication.

3.2.1 Spread-spectrum

Spread-spectrum techniques originated in answer to the unique needs of military communications, and this application is still the predominant one. For a communication system to be considered a spread-spectrum system, it is necessary that the transmitted signal satisfying two criteria. First, the bandwidth of the transmitted signal must be much greater than the message bandwidth. This, by itself, is however not sufficient because there are many modulation methods that can achieve this. For example, FM, Pulse Code Modulation (PCM), and Delta Modulation may have bandwidths that are much greater than the message bandwidth. The second criterion is that the transmitted bandwidth must be determined by some function that is independent of the message and is known to the receiver.

The bandwidth expansion does not combat white noise as it does in FM, PCM and other wide-band modulation methods. This is so because bandwidth expansion is achieved by something that is independent of the message, rather than being uniquely related to the message. Since a spread-spectrum system is not useful in combating white noise, it has other applications that make it worth considering. These applications include:

- Anti-jam capability – particularly for narrow-band jamming
- Interference rejection
- Multiple-access capability
- Multipath protection
- Covert operation or low probability of intercept
- Secure communications
- Improved spectral efficiency – in special circumstances
- Ranging

There are many different types of spread-spectrum systems; one way to classify them is by concept. On this basis spread-spectrum systems may be considered to be either averaging systems or avoidance systems. An averaging system is one in which the reduction of interference takes place because the interference can be averaged over a large time interval. An avoidance system, on the other hand, is one in which the reduction of interference occurs because the signal is made to avoid the interference a large fraction of the time.

A second method of classifying spread-spectrum system is by the modulation technique used, which may be:

- Direct-sequence (DS) (pseudonoise)
- Frequency-hopping (FH)
- Time-hopping
- Chirp

- Hybrid methods

The relation between these two methods of classification may be made clearer by noting that a direct-sequence system is an averaging system, whereas frequency-hoping, time-hopping, and chirp systems are avoidance systems. A hybrid modulation method may be averaging, avoidance, or both [Cooper86]. A typical CDMA system that utilises both wavelength-time resources is illustrated in figure 3.1(c). To demonstrate the process of averaging and avoidance with multiple-access capability, the DS and FH are discussed.

3.2.2 DS and FH spread-spectrum techniques

DS is usually used to encode digital information. The process is a form of spreading one information bit, of rate R_b, to a new form of binary stream of n chips. The chip rate R_c is defined as:

$$R_c = nR_b \quad , n = 1,2,3,.... \tag{3.1}$$

The process of spreading is depicted in figure 3.2, where $n = 5$. The spreading sequence is a random pattern of bits '0' and '1'. In unipolar signal modulation, an information bit '1' is spread to form the spreading sequence, whereas a '0' bit remains unchanged. In bipolar signal modulation, the positive signal is spread to form the spreading sequence, and the negative signal is spread to the complement of the spreading sequence. This process can be seen as a result of multiplication between the information and the spreading sequence. The spreading sequence can be duplicated and synchronised at the transmitter and receiver. The receiver recovers the original signal by performing a *correlation* function with the same sequence as that of the transmitter. The pattern of the spreading sequence is determined by a code. When a set of different codes is used, multiple-access communication is possible, whereby the system can operate at one carrier wavelength, but with increased processing time. The process is depicted in figure 3.1(c), where each code represents a channel.

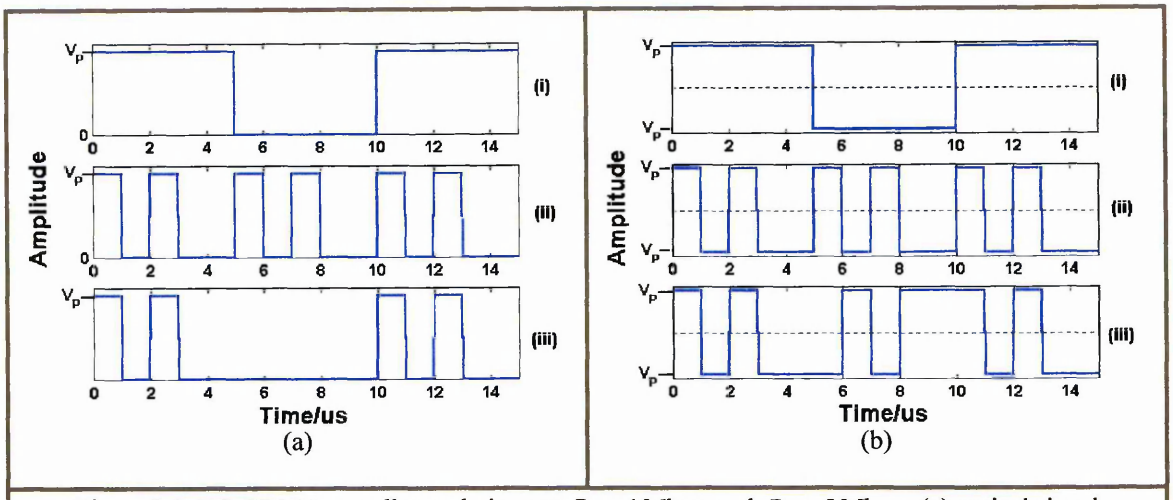

Figure 3.2: DS-CDMA encoding technique at $R_b = 1$ Mbps and $R_c = 5$ Mbps . (a) optical signal (unipolar). (b) electrical signal (bipolar); (i) is the information signal, (ii) is spreading sequence of pattern $\{1 \quad 0 \quad 1 \quad 0 \quad 0\}$ repeating at every $1/R_b$ duration, and (iii) is resulting waveform.

FH can encode both analogue and digital information. It is usually used in military systems, as it is extremely difficult for unauthorised receivers to decode. FH is a form of spreading in which the carrier frequency of the signal is altered many times a second in accordance with a list of pseudo-random frequencies, called the hop set [Rappaport96]. This process can be visualised with the aid of figure 3.3, which show a single FH sequence. FH can either be fast, i.e. several hops per one symbol, or slow, i.e. several symbols transmitted during one hop [Ojanperä01]. As shown in figure 3.3, for a data rate of 1 Mbps , the hoping rate is 7 Mbps . Ideally a slow-FH code, employing code diversity transmission, can facilitate simultaneous multiple-access communication [Ong95], provided there is no frequency-time overlap between the carriers.

A recent application of (RF) wireless FH-CDMA over a short distance (<10 meters) is the 'Bluetooth' standard recommended for personal area networking [Filanowski01]. FH can also be implemented in an optical wireless system using an offset bipolar signal in the frequency domain employing IM/DD. To the author's knowledge, FH wireless technology employing wavelengths as hop source has not yet been proposed. Nevertheless it is possible to implement a wavelength-hopping technique where a transmitter will have to employ multiple optical sources and receivers for modulating and demodulating multiple wavelengths. In optical fibre FH system, wavelengths hopping are achieved by employing a tuneable multiple-grating fibre [Fathallah97, Fathallah98].

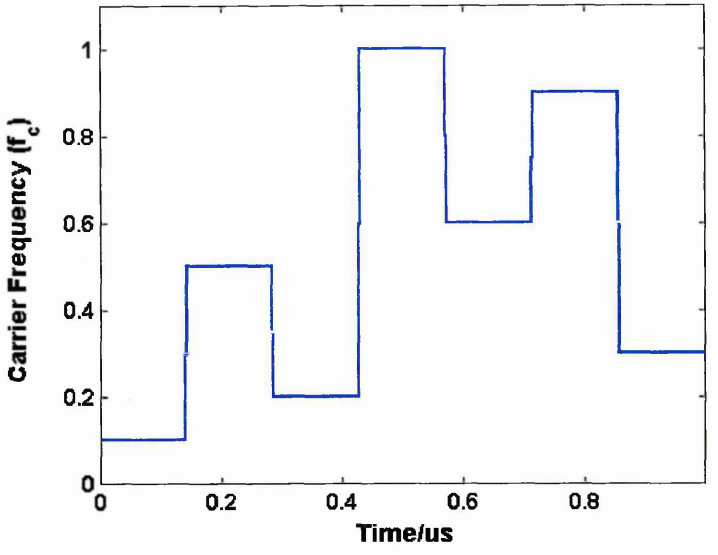

Figure 3.3: A typical FH sequence for one bit period.

3.2.3 Spreading sequence

One of the most important properties of the CDMA technique is demonstrated when the spreading sequence is used for message separation. The spreading sequence determines how well a CDMA system will perform. Its form is appropriately geared to the class of CDMA being used. For instance, in a DS system, a spreading sequence assigned for a communication channel is to appear as distinct as possible compared to the sequence used by another channel. A high degree of difference indicates a high quality of message separation. In electrical systems, the codes used for generating spreading sequences are called pseudonoise or PN code [ARRL91], whereas in optical systems, they are called Optical Orthogonal Codes or OOC [Salehi89a].

For FH systems, a spreading sequence determines the carrier frequency to which the base-band signal is to be hopped. A good spreading sequence will have a random hop-set so that the signal being encoded will appear as noise in a form that is unrecognisable to unwanted recipients. Hop-sets use different carrier frequencies for different channels ensuring that they will never overlap at any hop.

3.2.4 Correlation

Correlation is a fundamental process in a spread-spectrum system and forms a common method of receiving individual signals. It is the process of measuring the similarity between two signals. The degree of correlation is often normalised between zero and one. A value of one indicates a perfect match whereas a value zero indicates total mismatch. Correlation is usually carried out using a circuit known as a correlator. A correlator is typically composed of a mixer followed by a low-pass filter (LPF) that performs an averaging function, as shown in figure 3.4. The mixer is a multiplication function for comparing two signals. It will output a high value if the two signals are matched, and a lower output, depending on how different the signals are. The averaging circuit will determine the average output of the mixer. This value is therefore the correlation of the two signals.

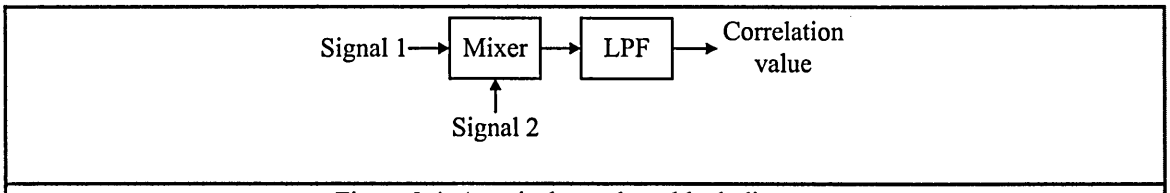

Figure 3.4: A typical correlator block diagram.

In a DS system, a correlator is used to identify and detect the signals with a particular spreading sequence. If the received signal matches with a locally generated spreading sequence, the correlator will yield a high value. In a noisy and interfering communication environment, some of the received signals from the channel (the spread sequences) will be corrupted. After mixing, the interfering signals (the undesired spreading sequences) are spread and resemble noise, while the desired signal is de-spread and the energy is focused onto a single chip period. The averaging circuit will then perform a low-pass filtering function, thereby reducing the noise while passing the time constrained information. A threshold circuit is then used to decide whether the received signal is either a match or mismatch. This is the heart of the DS interference-rejection process.

Auto-correlation is the process of correlating two identical sequences, and cross-correlation is the correlation of two different sequences. A correlation process for DS system is demonstrated in figure 3.5. In optical systems operating in the positive region only, the bit '1' of the spreading sequence is modulated with a positive square pulse, whereas the bit '0' is modulated with an empty chip, both are at rate R_c. The electrical systems will modulate the bit '1' with a positive square pulse and the bit '0' with a negative square pulse at the chip rate R_c. The intended client receiver will have a replica of the spreading sequence, as plotted in red colour in figure 3.5. The incoming signal to the receiver, plotted in blue, will be multiplied with the replica sequence. Figures 3.5 (a) and (b) shows the in-phase auto-correlation where both sequences are multiplied at exactly the same time frame. This will result in the maximum sum of products, where the total is 2 for the optical and 5 for the electrical. It is said that the 'auto-correlation peak' for an optical sequence is equal to the number of pulses (bit '1') in the sequence, and for the electrical it is equal to the sequence length. The number of pulses that contribute to the sum of products is usually known as the 'code weight'. An out-of-phase auto-correlation can be imagined as two sequences that are correlated at a different time frame. Figures 3.5 (c) and (d) show a typical out-of-phase correlation. Note that the sum of product of out-of-phase is less than the in-phase, which indicates dissimilarity. Thus the reconstructed signal occurs at the in-phase position, which is the position it was at when encoded with the spreading sequence at the transmitter. Note that in general, the name auto-correlation itself implies that the function includes both the in-phase and out-of-phase terms. Hence the specific term must be mentioned to signify the specific correlation function. This is also the case for cross-correlation. When a set of spreading sequences produce a peak equal to the code weight at the in-phase auto-correlation but zero value when out-of-phase, and the cross-correlation of any sequences in the set is always zero, this is termed 'orthogonal correlation'.

The correlation process in a FH system is implemented somewhat differently, but the concept is the same. In a FH system, the transmitter carrier frequency is changed many times a second according to the hop-set. The receiver uses the same hop-set to follow that of the transmitter,

moving from channel to channel in the exact step with the signal. If the receiver is out of step with the signal, it cannot recover the information signal being transmitted.

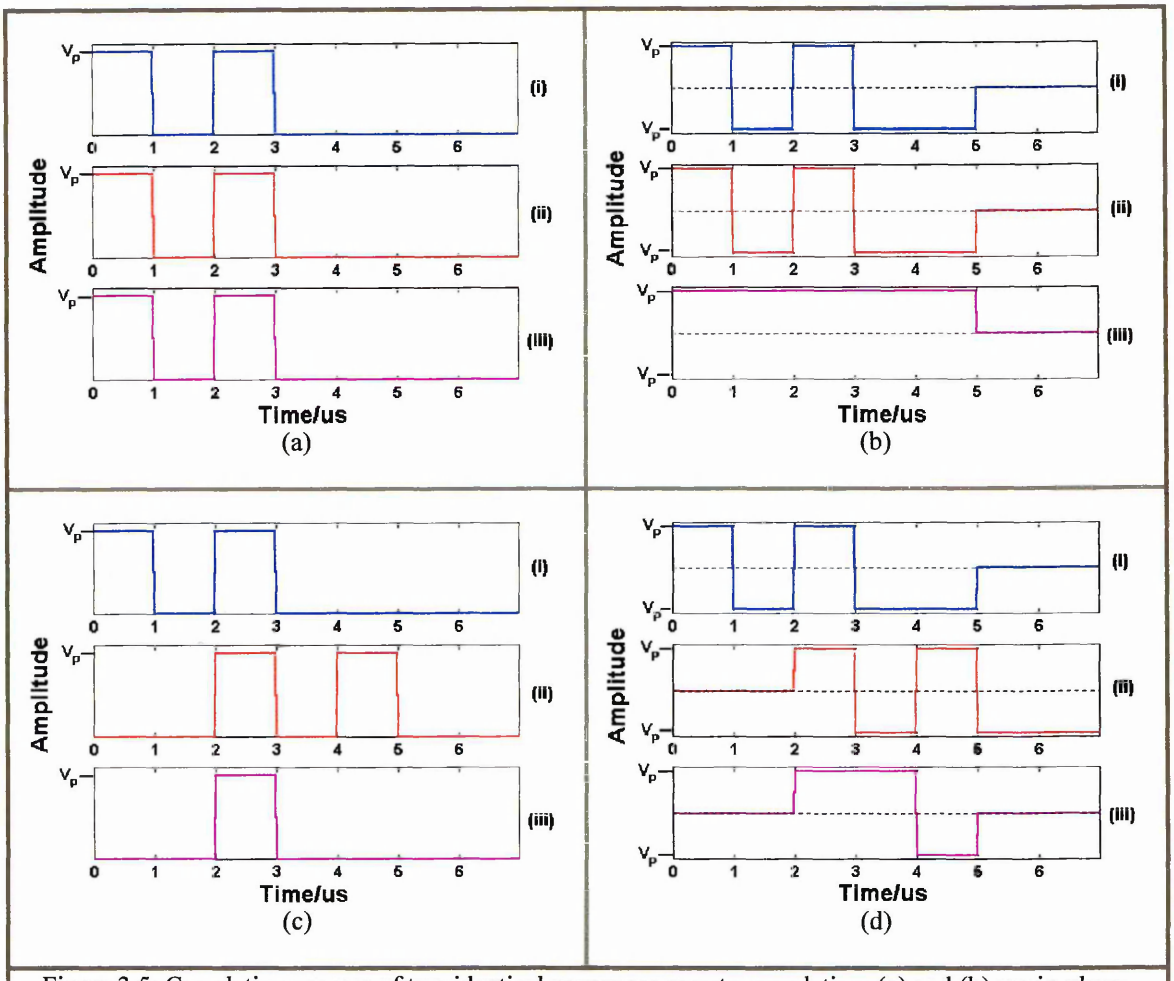

Figure 3.5: Correlation process of two identical sequences or auto-correlation; (a) and (b) are in-phase, and (c) and (d) are out-of-phase. (a) and (c) are optical signals, and (b) and (d) are electrical signals. (i) is transmitted or received signal, (ii) is replica sequence at receiver and (iii) is resulting waveform of mixer. *The signature sequence pattern is $\{1 \quad 0 \quad 1 \quad 0 \quad 0\}$.

3.2.5 Synchronisation

Synchronisation is the most difficult issue for a CDMA system. For a client receiver to demodulate the desired signal it must be able to synchronise its assigned spreading sequence with the one used by the transmitter, this operation often takes place at very high speeds. It is usually viewed as two processes: rough synchronisation that searches and acquires the receiver's spreading sequence within one chip, and fine synchronisation that maintains timing of the acquired chip rate. Rough and fine synchronisations can be visualised in figure 3.6.

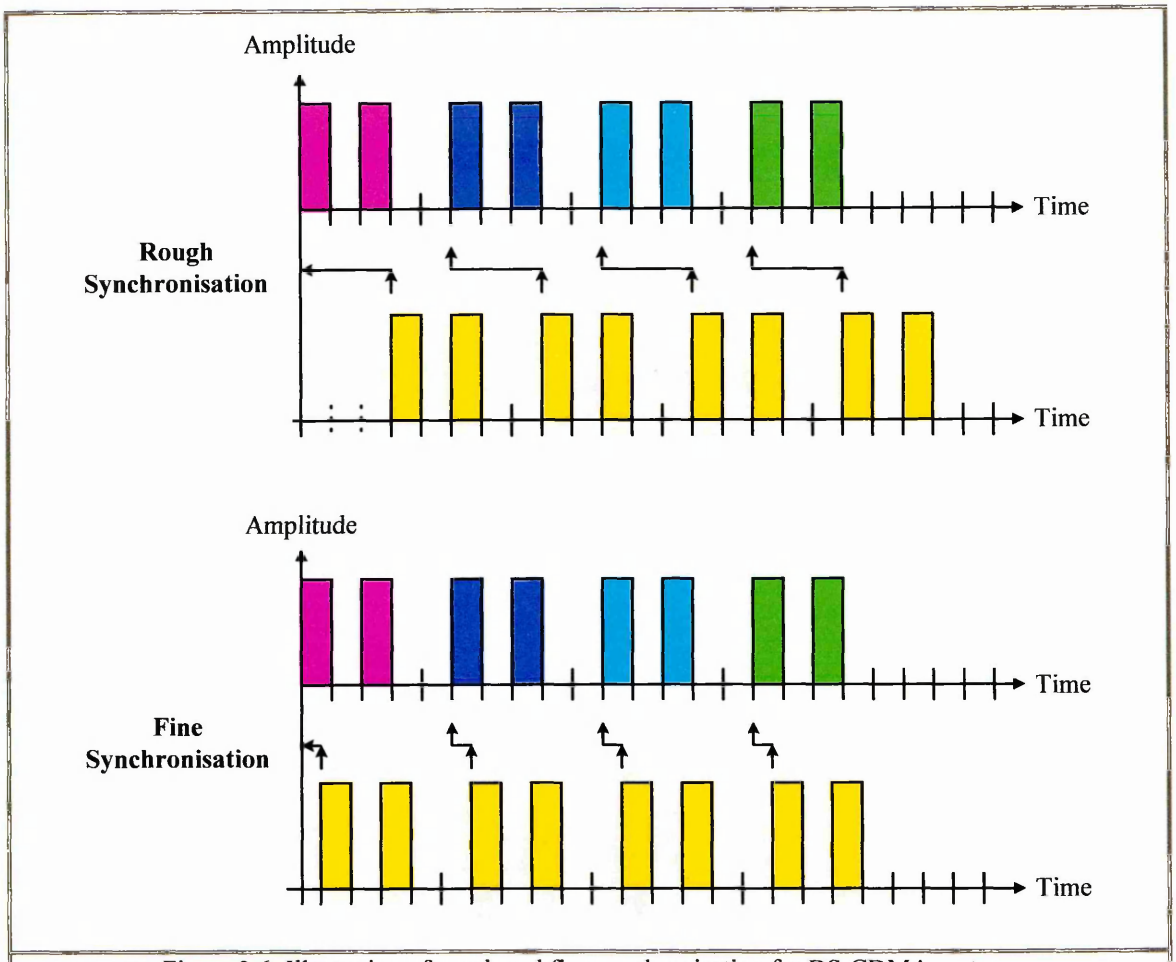

Figure 3.6: Illustration of rough and fine synchronisation for DS-CDMA system.
*The tope stream represents transmitted data and the different colours represent adjacent frames. The bottom stream is the replica sequence at receiver, which repeats at every period.

In rough synchronisation, the receiver attempts to align the in-phase auto-correlation between its spreading sequence and the transmitter's as close as possible. There are two methods. The first is called epoch synchronisation, in which the transmitter periodically sends a special synchronisation sequence. Commonly, this synchronisation sequence is unique and short and is chosen because it is easily detected by a simple correlator known as a digital matched filter. This filter consists of a shift register that clocks the received sequence by one chip at a time and compares it against the receiver's replica. The output of the matched filter produces the auto-correlation peak when the unique sequence is found in the input stream and is in-phase with the replica.

A second method of synchronisation is known as phase synchronisation. The receiver attempts to determine which of the n phases (the start of frame) the spreading sequence could be in,

where n is the spreading sequence length. A sliding correlator is employed to carry out the phase search. The sliding correlator operates by slowing down or speeding up the replica sequence at the mixer in such a way that it can search backward or forward in time to acquire the incoming sequence. This can be visualised as two wheels, with a red mark on each, rotating at different speeds on a same shaft. One of the wheels can be thought as "catching up" with the other. At one instant the red mark of the two wheels will meet together, thus representing the replica sequence that is in phase with the transmitted or incoming sequence. Momentarily, the mixer output will produce the auto-correlation peak and a local oscillator will be signalled to synchronise and lock the phase of the incoming sequence. A comprehensive discussion on phase synchronisation procedures including circuit schematic diagram can be found in [ARRL91].

A unique short spreading sequence will exhibit several repetitions periodically in a short amount of time. A digital matched filter can be constructed to signal the presence of this unique sequence, which is known as *preamble*. This is essentially a form of epoch synchronisation. Longer sequences will require more complex synchronisation methods, which is undesirable. Another method uses a sequence based on the time of the day. The receiver sets up a digital matched filter with a value slightly ahead of the current time and waits for the sequence to appear – this is related to the phase synchronisation method. The procedure may be useful for network operations in which clients can enter or leave the LAN at will [ARRL91].

3.2.5.1 preamble

A preamble signal is commonly sent by the transmitter immediately before it enters the signal-spreading mode. The preamble signal alerts the receiver to set up its synchronising procedure to acquire the spread signal. The format of the preamble is different from system to system.

In slow FH, which has hop rates of less than 100 times a second, a tone appearing on a prearranged frequency or home channel can be used. The falling edge of the tone signals the

beginning of hopping. At faster speeds, the precise instant that the tone falls may be difficult to measure accurately, and hence other preamble methods are typically employed. One such method calls for the frequency-hopping receiver to examine a specific set of channels continually. The transmitter pair would hop on these channels a prearranged number of times to allow the receiver to synchronise.

In DS (electrical system) transmissions the preamble performs three functions. First, the receiver must acquire the RF carrier frequency phase. This may be done by transmitting a run of chips with bit '0', which reveals the carrier's centre frequency to the receiver. Second, local clock synchronisation is established by transmitting a sequence of alternating ones and zeros. The receiver will detect these transitions and derive chip timing from them. Lastly, the spreading sequence is to be synchronised using the epoch synchronisation procedure. An optical system, which does not employ a carrier frequency, does not require carrier phase synchronisation and hence reduces system synchronisation component.

Once rough synchronisation is established, the receiver must track and maintain chip timing. There are several techniques to accomplish fine synchronisation. One involves a feedback loop mechanism that attempts to minimise the timing error between a transmitter and receiver pair spread-sequence at the fraction of the chip time. The feedback loop commonly consists of a differencing circuit that calculates the actual chip difference and a feedback path that adjusts the receiver spreading-sequence clock. In one technique called dithering, the spreading-sequence clock speed is continually rocked back and forth around the synchronisation point, causing the receiver to periodically move in and out of synchronisation a small amount. The point at which best synchronisation is achieved is used to resynchronise the receiver clock. Dithering can track a spreading-sequence whose timing may be changing, perhaps due to the transmitter moving, or in the case of FH, with changes in the height of the reflecting layers of ionosphere [ARRL91].

3.3 Summary

Three multiplexing schemes have been discussed. The WDMA scheme enables each communication channel to transmit information at higher data rates, but the channel capacity is limited by the available wavelength. TDMA can offer a large number of communication channels using one wavelength, however it trades off channel capacity with the reduction in system transmission rate. The CDMA technique utilises both wavelength (or frequency in RF) and time resources and provides flexibility in bandwidth and channel capacity management and allows for synchronous and asynchronous operation modes.

CDMA not requiring wavelength or time division technology alone for message separation is an added advantage, where using either WDMA or TDMA in conjunction with CDMA, can enhance channel capacity by a significant order of magnitude [Stok00]. This is illustrated in figure 3.7, where the extra three channels (4-6) were produced as a result of WCDMA-CDMA [Perrier88, Yang97, Andonovic99] joint technique, or the extra channels 7-8 produced as a result of the TDMA-CDMA [Vollmer01].

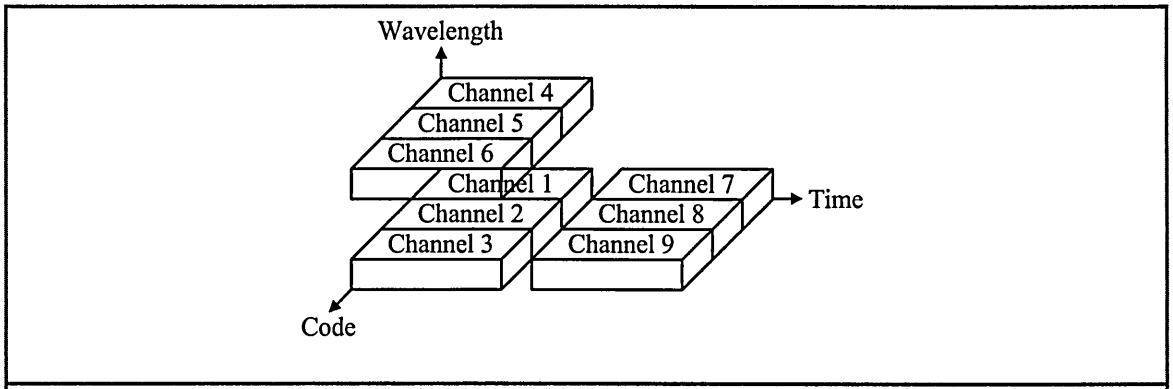

Figure 3.7: Joint multiple-access techniques.

Chapter 4

SPREADING CODES

4.1 Introduction

As discussed in the previous chapter, a DS-CDMA system requires a set of F spreading sequences to enable a number of F pairs of network clients to communicate in a common channel simultaneously. The spreading sequences play an important part in message separation as well as synchronisation. To be a good message separator, the spreading sequence must be distinct from other sequences that share the common channel. Both the auto- and cross-correlation constraints of a code set must be low in order to achieve low MAI and to aid rough synchronisation.

In an electrical DS-CDMA system, each spreading sequence of a set is usually designed to have an equal weight of '1' and '-1', and its pattern is random and different from those of the other sequences. Having equal weights, the out-of-phase auto-correlation and cross-correlation might result in zero values (as the equal number of '1' and '-1' may entirely cancel out each other), giving virtually no MAI. Numerous sets of code have been proposed such as the M-Sequence code, Gold code, Kasami code, Gordon-Mills-Welch code, No code and Walsh code [Chen99, Andonovic99]. However, none of these codes proved to be truly orthogonal where the correlation constraints are considerably high [Chen99, Tirkel96]. The only PN code that has perfect orthogonal correlation is the Walsh code, where the orthogonal correlation only occurs at zero time shifts [Lam02, Chen99].

The signature sequences for optical systems are different from those for electrical ones. The number of '1's and '0's in a sequence cannot be equal in order to achieve orthogonal correlation. This is because an optical signal only operates in the positive region. When correlation is carried out, the product-of-sum (result of correlation) between two streams of positive numbers always results in a positive value. The solution to design unipolar sequences that are distinct from each other is to have sufficiently small number of '1's and large number of '0's. This is because the correlation between a '0' and a '1' will result in zero. Recalling that only the weight, which is the number of '1's in a sequence, will only contribute to correlation magnitude. Therefore, with fewer '1's and many '0's in a sequence, the probability of a '1' from a sequence that will correspond with a '1' from another sequence will be very low as compared with the probability of a '1' will correspond with a '0'. In other words, the unique pattern of a PN sequence is determined by the randomness combination of '1' and '-1', whereas the OOC is determined by the distance between any pair of '1' in the sequence.

For OOC, the amplitude of the in-phase autocorrelation, when at a maximum, is equal to the code weight, w (the number of '1's in signature sequence). Whereas out-of-phase correlation has amplitudes range from 1 to $w-1$. A number of OOC have been proposed and are categorised to one of the following groups:

- $(n, w, \lambda_a, \lambda_c)$ OOC
- Prime Codes (PC)
- Truncated Costas (TC) Codes

Though their names are different, all of the above codes can be in general represented by the $(n, w, \lambda_a, \lambda_c)$ OOC [Marić95]. The parameter n is the sequence length, w is the code weight, and λ_a and λ_c are the auto- and cross- correlation constraints respectively [Salehi89a].

Before beginning to discuss all the three groups in detail, a standard way of matrix representation will be introduced so as to avoid any confusion that may be caused by the many

different terms introduced by different authors. This representation will be used throughout this thesis. Following this the codes are introduced and algorithms used to generate them are presented. Then a comparison of the algorithms is given in the discussion chapter and finally the summary.

4.1.1 Standard matrix representation

The matrix:

$$ {}^{'code'}_{n}CW^{F\times w}_{(i,j)} = \begin{pmatrix} cw_{1,1} & cw_{1,2} & \cdots & cw_{1,w} \\ cw_{2,1} & \ddots & & \vdots \\ \vdots & & \ddots & \vdots \\ cw_{F,1} & \cdots & \cdots & cw_{F,w} \end{pmatrix}, \tag{4.1} $$

represents a set of codeword for the '*code*' (where '*code*' is the code name) of $F \times w$ dimension. One entire row, denoted by i, is one codeword. The element in a row, denoted by j, is the location of a pulse in a sequence. For example, the codewords for the set (19,3,1,1) OOC with $F = 3$ sequences are represented as:

$$ {}^{(19,3,1,1)OOC}_{19}CW^{3\times 3}_{(i,j)} = \begin{pmatrix} 0 & 1 & 6 \\ 0 & 2 & 10 \\ 0 & 3 & 7 \end{pmatrix}. \tag{4.2} $$

The spreading sequences of (4.2) are illustrated in figure 4.1.

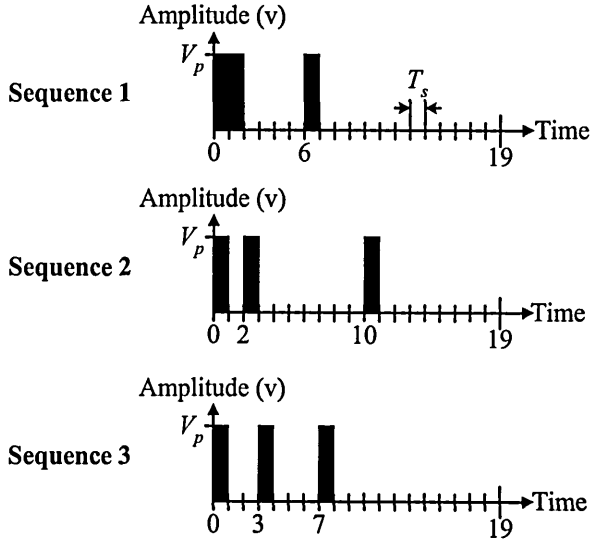

Figure 4.1: Example of $(n,3,1,1)$OOC spreading sequences.

Two other useful matrices, known as the relative-distance and the extended-relative-distance, are defined respectively as:

$$ {}^{'code'}_{n}RD^{F\times w}_{(i,j)} = \begin{cases} cw_{(i,j+1)} - cw_{(i,j)} & \text{, for } 1 \le j \le w-1 \\ n - cw_{(i,j)} & \text{, for } j = w \end{cases}, \tag{4.3} $$

and:

$$ {}^{'code'}_{n}ERD^{F\times w(w-1)}_{(I,J)} = \begin{cases} rd_{(i,j)} & \text{, for } J \le w, \text{ then } i = I \text{ and } j = J \\ \sum_{j'=J-w}^{J-w+1} rd_{(i,j)} & \text{, for } w < J \le 2w, \text{ then } i = I \text{ and } j = j'. \\ & \text{If } j' > w, \text{ then } j \text{ is forced to } j = j' \bmod_w \\ \sum_{j'=J-2w}^{J-2w+2} rd_{(i,j)} & \text{, for } 2w < J \le 3w, \text{ then } i = I \text{ and } j = j'. \\ & \text{If } j' > w, \text{ then } j \text{ is forced to } j = j' \bmod_w \\ \vdots & \\ \sum_{j'=J-(w-2)w}^{J-(w-2)w+(w-2)} rd_{(i,j)} & \text{, for } (w\text{-}2)w < J \le (w-1)w, \text{ then } i = I \text{ and } j = j'. \\ & \text{If } j' > w, \text{ then } j \text{ is forced to } j = j' \bmod_w \end{cases}. \tag{4.4} $$

Note that $cw_{(i,j)}$ is the element of the matrix ${}^{'code'}_{n}CW^{F\times w}_{(i,j)}$, where the terms '*code*', $F \times w$ and n have been omitted for the purpose of a simple representation. This is also true for $rd_{(i,j)}$, which belongs to ${}^{'code'}_{n}RD^{F\times w}_{(i,j)}$. The use of this matrix representation is helpful in reducing the number of variables used for representing each individual i^{th} codeword, relative-distance and extended-relative-distance. An example of *RD* matrix of the codeword in (4.2) is represented as:

$$ {}^{(19,3,1,1)OOC}_{19}RD^{3\times 3}_{(i,j)} = \begin{pmatrix} 1 & 5 & 13 \\ 2 & 8 & 9 \\ 3 & 4 & 12 \end{pmatrix}, \tag{4.5} $$

where the *ERD* matrix is represented as:

$$ {}^{(19,3,1,1)OOC}_{19}ERD^{3\times 6}_{(i,j)} = \begin{pmatrix} 1 & 5 & 13 & 6 & 18 & 14 \\ 2 & 8 & 9 & 10 & 17 & 11 \\ 3 & 4 & 12 & 7 & 16 & 15 \end{pmatrix}. \tag{4.6} $$

The need for the relative-distance and extended-relative-distance for code construction will become clear in the following sections.

4.2 $(n, w, \lambda_a, \lambda_c)$ Optical Orthogonal Codes

$(n, w, \lambda_a, \lambda_c)$ OOC were proposed by [Chung89]. There are a number of suggestions for constructing these codes with a different combination of the 4 parameters n, w, λ_a and λ_c [Chung89, Chung90, Azizoglu92, Yang95b, Yang95c, Ge01, Ho01, Weng01, Martirosyan02]. The magnitudes of λ_a and λ_c indicate the BER performance of the OOC, where the larger magnitudes indicates a poorer BER performance. There is no algebraic method for constructing this code; instead algorithms are used to rigorously search for a pattern for each sequence such that they are distinct from each other. Such an algorithm is known as a recursive algorithm, and is depicted in figure 4.2.

Generally, any set of codes based on this construction simply the name $(n, w, \lambda_a, \lambda_c)$ OOC. As with all recursive algorithms, if the correct number of codeword patterns cannot be obtained for a set, even where others have been obtained, the whole process will have to start again (refer to the loop directed by the red lines in figure 4.2). Some algorithms can guarantee that for certain values of parameters F, w and n, a set of valid codewords can be obtained [Chung89, Ge01]. Whereas, some algorithms cannot guarantee this and propose modified values of the parameters until a valid set of codewords is obtained [Chung89, Chung90, Martirosyan02]. This is time consuming and requires extensive computational power.

According to [Yang95c], the two correlation constraints λ_a and λ_c serve two purposes. Low λ_a enables the receiver to obtain synchronisation – to find the beginning of its message and locate the codeword boundaries. Low λ_c enables the receiver to estimate its message in the presence of interference from other clients. Thus a low cross-correlation constraint aids synchronisation in the presence of MAI and permits each receiver to "track" its message after rough synchronisation is achieved.

There were five recursive algorithms proposed by [Chung89] for constructing $(n, w, \lambda_a, \lambda_c)$ OOC of any values λ_a and λ_c. [Ge01, Martirosyan02] proposed algorithms for constructing $(n, w,1,1)$ OOC only. In [Chung90], developed algorithms for constructing $(n, w,2,2)$ OOC as well as $(n, w,1,1)$ OOC were proposed. [Yang95b, Yang95c] proposed algorithms for constructing unequal constraints for λ_a and λ_c such that $(n, w,2,1)$ OOC can be obtained. Some of these algorithms are limited to a certain value of F. All these algorithms are complex and lengthy, and will not be included in this thesis. For this, the reader is referred to the literature for more detailed information. Additional information on the Combinatorial Algorithm [Chung89] can be found in [Colbourn99]. All these are recursive algorithms and have similar structure as shown by the flow chart in figure 4.2.

Here, a new algorithm is proposed that is systematic and easy to implement as outlined in section 4.2.1. The algorithm is able to construct an optimal $(n,3,1,1)$ OOC only for any value of F and in the shortest time possible. Nevertheless, section 4.2.2 will show that a set of codewords of larger w, λ_a and λ_c can also be obtained, from a set of $(n,3,1,1)$ OOC.

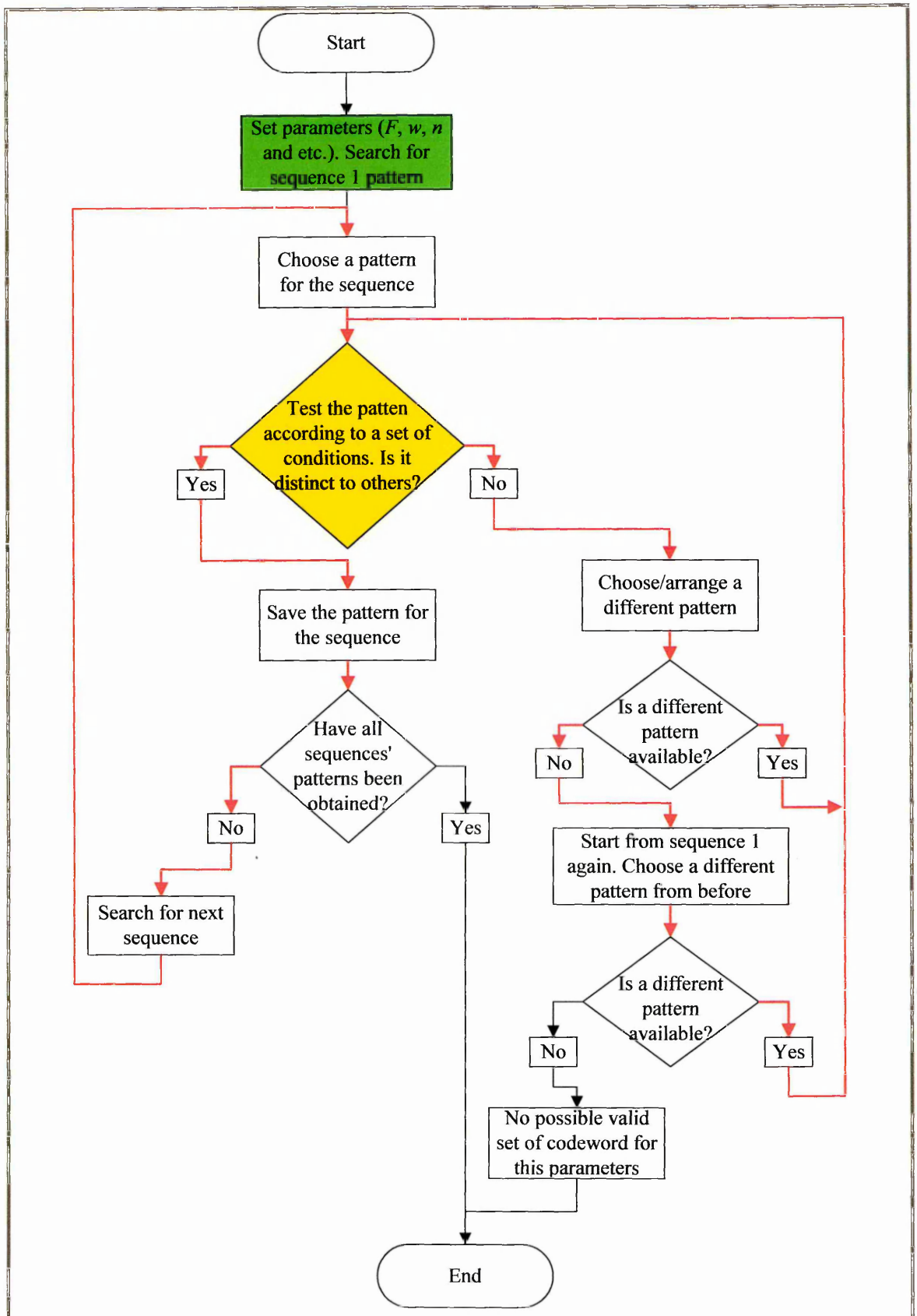

Figure 4.2: Flow chart for recursive algorithm.

4.2.1 Proposed algorithm

The main advantage of this novel algorithm is that it uses only one matrix (i.e. *ERD*) to generate a valid set of OOC codewords and utilises only half the matrix size compared with other algorithms [Yang95c] – this will be shown later in the analysis for C5. Each row represents a codeword and only one element in each row that needs to be searched for – this will be shown in the analysis for C4. This algorithm is also recursive and has a similar structure to figure 4.2, however the 'set of conditions for testing' (as highlighted in yellow) are reduced and simplified – thus the number of recursive loops is reduced. This has then led to easy implementations by computer programming and requires less computational time. To introduce the algorithm, this section will start with a definition and a number of analyses that led to the determination of the simplified conditions.

4.2.1.1 definition

The variable F for a set of $(n,w,1,1)$OOC codewords can be obtained from [Chung89]:

$$F \le \frac{n-1}{w(w-1)}. \tag{4.7}$$

If (4.7) is the upper bound such that:

$$F = \left\lfloor \frac{n-1}{w(w-1)} \right\rfloor, \tag{4.8}$$

then the generated set of codewords is known as optimal $(n,w,1,1)$OOC.

Fundamentally, a codeword set belongs to an $(n,w,1,1)$OOC if it satisfies only one condition, that is:

Condition 1 (C1). Each element belonging to the *ERD* set shall not be repeated more than once [Salehi89a]

The number of elements in *ERD* is limited to $Fw(w-1)$ [Salehi89a]. Here, additional rules/conditions for constructing $(n,3,1,1)$OOC are introduced, which are:

Condition 2 (C2). The value of each elements in *ERD* ranges from 1 to $n-1$

Condition 3 (C3). Each row of *ERD* can only have one element of value within the range 1 to F. For simplicity, this element is assigned to the first column of each row (ie. $erd_{(i,1)}$). This is also stated in the Combinatorial Methods given in [Chung89]

Condition 4 (C4). i) Since $erd_{(i,1)}$ has been assigned a value, then only $erd_{(i,2)}$ of each row in *ERD* needed to be searched for and ii) the range of $erd_{(i,2)}$ value has a minimum limit of $F+1$, but the maximum limit varies for each different row. The maximum limit is determined by the condition such that $erd_{(i,1)} + erd_{(i,2)} \leq (n+1)/2$

Condition 5 (C5). The size of *ERD* has been reduced from $F(w-1)w$ to $F((w-1)w/2+1)$. The reduced size will contain enough elements to obtain a valid set of codewords. Those discarded elements were found to be of no use and were taking up space or memory

❖ *Note that the elements of ERD, whose values represent the distance between any pair of '1' in a sequence, determine the patterns of sequences. Hence the values of all elements of ERD being different to each other will mean that the set of sequences obtained are distinct. Therefore the values of the elements are sometimes termed as the patterns.*

C1 is included to ensure that the correlation properties are always 1. C2 to C5 allow the algorithm to search for a valid set of patterns in the quickest time. Refer to figure 4.2, here C2 and C4 help by acknowledging the algorithm's 'test routine' (highlighted in yellow) to test only the values that will lead to a valid set of patterns. C3 predetermines the value of the first column of each row of *ERD* matrix before the matrix enters the 'test routine', where the matrix is

initialised in the block highlighted in green. It allows the 'test routine' to jump-start to testing possible values and avoids testing determined-impossible-values in the future. C5 reduces the *ERD* matrix size, hence requiring less computer memory and processing time.

Analysis for C2

Lets take an example of a ${}^{(19,3,1,1)OOC}_{19}CW^{3\times3}_{(i,j)}$ codeword, where $F=3$, $w=3$ and $n=19$.

For this code the *RD* and *ERD* are defined from (4.3) and (4.4), respectively as:

$$ {}^{(19,3,1,1)OOC}_{19}RD^{3\times3}_{(i,j)} = \begin{pmatrix} cw_{(1,2)}-cw_{(1,1)} & cw_{(1,3)}-cw_{(1,2)} & n-cw_{(1,3)} \\ cw_{(2,2)}-cw_{(2,1)} & cw_{(2,3)}-cw_{(2,2)} & n-cw_{(2,3)} \\ cw_{(3,2)}-cw_{(3,1)} & cw_{(3,3)}-cw_{(3,2)} & n-cw_{(3,3)} \end{pmatrix}, \tag{4.9} $$

and:

$$ {}^{(19,3,1,1)OOC}_{19}ERD^{3\times6}_{(i,j)} = \begin{pmatrix} rd_{(1,1)} & rd_{(1,2)} & rd_{(1,3)} & rd_{(1,1)}+rd_{(1,2)} & rd_{(1,2)}+rd_{(1,3)} & rd_{(1,3)}+rd_{(1,1)} \\ rd_{(2,1)} & rd_{(2,2)} & rd_{(2,3)} & rd_{(2,1)}+rd_{(2,2)} & rd_{(2,2)}+rd_{(2,3)} & rd_{(2,3)}+rd_{(2,1)} \\ rd_{(3,1)} & rd_{(3,2)} & rd_{(3,3)} & rd_{(3,1)}+rd_{(3,2)} & rd_{(3,2)}+rd_{(3,3)} & rd_{(3,3)}+rd_{(3,1)} \end{pmatrix}. \tag{4.10} $$

Taking the sum of *RD* for row 1, in (4.9), as:

$$ \varsigma = rd_{(1,1)}+rd_{(1,2)}+rd_{(1,3)}. \tag{4.11} $$

Substituting the elements $rd_{(i,j)}$ with $cw_{(i,j)}$ from (4.9) in (4.11) results in:

$$ \begin{aligned} \varsigma &= (cw_{(1,2)}-cw_{(1,1)})+(cw_{(1,3)}-cw_{(1,2)})+(n-cw_{(1,3)}) \\ &= n-cw_{(1,1)}. \end{aligned} \tag{4.12} $$

Since, $cw_{(i,1)}$ is always equal zero, then $\varsigma = n$. This is the same for all other rows.

Therefore in general, the code length can be expressed as:

$$ n = rd_{(i,1)}+rd_{(i,2)}+rd_{(i,3)}. \tag{4.13} $$

Substituting for $rd_{(i,3)}$ from (4.13) in (4.10) results in:

$$
{}^{(19,3,1,1)OOC}_{19}ERD^{3\times 6}_{(i,j)} =
\left(\begin{array}{ccc:ccc}
rd_{(1,1)} & rd_{(1,2)} & n-rd_{(1,1)}-rd_{(1,2)} & rd_{(1,1)}+rd_{(1,2)} & n-rd_{(1,1)} & n-rd_{(1,2)} \\
rd_{(2,1)} & rd_{(2,2)} & n-rd_{(2,1)}-rd_{(2,2)} & rd_{(2,1)}+rd_{(2,2)} & n-rd_{(2,1)} & n-rd_{(2,2)} \\
rd_{(3,1)} & rd_{(3,2)} & n-rd_{(3,1)}-rd_{(3,2)} & rd_{(3,1)}+rd_{(3,2)} & n-rd_{(3,1)} & n-rd_{(3,2)}
\end{array}\right). \quad (4.14)
$$

As can be seen from (4.14), the matrix can be divided into two regions. The left region contains columns 1 to 3 and the right region contains columns 4 to 6. Note that the elements on the right are reflections of the elements on the left, where an element on the right is obtained from an element on the left by deducting from n. The position of a reflected element (on the right) may not have an equal distance to the original element's (on the left) from a symmetry point (indicated by the dotted line). For $w=3$, there are six elements in a row of *ERD* and only the two corresponding elements, $erd_{(i,3)}$ and $erd_{(i,4)}$, have equal distance. The position of the elements on the right is not important, because at the final stage for constructing the codeword, only the elements on the left are required. Also, the right elements, $erd_{(i,5)}$ and $erd_{(i,6)}$, are not needed in the proposed algorithm for searching a distinct pattern. This will be discussed in further detail in the following analyses.

Since the minimum value in CW is 0, then the minimum value for *ERD* must be 1 (note, as mentioned previously no element in *ERD* can be repeated more than once, and it must be a positive integer). From (4.14), any elements of columns 1 and 2 could be at the minimum value 1, therefore the maximum value will be $n-\min\{rd_{(i,j)}\}=n-1$. Thus it was shown that the elements of *ERD* range from 1 to $n-1$.

Analysis for C3

Let row 1 of *ERD* contains two values in the range 1 to F, where $F=3$ has been chosen for this example, for $erd_{(1,1)}$ and $erd_{(1,2)}$. There are three possible combinations

for choosing the value for $erd_{(1,1)}$ and $erd_{(1,2)}$ as shown in table 4.1. The combination of values for $erd_{(1,1)}$ and $erd_{(1,2)}$ is not important. For example the row 1 from table 4.1, the combination $erd_{(1,1)}=1$ and $erd_{(1,2)}=2$ is the same as $erd_{(1,1)}=2$ and $erd_{(1,2)}=1$. This can be explained from (4.10) and (4.14). Observe that the right region of the *ERD*, which is the extended properties of *RD*, always result back to the same properties for all combination of $erd_{(i,1)}$, $erd_{(i,2)}$ and $erd_{(i,3)}$. The values in table 4.1 are tested using the lemma 4.1 below.

$erd_{(1,1)}$	$erd_{(1,2)}$
1	2
1	3
2	3

Table 4.1: Various combination values of $erd_{(1,1)}$ and $erd_{(1,2)}$.

Lemma 4.1

Assigning the first combination values for the row 1 of *ERD*, the resultant of summing $erd_{(1,1)}$ and $erd_{(1,2)}$ is 3. Then row 2, $erd_{(2,1)}$ and $erd_{(2,2)}$ must be a value higher than 3, e.g. 4 (or a higher available value). The *ERD* for this assignment is shown as:

$$ {}^{(19,3,1,1)OOC}_{19}ERD^{3\times 6}_{(i,j)} = \begin{pmatrix} 1 & 2 & 16 & 3 & 17 & 18 \\ 4 & 5 & 10 & 9 & 14 & 15 \\ rd_{(3,1)} & rd_{(3,2)} & n-rd_{(3,1)}-rd_{(3,2)} & rd_{(3,1)}+rd_{(3,2)} & n-rd_{(3,2)} & n-rd_{(3,1)} \end{pmatrix}. \quad (4.15) $$

Row 3, $erd_{(3,1)}$ and $erd_{(3,2)}$ must be a value that has not been used before between 1 and 18. It is obvious that the minimum value available is 6. Then rewriting (4.15) as:

$$ {}^{(19,3,1,1)OOC}_{19}ERD^{3\times 6}_{(i,j)} = \begin{pmatrix} 1 & 2 & 16 & 3 & 17 & 18 \\ 4 & 5 & 10 & 9 & 14 & 15 \\ 6 & 7 & 6 & 13 & 12 & 13 \end{pmatrix}. \quad (4.16) $$

From (4.16), it can be seen that row 3 has two numbers, which are 6 and 13, being repeated twice. Therefore this is not a valid arrangement for the $(19,3,1,1)\mathrm{OOC}$.

Applying lemma 4.1 to the others values in table 4.1 will also result in no valid arrangement for the $(19,3,1,1)\mathrm{OOC}$. This is due to the reflection property of the matrix at its mid point, which divides the left and the right regions. The mid point can be located by:

$$ n_{mid} = \frac{n}{2}. \quad (4.17) $$

It can be observed from (4.16) that $erd_{(i,1)}$ and $erd_{(i,2)}$ of rows 1 and 2, have values within the half minimum range (1 to $(n-1)/2$) that are less than the n_{mid}. Whereas, $erd_{(i,3)}$ of both rows is a reflection, has a value within the half maximum range ($(n+1)/2$ to $n-1$) that is larger than the n_{mid}. For this reason, the summation of $erd_{(i,1)}$ and $erd_{(i,2)}$ must result in a value that is in the minimum range, so that the value of $erd_{(i,3)}$ will be reflected in the maximum range. The value of $erd_{(i,3)}$ will certainly reflect to an identical value to $erd_{(i,1)}$ or $erd_{(i,2)}$ if the resultant of $erd_{(i,1)} + erd_{(i,2)}$ is large such that the reflection of $erd_{(i,3)}$ will result in the same minimum range as $erd_{(i,1)}$ and $erd_{(i,2)}$. This will only occur when usually the last codeword in the set is to be obtained, as was shown in Lemma 4.1.

Nevertheless, there is an exceptional case for $erd_{(i,3)}$ to reflect in the minimum range without overlapping with $erd_{(i,1)}$ or $erd_{(i,2)}$. The value of $erd_{(i,1)} + erd_{(i,2)}$ must be the number next to n_{mid} so that the reflection occurs at the other side and is also next to

n_{mid}. For example, let $erd_{(1,1)}=2$ and $erd_{(1,2)}=7$, for $n=19$ and $n_{mid}=9.5$. The result of summation will be $erd_{(1,4)}=9$ and the reflection will be $erd_{(1,3)}=10$ (where column 3 is reflected in the maximum range). On the other, let $erd_{(1,1)}=2$ and $erd_{(1,2)}=8$ then $erd_{(1,4)}=10$ and $erd_{(1,3)}=9$ (where column 3 is reflected in the minimum range). This condition is true for all rows except for one condition where $erd_{(1,1)}=1$ and $erd_{(1,2)}=9$. The reflection is $erd_{(1,3)}=9$ and resulted in overlapping.

It is impossible to provide a mathematical model to prove that each row of the *ERD* can only have one element with value within 1 to F in order to obtain a valid set of codewords. However, using lemma 4.1, tests for F (from 2 to 10) were carried out and it was found that all tests required the same condition as mentioned. From observation, this is also true for all values of F.

Analysis for C4

As mentioned in the analysis for C3, the *ERD* properties will never change if the values of $erd_{(1,1)}$, $erd_{(1,2)}$ and $erd_{(1,3)}$ are inter-changed. Therefore for simplicity, the first column of each row of *ERD* is assigned as $erd_{(1,1)}=F$, $erd_{(2,1)}=F-1$, ..., $erd_{(F-1,1)}=2$ and $erd_{(F,1)}=1$. Since, values from 1 to F have been assigned to $erd_{(i,1)}$ of each row, then the minimum value available for $erd_{(i,2)}$ will be $F+1$. It was shown in the analysis for C3 that $erd_{(i,1)}+erd_{(i,2)}\leq(n+1)/2$ so that $erd_{(i,3)}\geq(n-1)/2$. Therefore, according to these two conditions, each $erd_{(i,2)}$ of different rows will have a different maximum limit.

Note the values of $erd_{(i,1)}$ are assigned in the reverse order because this arrangement will lead to a valid codeword in the quickest time. According to the two conditions stated previously, for $erd_{(1,1)}$, which has the highest value, to sum with $erd_{(1,2)}$ without

exceeding the limit, then the value of $erd_{(1,2)}$ must be a small value (i.e. $F+1$). Next, choose a smallest value that is available for the $erd_{(2,2)}$, and so on, then leaving the highest value for the $erd_{(F,2)}$. This is because $erd_{(F,1)}$ has the smallest value and so adding to a higher value from $erd_{(F,2)}$ will only result in a slightly higher value – that is still meets the conditions.

Analysis for C5

Referring to (4.14), the right region is the reflection of the left region. This means that if each element in the left region is different from the other elements in the same region, then the reflection of each of the element occurring in the right region is also different from the other reflected elements. For example, if $erd_{(1,1)} \neq erd_{(I,J)} : I = \{1, F\}$ and $J = \{1,3\}$, where $I = 1$ and $J = 1$ cannot be together, and so $erd_{(1,6)} \neq erd_{(I',J')} : I' = \{1, F\}$ and $J' = \{4,6\}$, where $I' = 1$ and $J' = 6$ cannot be together – this equality is due to the reflection effect. Therefore, the elements $erd_{(i,5)}$ and $erd_{(i,6)}$ can be eliminated. However, $erd_{(i,4)}$ cannot be eliminated owing to it being obtained from $erd_{(i,1)} + erd_{(i,2)}$ and it reflects for $erd_{(i,3)}$. The *ERD* size has then been reduced to $F \times (w+1)$. As compared with [Salehi89a, Yang95c], where the actual *ERD* size is $F \times (w(w+1))$, the new *ERD* size is reduced by $2/3$ for every F.

Once a valid *ERD* is obtained, the codeword can be constructed by working backward from (4.4) and (4.3). The simplified codeword is given as:

$$ {}^{(n,3,1,1)OOC}_{n}CW^{F\times 3}_{(i,j)} = \begin{pmatrix} 0 & erd_{(F,1)} & erd_{(F,1)} + erd_{(F,2)} \\ 0 & erd_{(F-1,1)} & erd_{(F-1,1)} + erd_{(F-1,2)} \\ \vdots & \vdots & \vdots \\ 0 & erd_{(1,1)} & erd_{(1,1)} + erd_{(1,2)} \end{pmatrix}. \tag{4.18} $$

The proposed algorithm was implemented in MATLAB programming, see appendix and the CD provided. The programs contain many extra functions that help to speed up the searching process. The discussion for the functions is not included in the main text but the functions have been well commented in the program function files themselves

4.2.2 Proposed $(n,3\times \mathrm{K},\mathrm{K},\mathrm{K})$ OOC

The proposed algorithm can only construct OOC with w a multiple of 3 for $\mathrm{K}\geq 2$. The codewords are constructed from a valid set of $(n,3,1,1)$OOC. For example, a set ${}^{(74,6,2,2)}_{74}CW^{3\times 6}_{(i,j)}$ can be constructed from ${}^{(37,3,1,1)OOC}_{37}CW^{6\times 3}_{(i,j)}$, by cascading two codewords from the latter to form a new codeword for the former. The procedure is as follow, two codewords ${}^{(37,3,1,1)OOC}_{37}CW^{6\times 3}_{(1,j)}:j=[1,3]$ and ${}^{(37,3,1,1)OOC}_{37}CW^{6\times 3}_{(4,j)}:j=[1,3]$ are cascaded to form a new codeword as ${}^{(74,6,2,2)}_{74}CW^{3\times 6}_{(1,j)}:j=[1,6]$. The remaining 4 codewords of ${}^{(37,3,1,1)OOC}_{37}CW^{6\times 3}_{(i,j)}$ can be cascaded 2 by 2 to form for ${}^{(74,6,2,2)}_{74}CW^{3\times 6}_{(2,j)}:j=[1,6]$ and ${}^{(74,6,2,2)}_{74}CW^{3\times 6}_{(3,j)}:j=[1,6]$. This procedure can be best illustrated by:

$$ {}^{(74,6,2,2)OOC}_{n=2n'=74}CW^{3\times 6}_{(i,j)}=\begin{pmatrix} cw'_{(1,1)} & cw'_{(1,2)} & cw'_{(1,3)} & cw'_{(4,1)}+n' & cw'_{(4,2)}+n' & cw'_{(4,3)}+n' \\ cw'_{(2,1)} & cw'_{(2,2)} & cw'_{(2,3)} & cw'_{(5,1)}+n' & cw'_{(5,2)}+n' & cw'_{(5,3)}+n' \\ cw'_{(2,1)} & cw'_{(3,2)} & cw'_{(3,3)} & cw'_{(6,1)}+n' & cw'_{(6,2)}+n' & cw'_{(6,3)}+n' \end{pmatrix}, \quad (4.19) $$

where $cw'_{(i,j)}$ and n' belong to ${}^{(37,3,1,1)OOC}_{37}CW^{6\times 3}_{(i,j)}$. There is no particular order or combination for cascading two codeword to form a new codeword, as long as the two codewords are different. This is because each codeword of the ${}^{(n,3,1,1)OOC}_{n}CW^{F\times 3}_{(i,j)}$ set obtained from the proposed algorithm is distinct from each other. For a higher order of code weight, e.g. $w=9$, the codeword can be constructed by cascading 3 codewords from a set of ${}^{(n,3,1,1)OOC}_{n}CW^{F\times 3}_{(i,j)}$. For example, a set ${}^{(111,9,3,3)OOC}_{111}CW^{2\times 9}_{(i,j)}$ can be obtained from the source ${}^{(37,3,1,1)OOC}_{37}CW^{6\times 3}_{(i,j)}$. Similarly, the construction procedure is defined as:

$$
{}^{(111,9,3,3)OOC}_{111}CW^{2\times 9}_{(i,j)} =
\begin{pmatrix}
cw'_{(1,1)} & cw'_{(1,2)} & cw'_{(1,3)} & cw'_{(2,1)}+n' & \dots & cw'_{(2,3)}+n' & cw'_{(3,1)}+2n' & \dots & cw'_{(3,3)}+2n' \\
cw'_{(4,1)} & cw'_{(4,2)} & cw'_{(4,3)} & cw'_{(5,1)}+n' & \dots & cw'_{(5,3)}+n' & cw'_{(6,1)}+2n' & \dots & cw'_{(6,3)}+2n'
\end{pmatrix}. \qquad (4.20)
$$

Note that the length n of the new codeword is determined by the original n' and the order of cascading K. For example, the new length is obtained by:

$$
n = \mathrm{K}n'. \qquad (4.21)
$$

4.3 $(n,w,1,1)$ Strict OOC

Most of the $(n,w,1,1)$ OOC discussed above were designed for use in constant-bit-rate systems. However, when used in a variable-bit-rate (aperiodic) system, the correlation constrains will be increased by one, i.e. $\lambda'_a = 1+1$ and $\lambda'_c = 1+1$, due to the aperiodic data transmission [Petrovic90, Zhang97d, Zhang99d]. An increase in the correlation constraints is described mathematically in [See00] and graphically in [Zhang97d, Zhang99c, Zhang00a].

[Petrovic90] proposed a solution for maintaining the correlation constraints equal to 1 at all times and for all transmission conditions, e.g. whether periodic or aperiodic. It was suggested that all of the '1's (equal to the code weight) must lie within 0 and $(n-1)/2$ on the spreading sequence. This also means that any set of codewords must satisfy the following:

$$
{}^{(n,w,1,1)OOC}_{n}CW^{F\times w}_{(i,j)} \le (n-1)/2, \qquad (4.22)
$$

is a $(n,w,1,1)$SOOC.

Algorithms for constructing the $(n,w,1,1)$SOOC were given in [Zhang97d, Zhang99b, Zhang99c, Zhang00a]. These are more complex and are recursive owing to the conditions for the codeword validation being less discriminating. Only small sets of codewords were provided in the literature, however no large sets of codeword have been reported so far. This is because a recursive algorithm requires a huge amount of computation time to find a valid set (maybe up to months or years). This will be discussed in more detail in section 4.6.

From the proposed algorithm, most sets of codeword obtained are $(n,w,1,1)$SOOC or near to $(n,w,1,1)$SOOC. This can be proved by considering C4 and (4.18). In (4.18), where $cw_{(i,3)}$ has the highest value in the codeword, it is defined as:

$$cw_{(i,3)} = erd_{(i,1)} + erd_{(i,2)}. \tag{4.23}$$

According to C4:

$$erd_{(i,1)} + erd_{(i,2)} \leq \frac{n+1}{2}$$
$$rd_{(i,1)} + rd_{(i,2)} \leq \frac{n+1}{2}, \tag{4.24}$$

and so:

$$cw_{(i,3)} \leq \frac{n+1}{2}. \tag{4.25}$$

Therefore the codeword obtained is $(n,w,1,1)$SOOC if:

$$cw_{(i,3)} < \frac{n+1}{2}, \tag{4.26}$$

and not if:

$$cw_{(i,3)} = \frac{n+1}{2}. \tag{4.27}$$

For the case of (4.27), the codeword can be converted to $(n,w,1,1)$SOOC by adding 2 to sequence length n to a new length of $n' = n+2$, such that:

$$cw_{(i,3)} = \frac{n+1}{2} \Rightarrow \frac{n'-1}{2}. \tag{4.28}$$

The last term of (4.28) is the limit of the condition for $(n,w,1,1)$SOOC as defined in (4.22).

4.4 Prime Codes (PC)

The family of PC and their derivatives are defined in relative to a prime number P. Compared with $(n,w,\lambda_a,\lambda_c)$OOC, all codeword sets of PC have an algebraic way of

construction. This section describes the construction of a number of such codes that have been reviewed.

4.4.1 Prime-sequences

A Prime-Sequence (P) (PS(P)) code is the easiest of all codes to construct. The algebraic algorithm for constructing PS(P) is given in [Shaar83, Prucnal86, Yang95a, Nikolajević98a]. The number of codewords that can be generated in a set is $F = P$. The code weight is $w = P$ and the sequence length is $n = P^2$. Substituting these values into the standard form, of (4.1), the algebraic algorithm for constructing the codeword set can be summarised as:

$$ {}^{PS(P)}_{n=P^2}CW^{P\times P}_{(i,j)} = [([i-1]\times[j-1])\bmod_P] + [(j-1)\times P], \tag{4.29} $$

where $1 \le i, j \le P$. An example of PS(5) codeword is shown below:

$$ {}^{PS(5)}_{25}CW^{5\times 5}_{(i,j)} = \begin{pmatrix} 0 & 5 & 10 & 15 & 20 \\ 0 & 6 & 12 & 18 & 24 \\ 0 & 7 & 14 & 16 & 23 \\ 0 & 8 & 11 & 19 & 22 \\ 0 & 9 & 13 & 17 & 21 \end{pmatrix}. \tag{4.30} $$

PS(P) has been shown to be a very poor signature sequences for optical DS-CDMA system, as its auto- and cross- correlation constraints are $\lambda_a \le P-1$ and $\lambda_c \le 2$ [Marić93]. Therefore, other algorithms are proposed to modify or improve PS(P) in order to achieve a lower λ_a and λ_c, as described below.

4.4.2 Modified prime codes (MPR)

A codeword set constructed based on the modification from a set of PS(P) code is grouped as MPR [Zhang97b, Zhang97c]. MPR construction may involve only algebraic algorithm or both algebraic and recursive algorithms.

4.4.2.1 quasi-prime sequences

The Quasi-Prime Sequence (P) (QSP(P)) is a slight modification from PS(P). It was proposed as an alternative for optical DS-CDMA system, where a fibre-optic lattice was used as the codeword encoder and decoder [Holmes92].

The algorithm for obtaining the codewords is similar to the PS(P) and is defined as:

$$ {}^{QPS(P)}_{n=QP}CW^{P\times Q}_{(i,j)} = [([i-1]\times[(j-1)+\breve{q}])\bmod_P]+[(j-1)\times P], \tag{4.31} $$

where $0\le\breve{q}\le P-1$, $1\le i\le P$, $1\le j\le Q$ and Q is any positive integer [Holmes92]. The $\breve{q}$ is to be chosen and it represents the number of times for cyclically shifting the frames of PS(P) codeword to the left. The Q is usually chosen to be larger than P as the code weight is $w=Q$ and the sequence length is $n=QP$. Note that (4.31) is similar to (4.29), this is because they are defined in a similar way. An example of a codeword is shown below for $P=5$ and $Q=6$. The value for $\breve{q}$ is chosen such that the first and last columns of the codeword matrix have constant values, except for the 1st codeword. The value of $\breve{q}$ for each codeword, from number 1 to 5 respectively, is $\breve{q}=\{0,2,1,4,3\}$. With these values, the elements of the first and last columns are 2 and 27, respectively.

$$ {}^{QPS(5)}_{30}CW^{5\times 6}_{(i,j)} = \begin{pmatrix} 0 & 5 & 10 & 15 & 20 & 25 \\ 2 & 8 & 14 & 15 & 21 & 27 \\ 2 & 9 & 11 & 18 & 20 & 27 \\ 2 & 5 & 13 & 16 & 24 & 27 \\ 2 & 6 & 10 & 19 & 23 & 27 \end{pmatrix}. \tag{4.32} $$

4.4.2.2 $2^{\breve{n}}$ prime-sequences

$2^{\breve{n}}$ Prime-Sequence (P) ($2^{\breve{n}}$PS(P)) codes were proposed by [Kwong94a, Kwong94b, Kwong96]. In [Kwong94a, Kwong94b, Zhang98a, Zhang99a], $2^{\breve{n}}$ is referred to as 2^n, but because the variable n has been used as the sequence length, it is renamed here as $2^{\breve{n}}$. $2^{\breve{n}}$PS(P) is a modified version of PS(P) where the code weight and number of codewords are reduced. The new code weight is $w=2^{\breve{n}}$, where $2^{\breve{n}}<P$. The algorithm for the modification is recursive.

The ${}^{PS(P)}_{P^2}RD^{F\times w}_{(i,j)}$ from a ${}^{PS(P)}_{P^2}CW^{F\times w}_{(i,j)}$ has to be tested against a condition before it can be modified, and the condition is defined as [Kwong94a]:

$$rd_{(i,x\oplus(2^{Z-1}-1)\oplus m)} = rd_{(i,y\oplus(2^{Z-1}-1)\oplus m)}, \tag{4.33}$$

where x, y, Z and m are integers such that $x \neq y$, $0 \le x, y \le 2^{\tilde{n}} - 2$, $1 \le Z \le \tilde{n} - 1$, and $m \in [0, 2^{\tilde{n}} - 1]$. The symbol $\oplus$ represents modulo $2^{\tilde{n}}$ addition. The variables x and y must be divisible by $2^{\tilde{n}}$. The $rd_{(i,j)}$ in (4.33) correspond to ${}^{PS(P)}_{P^2}RD^{F\times w}_{(i,j)}$.

When (4.33) is true for x and y, where both variables are divisible by $2^{\tilde{n}}$, then the condition is to be tested on each row of ${}^{PS(P)}_{P^2}RD^{F\times w}_{(i,j)}$. Elements in each row that satisfy the condition will remain unchanged otherwise they are discarded. If there is no element in a row that satisfies the condition, then the entire row is discarded. Once all elements in ${}^{PS(P)}_{P^2}RD^{F\times w}_{(i,j)}$ have been tested and necessary modifications have been made, then the new set of codewords is obtained by working backward using (4.3). Since the code weight has been reduced, the sequence length can also be reduced, provided that the properties of the new set of codewords, where $\lambda_a \le P-1$ and $\lambda_c = 2$, remain unchanged [Kwong96]. Sometimes there are rows of ${}^{PS(P)}_{P^2}RD^{F\times w}_{(i,j)}$ being discarded and this resulted in a reduced number of codewords (i.e. $F < P$). A good tutorial for obtaining a $2^{\tilde{n}}$ PS(P) from a PS(P) is shown in [Kwong96].

The advantages of reducing the code weight and codewords are a reduction in the probability of occurrence of λ_a and λ_c, and thus the MAI, resulting in improved BER performance. Additionally, the $2^{\tilde{n}}$ PS(P) codeword has a symmetric pulse distribution that can be encoded using a tuneable prime encoder and decoded using a $2^{\tilde{n}}$ decoder [Kwong96, Zhang97a, Zhang00b].

4.4.2.3 extended prime-sequences

As the name implies, Extended Prime-Sequence (P) (EPS(P)) codewords can be obtained by extending the codeword from PS(P). The extension is carried out by adding a $P-1$ distance between two adjacent '1's in a codeword [Zhang98b], which can be defined as:

$$\underset{n=P(2P-1)}{\overset{EPS(P)}{}}CW_{(i,j)}^{P\times P}=[([i-1]\times[j-1])\bmod_P]+[(j-1)\times(2P-1)], \tag{4.34}$$

where $1\le i,j\le P$.

In this codeword, $\lambda_a\le P-1$ and λ_c is reduced from 2 to 1, as compared with PS(P). Lower values of λ_c mean a reduced MAI and hence improved BER performance. However, a longer n results in a reduced data rate.

4.4.2.4 $2^{\tilde{n}}$ extended prime-sequences

A $2^{\tilde{n}}$ PS(P) code is interesting for system design as it has symmetric pulse distribution for fast encoder and decoder configuration [Zhang98b]. Nevertheless, the correlation properties λ_a and λ_c remain the same as the PS(P). Therefore λ_c of $2^{\tilde{n}}$ PS(P) can be reduced to 1 by extending the distance between two adjacent '1's of a codeword in a similar way to EPS(P). Thus this codeword is known as $2^{\tilde{n}}$ Extended Prime-Sequence (P) ($2^{\tilde{n}}$ EPS(P)).

The algorithm introduced in [Zhang98b] can be implemented by adding $P-1$ to each relative-distance of the $2^{\tilde{n}}$ PS(P) as shown:

$$\underset{n\le P(2P-1)}{\overset{2^{\tilde{n}}EPS(P)}{}}RD_{(i,j)}^{F\times w}=\underset{n\le P^2}{\overset{2^{\tilde{n}}PS(P)}{}}RD_{(i,j)}^{F\times w}+(P-1). \tag{4.35}$$

The codeword is then obtained by working backwards using (4.3).

4.5 Other OOC

There are many others OOC that have been proposed, two such codes are the Quadratic Congruence (QC) code [Marić93] and the Truncated Costas (TC) code [Marić95]. They are

similar to any of the code above where QC code can be categorised as $(n,w,2,4)$OOC and TC code as $(n,w,1,1)$OOC. Both codes can be constructed algebraically. QC code was proposed to improve from PS(P) in which λ_a has been reduced from $P-1$ to 2, in order to assist DS-CDMA system tracking and synchronisation. However, λ_c has been increased to 4 and this subsequently increases the effect of MAI. The position of the '1's in QC code is based on quadratic placement.

TC code construction is based on the Welch-Costas array. Unlike other recursive algorithms, TC code algebraic construction can generate a large set of $(n,w,1,1)$OOC easily. Nevertheless, there is a drawback where the code obtained is not optimal and that the sequence length n is the longest compared with others. For DS-CDMA modulation, the variable n determines the bandwidth requirement and system throughput, where n is made preferably small to increase throughput and fit within bandwidth limitations. This will be discussed in further detail in the next chapter.

4.6 Discussions

Apart from TC codes, all others $(n,w,1,1)$OOC require recursive algorithm for code construction. All recursive algorithms consume large amount of computational time. Although some algorithms have refined conditions, only small sets of codes can be generated, large sets of codes are difficult to obtain. This cannot be proved using other algorithms, as computer programs for the algorithms can be written in many ways. However, the refined (proposed) algorithm can be used to show in principal why a recursive algorithm is time consuming. In the proposed algorithm for constructing $(n,3,1,1)$OOC, only one matrix is required, which is the ERD, with reduced size for code construction (as indicated by C5). For codeword validation, only three conditions needed to be satisfied, which are indicated by C1, C2 and C4. C1 is the primary test for a valid codeword; C2 and C4 are end limits for searching for available patterns. C3 initialises ERD to avoid known invalid arrangements to be carried out in the searching

process, thus reducing searching time. Compared with the Combinatorial Methods in [Chung89], which has four groups of conditions and each group has 6 conditions.

In the ERD matrix, only the element $erd_{(i,2)}$ needs to be searched. The searching procedure starts from the top row to the bottom row. Since C1 defines that no element in ERD can be repeated twice, then each $erd_{(i,2)}$ for each different rows has a different number of arrangements due to the different number of available values (patterns). This phenomenon can be seen from the following example.

Let $F=5$ and the code weight $w=3$, the ERD is initialised as:

$$ {}^{(31,3,1,1)OOC}_{31}ERD^{5\times 4}_{(i,j)} = \begin{pmatrix} 5 & 0 & 0 & 0 \\ 4 & 0 & 0 & 0 \\ 3 & 0 & 0 & 0 \\ 2 & 0 & 0 & 0 \\ 1 & 0 & 0 & 0 \end{pmatrix}. \tag{4.36} $$

Elements $erd_{(i,3)}$ and $erd_{(i,4)}$ are obtained using (4.14) when a value for $erd_{(i,2)}$ is chosen. Starting with $erd_{(1,2)}$, the minimum and maximum numbers available for arrangement are ranging from $F+1=6$ and $(n+1)/2-F=11$ respectively, and there are 6 possible numbers for arrangement. Once a number has been chosen for $erd_{(1,2)}$, obtain a value for $erd_{(1,3)}$ and $erd_{(1,4)}$. Then choose $erd_{(2,2)}$. The minimum and maximum ranges are $F+1=6$ and $(n+1)/2-(F-1)=12$. Since row 1 has been arranged, the available numbers within the range for row 2 becomes $7-2=5$. The deduction by 2 is due to a number in the range been chosen by $erd_{(1,2)}$ and a number been reflected by $erd_{(1,3)}$ (which is itself the reflection of $erd_{(1,4)}$), these two numbers cannot be chosen again by $erd_{(2,2)}$ or reflected by $erd_{(2,3)}$. As this procedure will carry on arranging for the other rows, the possible arrangements for each row can be summarised in table 4.2.

No.	$\begin{pmatrix}\text{End}\\ \text{limit}\end{pmatrix}-\begin{pmatrix}\text{Min.}\\ \text{number}\end{pmatrix}-\left(erd_{(i,1)}\right)$	Total numbers	$\begin{pmatrix}\text{Total}\\ \text{numbers}\end{pmatrix}-\begin{pmatrix}\text{Chosen}\\ \text{numbers}\end{pmatrix}$	Available numbers or Possible arrangements
1.	$(3F+1)-(F)-(F)$	$=F+1=6$	$(F+1)-(2\times 0)$	$=F+1=6$
2.	$(3F+1)-(F)-(F-1)$	$=F+2=7$	$(F+2)-(2\times 1)$	$=F=5$
3.	$(3F+1)-(F)-(F-2)$	$=F+3=8$	$(F+3)-(2\times 2)$	$=F-1=4$
4.	$(3F+1)-(F)-(F-3)$	$=F+4=9$	$(F+4)-(2\times 3)$	$=F-2=3$
5.	$(3F+1)-(F)-(F-4)=\cdots$ $\cdots(3F+1)-(F)-(F-(F-1))$	$=F+5=10$	$(F+5)-(2\times 4)=\cdots$ $\cdots(F+5)-(2\times(F-1))$	$=F-3=2$

Table 4.2: Possible arrangements in every row of ERD for $F=5$.

Thus the total possible arrangement or recursive loops that the proposed recursive algorithm can carry out, whilst searching for valid patterns for ${}^{(31,3,1,1)OOC}_{31}CW^{5\times 3}_{(i,j)}$, is the total product of all possible arrangements for ${}^{(31,3,1,1)OOC}_{31}ERD^{5\times 4}_{(i,j)}$, which is $6!=720$. Nevertheless, a valid codeword arrangement lies within the total 720 arrangements, which means that a valid codeword will be found before 720 loops have been completed.

Note the last row of table 4.2, which is also the last row of ERD, the equations for obtaining the 'Total numbers' and 'Available numbers' are the same for all F, and the 'Available numbers' always equals 2. This can be proved by solving both equations, resulting in:

$$(3F+1)-(F)-(F-(F-1))-(2\times(F-1))=2. \tag{4.37}$$

Observe from the grey column, the total possible arrangements can be generalised as:

$$Total_{Arr}=\frac{(F+1)!}{1!}=(F+1)!. \tag{4.38}$$

In a computer program, a subroutine is usually used to carry out a recursive loop. A subroutine may contain many program lines, denotes by a, and one program line may be compiled into a large number of machine codes, denotes these as b. Assuming that a machine code only requires 1 cycle of the computer time to carry out the operation, the total computer time (estimated) required to evaluate $Total_{Arr}$ can be expressed as:

$$Total_{Com} = \frac{ab \cdot (F+1)!}{c_{Com}}, \tag{4.39}$$

where c_{Com} is the computer clock frequency in Hz.

The time taken to execute a recursive algorithm, is determined by the product of a and b. This differs from one programmer to another due to the efficiency or size of the program code. Therefore it is difficult to evaluate the actual computational time. Nevertheless, the efficiency of recursive algorithm can still be evaluated by letting a and b remain as variables, and $c_{Com} = 1.5\,\text{GHz}$ (the clock of the computer used for obtaining the results in table 4.3). The theoretical results for various F obtained from (4.39) are shown in table 4.3, and the practical results obtained from written programs listed in the appendix are also included for comparison.

As can be seen from table 4.3, the theoretical results show that the times required to try all the possible arrangements are immense for large values of F. Though the program size (the product of a and b) can be kept small by efficient programming skill, the total numbers of arrangement is still large. From the programs written as part of this work, the times obtained do not increase linearly with the value of F. As discussed before, a valid codeword pattern lies within the total possible arrangement. The proposed algorithm can obtain the codeword with small amount of time for some large F as the algorithm has the conditions for code construction is well refined.

F	Theory	Practical	F	Theory	Practical
2	$ab \times 4 \times 10^{-9}$ sec	< 1 sec	⋮	⋮	⋮
3	$ab \times 1.6 \times 10^{-8}$ sec	< 1 sec	37	$ab \times 1.11 \times 10^{28}$ years	≅ 9 hours 32 min
4	$ab \times 8 \times 10^{-8}$ sec	< 1 sec	38	$ab \times 4.33 \times 10^{29}$ years	≅ 1 sec
5	$ab \times 4.8 \times 10^{-7}$ sec	< 1 sec	39	$ab \times 1.73 \times 10^{31}$ years	≅ 3 sec
6	$ab \times 3.36 \times 10^{-6}$ sec	< 1 sec	40	$ab \times 7.1 \times 10^{32}$ years	≅ 3 days 18 hours
7	$ab \times 2.69 \times 10^{-5}$ sec	≅ 1 sec	41	$ab \times 2.98 \times 10^{34}$ years	≅ 6 min 7 sec
8	$ab \times 2.42 \times 10^{-4}$ sec	≅ 1 sec	42	$ab \times 1.28 \times 10^{36}$ years	≅ 53 min
9	$ab \times 2.42 \times 10^{-3}$ sec	≅ 1 sec	43	$ab \times 5.64 \times 10^{37}$ years	≅ 2 sec
10	$ab \times 2.66 \times 10^{-2}$ sec	≅ 1 sec	44	$ab \times 2.54 \times 10^{39}$ years	≅ 32 min
11	$ab \times 3.19 \times 10^{-1}$ sec	≅ 1 sec	⋮	⋮	⋮
12	$ab \times 4.15$ sec	≅ 1 sec	67	$ab \times 5.26 \times 10^{79}$ years	> 4 weeks. Therefore, program was intentionally terminated.
13	$ab \times 58$ sec	≅ 1 sec	68	$ab \times 3.63 \times 10^{81}$ years	≅ 3 sec
14	$ab \times$ 14 mins 32 sec	≅ 1 sec	69	$ab \times 2.54 \times 10^{83}$ years	≅ 5 hours 28 min
15	$ab \times$ 3 hours 52 mins 29 sec	≅ 1 sec	70	$ab \times 1.8 \times 10^{85}$ years	> 4 weeks. Therefore, program was intentionally terminated.
16	$ab \times$ 2 days 18 hours	≅ 1 sec	71	$ab \times 1.3 \times 10^{87}$ years	≅ 8 min 16 sec
17	$ab \times$ 1 months 3 weeks	≅ 1 sec	72	$ab \times 9.48 \times 10^{88}$ years	≅ 20 hours 26 min
18	$ab \times$ 2 years 6 months	≅ 1 sec	73	$ab \times 7.02 \times 10^{90}$ years	≅ 25 sec
19	$ab \times$ 51 years 7 months	≅ 1 sec	74	$ab \times 5.26 \times 10^{92}$ years	≅ 21 sec
20	$ab \times 1.08 \times 10^{3}$ years	≅ 1 sec	75	$ab \times 4 \times 10^{94}$ years	≅ 29 min 13 sec

Table 4.3: Comparison between theoretical and practical results of computational time require to obtain for valid sets of codewords using proposed recursive algorithm.
*Numbers were rounded up to the nearest integer.

To date, it is found that the largest set of codewords of $F = 53$ and $w = 4$ was reported so far [Ge01]. The largest set of codeword obtained from the proposed algorithm for $F = 75$ and $w = 3$ is given below:

$$
{}^{(451,3,1,1)SOOC}_{451}CW^{75\times 3}_{(i,j)} = \begin{pmatrix} 0 & 75 & 151 \\ 0 & 74 & 152 \\ 0 & 73 & 150 \\ 0 & 72 & 153 \\ 0 & 71 & 154 \\ 0 & 70 & 149 \\ 0 & 69 & 155 \\ 0 & 68 & 148 \\ 0 & 67 & 156 \\ 0 & 66 & 161 \\ 0 & 65 & 147 \\ 0 & 64 & 157 \\ 0 & 63 & 159 \\ 0 & 62 & 146 \\ 0 & 61 & 165 \\ 0 & 60 & 145 \\ 0 & 59 & 158 \\ 0 & 58 & 160 \\ 0 & 57 & 144 \\ 0 & 56 & 169 \\ \vdots & \vdots & \vdots \end{pmatrix} \begin{pmatrix} \vdots & \vdots & \vdots \\ 0 & 55 & 143 \\ 0 & 54 & 162 \\ 0 & 53 & 163 \\ 0 & 52 & 175 \\ 0 & 51 & 141 \\ 0 & 50 & 142 \\ 0 & 49 & 140 \\ 0 & 48 & 164 \\ 0 & 47 & 179 \\ 0 & 46 & 166 \\ 0 & 45 & 139 \\ 0 & 44 & 168 \\ 0 & 43 & 210 \\ 0 & 42 & 170 \\ 0 & 41 & 138 \\ 0 & 40 & 171 \\ 0 & 39 & 137 \\ 0 & 38 & 211 \\ 0 & 37 & 172 \\ \vdots & \vdots & \vdots \end{pmatrix} \begin{pmatrix} \vdots & \vdots & \vdots \\ 0 & 36 & 136 \\ 0 & 35 & 209 \\ 0 & 34 & 212 \\ 0 & 33 & 214 \\ 0 & 32 & 133 \\ 0 & 31 & 134 \\ 0 & 30 & 206 \\ 0 & 29 & 213 \\ 0 & 28 & 205 \\ 0 & 27 & 207 \\ 0 & 26 & 208 \\ 0 & 25 & 130 \\ 0 & 24 & 215 \\ 0 & 23 & 129 \\ 0 & 22 & 217 \\ 0 & 21 & 218 \\ 0 & 20 & 221 \\ 0 & 19 & 222 \\ 0 & 18 & 220 \\ \vdots & \vdots & \vdots \end{pmatrix} \begin{pmatrix} \vdots & \vdots & \vdots \\ 0 & 17 & 126 \\ 0 & 16 & 127 \\ 0 & 15 & 219 \\ 0 & 14 & 121 \\ 0 & 13 & 125 \\ 0 & 12 & 198 \\ 0 & 11 & 194 \\ 0 & 10 & 226 \\ 0 & 9 & 199 \\ 0 & 8 & 200 \\ 0 & 7 & 196 \\ 0 & 6 & 193 \\ 0 & 5 & 119 \\ 0 & 4 & 122 \\ 0 & 3 & 188 \\ 0 & 2 & 117 \\ 0 & 1 & 224 \end{pmatrix}. \quad (4.40)
$$

4.7 Summary

One can see that a recursive algorithm is complex (as a result of the number of conditions for codeword validation) and time consuming. Due to the complexity of the algorithm it was also time consuming to develop a computer program. Although the proposed algorithm has been refined to search for only one variable ($erd_{(i,2)}$), large sets of codewords are still difficult to obtain. As compared with other algorithms where more than one variable is required, the computer programming will become more complicated and computational time is intolerable.

Another option for obtaining large sets of codeword is to employ PS(P), as the codeword can be easily obtained algebraically. However this code was found to be a $(P^2, P, P-1, 2)$OOC where the auto-correlation constraint is very high affecting synchronisation performance. The high cross-correlation constraint also reduces system performance in terms of the BER. This has then

led to MPR being proposed to obtain codewords with lower λ_a and λ_c. Alternatively, a large set of $(n, w, 1, 1)$OOC can be easily obtained employing the TC code, but the drawback is that the sequence length n is greatly increased.

Chapter 5

DIRECT-SEQUENCE CDMA SYSTEMS

5.1 Introduction

In optical DS-CDMA system, the encoding and decoding of signature sequence can be carried out in optical or in electrical domain. In all-optical DS-CDMA systems [Oksa97], the output of the modulator is first converted to an optical signal using intensity-modulation (IM) of a light source before being encoded by the CDMA encoder, see figure 5.1. At the receiver the output of CDMA decoder is converted to an electrical signal using a direct-detection (DD), followed by demodulation to recover the original data. In conventional optical DS-CDMA systems, encoding and decoding of the signal is performed in the electrical domain, before the IM and after the DD at the transmitter and receiver respectively.

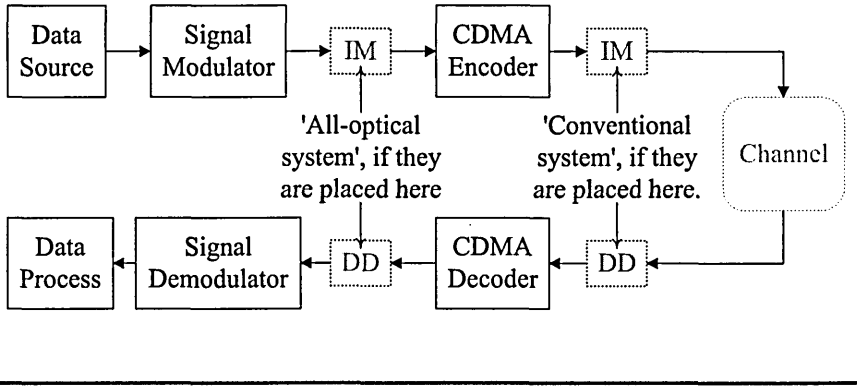

Figure 5.1: Optical DS-CDMA system block diagram.

The all-optical DS-CDMA system is normally classified as a non-coherent system, where the signature encoding is performed by an optical waveguide structure [Oksa97, Hui85]. However, in wireless diffuse systems, signature encoding and decoding can only be implemented in the

electrical domain. Hence only the conventional DS-CDMA encoding and decoding techniques will be considered in the following.

This chapter will discuss the implementation of optical wireless DS-CDMA systems employing two devices, which are the multiplier and tap-delay structure, which can both perform encoding and decoding. In section 5.2, the transmitter configurations based on these devices will be discussed. Section 5.3 will discuss the multiple-access optical wireless diffuse channel characteristics. The receiver configurations employing both the devices will be presented in section 5.4. Section 5.5 will discuss the synchronisation methods. The comparison of multiplier and tap-delay structure for CDMA decoding is carried out in section 5.6. A description of DS-CDMA systems employing various modulation techniques such as OOK-CDMA, PPM-CDMA and *h*PPM-CDMA are presented in sections 5.7, 5.8 and 5.9, respectively. Finally, the summary is presented in section 5.10. The set of signature sequences that will be used in the following examples is only for two users that can be obtained from the following set of codewords:

$$ {}^{(5,2,1,1)OOC}_{5}CW^{2\times 2}_{(i,j)} = \begin{pmatrix} 0 & 1 \\ 0 & 2 \end{pmatrix}. \tag{5.1} $$

5.2 Transmitter

There are two devices that can be used for encoding signature sequences and they will be discussed individually in the following sub-sections.

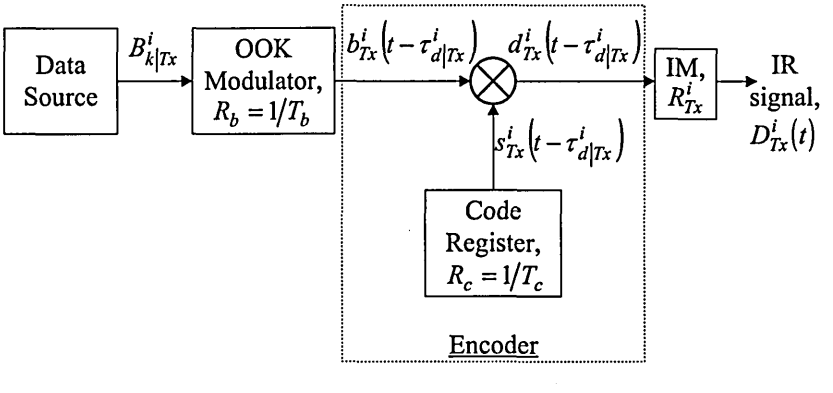

Figure 5.2: Transmitter block diagram of optical wireless DS-CDMA employing multiplier as encoder.

5.2.1 Encoder employing multiplier

A block diagram of a transmitter encoder employing a multiplier is shown in figure 5.2. The information bits $B^i_{k|Tx} \in \{0,1\}$ from the i^{th} data source are converted to an OOK format of bit duration T_b, represented as:

$$b^i_{Tx}\left(t-\tau^i_{d|Tx}\right)=\sum_{k=0}^{\infty}V_b B^i_{k|Tx} g_b\left(t-kT_b-\tau^i_{d|Tx}\right), \tag{5.2}$$

where $\tau^i_{d|Tx}$ is the time delay of the i^{th} transmitter, $g_b(t)$ is the OOK signal of duration T_b and amplitude V_b, and k represents the k^{th} information bits. The spreading sequence is generated periodically every nT_c interval by a code register and is expressed as:

$$s^i_{Tx}\left(t-\tau^i_{d|Tx}\right)=\sum_{k=0}^{\infty}\sum_{j=1}^{w}V_s g_c\left(t-cw_{(i,j)}T_c-knT_c-\tau^i_{d|Tx}\right), \tag{5.3}$$

where $g_c(t)$ is a square pulse of duration T_c and $T_c = T_b/n$, and V_s is the signature sequence amplitude. The code register must have the same time delay $\tau^i_{d|Tx}$ as the OOK modulator in order for encoding the signature sequence correctly. The encoding process at the multiplier can be modelled as:

$$\begin{aligned} d^i_{Tx}\left(t-\tau^i_{d|Tx}\right) &= b^i_{Tx}\left(t-\tau^i_{d|Tx}\right)\times s^i_{Tx}\left(t-\tau^i_{d|Tx}\right) \\ &= \sum_{k=0}^{\infty}\sum_{j=1}^{w}V_d B^i_{k|Tx} g_c\left(t-cw_{(i,j)}T_c-kT_b-\tau^i_{d|Tx}\right), \end{aligned} \tag{5.4}$$

where V_d is the output amplitude of the multiplier. The process can be illustrated in the timing diagram for user-2 only as shown in figure 5.3. The encoded signal is then directly modulate the optical signal, which is modelled as:

$$D^i_{Tx}\left(t-\tau^i_{d|Tx}\right)=R^i_{Tx} d^i_{Tx}\left(t-\tau^i_{d|Tx}\right), \tag{5.5}$$

where R^i_{Tx} is the i^{th} transmitter optical source responsivity of units W/A.

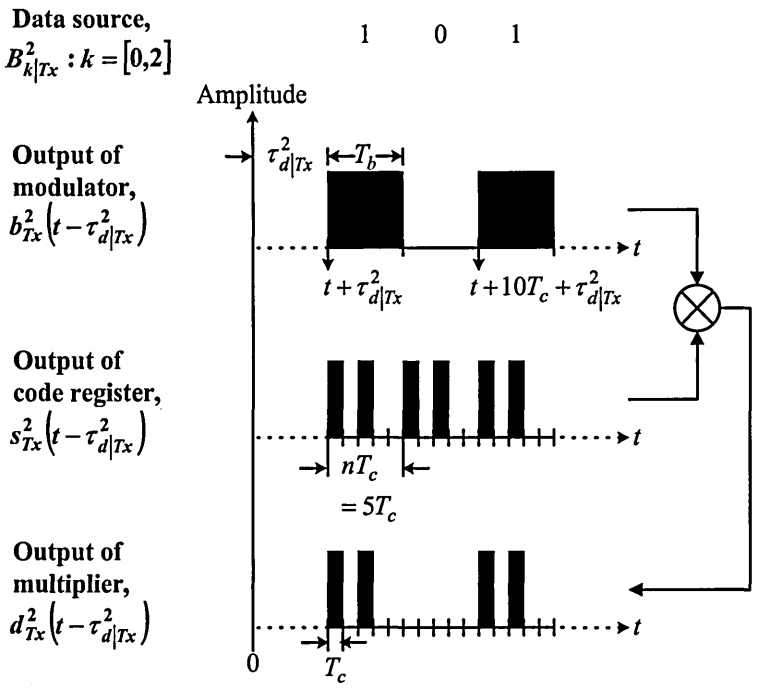

Figure 5.3: Timing waveforms showing the process of encoding in figure 5.2 for user-2 only.
*The codeword is ${}^{(5,2,1,1)OOC}_{5}CW^{2\times 2}_{(2,j)} = (0 \quad 2)$.

5.2.2 Encoder employing tap-delay structure

Tap-delay is made of charge-couple-devices (CCD) or Complementary Metal Oxide Semiconductor (CMOS), which are programmable and have been used to perform analogue convolution or matched filter function [Kapur80, ARRL91, WWW1, WWW3, WWW4]. A tap-delay structure for a CDMA encoder is shown in figure 5.4. Note that the property of OOK modulator is different to the one in figure 5.2.

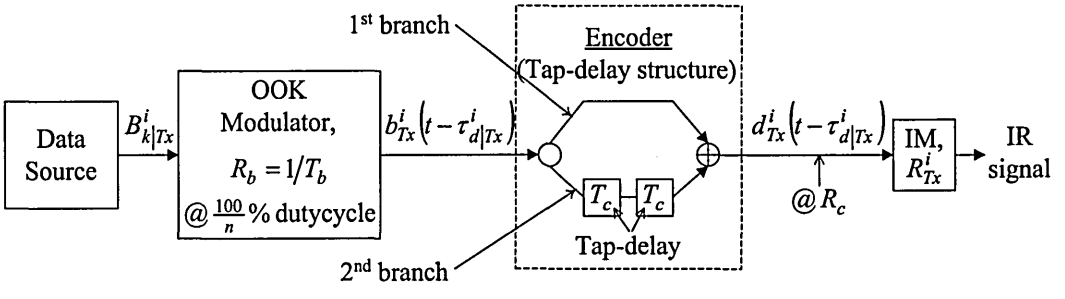

Figure 5.4: Transmitter block diagram of optical wireless DS-CDMA employing tap-delay structure as encoder.

The data from the source is converted to OOK signal format with a $\frac{100}{n}\%$ duty cycle of T_b (which is equivalent to T_c), expressed as:

$$b_{Tx}^{i}\left(t-\tau_{d|Tx}^{i}\right)=\sum_{k=0}^{\infty}V_b B_{k|Tx}^{i} g_c\left(t-kT_b-\tau_{d|Tx}^{i}\right). \tag{5.6}$$

The encoder is composed of a structure of parallel tap-delay, where each branch's delay value is determined by the codeword of the signature sequence, see figures 5.4 and 5.5. For the codeword of ${}^{(5,2,1,1)OOC}_{5}CW_{(2,j)}^{2\times 2}=\begin{pmatrix}0 & 2\end{pmatrix}$, the first and second elements' values of 0 and 2 correspond to the zero delay of the top branch and $2T_c$ delays of the bottom branch, respectively. The OOK signals duplicated and being delayed at the end of each branch are then combined to form the encoded signal (signature sequence) at the output of the tap-delay structure, which can be represented as:

$$d_{Tx}^{i}\left(t-\tau_{d|Tx}^{i}\right)=\sum_{k=0}^{\infty}\sum_{j=1}^{w}V_d B_{k|Tx}^{i} g_c\left(t-cw_{(i,j)}T_c-kT_b-\tau_{d|Tx}^{i}\right). \tag{5.7}$$

Then the encoded signal in (5.7) is used to intensity modulate the optical signal, which can be modelled using (5.5).

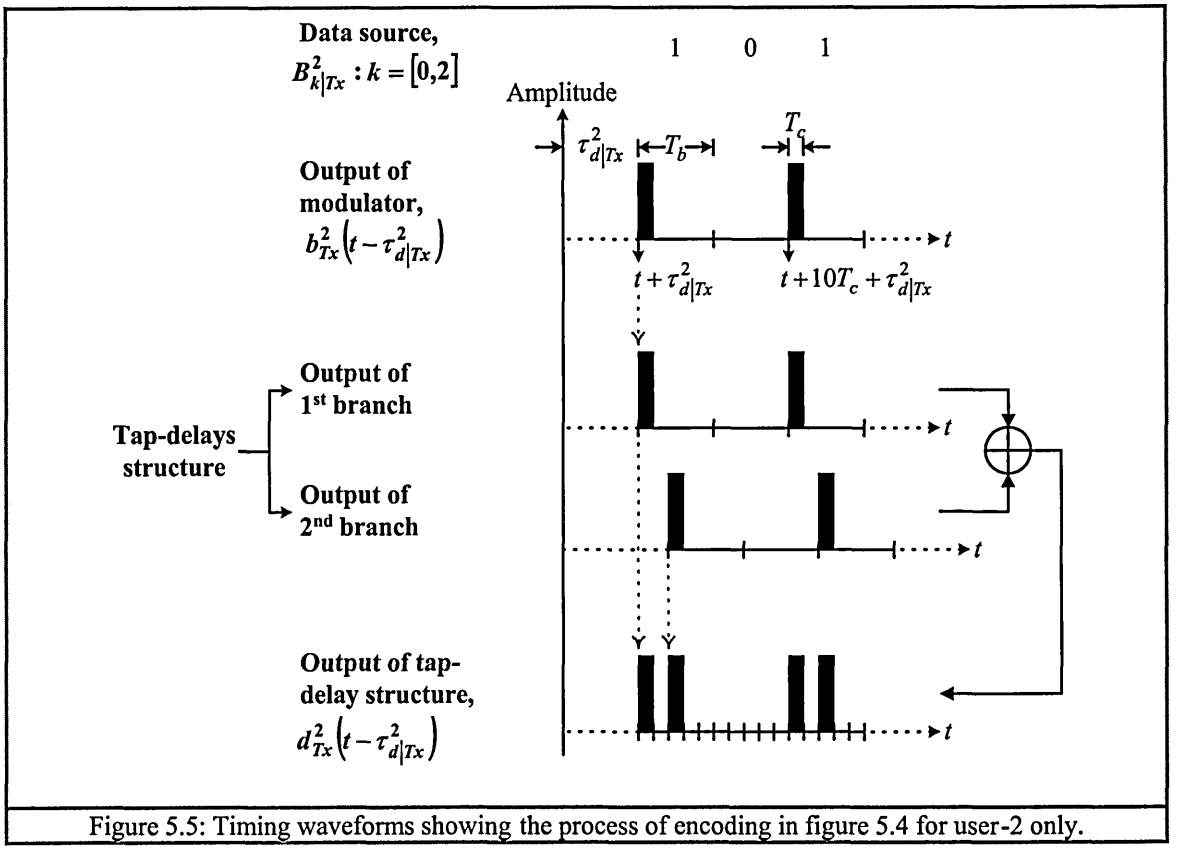

Figure 5.5: Timing waveforms showing the process of encoding in figure 5.4 for user-2 only.

For such a tap-delay encoder no synchronisation is required with the OOK modulator but precise tuning of the tap's delay is essential. Note that the output of both encoders (figures 5.3 and 5.5) are the same as can be seen from (5.4) and (5.7).

5.3 Channel Characteristics

The effective impulse response of an optical wireless diffuse channel can be modelled as [Carruthers96a, Carruthers97]:

$$h^{I|i}(t) = G_{OC}^{I|i} \frac{h_c(t, a_h)}{\int_{-\infty}^{\infty} h_c(t, a_h) dt}, \tag{5.8}$$

where a_h (determines the value of D_{RMS}) and the optical gain $G_{OC}^{I|i}$ are determined by the locations and orientations of the I^{th} transmitter and the i^{th} receiver within a room. The notation $h^{I|i}(t)$ denotes the effective channel impulse response of the signal from the I^{th} transmitter to the i^{th} receiver. In DS-CDMA systems where transmitter-receiver pairs have different locations

and orientations, a diffuse wireless channel can be modelled as a base-band linear and multiple-access system as shown in figure 5.6.

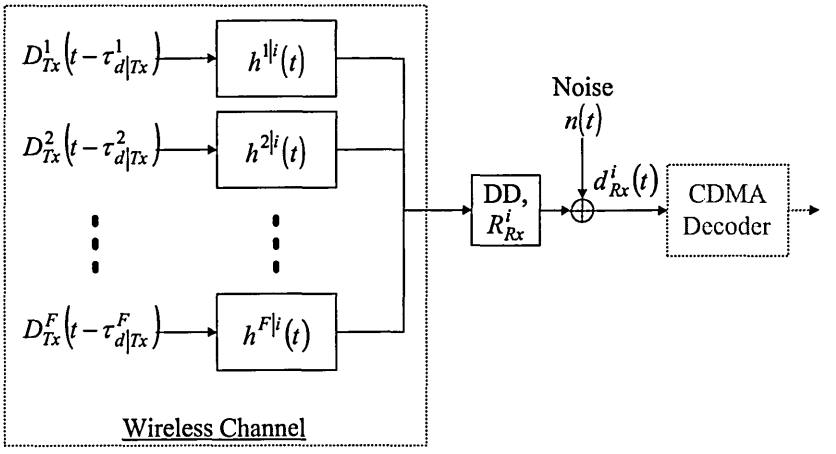

Figure 5.6: Diffuse optical wireless DS-CDMA system link channel model.

The output of the model can be expressed as:

$$d_{Rx}^{i}(t) = R_{Rx}^{i} \sum_{I=1}^{F} D_{Tx}^{I}\left(t-\tau_{d|Tx}^{I}\right) \otimes h^{I|i}(t) + n(t), \tag{5.9}$$

where R_{Rx}^{i} is the individual receiver photodiode responsivity.

5.4 Receiver

As with the transmitter, the multiplier and tap-delay structure are also used for decoding. The former is usually known as correlator whereas the latter is known as matched filter (MF).

5.4.1 Decoder employing multiplier – Correlator

The receiver block diagram is shown in figure 5.7, where the received optical signal is first converted to an electrical signal by means of a DD technique. The correlator is composed of a multiplier, a code register and the modules labelled A, B and C to correlate the signal intended for the receiver.

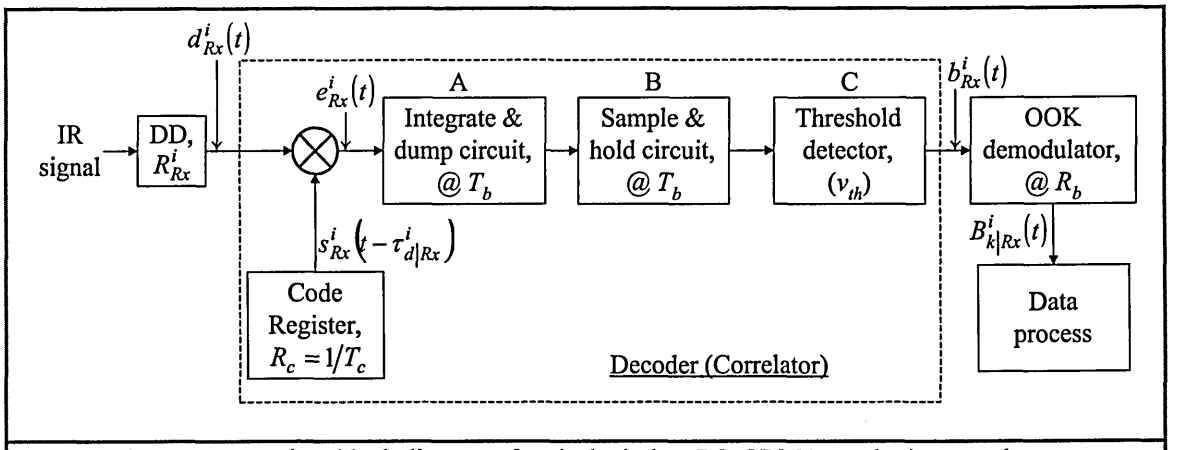

Figure 5.7: Receiver block diagram of optical wireless DS-CDMA employing correlator.

The output of the multiplier is given as:

$$\begin{aligned} e^i_{Rx}(t) &= d^i_{Rx}(t) \times s^i_{Rx}\left(t-\tau^i_{d|Rx}\right) \\ &= \left(R^i_{Rx} D^i_{Tx}\left(t-\tau^i_{d|Tx}\right) \otimes h^{i|i}(t) + \left[R^i_{Rx} \sum_{I=1}^{F} D^I_{Tx}\left(t-\tau^I_{d|Tx}\right) \otimes h^{I|i}(t) \right] + n(t) \right) \\ &\quad \times s^i_{Rx}\left(t-\tau^i_{d|Rx}\right), \end{aligned} \tag{5.10}$$

where $I \neq i$, $\tau^i_{d|Rx}$ is the time delay of the receiver and $s^i_{Rx}(t)$ is the signal of spreading sequence. The first term in the round bracket is the desired signal, the second term is the superposition of all other users' transmitted signals, and the third term is additive white Gaussian noise. Assuming that tracking and synchronisation are achieved where $\tau^i_{d|Rx} \bmod_{nT_c} = \tau^i_{d|Tx}$ then only the first term in (5.10), which is the desired de-spread signal, will emerge at the output of the multiplier. The de-spread signal is then passed through an integrator and a sampler. The output of the sampler (highest amplitude at $t = T_b$) is then compared with a threshold level, v_{th}, to determine if a pulse is being received, see figure 5.8. The uncorrelated signals emerging at the output of the multiplier will become constrained to the correlated signal, which is termed MAI. The amplitude of the constraint is determined by the value of λ_c for the codeword used. The correlated signal, $b^i_{Rx}(t)$, at the output of the correlator is then feed into the modulator for recovering the data bits, $B^i_{k|Rx}$, to be processed.

On the other hand if $\tau^i_{d|Rx} \bmod_{nT_c} \neq \tau^i_{d|Tx}$ then no signal correlation is produced from (5.10), where the first term is in out-of-phase auto-correlation with the replica sequence $s^i_{Rx}(t)$, which will then induce the auto-correlation constraints of maximum amplitude λ_a. The others will act as MAI and Gaussian noise. Thus, the phase or epoch synchronisation is essential in order to align the first term with $s^i_{Rx}(t)$ to achieve $\tau^i_{d|Rx} \bmod_{nT_c} = \tau^i_{d|Tx}$ for successful decoding.

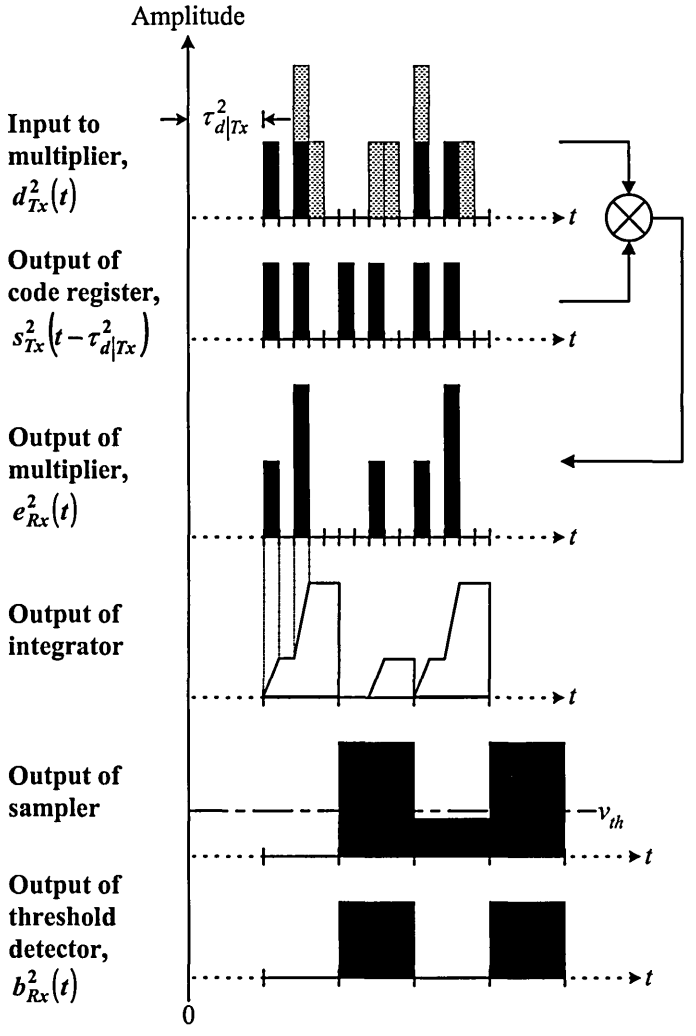

Figure 5.8: Sample waveforms observed from figure 5.7 for user-2 only.
*The shaded pulses are the signals of user 1. The transmission time delays of both transmitters are related to $\tau^1_{d|Tx} = \tau^2_{d|Tx} + 2T_c$. The time constant of the integrator is designed such that $RC = T_c$.

5.4.2 Decoder employing tap-delay structure – Matched filter

The receiver block diagram employing a matched filter is shown in figure 5.9. The output of a DD detector is passed to the tap-delay structure. The tap-delay structure function in

the opposite order to that of the transmitter, where by tuning the delay values a high amplitude signal pulse can be formed by each of the pulses in the signature sequence. The tap-delay value for each branch is obtained by making sure that each pulse in the signature sequence is collected at the last chip time (i.e. $(n-1)T_c$) of the sequence, given by:

$$\text{Tap - delay value} = \left(n-1-cw_{(i,j)}\right)T_c . \tag{5.11}$$

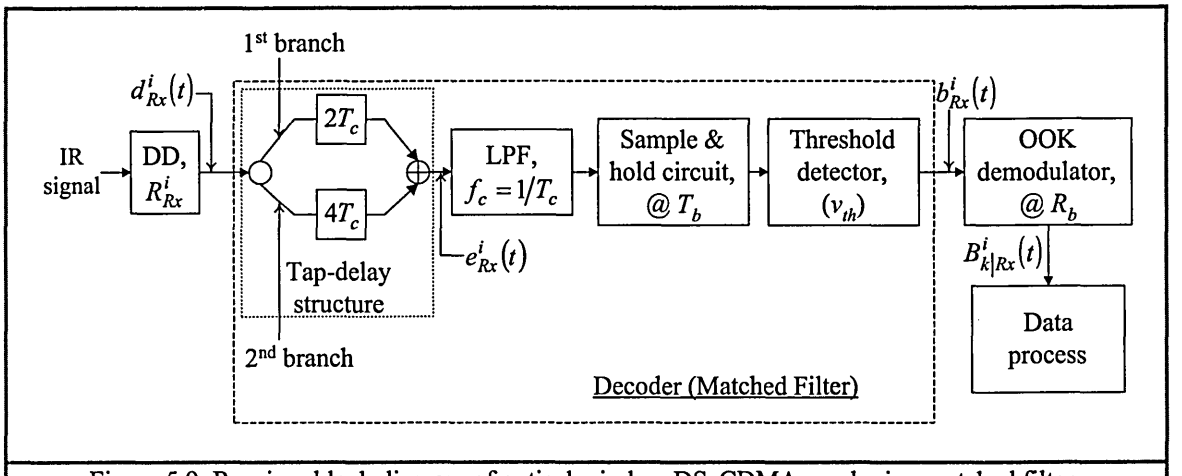

Figure 5.9: Receiver block diagram of optical wireless DS-CDMA employing matched filter.

Hence, the output of the tap-delay structure is given as:

$$e^i_{Rx}(t) = \sum_{j=1}^{w} d^i_{Rx}\left(t-\left(n-1-cw_{(i,j)}\right)T_c\right). \tag{5.12}$$

Substituting (5.7) and (5.9) into (5.12), will result in:

$$
\begin{aligned}
e^i_{Rx}(t) &= V_d R^i_{Tx} R^i_{Rx} \sum_{k=0}^{\infty} \sum_{j=1}^{w} B^i_{k|Tx} g_c\left(t - cw_{(i,j)} T_c - \left(n-1-cw_{(i,j)}\right) T_c - kT_b - \tau^i_{d|Tx}\right) \otimes h^{i|i}(t) \\
&+ V_d R^i_{Tx} R^i_{Rx} \sum_{k=0}^{\infty} \sum_{j=1}^{w} \sum_{J=1}^{w} B^i_{k|Tx} g_c\left(t - cw_{(i,j)} T_c - \left(n-1-cw_{(i,J)}\right) T_c - kT_b - \tau^i_{d|Tx}\right) \otimes h^{i|i}(t) \\
&+ R^i_{Rx} \sum_{j=1}^{w} \sum_{I=1}^{F} D^I_{Tx}\left(t - \left(n-1-cw_{(I,j)}\right) T_c - \tau^I_{d|Tx}\right) \otimes h^{I|i}(t) \\
&+ n(t) \\
&= V_d R^i_{Tx} R^i_{Rx} \sum_{k=0}^{\infty} B^i_{k|Tx} g_c\left(t - (n-1) T_c - kT_b - \tau^i_{d|Tx}\right) \otimes h^{i|i}(t) \\
&+ V_d R^i_{Tx} R^i_{Rx} \sum_{k=0}^{\infty} \sum_{j=1}^{w} \sum_{J=1}^{w} B^i_{k|Tx} g_c\left(t - cw_{(i,j)} T_c - \left(n-1-cw_{(i,J)}\right) T_c - kT_b - \tau^i_{d|Tx}\right) \otimes h^{i|i}(t) \\
&+ R^i_{Rx} \sum_{j=1}^{w} \sum_{I=1}^{F} D^I_{Tx}\left(t - \left(n-1-cw_{(I,j)}\right) T_c - \tau^I_{d|Tx}\right) \otimes h^{I}(t) \\
&+ n(t),
\end{aligned}
\tag{5.13}
$$

where $i \neq I$ and $j \neq J$. The first term is the decoded signal that resulted from at the in-phase auto-correlation. This is because the tap-delay values (circled in blue dotted line) match with the signature sequence codeword (circled in red dotted line) and resulted in the correlated signal occurred on the last chip position of the sequence, as circled in the green dotted line. The second term is the result of a mismatch between other pulses in within the sequence itself that causes auto-correlation constraints. The third term is the MAI and the last term is Gaussian noise. Then (5.13) is passed to the LPF to filter the Gaussian noise and to the sampler to regenerate recovered signal. The threshold detector is used to decide whether the recovered signals are correlated signals if the amplitudes are above the threshold level. The process is illustrated in figure 5.10 where Gaussian noise has been neglected, it is also assumed that the channel is ideal, and tracking and synchronisation are achieved.

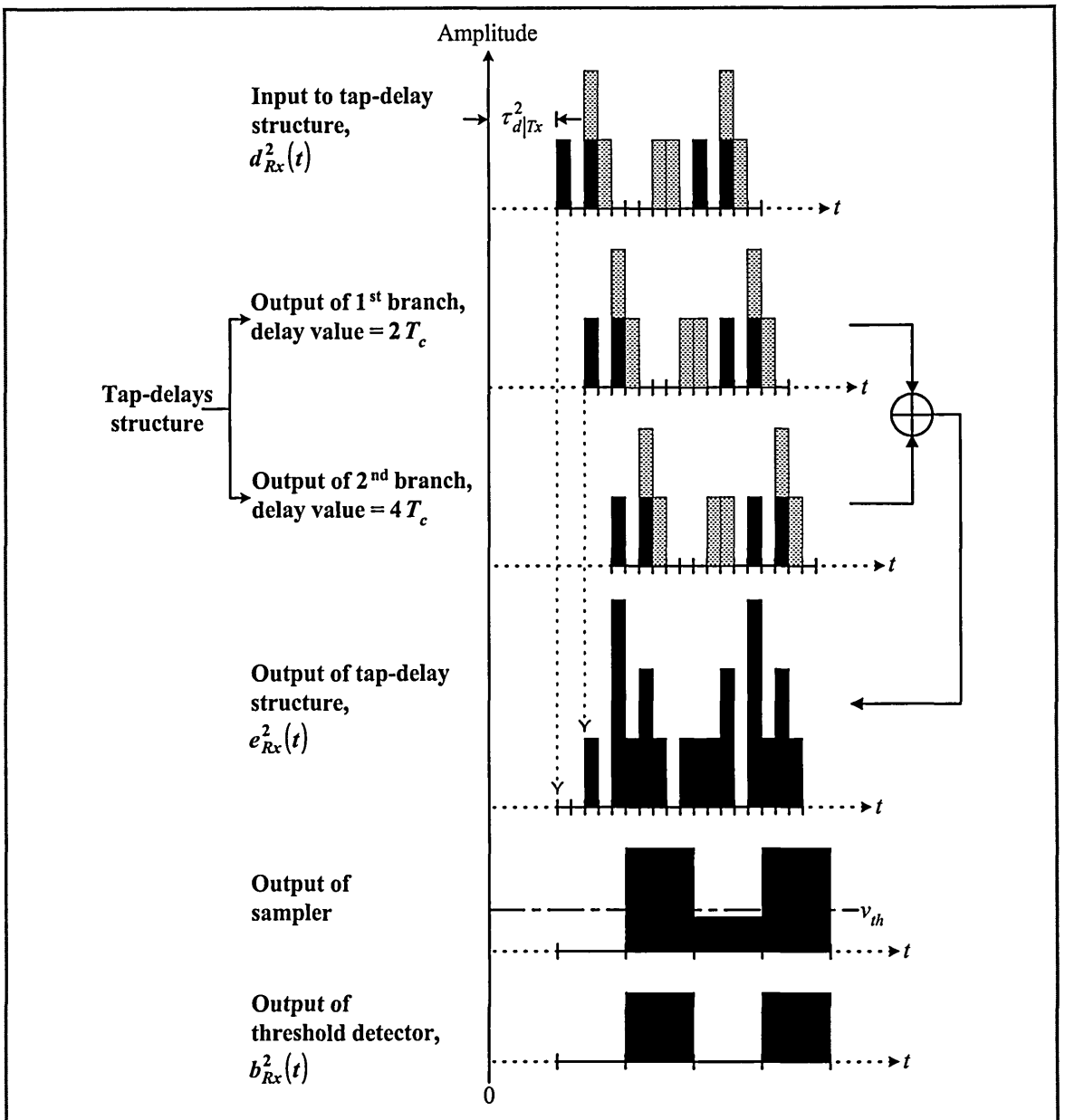

Figure 5.10: Sample waveforms observed from figure 5.9 for user-2 only.
*The shaded pulses are the signals of user 1. The codeword of user 1 is ${}^{(5,2,1,1)OOC}_{5}CW^{2\times2}_{(1,j)} = (0 \quad 1)$ and of user 2 is ${}^{(5,2,1,1)OOC}_{5}CW^{2\times2}_{(2,j)} = (0 \quad 2)$. The transmission time delays of both transmitters are related to $\tau^1_{d|Tx} = \tau^2_{d|Tx} + 2T_c$.

5.5 DS-CDMA Operating Modes

DS-CDMA system can be configured to operate in symbol synchronous, asynchronous (but chip synchronous) or fully asynchronous mode. A synchronous DS-CDMA system is similar to a TDMA system, but unlike the TDMA where each user must transmit one after another, DS-CDMA allows all users to transmit at the same time but at a lower rate [Kwong90, Kwong91, Lam02]. In the scope of this thesis, only the asynchronous system is considered.

System synchronisation can be achieved in several ways [ARRL91]:

1. Recovery of the transmitter clock at the receiver
2. Transmit clock and signal separately
3. Transmit clock as part of the signal
4. Use an external reference to synchronise both transmitter and receiver

For asynchronous systems, chip synchronisation is achieved by using an external reference signal (option 4) where a base station is used to synchronise all users with a biased AM signal [ARRL91] or with a short signature sequence [Holejko99] at a different wavelength, as shown in figure 5.11.

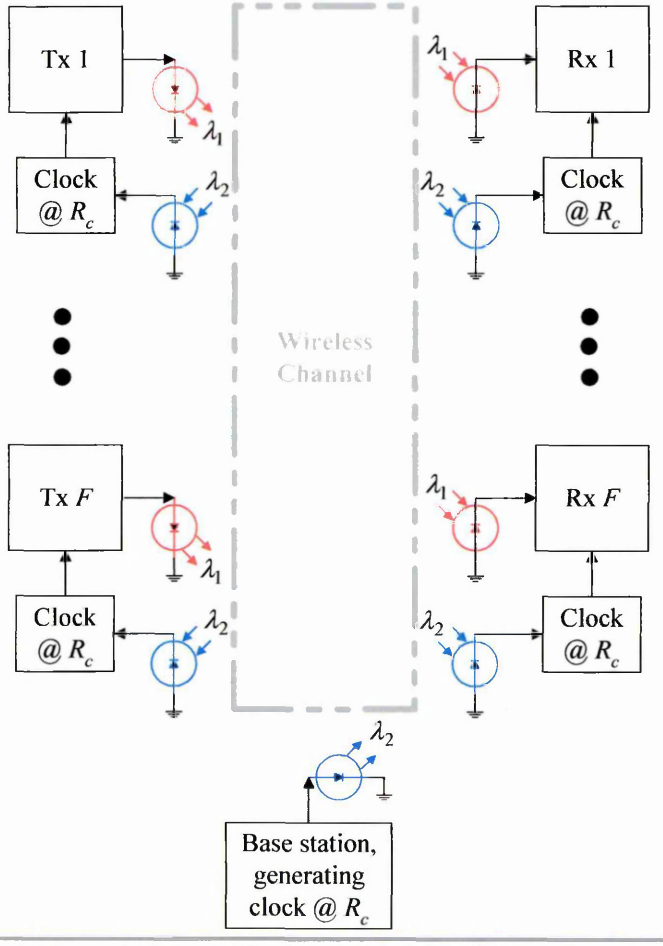

Figure 5.11: Synchronisation technique employing a base station for global synchronisation at the clock rate R_c [ARRL91].

*The wavelength λ_1 is reserved for signal transmission and the wavelength λ_2 is reserved for clock signal only.

5.6 Comparison of Correlator and MF Receivers

This section compares the performance of the multiplier and the tap-delay structure used for encoding and decoding unipolar signals for optical DS-CDMA systems. The comparison is carried out for three cases: i) the minimum dispersion, ii) severe dispersion and iii) near far effect.

Here, a system of two clients employing the set of codeword in (5.1) is used as model. The chip rate is set at $R_c = 10\,\text{Mbps}$, and all transmitter-receiver pairs are assumed chip synchronised and tracking has been obtained.

5.6.1 Case 1 – Minimum dispersion effect

Transmitters and receivers are placed at an equal distance such that the channel impulse responses observed at the user-2 receiver (desired receiver) are equal, i.e. $h^{1|2}(t) = h^{2|2}(t)$. The value of $D_T \leq 0.3$ is found to correspond to $\leq 10\%$ of dispersed power, which is chosen as the upper bound for minimum dispersion (i.e. $D_T^{1|2} = D_T^{2|2} = 0.3$ in this study). It is assumed that there is no optical path loss where $G_{OC}^{1|2} = G_{OC}^{2|2} = 1$ and the electrical-optical-electrical conversion is ideal such that $R_{Tx}^{i} \times R_{Rx}^{I} = 1 : i, I = [1,2]$. The data bits for the user-1 and user-2 transmitters are $B_{k|Tx}^{1} = \{1 \;\; 1 \;\; 1\}$ and $B_{k|Tx}^{2} = \{1 \;\; 0 \;\; 1\}$, for $k = [0,2]$, respectively. The transmission delay of the user-1 is arbitrarily set to $\tau_{d|Tx}^{1} = 4T_c$ and the delay the user 2 is set to $\tau_{d|Tx}^{2} = 1T_c$ so that no pulses from either transmitted signals will overlap, see figure 5.12.

Figures 5.12 (i) and (ii) show the dispersed waveforms, at the output of user-2 photo-detector, for user-1 and user-2. The combined output observed at the output of the user-2 photo-detector is shown in figure 5.12 (iii). Also shown for comparison are the waveforms for an ideal channel, indicated by the dotted magenta lines. Using the correlator following the photo-detector, the waveforms observed are shown in figure 5.13. Figure 5.13 (i) shows the recovered signal

overlaid with the signature sequence of user-2 (indicated by the cyan dash-dotted line) and figure 5.13 (ii) shows the correlation process. As can be seen from figure 5.13 (i), the 'centre point' (where most power is concentrated) of each signal pulse has been shifted slightly to the right due to channel dispersion. Hence the code register at the correlator detector (see figure 5.7) needs to be synchronised with the photo-detector output $d_{Rx}^2(t)$ at the chip rate where the optimum power is to be recovered from each dispersed pulse. The output of the multiplier for user-2 as in (5.10), can be rewritten as:

$$e_{Rx}^2(t) = d_{Rx}^2(t) \times s_{Rx}^2\left(t - \tau_{SP|C}^2 - \tau_{d|Rx}^2\right), \tag{5.14}$$

where $\tau_{SP|C}^2$ is time shift of the 'centre' of the dispersed signal. Simulations show that $\tau_{SP|C}^i$ of the i^{th} correlator code register $s_{Rx}^i(t)$ can be generally represented as:

$$\tau_{SP|C}^i \approx \frac{D_T^{i|i} T_c}{10}. \tag{5.15}$$

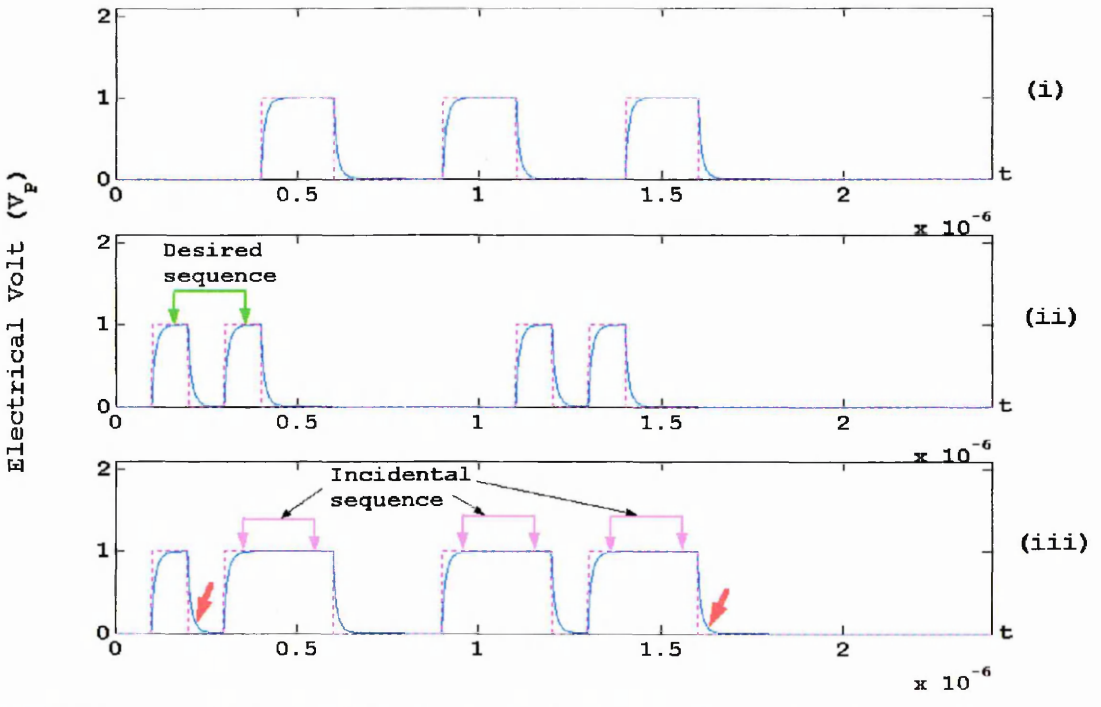

Figure 5.12: Sample waveforms for minimum dispersion case; (i) user-1 transmitted signal, (ii) user-2 transmitted signal and (iii) user-2 photo-detector output $d_{Rx}^2(t)$.
Legend references: (1) Magenta dotted plot: Ideal signal, (2) Blue plot: Electrical signal.
*Note, for simplicity, the peak amplitudes are normalised to a peak voltage V_P.

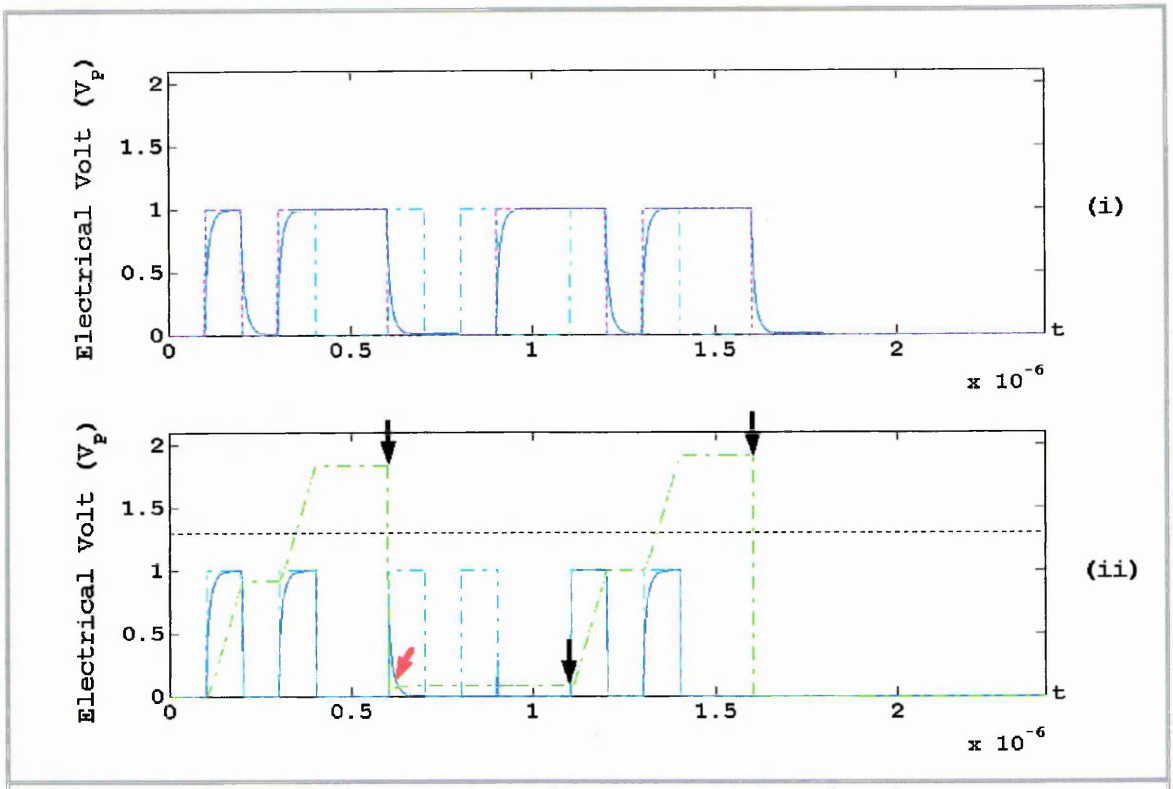

Figure 5.13: Sample waveforms of correlator for minimum dispersion case.
Legend references: (1) Magenta dotted plot: Ideal signal, (2) Blue plot: Electrical signal, (3) Cyan dotted plot: Code register output signal, (4) Green dotted plot: Integrator output signal and (5) Black dotted line: Threshold detector level.

For $D_T = 0.3$, $\tau^i_{SP|C} = 0.03T_c$, which is small and there is no need to adjust the code register delay. Using a MF following the photo-detector, the waveforms are shown in figure 5.14. The dispersed signal peak always occurs at the last chip slot of the sequence as indicated by the sampling point (the black arrows). Referring to figures 5.13 (i) and 5.14, it can be seen that for a small delay the dispersed signals are almost the same as the equivalent ideal signal (magenta dotted plots). This is because the small delay spread does not affect the correlation properties. The exponential dispersed tail of up to 0.3 pulse length (indicated by the red arrows) only contributes to 10% of the total power and is therefore considered negligible.

Comparing figure 5.13 (ii) with 5.14, it can be seen that the correlator multiplier only produces the output of the correlated signals when synchronisation is achieved; whereas the MF tap-delay structure carries out correlation at every time chip, producing both the desired signals and the false alarm pulses (as indicated by the cyan arrows). However the MF sampler is able to detect the desired signals at the correct time chip when it is synchronised. If synchronisation hasn't

been achieved, then the correlator will have to struggle to locate the desired signature sequence and to locate the symbol boundary by performing a rigorous search at every time chip. This searching employs a technique known as the sliding correlator that is described in section 3.2.5.

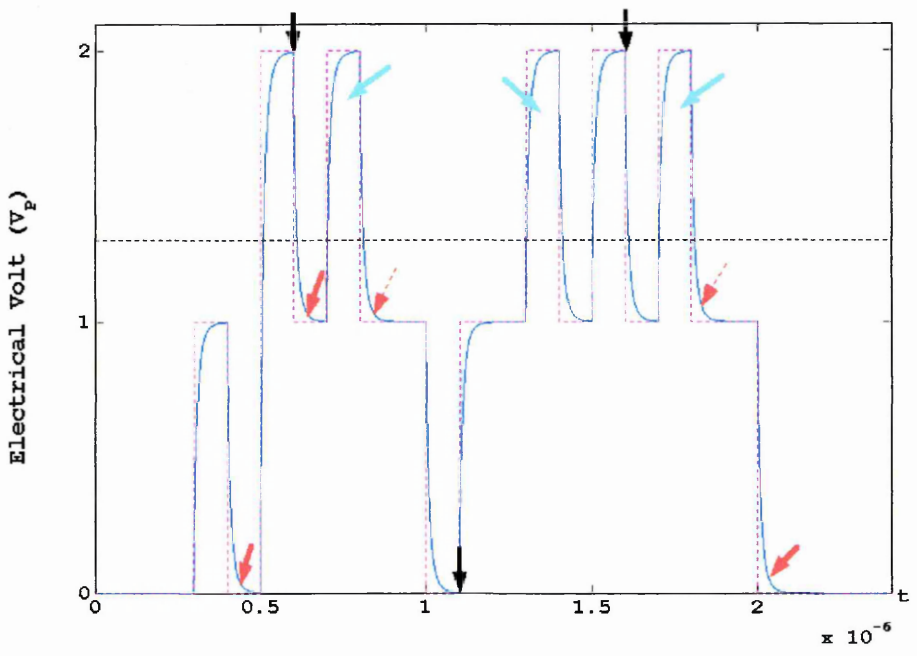

Figure 5.14: Sample waveforms of MF for minimum dispersion case.
Legend references: (1) Magenta dotted plot: Ideal signal, (2) Blue plot: Electrical signal, (3) Black dotted line: Threshold detector level.

Referring to figure 5.14 and 5.12 (iii), the false alarm pulses occur as a result of interfering signals falling at the chip position that corresponds to the desired signal, creating an identical spreading sequence (as indicated by the magenta arrows). This is termed an incidental sequence as apposed to the desired one (indicated by the green arrows). The correlator receiver will also detect these false alarm pulses when it carries out the sliding correlation process.

5.6.2 Case 2 – Severe dispersion effect

Increasing the channel dispersion, i.e. setting $D_T^{1|2} = D_T^{2|2} = 1.5$, will reduce the signal power by distributing the signal power to adjacent chips, see figure 5.15. The effect will destroy the original patterns of the signature sequences as more incidental sequences have been generated.

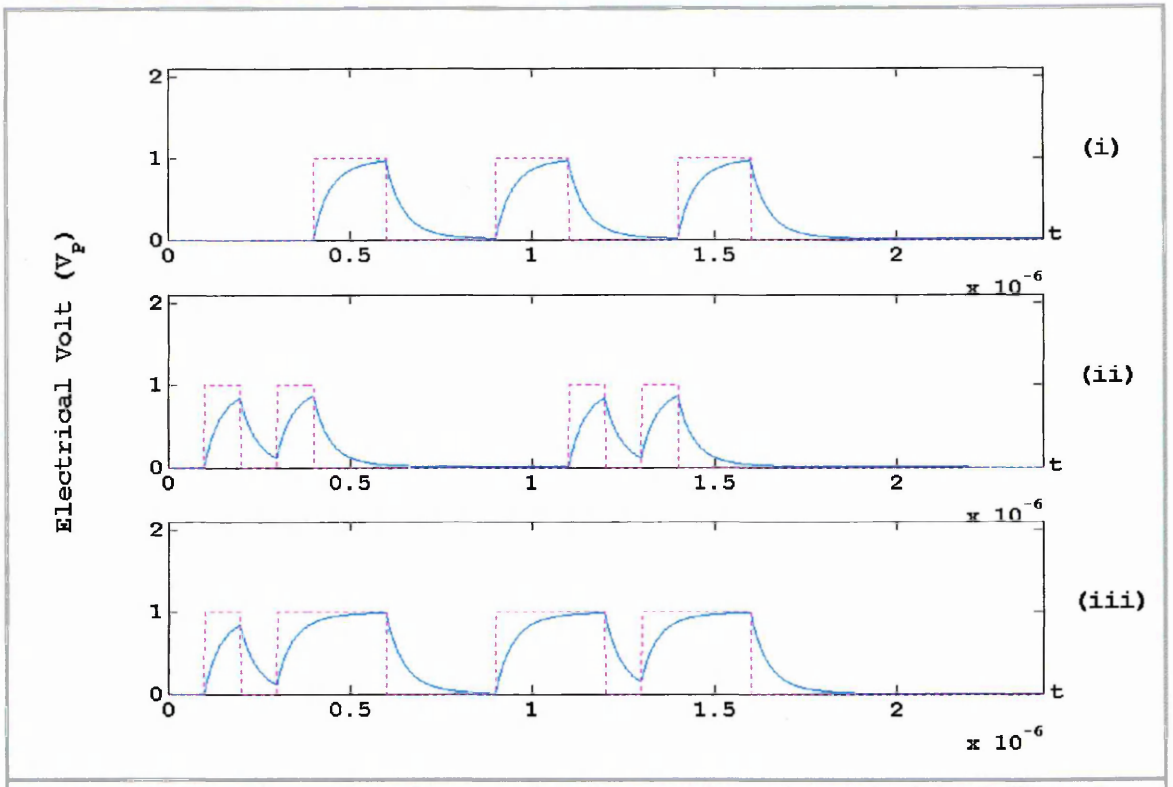

Figure 5.15: Sample waveforms for severe dispersion case; (i) user-1 transmitted signal, (ii) user-2 transmitted signal and (iii) user-2 photo-detector output $d_{Rx}^2(t)$.
Legend references: (1) Magenta dotted plot: Ideal signal, (2) Blue plot: Electrical signal.

This is best illustrated in figures 5.16 (ii) and 5.17, where the uncorrelated signal magnitude ('bit 2' position) has increased. As shown in figure 5.16, the code register (indicated by the cyan dotted plot) of the correlator is synchronised at the position of $\tau_{SP|C}^2 = 0.15T_c$ away from the equivalent ideal signal (indicated by the magenta dotted plot) in order to achieve the optimum signal detection. As for MF detection (figure 5.17), the signal peaks also occur at the last chip position, and is similar to the case in figure 5.14. Compared with the correlator, the MF detector is more robust against the variance of signal dispersion, which can be caused by the mobility of the communicating pairs.

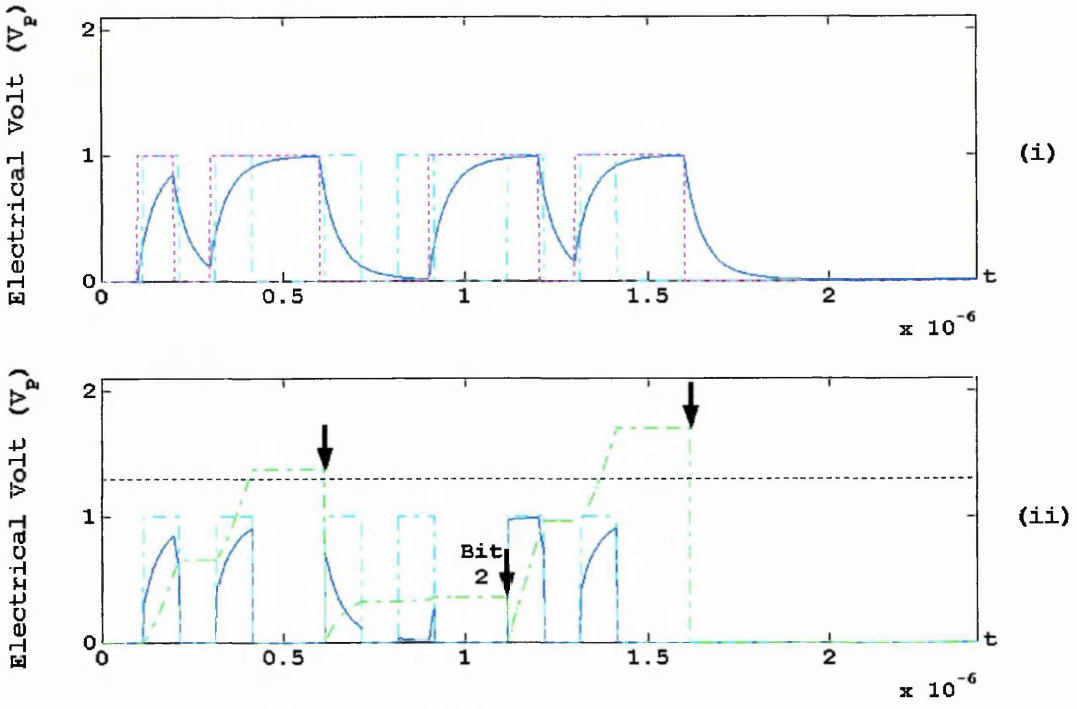

Figure 5.16: Sample waveforms of correlator for severe dispersion case.
Legend references: (1) Magenta dotted plot: Ideal signal, (2) Blue plot: Electrical signal, (3) Cyan dotted plot: Code register output signal, (4) Green dotted plot: Integrator output signal and (5) Black dotted line: Threshold detector level.

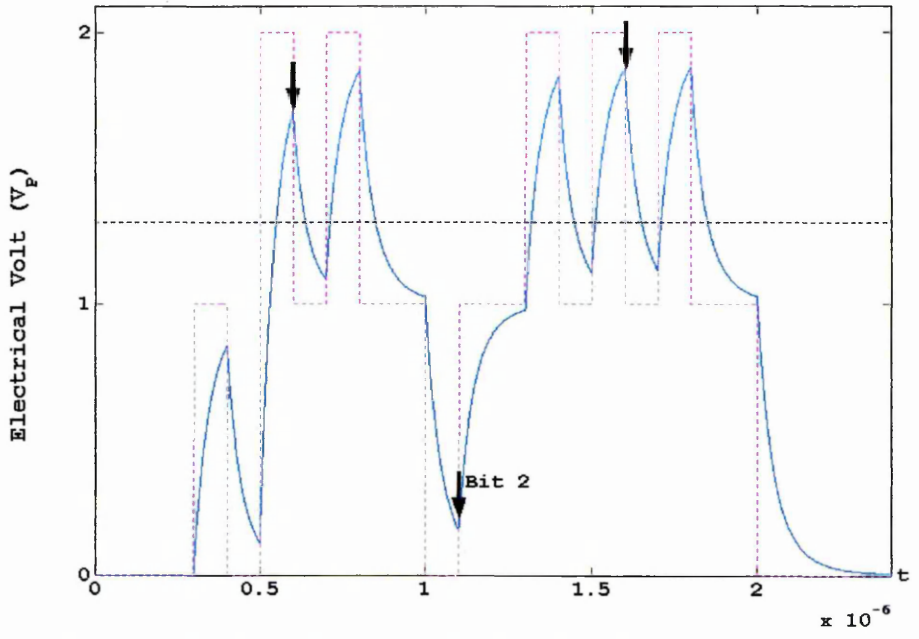

Figure 5.17: Sample waveforms of MF for severe dispersion case.
Legend references: (1) Magenta dotted plot: Ideal signal, (2) Blue plot: Electrical signal, (3) Black dotted line: Threshold detector level.

5.6.3 Case 3 – Near-far effect

This effect is evident when the desired signal that arrives at the desired receiver is weaker than the interfering signals. This will result in the desired receiver being more likely to detect the interfering signal. To simulate this, the parameters are set to $D_T^{1|2}=0.6$, $D_T^{2|2}=1.9$, $G_{OC}^{1|2}=0.95$, $G_{OC}^{2|2}=0.75$ and $R_{Tx}^{i}\cdot R_{Rx}^{I}=1:i,I=[1,2]$, to imply that the user-1 transmitter is placed closer to the user-2 receiver than user-2 transmitter. User-2 receiver will detect the interfering signals if: there are large signal pulses from the user-1 that overlap with the desired signals, and the particular desired signal being interfered is modulating bit '0'. Hence the data bits are set as $B_{k|Tx}^{1}=\{1\ \ 1\ \ 1\}$ and $B_{k|Tx}^{2}=\{1\ \ 0\ \ 0\}$, and transmission delays are set to $\tau_{d|Tx}^{1}=5T_c$ and $\tau_{d|Tx}^{2}=1T_c$, so that the previously mentioned interference will occur – as shown in figure 5.18.

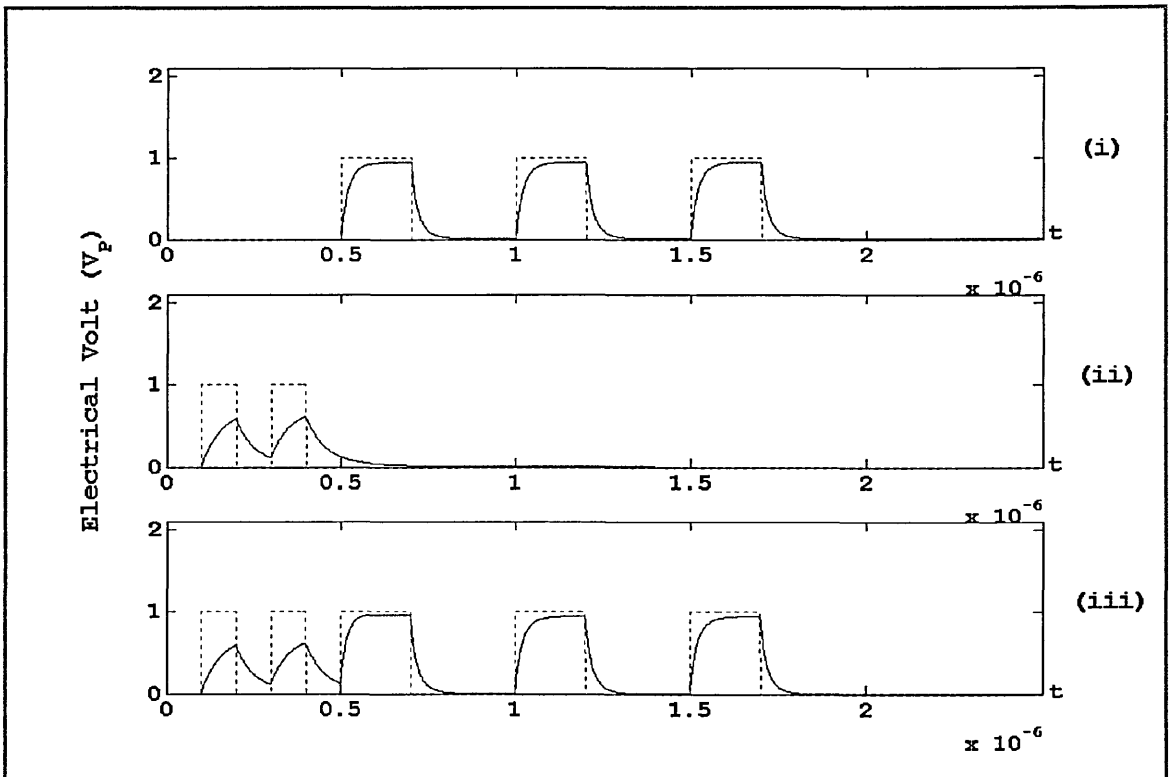

Figure 5.18: Sample waveforms for near-far effect case; (i) user-1 transmitted signal, (ii) user-2 transmitted signal and (iii) user-2 photo-detector output $d_{Rx}^{2}(t)$.
Legend references: (1) Magenta dotted plot: Ideal signal, (2) Blue plot: Electrical signal.

In the near-far case, there is a greater probability of detecting (correlating) the interfering signals than the desired one. The probability is dependant on the signal pulses from the interfering transmitter appearing on the chip position corresponding to the patterns of the desired signature sequence, as indicated by the blue arrows in figure 5.19 (i) which shows one pulse interference. Note that the delays for user-1 and user-2 transmitters are different to those discussed above. The desired signal travelling a longer path arrives at the receiver with much reduced power compared to the interfering channel, see figure 5.18. Therefore, in order to detect small signals, the threshold detector level needs adjusting (as indicated by the red dotted line in figures 5.19 (ii) and 5.20) for both the correlator and MF detectors. However by doing so, the uncorrelated signals due to the interfering signal have the potential to exceed the threshold level, thus increasing the signal-to-interference ratio (SIR). The desired transmitter may increase the signal power level to compensate for the channel loss. Nevertheless, amplifying the desired signal (from user-2) may potentially increase the magnitude of interference to the other receiver (the user-1), or vice versa.

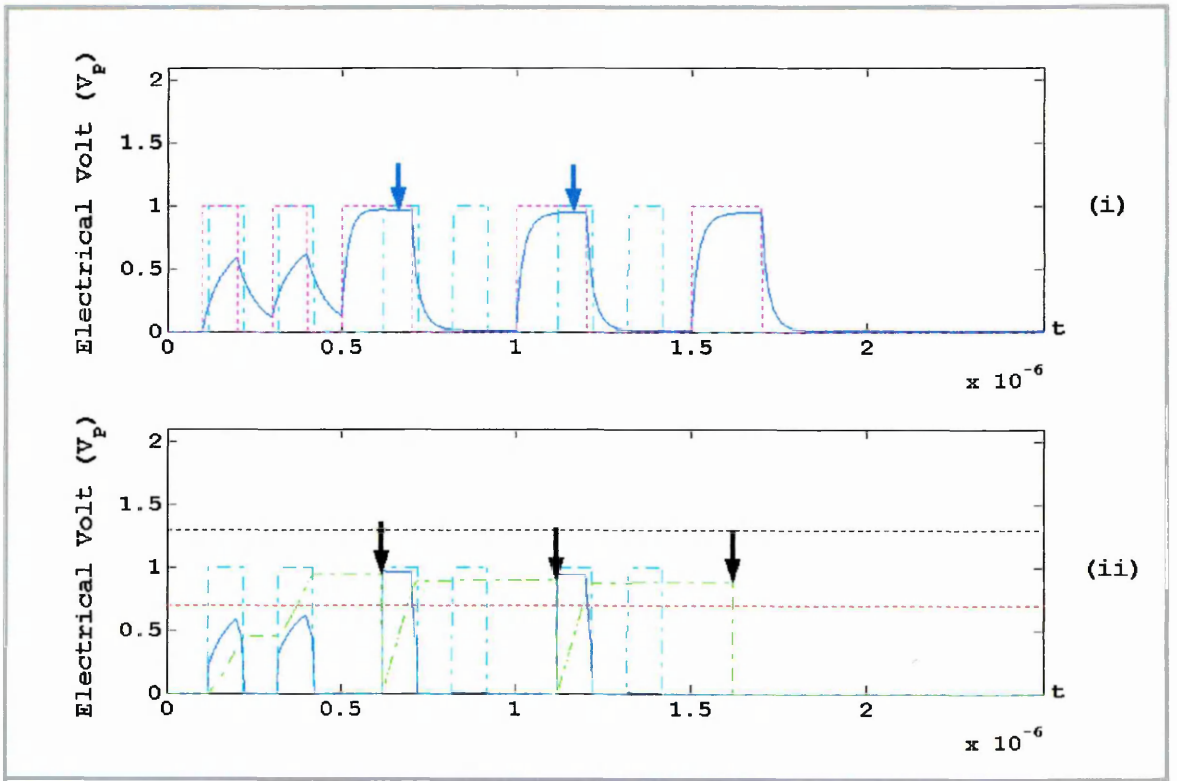

Figure 5.19: Sample waveforms of correlator for near-far effect case.
Legend references: (1) Magenta dotted plot: Ideal signal, (2) Blue plot: Electrical signal, (3) Cyan dotted plot: Code register output signal, (4) Green dotted plot: Integrator output signal and (5) Black dotted line: Threshold detector level.

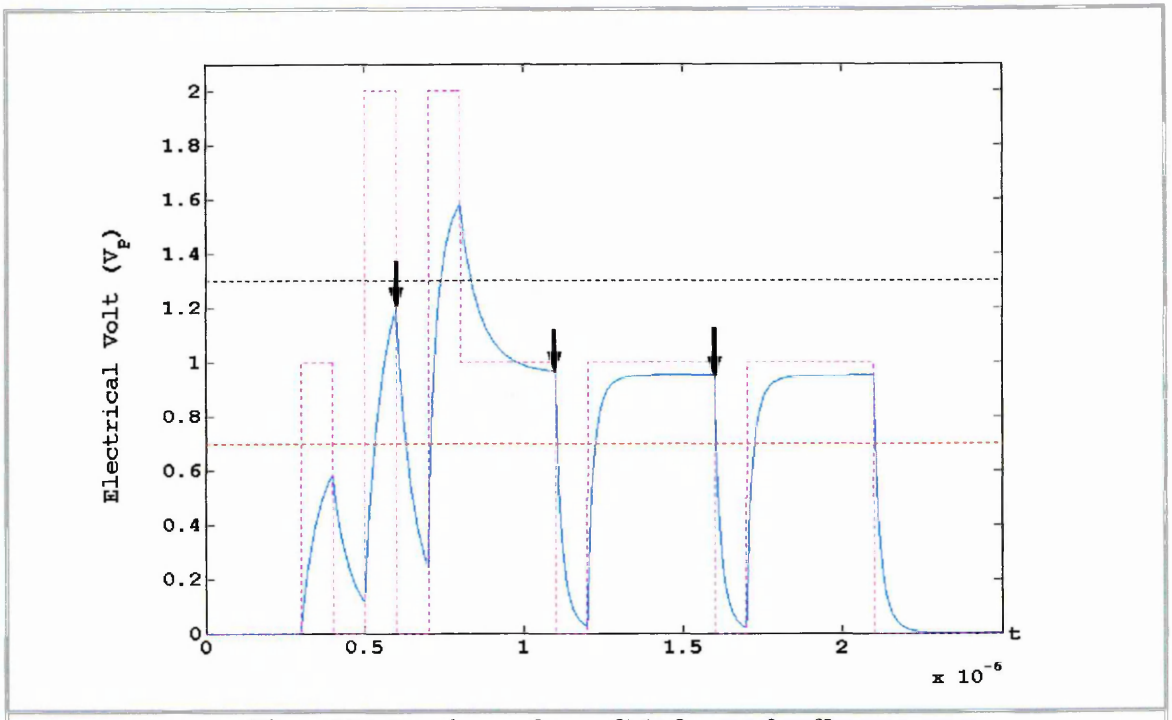

Figure 5.20: Sample waveforms of MF for near-far effect case.
Legend references: (1) Magenta dotted plot: Ideal signal, (2) Blue plot: Electrical signal, (3) Black dotted line: Threshold detector level.

5.7 OOK-CDMA

The optical DS-CDMA system that uses an OOK signal format is also known as OOK-CDMA system. The performances of an OOK-CDMA system in terms of BEF and power efficiency are discussed in this section. The data rate for OOK-CDMA can be expressed as:

$$R_{b|OOK-CDMA} = \frac{1}{T_b} = \frac{1}{nT_c}. \tag{5.16}$$

As can be seen from (5.16), the bandwidth increases with the sequence length n for the same data rate. In diffuse optical wireless DS-CDMA systems, the bandwidth is limited by:

$$D_{T|\min} \leq 0.3. \tag{5.17}$$

The throughput performance normalised to OOK is measured by BEF defined as:

$$BEF_{\frac{OOK-CDMA}{OOK}} = \frac{1}{n}. \tag{5.18}$$

The power efficiency is given as:

$$W_{Eff\left|\frac{OOK-CDMA}{OOK}\right.} = -10\log\frac{Fw}{Fw(w-1)+1}(\mathrm{dB}). \tag{5.19}$$

The BEF and W_{Eff} performances are shown in figures 5.21 and 5.22 respectively. As shown in figure 5.21, OOK-CDMA BEF reduces with increasing F and w. On the other hand, the power efficiency increases with w, see figure 5.22. For a constant w, the power efficiency remains constant for all values of F. This is because the condition in (4.8) ensures that the sets of codewords constructed are always orthogonal for all F. However this does increase the signature sequence length n linearly with F, resulting in constant power efficiency. Increasing w will increase n exponentially whilst increasing the power efficiency.

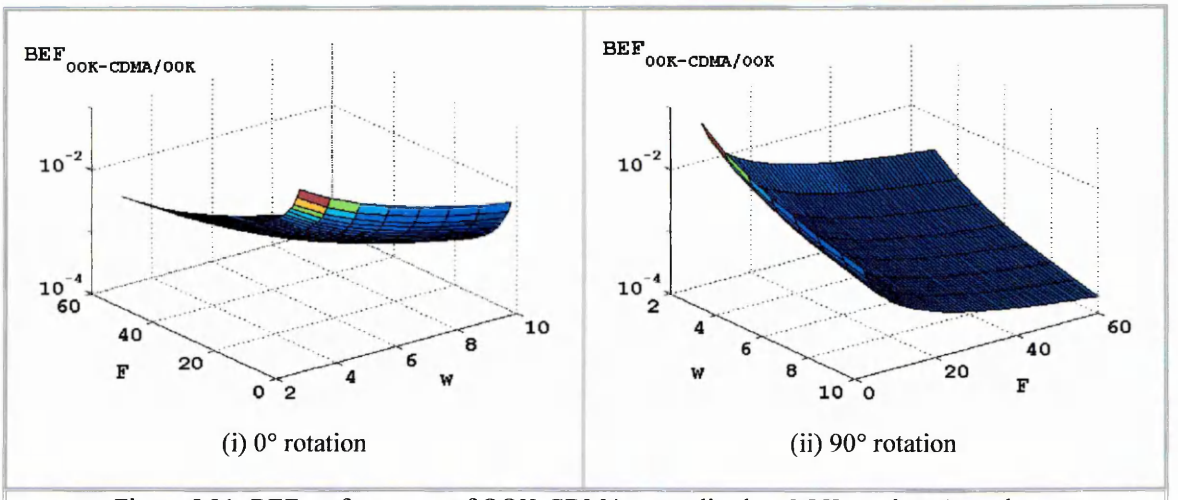

(i) 0° rotation (ii) 90° rotation

Figure 5.21: BEF performance, of OOK-CDMA normalised to OOK, against F and w.

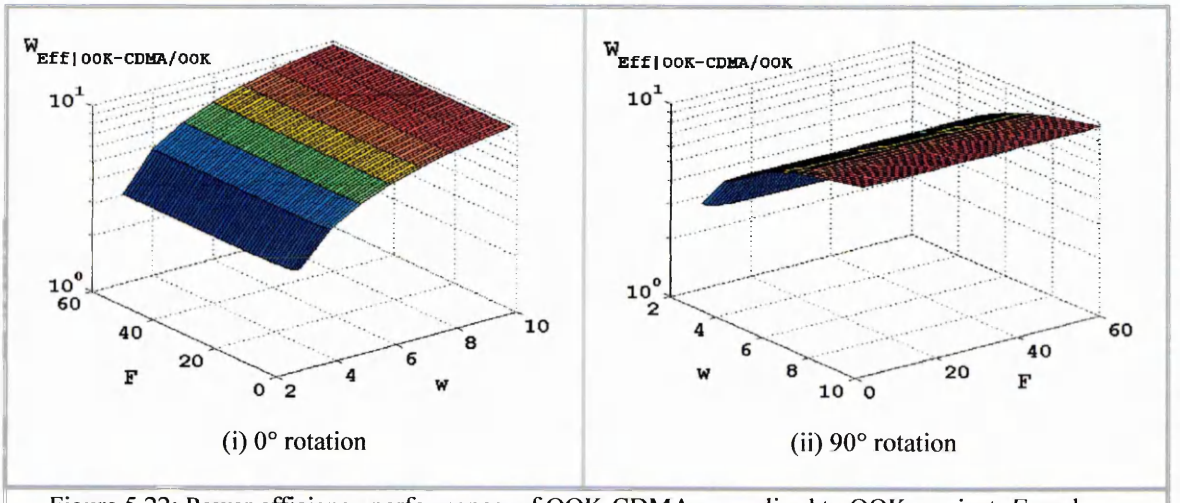

(i) 0° rotation (ii) 90° rotation

Figure 5.22: Power efficiency performance, of OOK-CDMA normalised to OOK, against F and w.

5.8 PPM-CDMA

PPM-CDMA encoding is similar to PPM technique, where a signature sequence is located at a position corresponding to the information [Khansefid90, Gagliardi93, Hwang97a, Hwang97b, Kamakura99]. An example of two 4-PPM-CDMA symbols is shown in figure 5.23.

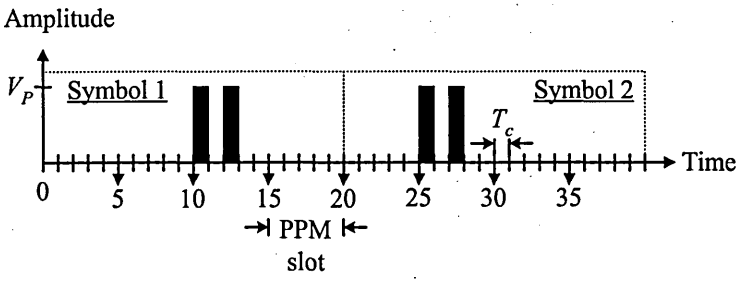

Figure 5.23: 4-PPM-CDMA signal stream of 2 symbols mapping information $B_{k|Tx} = \{1 \quad 0 \quad 0 \quad 1\}$.

The PPM-CDMA symbol duration is governed by the order of mapping $L = 2^M$ and is fixed to:

$$T_{S|PPM-CDMA} = nLT_c = n2^M T_c. \tag{5.20}$$

The location of the signature sequence of $nS_k^i T_c$ away from the symbol's origin represents the mapping of M bits information, where S_k^i is the decimal value of the M bits information. For example, the information for the two symbols in figure 5.23 is $S_k^i \in (2 \quad 1) : k = [1,2]$ mapping 2 bits of information. The PPM-CDMA signal stream can be modelled as:

$$d_{Tx}^i\left(t - \tau_{d|Tx}^i\right) = V_d \sum_{k=0}^{\infty} \sum_{j=1}^{w} g_c\left(t - \left(cw_{(i,j)} - kn2^M - nS_k^i\right)T_c - \tau_{d|Tx}^i\right). \tag{5.21}$$

The data rate for PPM-CDMA is:

$$R_{b|PPM-CDMA} = \frac{M}{n2^M T_c}. \tag{5.22}$$

The throughput performance of PPM-CDMA normalised to OOK-CDMA, under bandwidth limitation, is best given as:

$$BEF_{\frac{PPM-CDMA}{OOK-CDMA}} = \frac{R_{b|PPM-CDMA}}{R_{b|OOK-CDMA}} = \frac{MnT_c}{2^M nT_c} = \frac{M}{2^M}. \tag{5.23}$$

The power efficiency of PPM-CDMA normalised to OOK-CDMA is given as:

$$W_{Eff|\frac{PPM-CDMA}{OOK-CDMA}} = -10\log\frac{2}{2^M}(\text{dB}). \tag{5.24}$$

As can be observed from (5.23), the PPM-CDMA BEF decreases exponentially as M increases, but the power efficiency increases linearly (refer (5.24)).

To improve the PPM-CDMA throughput further, a new technique known as overlapping PPM-CDMA has been proposed [Shalaby99a, Shalaby99b], this uses a shorter symbol durations and allows the signature sequence to spread onto adjacent PPM slots.

5.9 Hybrid PPM-CDMA

The PPM-CDMA BEF decreases with an increasing number of PPM slot by a value nT_c as shown in figure 5.23. This resulted in a large number of redundant slots. The redundant slots, however can be eliminated by reducing L-PPM-CDMA symbol length (refer to (5.20)) to:

$$T_{S|hPPM-CDMA} = \left(n + 2^M - 1\right)T_c. \tag{5.25}$$

The signature sequence is encoded as a new symbol of length governed by (5.25) and is located at $S_k^i T_c$ chips away from the symbol's origin, see figure 5.24. This new technique is known as hybrid PPM-CDMA or in short as *h*PPM-CDMA [Elmirghani94, Chan96, Chan98, Chan99].

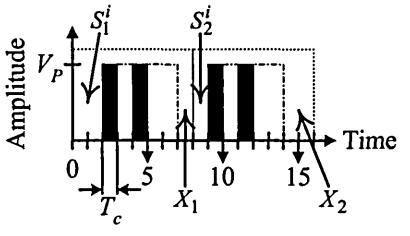

Figure 5.24: 4-*h*PPM-CDMA signal stream of 2 symbols mapping information $B_{k|Tx} = \{1\ \ 0\ \ 0\ \ 1\}$.

Comparing figure 5.24 with 5.23, it can be seen that the duration for transmitting two *h*PPM-CDMA symbols is shorter than the equivalent PPM-CDMA symbols once the redundant chips have been eliminated. *h*PPM-CDMA signal stream can be modelled as:

$$d_{Tx}^{i}\left(t-\tau_{d|Tx}^{i}\right)=V_d\sum_{k=0}^{\infty}\sum_{j=1}^{w}g_c\left(t-\left(cw_{(i,j)}-k\left(n+2^M-1\right)-S_k^i\right)T_c-\tau_{d|Tx}^{i}\right). \tag{5.26}$$

From (5.26), the term $k\left(n+2^M-1\right)T_c$ is periodic but $S_k^iT_c$ is not. The implication as far as the encoder and decoder are concerned is that, only the tap-delay structure can be used. This is because the tap-delay structure is passive and does not require synchronisation. The decoded signal using the tap-delay structure, considering the desired signal only, can be modelled similarly to (5.13) as:

$$\begin{aligned}e_{Rx}^{i}(t)=&V_dR_{Tx}^{i}R_{Rx}^{i}\sum_{k=0}^{\infty}\sum_{j=1}^{w}g_c\left(t-(n-1)T_c-\left(k\left(n+2^M-1\right)+S_k^i\right)T_c-\tau_{d|Tx}^{i}\right)\otimes h^{i|i}(t)\\&+V_dR_{Tx}^{i}R_{Rx}^{i}\sum_{k=0}^{\infty}\sum_{j=1}^{w}\sum_{J=1}^{w}g_c\left(t-\left(n-1-cw_{(i,J)}\right)T_c-\left(cw_{(i,j)}+k\left(n+2^M-1\right)+S_k^i\right)T_c\right.\\&\left.-\tau_{d|Tx}^{i}\right)\otimes h^{i|i}(t),\end{aligned} \tag{5.27}$$

where $j\neq J$.

The data rate for *h*PPM-CDMA is:

$$R_{b|hPPM-CDMA}=\frac{M}{\left(n+2^M-1\right)T_c}. \tag{5.28}$$

The BEF and power efficiency of *h*PPM-CDMA normalised to OOK-CDMA are given respectively as:

$$BEF_{\frac{hPPM-CDMA}{OOK-CDMA}}=\frac{nM}{n+2^M-1}, \tag{5.29}$$

and

$$W_{Eff}\Big|_{\frac{hPPM-CDMA}{OOK-CDMA}}=-10\log\frac{2n}{n+2^M-1}(\text{dB}). \tag{5.30}$$

Note that both the BEF and power efficiency are functions of the signature sequence length n. As discussed in chapter 4, n increases with the number of sequences F for all groups of codewords. For simplicity, the optimal $(n,w,1,1)$ OOC is chosen to evaluate both performances. Since n is related to F and w as defined in (4.8), (5.29) and (5.30) can be rewritten respectively as:

$$BEF_{\frac{hPPM-CDMA}{OOK-CDMA}} = \frac{[Fw(w-1)+1]M}{[Fw(w-1)+1]+2^M-1}, \tag{5.31}$$

and

$$W_{Eff}\Big|_{\frac{hPPM-CDMA}{OOK-CDMA}} = -10\log\frac{2[Fw(w-1)+1]}{[Fw(w-1)+1]+2^M-1}(\text{dB}). \tag{5.32}$$

The BEF and power efficiency performances for various F, M and w are shown in figures 5.25 and 5.26, respectively.

In contrast to PPM-CDMA, *h*PPM-CDMA achieves a higher BEF but with a lower power efficiency. At $M=2$, the BEF is 1 for all F, which means that *h*PPM-CDMA does not achieve a higher throughput. As M increases, the BEF increases and reaches an optimum point. As M increases further, the BEF starts to decrease and will eventually fall below 1 – which means that the throughput is lower than the OOK-CDMA. As can be observed, the optimum point varies for different w. It also varies for different F but the variation is only significant at small F. Comparing figures 5.25 and 5.26, it can be seen that *h*PPM-CDMA does not achieve high power efficiency in the region before the BEF optimum point but does so in the region after the optimum point. Hence *h*PPM-CDMA gives improved BEF and power efficiency at higher bit resolutions, M, and improved BEF only at a lower order of M. However at lower bit resolutions, *h*PPM-CDMA decreased power efficiency is limited to -3dB. This can be observed from (5.32), where for small M the power efficiency will reduce to $-10\log 2 \approx -3$ as F increases. As M increases the power efficiency will continually improve. However, large M will reduce the BEF. Therefore, the advantage of *h*PPM-CDMA is that it offers enhanced data throughput at the cost of reduced power efficiency by not more than -3dB.

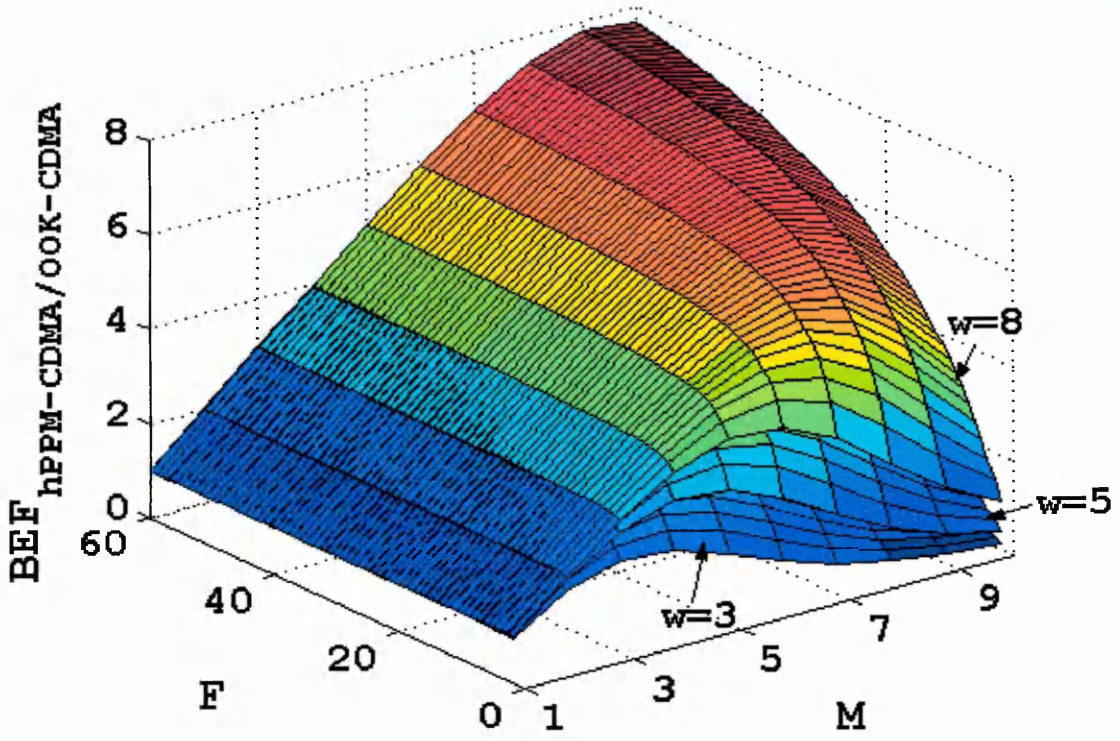

(i) 0° rotation

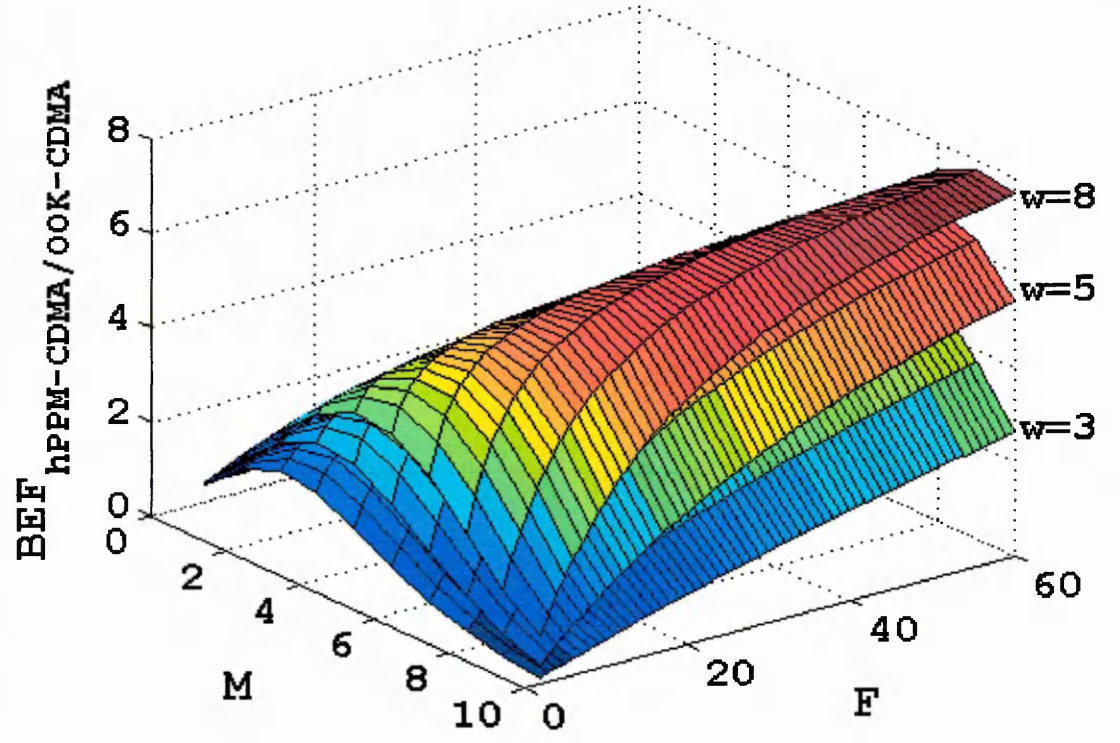

(ii) 90° rotation

Figure 5.25: BEF performance, of *h*PPM-CDMA normalised to OOK-CDMA, against F and M for $w = 3, 5,$ and 8.

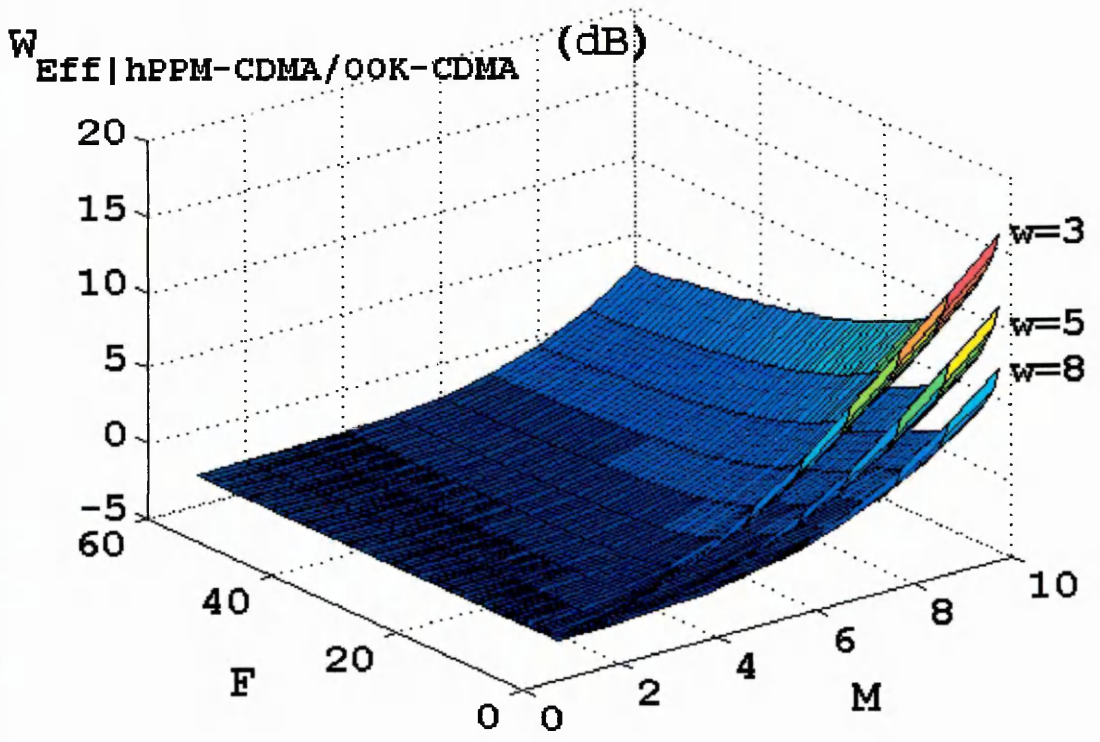

(i) 0° rotation

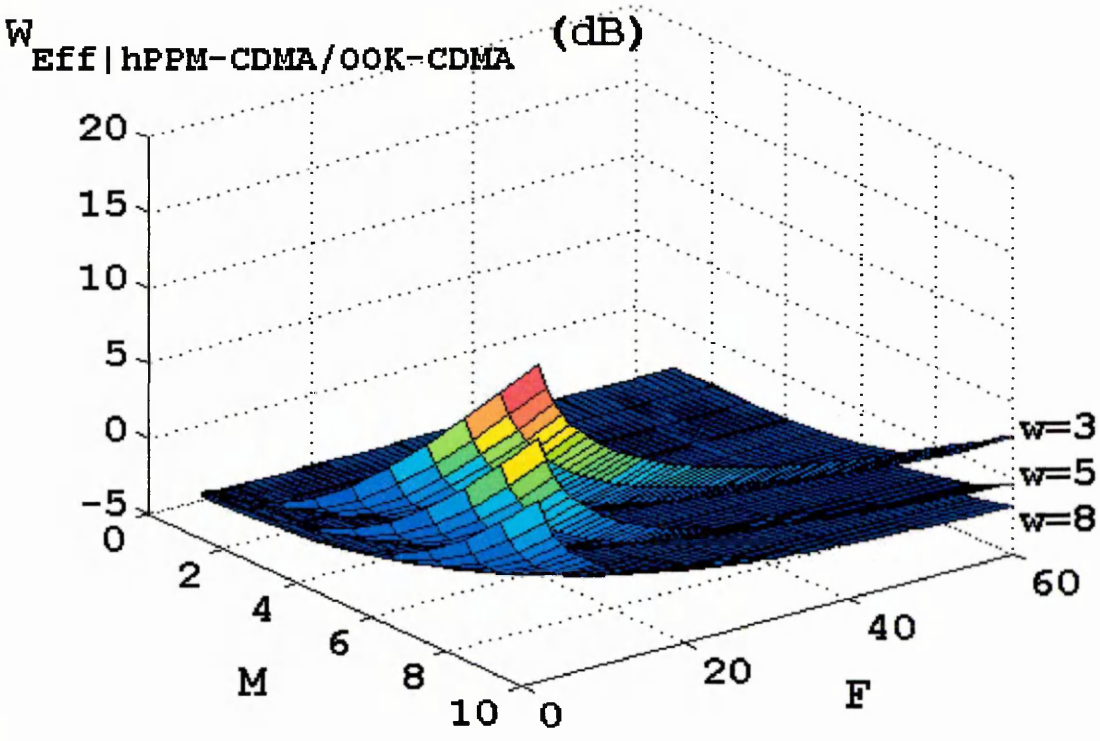

(ii) 90° rotation

Figure 5.26: Power efficiency performance, of *h*PPM-CDMA normalised to OOK-CDMA, against F and M for $w = 3, 5$ and 8.

5.10 Summary

In this chapter, optical wireless diffuse DS-CDMA (OOK- CDMA) systems employing either the multiplier or tap-delay structures for encoding and decoding have been studied. Matched filters based on a tap-delay structure have shown to achieve fast rough synchronisation and has more robust fine synchronisation for a range of D_T compared with the correlator detector. Nevertheless, both detectors are equally affected by the MAI and should operate under the condition (5.17) (where the correlation performance of the signature sequences will be preserved) to achieve high SIR.

For multiple-access communications, OOK-CDMA offers advantages over OOK with an increased number of channels, but at the cost of reduced data throughput. Nevertheless, OOK-CDMA is still a suitable candidate for optical wireless diffuse system where the transmitted optical power is regulated. The total power of an OOK-CDMA system, even when all F users are transmitting simultaneously, was shown to be less than a single channel OOK system. Hence the excess power in OOK-CDMA could be used to achieve a higher SNR performance compared with OOK.

PPM-CDMA was shown to improve the power efficiency but at the cost of a reduced BEF as compared with OOK-CDMA. The BEF can be improved without the need for bandwidth expansion by employing *h*PPM-CDMA scheme. *h*PPM-CDMA achieves this by utilising a shorter symbol length to convey the same information by means of data compression. *h*PPM-CDMA will improve the BEF at low values of M only but is power inefficient, or vice versa.

Chapter 6

HYBRID PIM-CDMA SYSTEM

6.1 Introduction

It was discussed in chapter 2 that PPM and PIM can be employed to achieve low power transmission over OOK in a diffuse IR wireless system. However both PPM and PIM require a higher transmission bandwidth to achieve power efficiency and suffer from severe channel dispersion effects. PIM has been shown to achieve not only power efficiency but also higher throughput compared with OOK and PPM.

In chapter 5, it was shown that a CDMA system relies on a distinct signature sequence to achieve a high SIR. For the sequence to preserve its correlation properties it needs to operate in a low dispersion channel. Under such circumstances, the modulation bandwidth is limited thus affecting the system throughput in the case of OOK-CDMA compared with OOK. In the case of *h*PPM-CDMA, a higher throughput is achieved without the need for additional bandwidth. Further improvement in the throughput can be achieved using a *h*PIM-CDMA scheme, which is the subject of this chapter.

Section 6.2 will present the proposed *h*PIM-CDMA scheme. A discussion of the performance of all schemes will be given in section 6.3 followed by a summary in section 6.4.

6.2 Hybrid PIM-CDMA

Similar to PIM, *h*PIM-CDMA offers improved BEF performance. This is achieved by eliminating the redundant chips (denoted by X_k in figure 5.24) in *h*PPM-CDMA symbol [See01, Ghassemlooy01] by reducing $T_{S|hPPM-CDMA}$ in (5.25) to:

$$T_{S|hPIM-CDMA} = \left(n + S_k^i\right)T_c . \tag{6.1}$$

Each symbol is composed of a signature sequence at the beginning followed by $S_k^i T_c$ empty chips. Examples of *h*PIM-CDMA symbols modulating the same information (as in figure 5.24) as other DS-CDMA schemes are shown in figure 6.1.

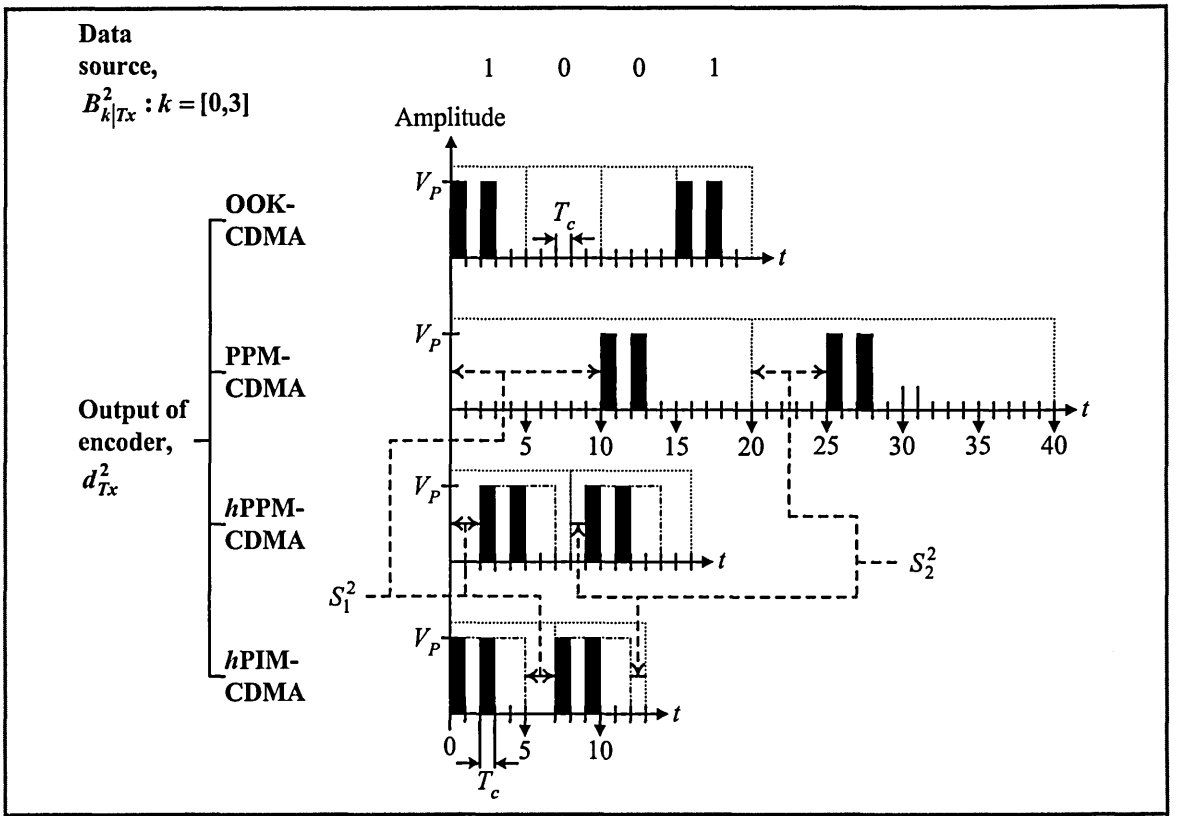

Figure 6.1: 4-*h*PIM-CDMA signal stream of 2 symbols mapping information $B_{k|Tx} = \{1\ 0\ 0\ 1\}$.

The *h*PIM-CDMA system transmitter and receiver block diagrams are shown in figure 6.2 (a) and (b) respectively. Note, the transmitter and receiver are based on a tap-delay structure. The *h*PIM signal at the output of modulator is represented as:

$$b_{Tx}^{i}\left(t-\tau_{d|Tx}^{i}\right)=V_b\sum_{k=0}^{\infty}g_c\left(t-\left(nk+\sum_{l=-1}^{k-1}S_l^i\right)T_c-\tau_{d|Tx}^{i}\right). \tag{6.2}$$

Note that the *h*PIM signal is non-periodic. This is because the start time for modulating each k^{th} symbol is determined by the previous information $\sum_{l=-1}^{k-1}S_l^i$ being modulated. Thus, as with *h*PPM-CDMA, *h*PIM-CDMA can only employ a tap-delay structure and matched filter for encoding and decoding. The encoded *h*PIM-CDMA signal can be modelled as:

$$d_{Tx}^{i}\left(t-\tau_{d|Tx}^{i}\right)=V_d\sum_{k=0}^{\infty}\sum_{j=1}^{w}g_c\left(t-cw_{(i,j)}-\left(nk+\sum_{l=-1}^{k-1}S_l^i\right)T_c-\tau_{d|Tx}^{i}\right). \tag{6.3}$$

The encoding process is shown in figure 6.2 (c).

In a multiple-access communication system, the decoded signal at the receiver can be modelled as:

$$\begin{aligned}e_{Rx}^{i}(t)=&V_d R_{Tx}^{i}R_{Rx}^{i}\sum_{k=0}^{\infty}wg_c\left(t-(n-1)T_c-\left(nk+\sum_{l=-1}^{k-1}S_l^i\right)T_c-\tau_{d|Tx}^{i}\right)\otimes h^{i|i}(t)\\&+V_d R_{Tx}^{i}R_{Rx}^{i}\sum_{k=0}^{\infty}\sum_{j=1}^{w}\sum_{J=1}^{w}g_c\left(t-cw_{(i,J)}T_c-\left(n-1-cw_{(i,j)}\right)T_c-\left(nk+\sum_{l=-1}^{k-1}S_l^i\right)T_c\right.\\&\left.-\tau_{d|Tx}^{i}\right)\otimes h^{i|i}(t)\\&+R_{Rx}^{i}\sum_{j=1}^{w}\sum_{I=1}^{F}D_{Tx}^{I}\left(t-\left(n-1-cw_{(i,j)}\right)T_c-\tau_{d|Tx}^{I}\right)\otimes h^{I|i}(t)\\&+n(t)\end{aligned} \tag{6.4}$$

where $i\neq I$, $j\neq J$ and $D_{Tx}^{I}\left(t-\tau_{d|Tx}^{I}\right)=R_{Tx}^{I}d_{Tx}^{I}\left(t-\tau_{d|Tx}^{I}\right)$. The first term is the decoded *h*PIM signal or the auto-correlated peaks and the second term is the auto-correlation constraints. The thirst term is the MAI and the last term is the Gaussian noise contribution. Observing the first term from (6.4), the decoded signal stream is delayed by $(n-1)T_c$ from the transmitting time $\tau_{d|Tx}^{i}$ due to the tap-delay structure.

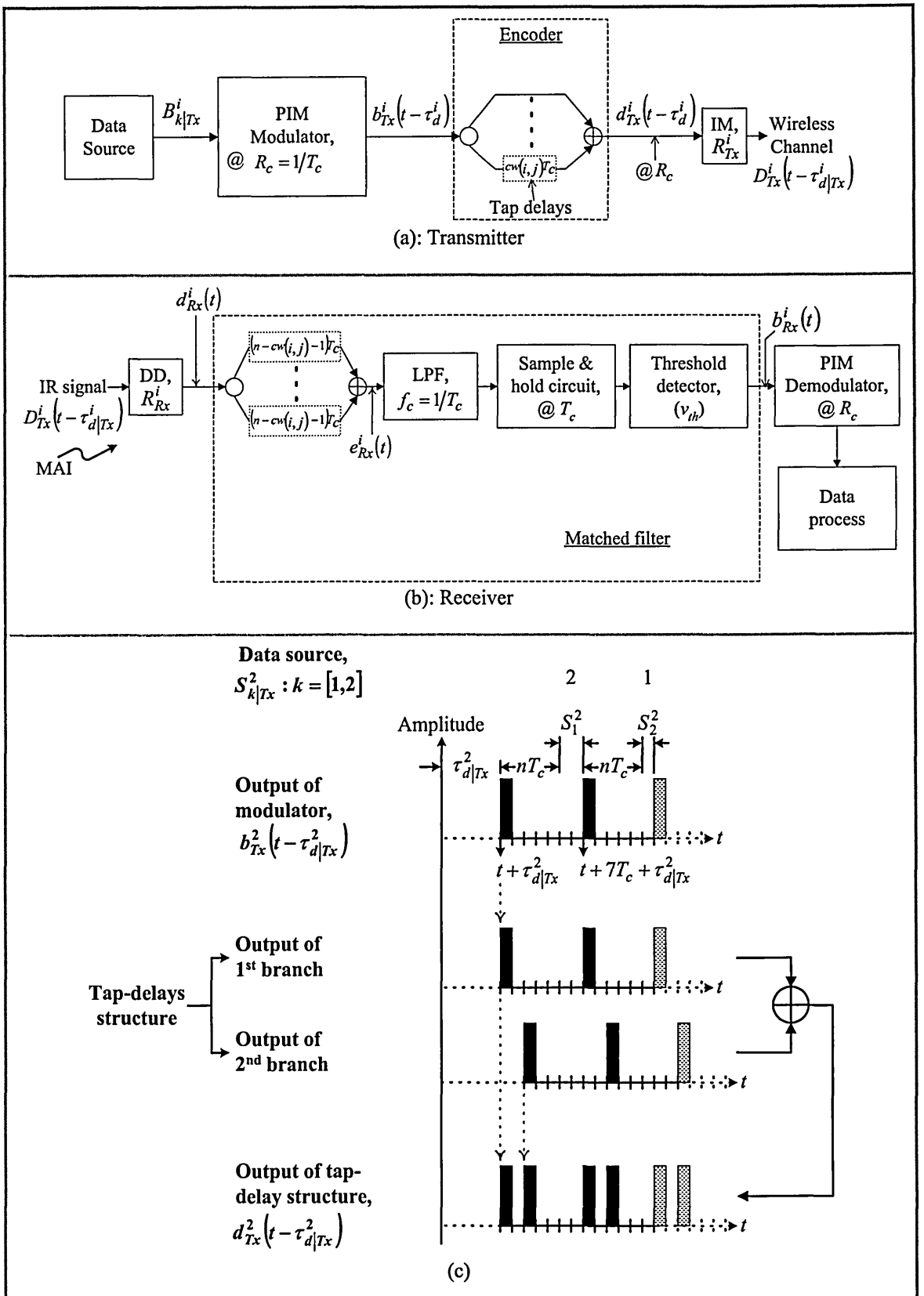

Figure 6.2: *h*PIM-CDMA; (a) transmitter block diagram, (b) receiver block diagram and (c) timing waveforms showing the process of encoding.

The recovered *h*PIM signal at the output of MF in figure 6.2 (b), assuming no MAI and Gaussian noise, is represented as:

$$b_{Rx}^{i}(t) = V_T R_{Tx}^{i} R_{Rx}^{i} \sum_{k=0}^{\infty} g_c\left(t - \left(k + \sum_{l=-1}^{k-1} S_l^i\right) T_c - \tau_{d|Tx}^{i}\right), \tag{6.5}$$

where V_T is the peak voltage of the threshold detector output. This (i.e. (6.5)) is similar to the PIM signal, and therefore the PIM demodulator developed by [Kaluarachi96a, Ghassemlooy98a, Hayes02] may be employed to recover the data from a *h*PIM signal with a minor change. Since *h*PIM symbol contains an extra $(n-1)$ chips (redundancy resulting from CDMA decoding), when the demodulator detects a pulse of $1T_c$ duration at the start of a symbol it should ignore the following $(n-1)T_c$ chips; then count the number of empty chips of $S_k^i T_c$ that correspond to the information [See01, Ghassemlooy01]. This is illustrated in figure 6.3.

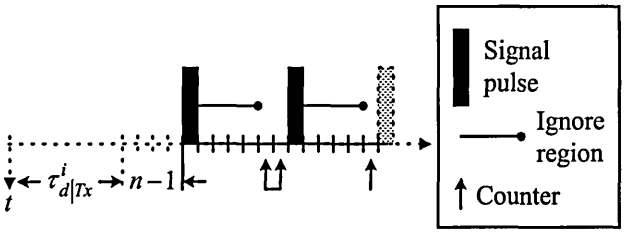

Figure 6.3: *h*PIM-CDMA signal demodulation.

Since the *h*PIM symbol length varies with the information content, the actual data rate is indeterminable. Nevertheless, the data rate can be approximated by considering the average symbol's length, and assuming that the data modulated is IID, and is given as:

$$T_{S|hPIM-CDMA} = \frac{2n + 2^M - 1}{2} T_c, \tag{6.6}$$

the average data rate is:

$$R_{b|hPIM-CDMA} = \frac{2M}{\left(2n + 2^M - 1\right) T_c}. \tag{6.7}$$

To compare this with *h*PPM-CDMA, the BEF and power efficiency of *h*PIM-CDMA normalised to *h*PPM-CDMA are investigated, and are defined respectively as:

$$BEF_{\frac{hPIM-CDMA}{hPPM-CDMA}} = \frac{2\left(n+2^M-1\right)}{2n+2^M-1}$$

$$= \frac{2\left(\left[Fw(w-1)+1\right]+2^M-1\right)}{2\left[Fw(w-1)+1\right]+2^M-1}, \tag{6.8}$$

and:

$$W_{Eff\left|\frac{hPIM-CDMA}{hPPM-CDMA}\right.} = -10\log\frac{2\left(n+2^M-1\right)}{2n+2^M-1}(\text{dB})$$

$$= -10\log\frac{2\left(\left[Fw(w-1)+1\right]+2^M-1\right)}{2\left[Fw(w-1)+1\right]+2^M-1}(\text{dB}). \tag{6.9}$$

BEF and power efficiency plotted against F and M for various w are shown in figures 6.4 and 6.5. It can be seen that *h*PIM-CDMA throughput increases as the mapping order M increases, and decreases as F increases. The BEF increases exponentially with M and will reach a peak at 2; this can easily be seen from (6.8). On the other hand, the BEF reduces to 1 as F increases. Though *h*PIM-CDMA achieves higher throughput at high value of M compared with *h*PIM-CDMA, its throughput becomes lower than OOK-CDMA. As shown in figure 6.4, *h*PIM-CDMA has a higher throughput than the *h*PPM-CDMA. This is because *h*PIM-CDMA symbol's duration varies and results in a shorter average duration. This affects *h*PIM-CDMA power efficiency, where the average signal power is higher than the *h*PPM-CDMA, which has fixed and longer symbol duration. Referring to figure 6.5, *h*PIM-CDMA power efficiency performance is in contrast to its BEF performance and in the worst-case reaches $-3\,\text{dB}$. Correspondingly the BEF best performance will peak at 2. As the code weight w increases, the BEF performance gradually degrades but power efficiency improves.

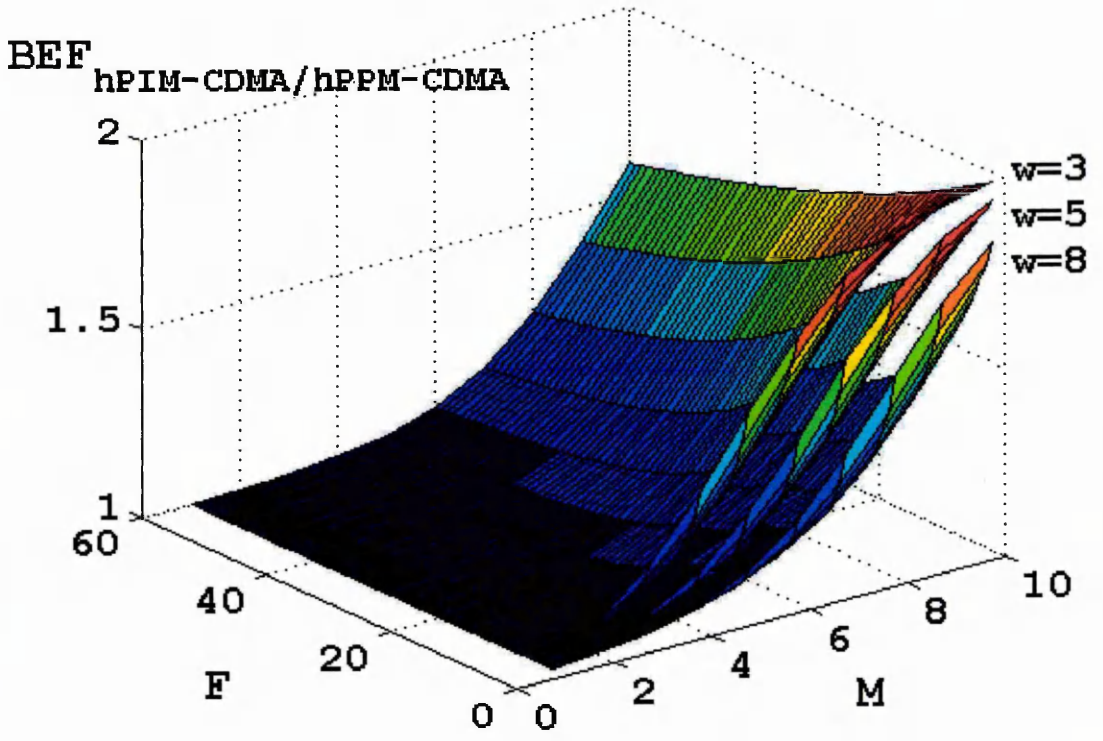

(i) 0° rotation

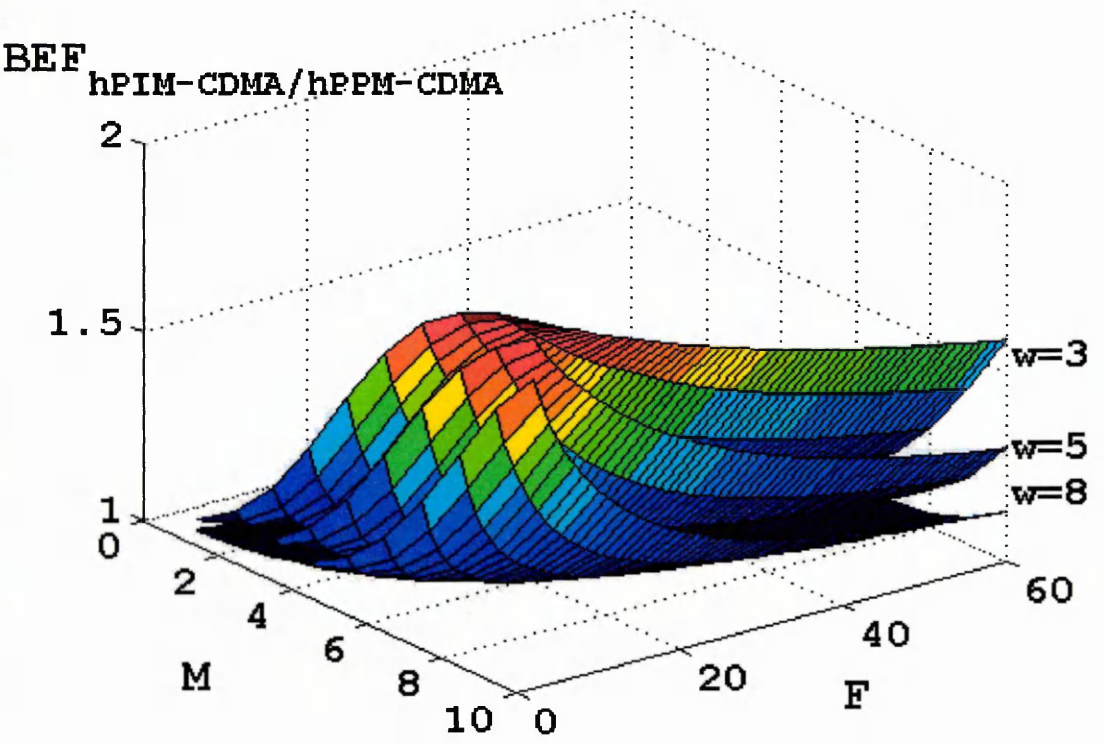

(ii) 90° rotation

Figure 6.4: BEF performance, of *h*PIM-CDMA normalised to *h*PPM-CDMA, against F and M for $w = 3, 5$ and 8 .

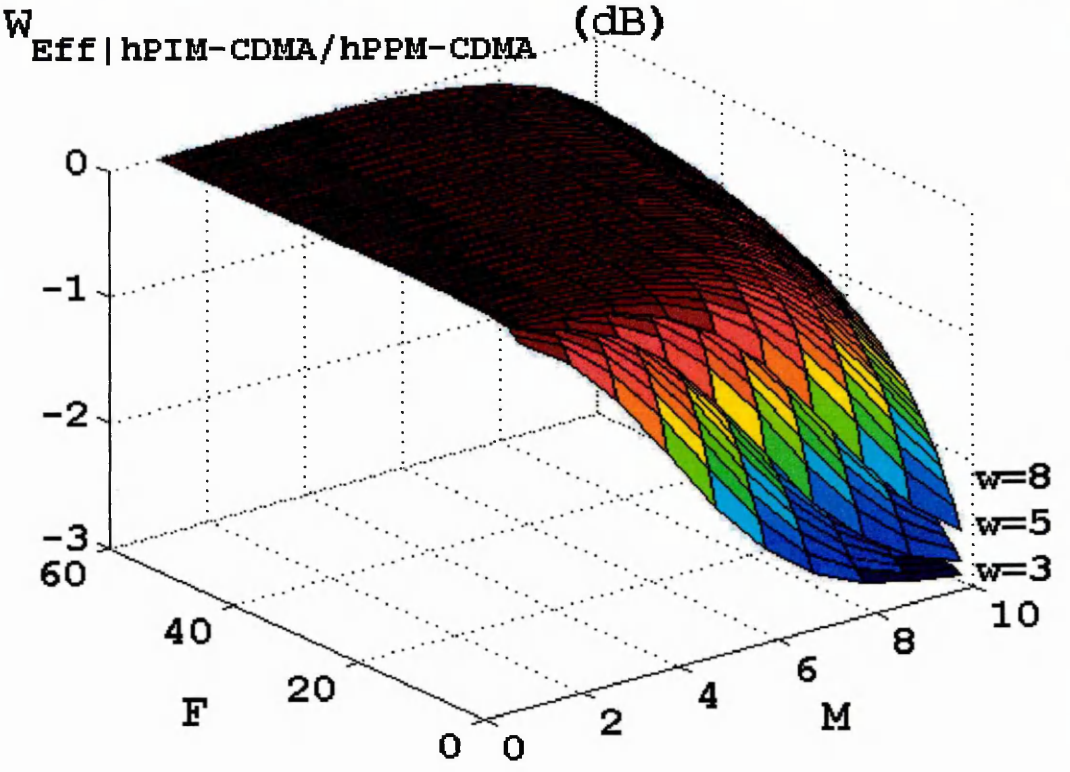

(i) 0° rotation

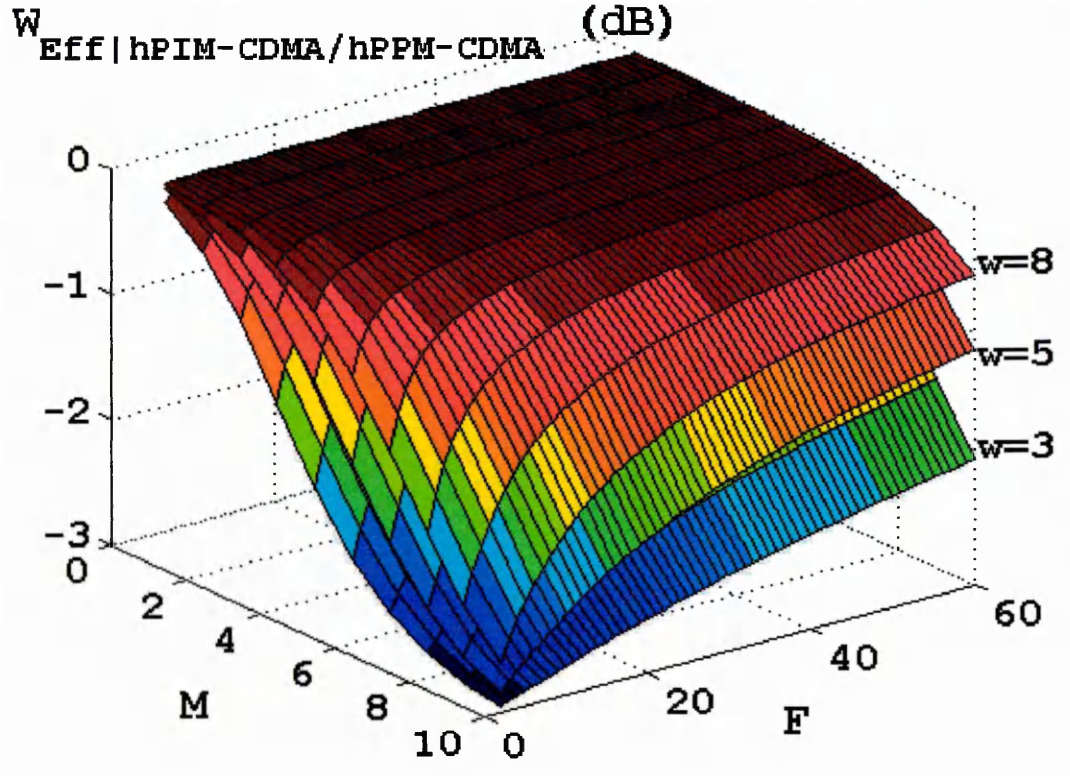

(ii) 90° rotation

Figure 6.5: Power efficiency performance, of *h*PIM-CDMA normalised to *h*PPM-CDMA, against F and M for $w = 3, 5$ and 8.

6.3 Comparison of DS-CDMA systems

In this section, further investigations and comparisons of BEF and power efficiency of OOK-CDMA, PPM-CDMA, *h*PPM-CDMA and *h*PIM-CDMA normalised to OOK for optical wireless environment are presented. It is assumed that all schemes have the same pulse duration $T_{c|0.3}$ limited by $D_{T|0.3}=0.3$ and peak optical power of W_P. The codeword set used in the following analysis is optimal $(n,8,1,1)$ OOC. In addition, all transmitted information is assumed IID. The power entering the neighbouring chip due to dispersion is assumed to be very small (i.e. $\leq 10\%$ of the total power). Since the steps for determining BEF and W_{Eff} are similar for all modulation schemes, only an analysis for *h*PIM-CDMA scheme is presented here. The others' BEF and W_{Eff} are tabulated in table 6.1.

The average optical power for OOK signal is:

$$W_{ave|OOK}=\frac{W_P T_{c|0.3}}{2T_{c|0.3}}=\frac{W_P}{2}. \tag{6.10}$$

*h*PIM-CDMA symbol consists of only one signature sequence of w pulses, thus the average optical power for one user is given as:

$$W_{ave|hPIM-CDMA}=\frac{2wW_P}{\left(2n+2^M-1\right)}. \tag{6.11}$$

Considering all F simultaneous users, the power efficiency of *h*PIM-CDMA normalised to OOK is given as:

$$W_{Eff}\Big|_{\frac{hPIM-CDMA}{OOK}}=-10\log\frac{4wF}{2n+2^M-1}(\text{dB}). \tag{6.12}$$

The normalised BEF is given by:

$$BEF_{\frac{hPIM-CDMA}{OOK}}=\frac{R_{b|hPIM-CDMA}}{R_{b|OOK}}$$

$$=\frac{\frac{2MR_{c|0.3}}{2n+2^M-1}}{R_{c|0.3}}=\frac{2M}{2n+2^M-1}. \tag{6.13}$$

System	W_{Eff}	BEF
OOK-CDMA	$-10\log\frac{wF}{n}(\text{dB})$	$\frac{1}{n}$
PPM-CDMA	$-10\log\frac{2wF}{n2^M}(\text{dB})$	$\frac{M}{n2^M}$
*h*PPM-CDMA	$-10\log\frac{2wF}{n+2^M-1}(\text{dB})$	$\frac{M}{n+2^M-1}$
*h*PIM-CDMA	$-10\log\frac{4wF}{2n+2^M-1}(\text{dB})$	$\frac{2M}{2n+2^M-1}$

Table 6.1: Power efficiency and BEF expressions for various DS-CDMA schemes normalised to OOK. *Note that $n=Fw(w-1)$ for optimal $(n,w,1,1)$ OOC.

Figure 6.6 shows W_{Eff} against F and M for $w=8$ for all the four schemes. As can be seen, all the schemes achieve higher power efficiency with PPM-CDMA being the best followed by OOK-CDMA, *h*PPM-CDMA and *h*PIM-CDMA. For the hybrid schemes, power efficiency is highly dependent on the set of signature sequences that one could use and the bit resolution M. As shown in figure 6.7, the hybrid schemes average transmitted power is low by employing optimum $(n,w,1,1)$ OOC of $w\geq 4$. For $w=3$, the average power is low at low values of F but the power efficiency decreases to near 0, as F tends to infinity. For $w=2$, which is not shown in figure 6.7, *h*PIM-CDMA achieves no power efficiency change relative to OOK.

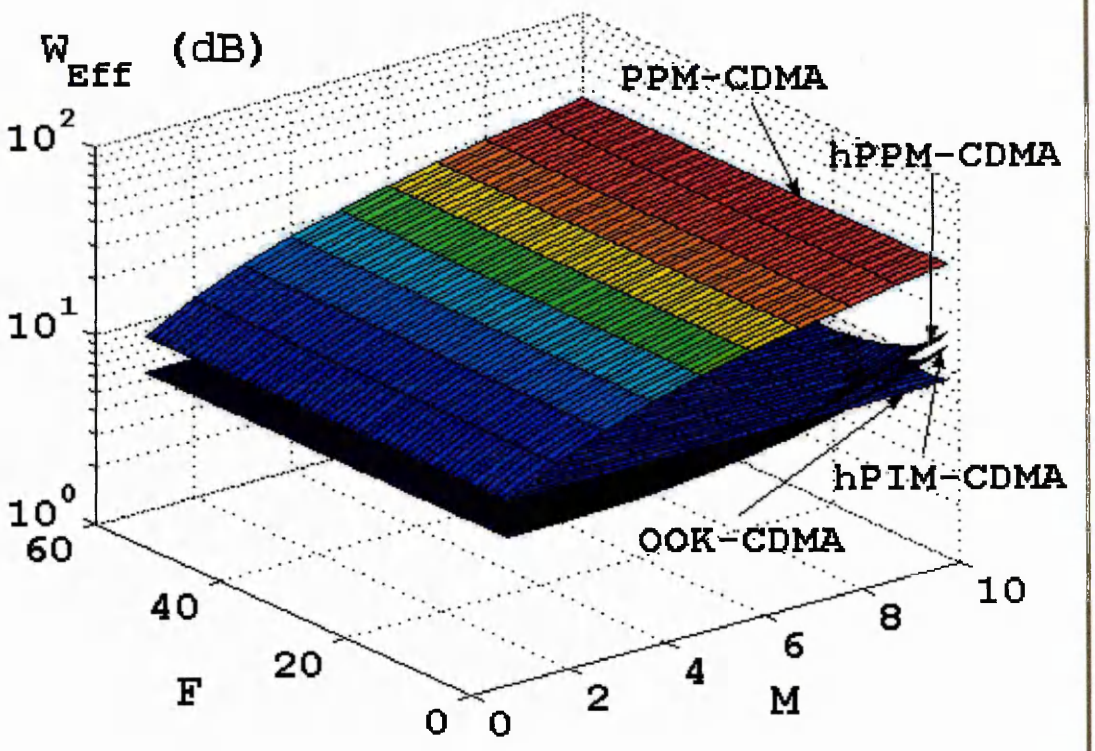

(i) 0° rotation

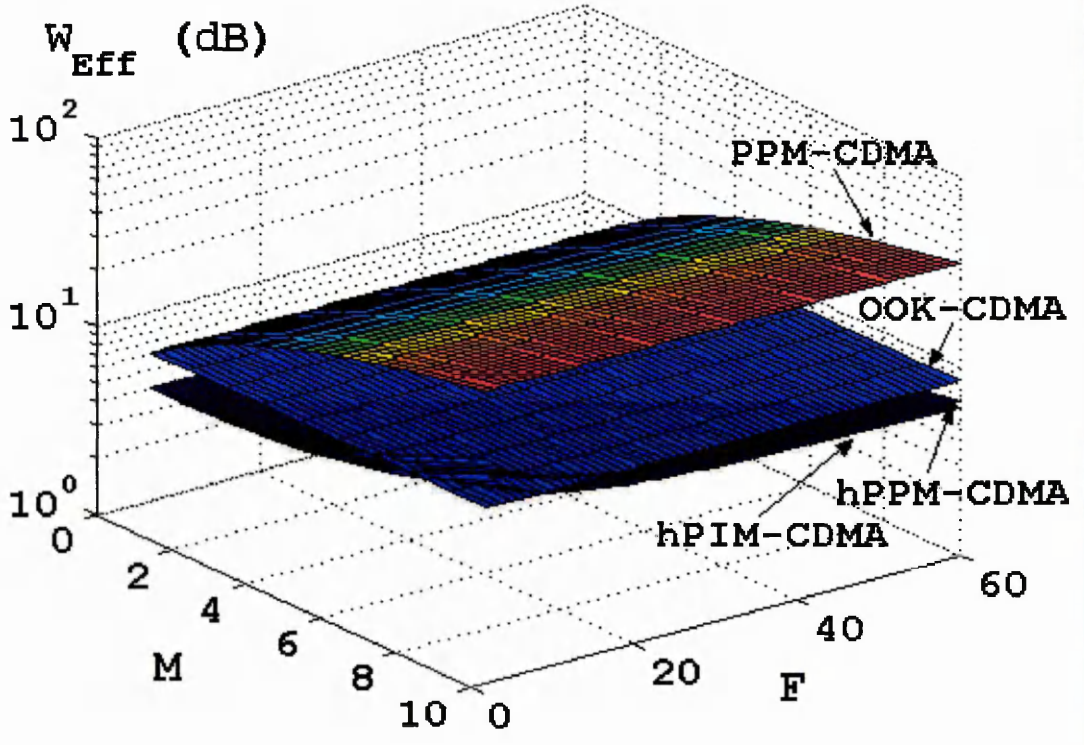

(ii) 90° rotation

Figure 6.6: Power efficiency performance normalised to OOK, against F and M for $w = 8$.

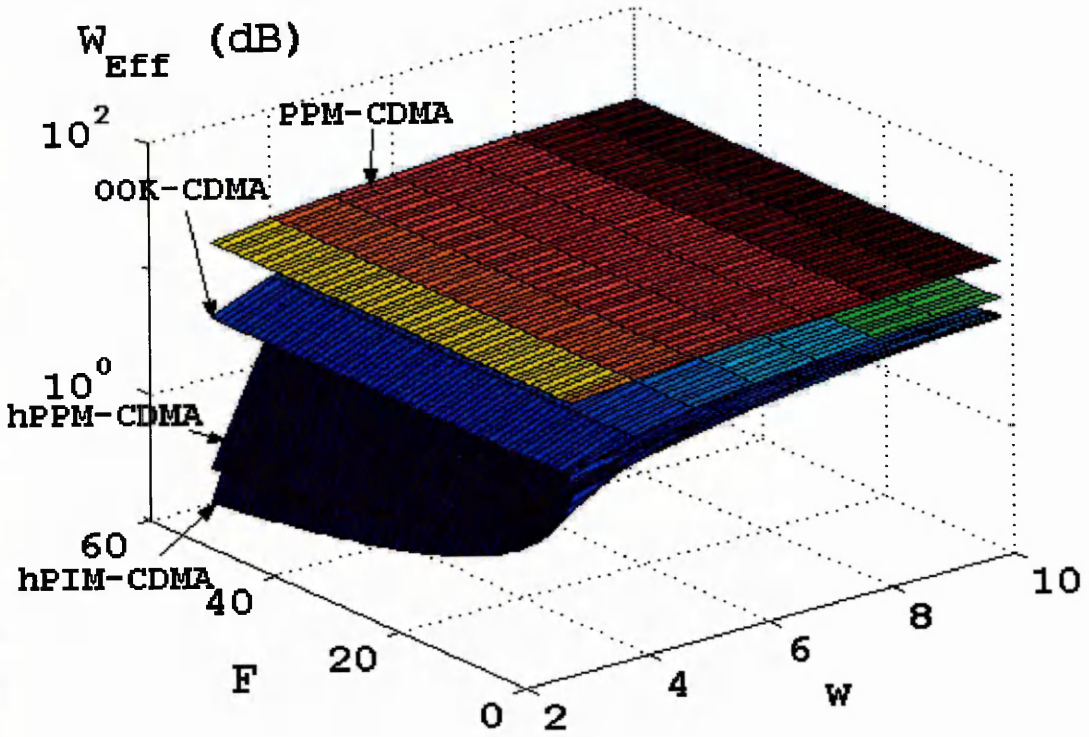

(i) 0° rotation

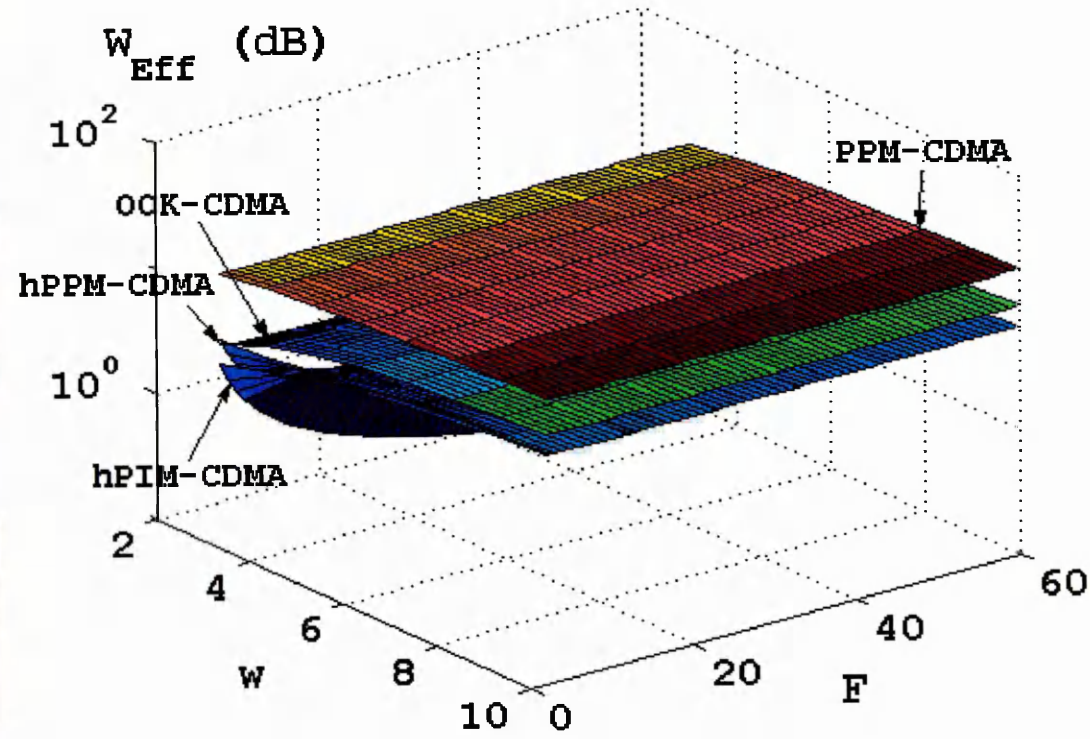

(ii) 90° rotation

Figure 6.7: Power efficiency performance normalised to OOK, against F and w for $M = 4$.

The BEF against F and M for $w=8$ for all schemes are shown in figure 6.8. As observed, for all schemes the BEF is below 1, which means that their throughput is lower than OOK. The lowest performance is displayed by PPM-CDMA followed by OOK-CDMA. *h*PIM-CDMA and *h*PPM-CDMA show a similar behaviour offering higher BEF as expected (where *h*PIM-CDMA is the highest). Increasing F will gradually deteriorate the BEF of all schemes. For PPM-CDMA, increasing M will reduce the BEF severely, whereas for OOK-CDMA, the BEF is unchanged. For both hybrid schemes the BEF will increase with M, then reach an optimum point and decrease as M increase further. Eventually, both hybrid BEFs will fall below the OOK-CDMA BEF as M tends toward infinity. Such behaviour has resulted in both hybrids BEF having a saddle shape. Figure 6.9 shows the BEF against F and w, for $M=4$, and for all schemes. Once again, *h*PIM-CDMA displays the best performance. The BEF for all schemes has the same behaviour, which decreases as F and w increasing. In figure 6.10, only the *h*PIM-CDMA BEF is shown for various values of w. As can be seen, the BEF profiles for all values of w are a saddle shape, which will mean that choosing a low value of M on the left of BEF_{OP} gives a similar BEF as compared to a high value of M chosen from the right of BEF_{OP}. The optimum point of each saddle is slightly different and is determined from n and 2^M, this may be defined as:

$$z_{BEF} = \frac{\text{Sequence length - 1}}{\text{Information length}} = \frac{n-1}{2^M - 1}. \qquad (6.14)$$

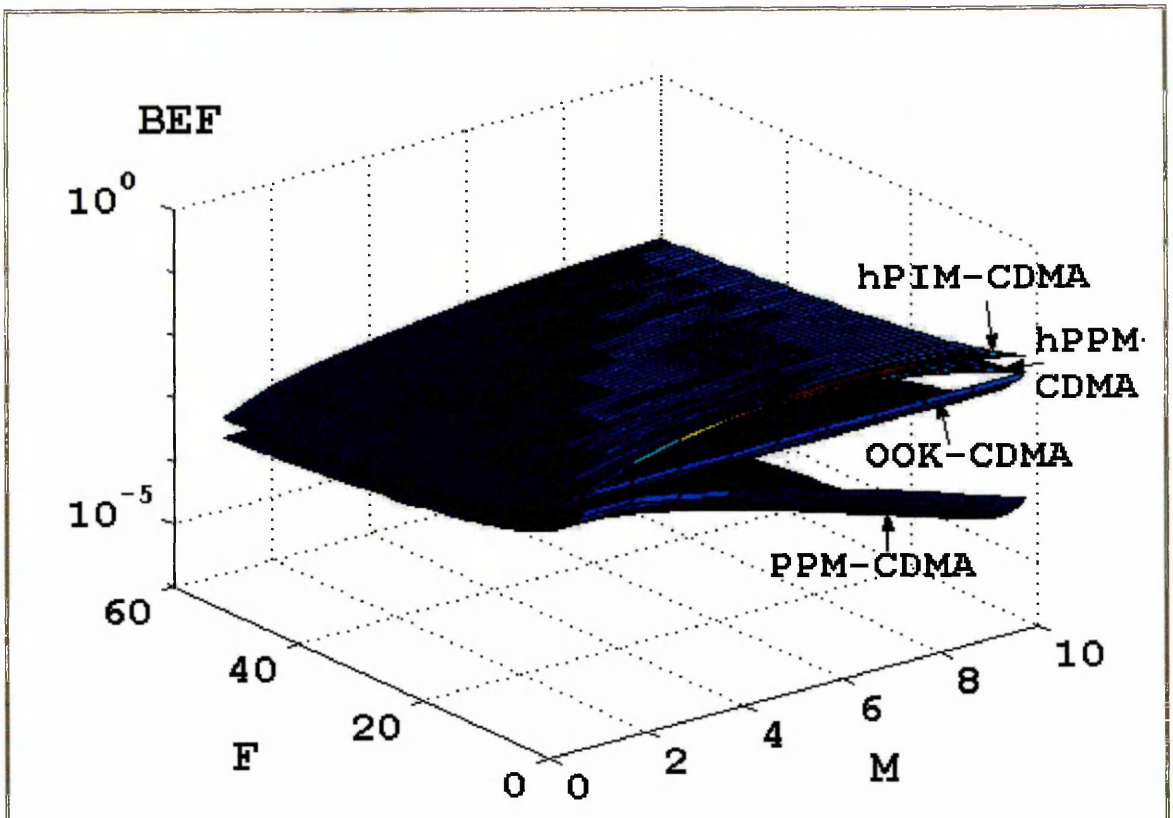

(i) 0° rotation

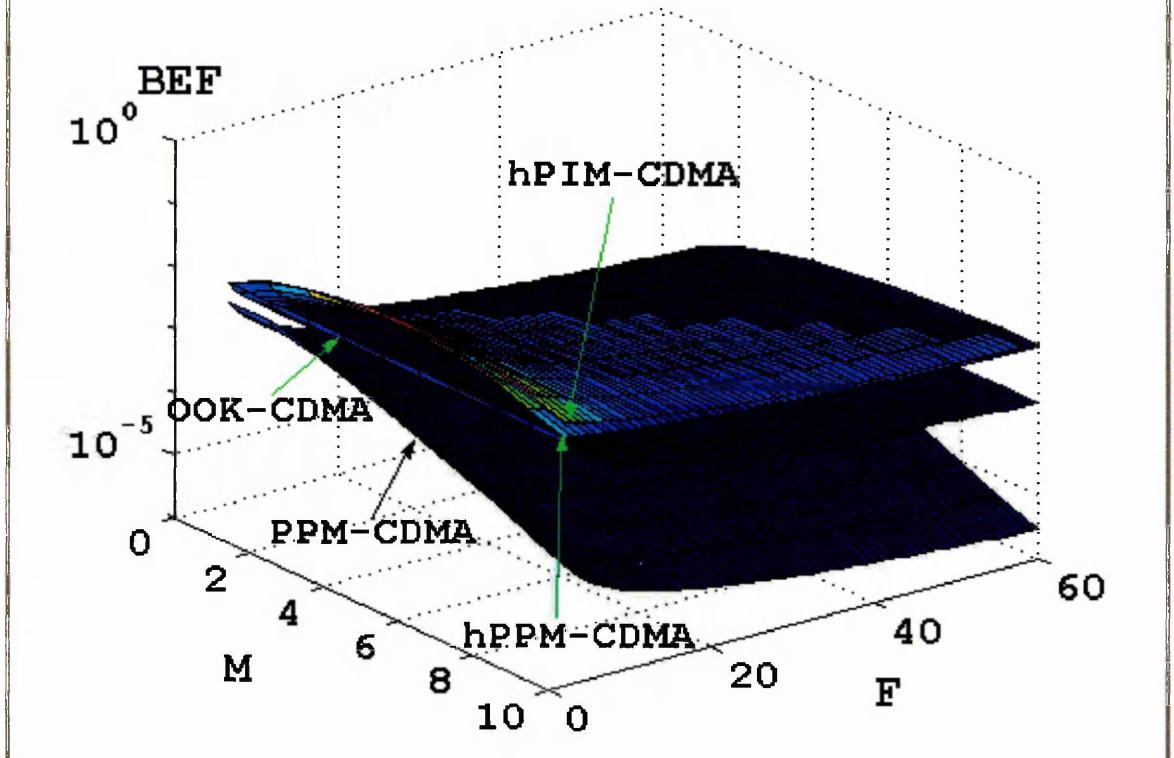

(ii) 90° rotation

Figure 6.8: BEF performance normalised to OOK, against F and M for $w = 8$.

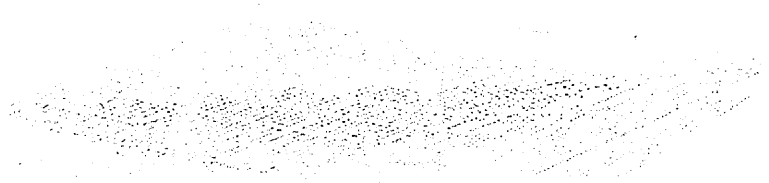

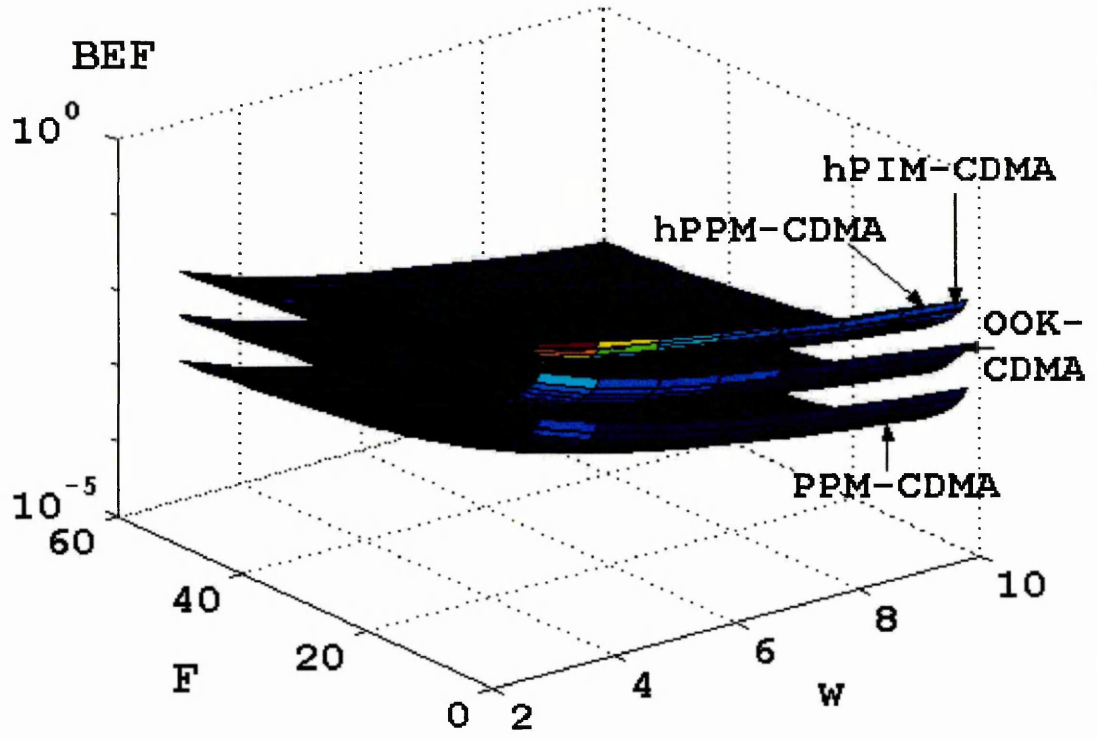

(i) 0° rotation

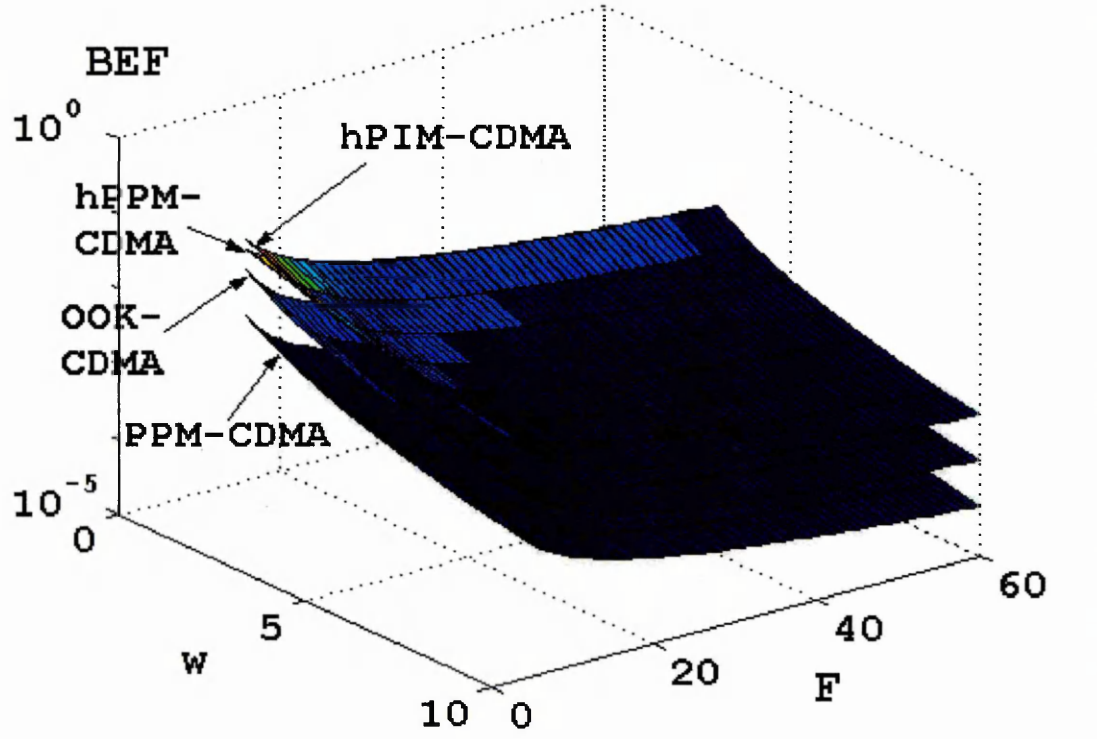

(ii) 90° rotation

Figure 6.9: BEF performance normalised to OOK, against F and w for $M = 4$.

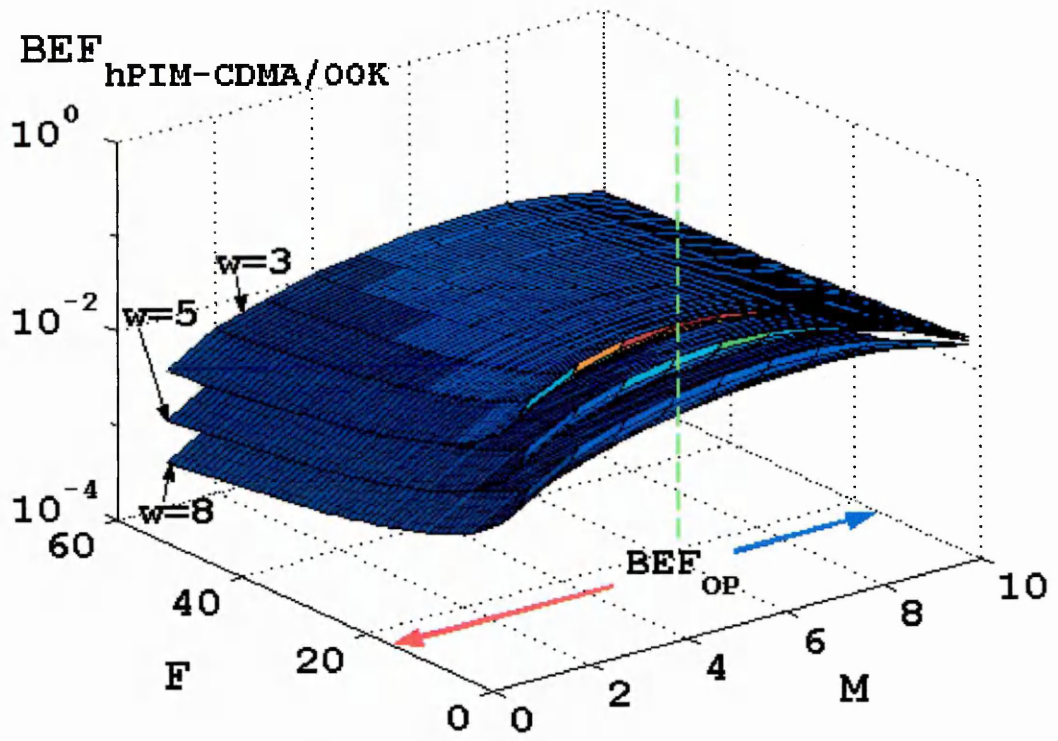

(i) 0° rotation

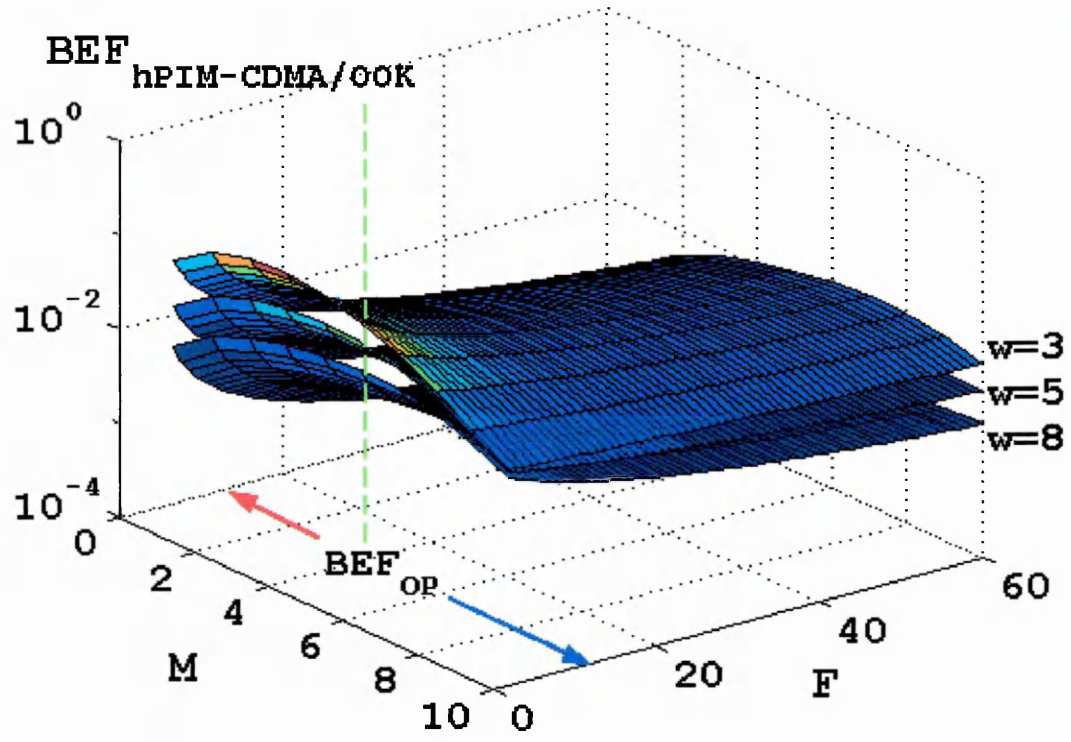

(ii) 90° rotation

Figure 6.10: BEF performance, of *h*PIM-CDMA normalised to OOK, against F and M for $w = 3, 5$ and 8.

*BEF_{OP} (BEF optimum point) is not drawn to scale and it does not represent the exact location of an optimum point. It is only used as a reference.

Figure 6.11 shows the z_{BEF} against F for various w. As can be seen, z_{BEF} is non-linear and is difficult to obtain analytically. However, it is obtained from simulation by searching for the optimum points, the corresponding values of n and M are then substituted in (6.14). The results shown provide enough information to evaluate the BEF performance of *h*PIM-CDMA for a given BER, which will be discussed in chapter 7. The area above the curves represents the region of low value M (to the left of BEF_{OP} in figure 6.10) and the area below the curves represents the region of high value M (to the right of BEF_{OP} in figure 6.10).

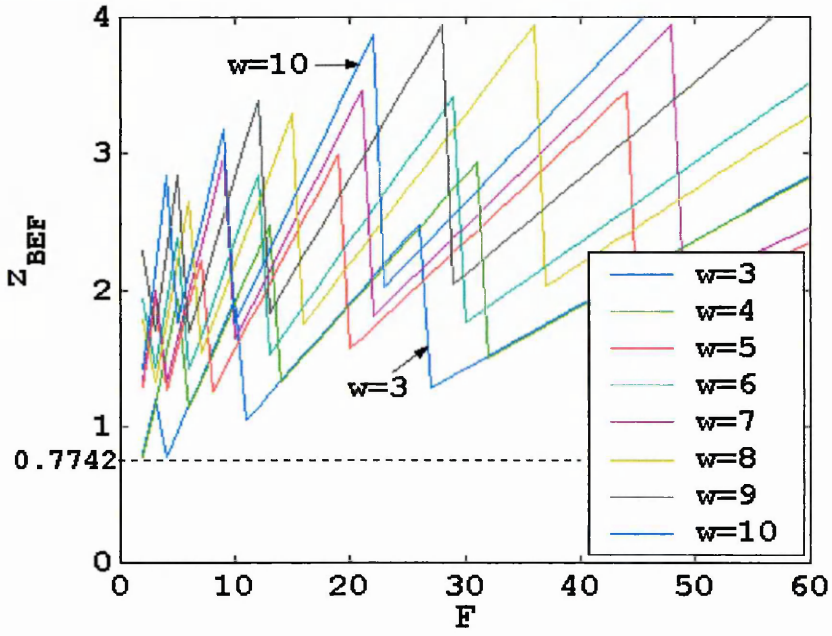

Figure 6.11: The ratio of sequence length over information length of optimum BEF, of *h*PIM-CDMA system.

As indicated earlier in this section, the improvement in W_{Eff} and BEF depends on the set of signature sequences used. In chapter 4, a number of signature sequences were presented, amongst them, PS(P) has the shortest sequence length and largest code weights and this will affect both the BEF and power efficiency of any DS-CDMA system. To investigate this, the performances of *h*PIM-CDMA using PS(P) signature sequences are investigated and are compared with OOK-CDMA. The performances of *h*PPM-CDMA will not be shown since they display similar characteristics to *h*PIM-CDMA. Figure 6.12 shows the power efficiency against F and w for a range of bit resolution M. Note that $F = w = P$ and $n = P^2$ for PS(P) codes.

As a result, the *h*PIM-CDMA power efficiency decreases exponentially as F and w increase and will fall below zero. For low values of F and w (i.e. <20), the power efficiency improves when $M > 3$. Referring to (6.12), smaller M (*h*PIM-CDMA symbol length is shorter) and larger w (more optical power per *h*PIM-CDMA symbol), the denominator will dominates and leading to a reduced power efficiency. As M increases, the (6.12) denominator will dominate (i.e. the average optical power reduces as symbol length increases) and the power efficiency will improve. As F and w increase toward infinity, the power efficiency for all values of M will go below zero and reaches a steady state at $-10\log 2(\mathrm{dB})$. For OOK-CDMA using PS(*P*), the power efficiency is constant as in OOK.

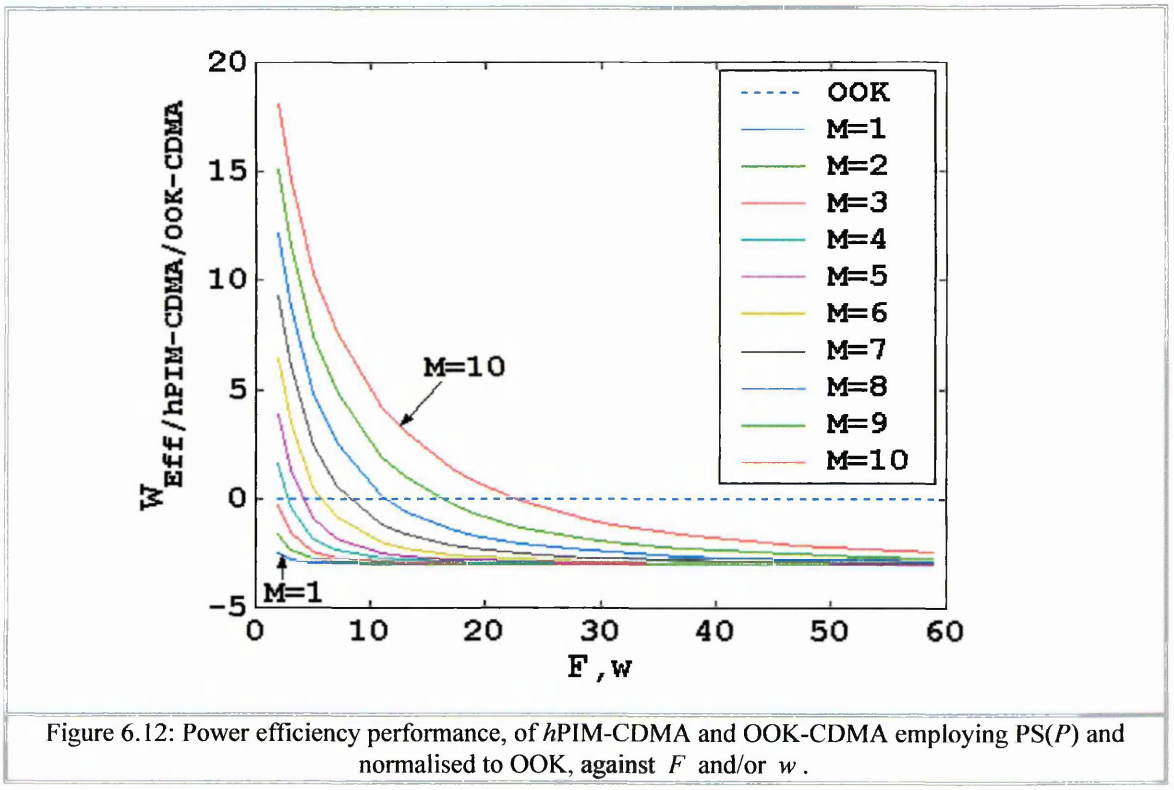

Figure 6.12: Power efficiency performance, of *h*PIM-CDMA and OOK-CDMA employing PS(*P*) and normalised to OOK, against F and/or w.

Figure 6.13 shows the BEF against F, w and M for *h*PIM-CDMA and OOK-CDMA schemes employing PS(*P*) codes. For low value of F and w (i.e. 3), and for $M = 1$, *h*PIM-CDMA the BEF (of value 0.2222) is lower than the OOK-CDMA (of value 0.25). As M increases, *h*PIM-CDMA BEF improves and will reach an optimum point. It then decreases as M increases further and eventually falls below OOK-CDMA again, and falling exponentially. This is because the PS(*P*) sequence length is shorter for smaller value of F and w when $M = 1$, hence

the OOK-CDMA symbol length will be shorter than the *h*PIM-CDMA symbol. As M increases, the *h*PIM-CDMA symbol length increases however the number of information bits carried by one *h*PIM-CDMA symbol is a multiple of the number (which is one bit only) carried by one OOK-CDMA symbol. Thus, a *h*PIM-CDMA BEF is achieved due to the data compression. As M keeps on increasing, the *h*PIM-CDMA BEF will deteriorate when it has reached an optimum point, as the symbol length becomes longer than the number of bits it compresses, compared with the OOK-CDMA. For $M=1$, *h*PIM-CDMA BEF is lower than the OOK-CDMA for small values of F and w (i.e. <17). When F and w are larger than 17, *h*PIM-CDMA BEF will coincide with the OOK-CDMA BEF. For a larger value of M (e.g. value of 10), the *h*PIM-CDMA BEF is lower than the OOK-CDMA for a F and w less than 7, it does become higher than OOK-CDMA when F and w increase further. Both BEF will decrease gradually as F and w tend toward infinity, but with *h*PIM-CDMA BEF always higher than the OOK-CDMA. At larger F and w, the sequence is much longer than the information length in one *h*PIM-CDMA symbol and so *h*PIM-CDMA scheme able to compress more data.

Figure 6.14 shows the BEF performance of *h*PIM-CDMA against F, w and M using PS(*P*) and optimal $(n,8,1,1)$OOC. The results are obtained using (6.13), where the F, w and M are varied for PS(*P*) but F and M are various but $w=8$ for $(n,8,1,1)$OOC. Note that the BEF profile employing PS(*P*) is similar to that for optimal $(n,w,1,1)$OOC, with the PS(*P*) BEF performance considerably higher at low values of F, w and M as compared with optimal $(n,8,1,1)$OOC. At high values of F, the BEF of optimal $(n,8,1,1)$OOC is higher than PS(*P*). In figure 6.10, it was shown that a lower value of w with an optimal $(n,w,1,1)$OOC would have a higher BEF performance than a higher value of w. Therefore *h*PIM-CDMA employing a low w with an optimal $(n,w,1,1)$OOC will have BEF closer to the PS(*P*) at low values of F, and the BEF will be higher than PS(*P*) at high values of F.

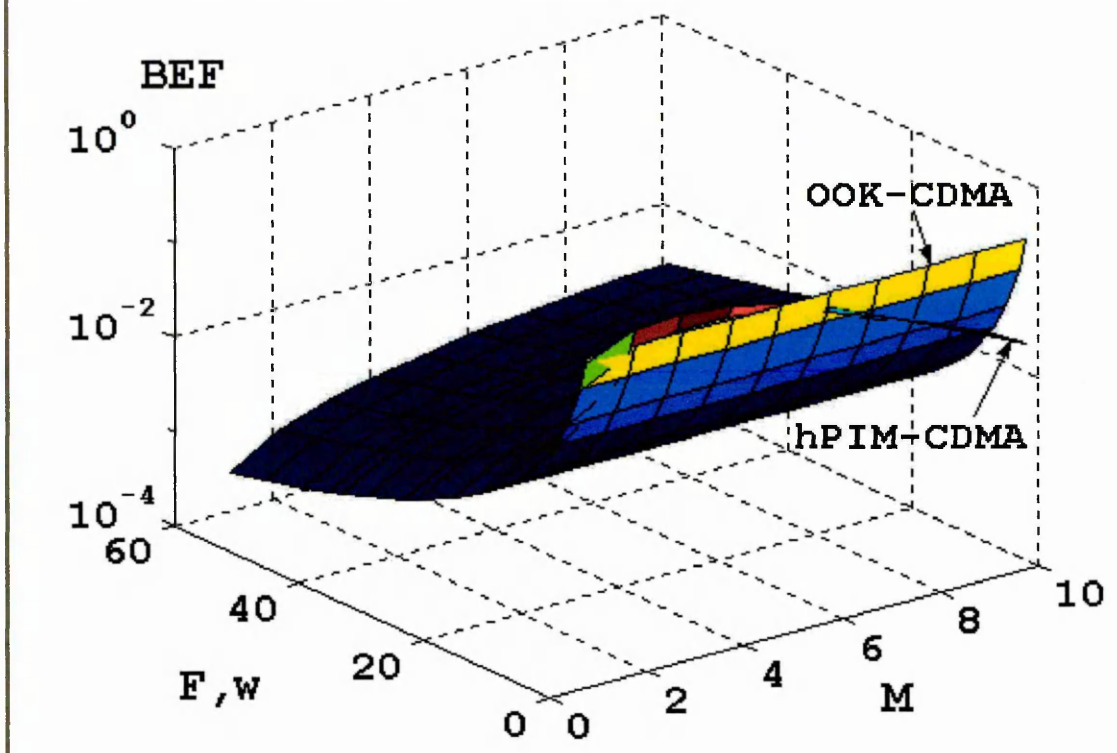

(i) 0° rotation

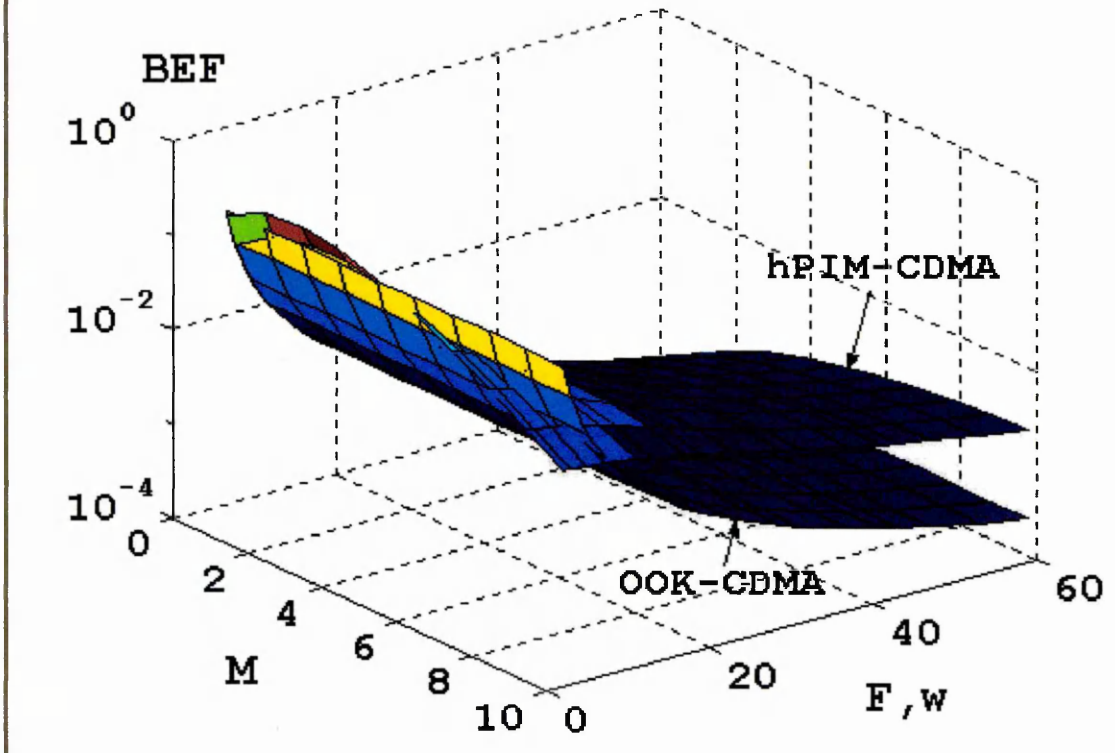

(ii) 90° rotation

Figure 6.13: BEF performance, of *h*PIM-CDMA and OOK-CDMA employing PS(P) and normalised to OOK, against F and/or w and M.

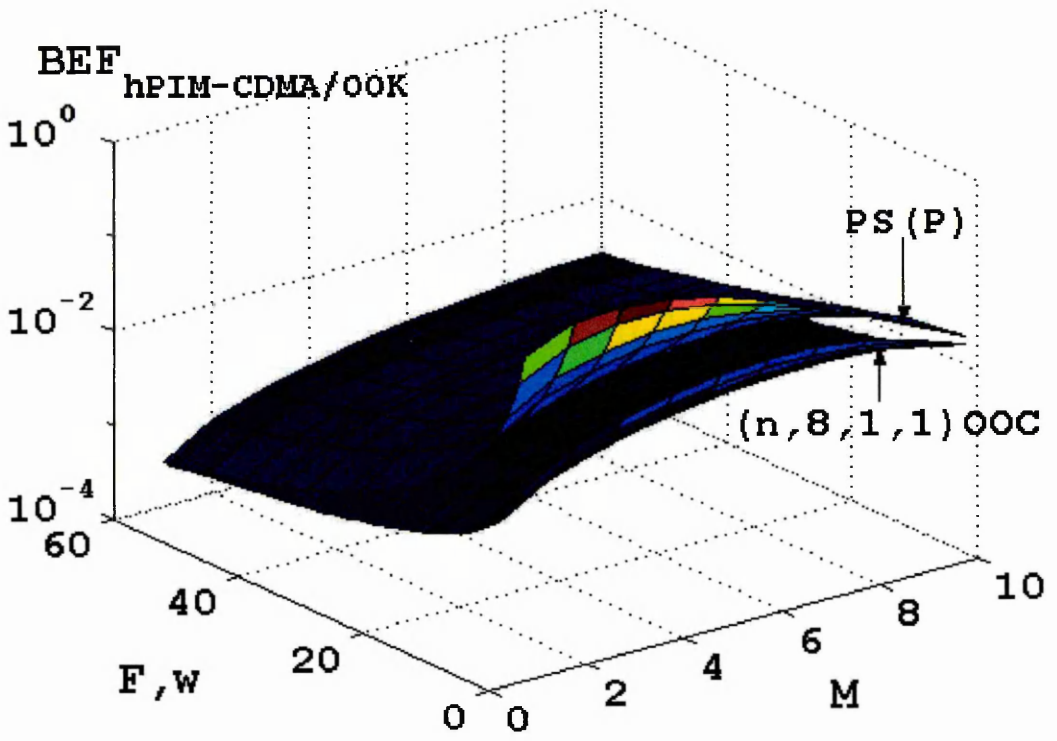

(i) 0° rotation

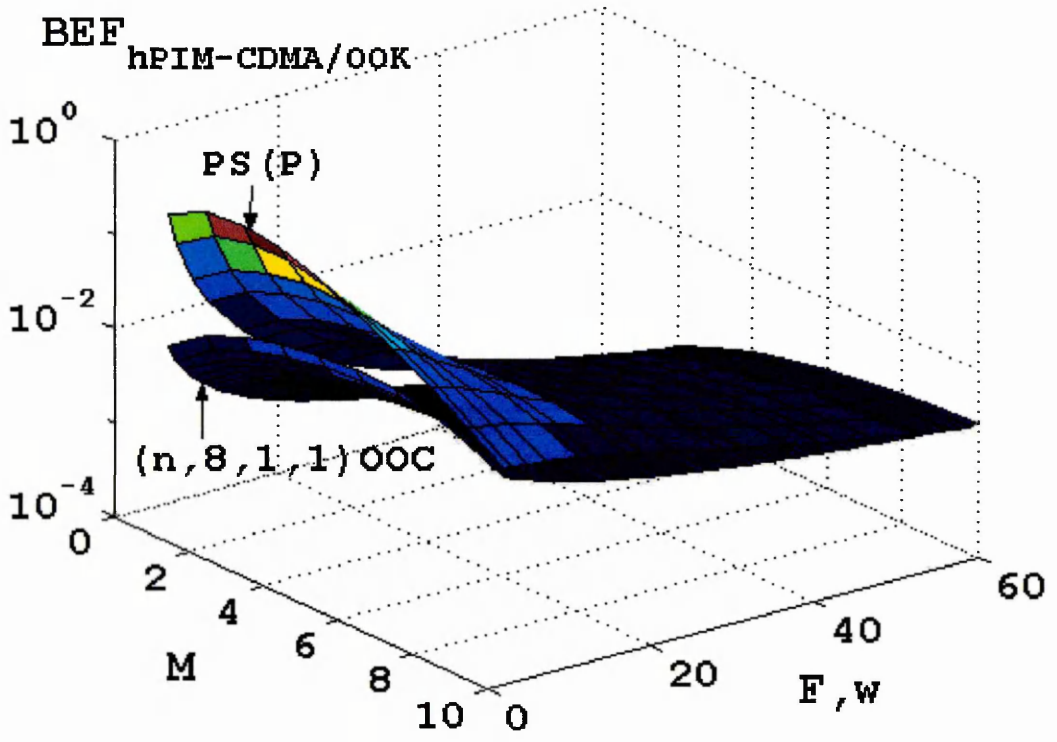

(ii) 90° rotation

Figure 6.14: BEF performance, of *h*PIM-CDMA employing PS(P) and optimal $(n,8,1,1)$OOC and normalised to OOK, against F and/or w and M.

6.4 Summary

In this chapter, the basic principle of proposed *h*PIM-CDMA, and its BEF and power efficiency compared with OOK-CDMA, PPM-CDMA and *h*PPM-CDMA were presented. It was shown that *h*PIM-CDMA offers improved system throughput with lower power efficiency as compared with OOK-CDMA, PPM-CDMA and *h*PPM-CDMA. The *h*PIM-CDMA power efficiency is higher compared with OOK.

The *h*PIM-CDMA system is simple to implement compared with OOK-CDMA, PPM-CDMA and *h*PPM-CDMA, as it does not require symbol synchronisation at the demodulation. However it does require fine synchronisation at the CDMA decoder to generate high magnitude pulses at the decoder output.

Chapter 7

ERROR RATE ANALYSIS OF *h*PIM-CDMA

7.1 Introduction

A CDMA system can be classed as synchronous, asynchronous or fully asynchronous modes. The error rate performance of each mode is different even when the same set of signature sequences is used [Salehi89b, Kwong91]. Synchronous OOK-CDMA systems employing a modified version of PS(*P*) can accommodate an extra $P^2 - P$ users compared to its equivalent asynchronous system. It has been shown that in certain same cases with more than P users transmitting simultaneously, the synchronous system can have lower error rate [Kwong91, Nikolajević98b, Liu01]. This is because any set of PS(*P*) sequences are always orthogonal to each other with in-phase auto-correlation. Whereas, an asynchronous OOK-CDMA system employing PS(*P*) will have a very high error rate owing to the code property $\lambda_c \leq 2$, thus producing severe MAI [Kwong91].In addition, the property $\lambda_a \leq 4$ is high which affects the phase synchronisation. When using a set of sequences with improved properties such as $(n, w,1,1)$OOC this will lower the error rate, as $\lambda_c = 1$ and $\lambda_a = 1$ are the minimum values. Apart from employing a set of sequences with improved properties, the error rate can be further reduced by changing the mode from asynchronous to fully asynchronous [Salehi89b]. The error rate characteristics are similar with the asynchronous mode one being the upper bound and the fully asynchronous one being the lower bound.

In a *h*PIM-CDMA system employing $(n, w,1,1)$SOOC, the distribution of MAI and self-interference are found to be binomial, whereas employing $(n, w,1,1)$OOC, the distribution is

multinomial. In this chapter, the error rate performance of asynchronous *h*PIM-CDMA employing $(n,w,1,1)$SOOC is investigated, and the investigation for employing $(n,w,1,1)$OOC is left for future work as outlined in chapter 8. In carrying out the analysis, a number of assumptions were made such as:

i. Chip is synchronous between transmitters and receivers
ii. The dominant interferences are due to self-interference and MAI, and Gaussian noise is considered negligible
iii. Near-far effect is not taken into account. For this, the channel response $h^{I|i}(t)$ is considered ideal for $D_T \leq 0.3$; V_d, $R_{Tx}^i \times R_{Rx}^i$ and $G_{OC}^{I|i}$ are equal to unity

The chapter is organised into three main sections. Section 7.2 will present a comprehensive BER analysis for *h*PIM-CDMA. The BER expression for *h*PPM-CDMA presented in [Elmirghani94] does not include self-interference and the type of *h*PPM-CDMA demodulation employed. In this section, a new modified expression for *h*PPM-CDMA is given. The BER performance of *h*PIM-CDMA will be discussed and compared with OOK-CDMA and *h*PPM-CDMA. Section 7.3 will present an analysis for the three DS-CDMA system's BER (that is Binomial) using Gaussian approximation. For OOK-CDMA, Gaussian approximation is often used in some reports by assuming the MAI is large. However, this assumption is not good enough as there are certain mandatory conditions. These conditions will be studied based on OOK-CDMA and the results obtained can be equally applied to *h*PIM-CDMA and *h*PPM-CDMA. Section 7.4 is devoted to the summary of this thesis.

7.2 Analysis of Asynchronous *h*PIM-CDMA

Substituting (6.3) into (6.4) and considering the assumptions made, the decoded signal is given as:

$$
\begin{aligned}
e^{i}_{Rx}(t) = &\sum_{k=0}^{\infty} w g_c\left(t-(n-1)T_c-\left(nk+\sum_{l=-1}^{k-1}S^{i}_{l}\right)T_c-\tau^{i}_{d|Tx}\right) \\
&+\sum_{k=0}^{\infty}\sum_{j=1}^{w}\sum_{J=1}^{w} g_c\left(t-cw_{(i,J)}T_c-\left(n-1-cw_{(i,j)}\right)T_c-\left(nk+\sum_{l=-1}^{k-1}S^{i}_{l}\right)T_c-\tau^{i}_{d|Tx}\right) \\
&+\sum_{k=0}^{\infty}\sum_{j=1}^{w}\sum_{J'=1}^{w}\sum_{I=1}^{F} g_c\left(t-cw_{(I,J')}T_c-\left(n-1-cw_{(i,j)}\right)T_c-\left(nk+\sum_{l=-1}^{k-1}S^{I}_{l}\right)T_c-\tau^{I}_{d|Tx}\right),
\end{aligned}
\tag{7.1}
$$

where $i \neq I$ and $j \neq J$. The first term is the decoded hPIM-CDMA signal, the second term is the self-interference (or auto-correlation constraint); and the third term represents the MAI.

$(n,w,1,1)$SOOC is designed such that λ_a and λ_c are always 1 for aperiodic systems. Observing the second term in (7.1), there are $w-1$ pulses, represented by J, whose positions do not match with the w tap-delay lines, represented by j, this produces $w(w-1)$ uncorrelated pulses of amplitude $\lambda_a = 1$ at the output of the MF detector. Note from section 4.3, all pulses in $(n,w,1,1)$SOOC are located within the first half region of $n/2$, consequently at the output of the MF detector, the $w(w-1)$ pulses will spread into two regions of duration $(n-1)/2$ chips alongside the signal pulse, see figure 7.1. From (7.1), the distance (rather than the delay) that the uncorrelated pulses will spread is given as:

$$
D_{Spread} = cw_{(i,J)} + \left(n-1-cw_{(i,j)}\right). \tag{7.2}
$$

As the chip duration T_c is irrelevant it has been omitted here. The length where all the $w(w-1)$ uncorrelated pulses are contained, is given as:

$$
D_{L|Spread} = D_{Spread|\max} - D_{Spread|\min}, \tag{7.3}
$$

where the shortest distance $D_{Spread|\min}$ is determined by substituting $\min\left(cw_{(i,J)}\right)$ and $\max\left(cw_{(i,j)}\right)$ into (7.2), whereas the longest distance $D_{Spread|\max}$ is determined by substituting $\max\left(cw_{(i,J)}\right)$ and $\min\left(cw_{(i,j)}\right)$. The position of the correlated signal pulse is $D_{Signal} = n-1$, e.g. chip position 4 in figure 7.1. In figure 7.1, the value for $D_{Spread|\min} = 2$ is obtained by substituting $\min\left(cw_{(i,J)}\right) = 0$ and $\max\left(cw_{i,j}\right) = (n-1)/2$ into (7.2). Similarly for $D_{Spread|\max} = 6$,

the variables are $\max(cw_{(i,J)}) = (n-1)/2$ and $\min(cw_{i,j}) = 0$. The minimum and maximum limits of 0 and $(n-1)/2$ respectively can be obtained from section 4.3. It is found that $D_{L|Spread} = n-1$ for all $(n,w,1,1)$SOOC sets.

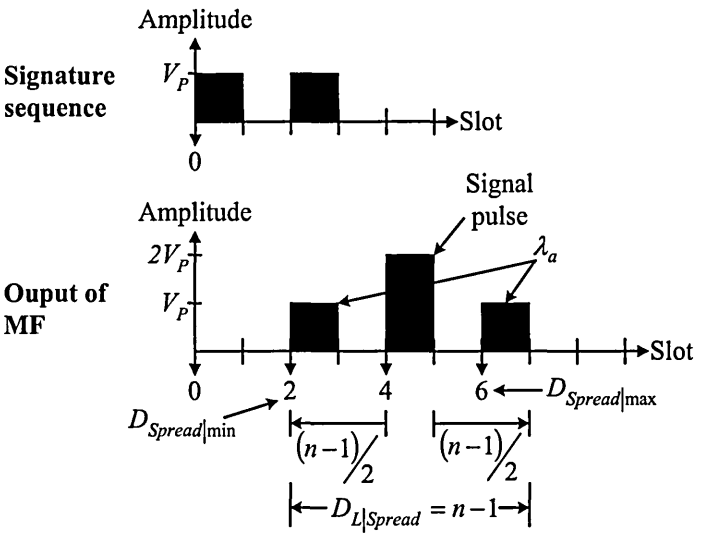

Figure 7.1: Auto-correlation constraints of $(5,2,1,1)$SOOC.

Referring to the second term in (7.1) again, the information variable S_k^i does affect the distance of the $w(w-1)$ pulses with relation to the reference time t. Hence, the probability of self-interference from every symbol taken independently is defined as:

$$P_{\lambda_a|hPIM-CDMA} = \frac{w(w-1)}{D_{L|Spread} + S_k^i}. \tag{7.4}$$

Assuming IID information S_k^i, then (7.4) can be generalised to:

$$P_{\lambda_a|hPIM-CDMA} = \frac{2w(w-1)}{2n + 2^M - 3}. \tag{7.5}$$

The major interference in a CDMA system is caused by MAI. As can be seen from the third term in (7.1), each of other simultaneous users I has w pulses with positions that do not match with the i desired user MF detector tap-delay values. There are w parallel tap-delay lines of the i MF detector and hence the output produces w^2 uncorrelated pulses, the cross-correlation

constraint. Employing the same procedures defined above, the probability of every other user causing interference is given as:

$$P_{\lambda_c|hPIM-CDMA} = \frac{2w^2}{2n + 2^M - 1}. \tag{7.6}$$

It is to be noted that $D_{L|Spread}$ is n for MAI, since none of the MAI signal pulses match the desired i codeword and hence all w^2 pulses are spread over the entire n chip region. Each interfering signal is transmitting at random i.e. $0 \le \tau^i_{d|Tx} \bmod_{n+2^M-1} < \left(n + 2^M - 1\right)T_c$ where $\tau^i_{d|Tx}$ is an integer multiple of T_c. The time delay limit is the worst case where all users are transmitting simultaneously. Each signal interfering the desired signal at a single chip position display a PDF given as:

$$PDF_{SI|hPIM-CDMA}(x) = \left(1 - P_{\lambda_c|hPIM-CDMA}\right)\delta(x) + P_{\lambda_c|hPIM-CDMA}\,\delta(x-1). \tag{7.7}$$

Therefore, the MAI effect on the desired signal at a single chip position will display a Binomial distribution expressed as:

$$PDF_{B.MAI|hPIM-CDMA}(x) = \sum_{i=0}^{F-1} \binom{F-1}{i} \left(P_{\lambda_c|hPIM-CDMA}\right)^i \cdot \left(1 - P_{\lambda_c|hPIM-CDMA}\right)^{F-1-i} \delta(x-i). \tag{7.8}$$

Note that the initial '*B*.' used before the abbreviation MAI denotes for the Binomial distribution that differentiate it from the Gaussian distribution.

For all F users transmitting simultaneously, each desired signal is interfered by $F-1$ other signals and as well as self-interference. Thus the probability a false alarm pulse will occur at a single chip position due to both interferences and exceeding the threshold level v_{th} is found to be:

$$P_{B.Self|hPIM-CDMA} = P_{\lambda_a|hPIM-CDMA} \sum_{i=v_{th}-1}^{F-1} \binom{F}{i+1} \left(P_{\lambda_c|hPIM-CDMA}\right)^i \cdot \left(1 - P_{\lambda_c|hPIM-CDMA}\right)^{F-1-i}. \tag{7.9}$$

where v_{th} is an integer.

There is a probability, $1 - P_{\lambda_a|hPIM-CDMA}$ that the MAI will occur at one chip position where there is no self-interference. Thus the probability of false alarm due to MAI only is found to be:

$$P_{B.MAI|hPIM-CDMA} = \left(1 - P_{\lambda_a|hPIM-CDMA}\right)\sum_{i=v_{th}}^{F-1}\binom{F}{i}\left(P_{\lambda_c|hPIM-CDMA}\right)^{i}\cdot\left(1 - P_{\lambda_c|hPIM-CDMA}\right)^{F-1-i}. \quad (7.10)$$

In *h*PIM-CDMA system, demodulation is carried out by detecting a pulse at the start of a symbol, then ignoring $n-1$ chips and counting the number of empty chips γ until the next pulse is detected. In an error free case, the next pulse detected is the beginning of the next symbol. However, due to a false alarm, a new pulse could be generated within the information slots (i.e. γ) which will result in a symbol being in error. The probability of a false alarm pulse occurring in the γ-slots causing a symbol in error can be simply related to:

$$\begin{aligned} P_{SFA|hPIM-CDMA} &= \gamma\left(P_{B.Self|hPIM-CDMA} + P_{B.MAI|hPIM-CDMA}\right) \\ &= \gamma P_{CFA|hPIM-CDMA}, \end{aligned} \quad (7.11)$$

where $P_{CFA|hPIM-CDMA}$ is the probability of a false alarm occurring in a single chip.

There are two conditions by which the *h*PIM-CDMA error rate could be defined by means of symbol-error-rate (SER) and/or BER. One of the conditions is that a symbol cannot be divided into two, which will result in more than two symbols in error. In a PIM system, a symbol in a packet due to false alarm error will affect not only the next symbol in error but also the remaining symbols in the packet by changing their relative positions [Hayes02], see figure 7.2 (a). In such cases, the system error rate is determined by the packet-error-rate (PER) rather than SER or BER. In *h*PIM-CDMA, an error in a symbol only affect the next symbol but not the rest of the symbols, see figure 7.2 (b). This is because the false alarm has been treated as the next symbol pulse and the pulse of the next symbol has been ignored. This will only result in the current symbol duration being shorter whereas the next symbol is longer.

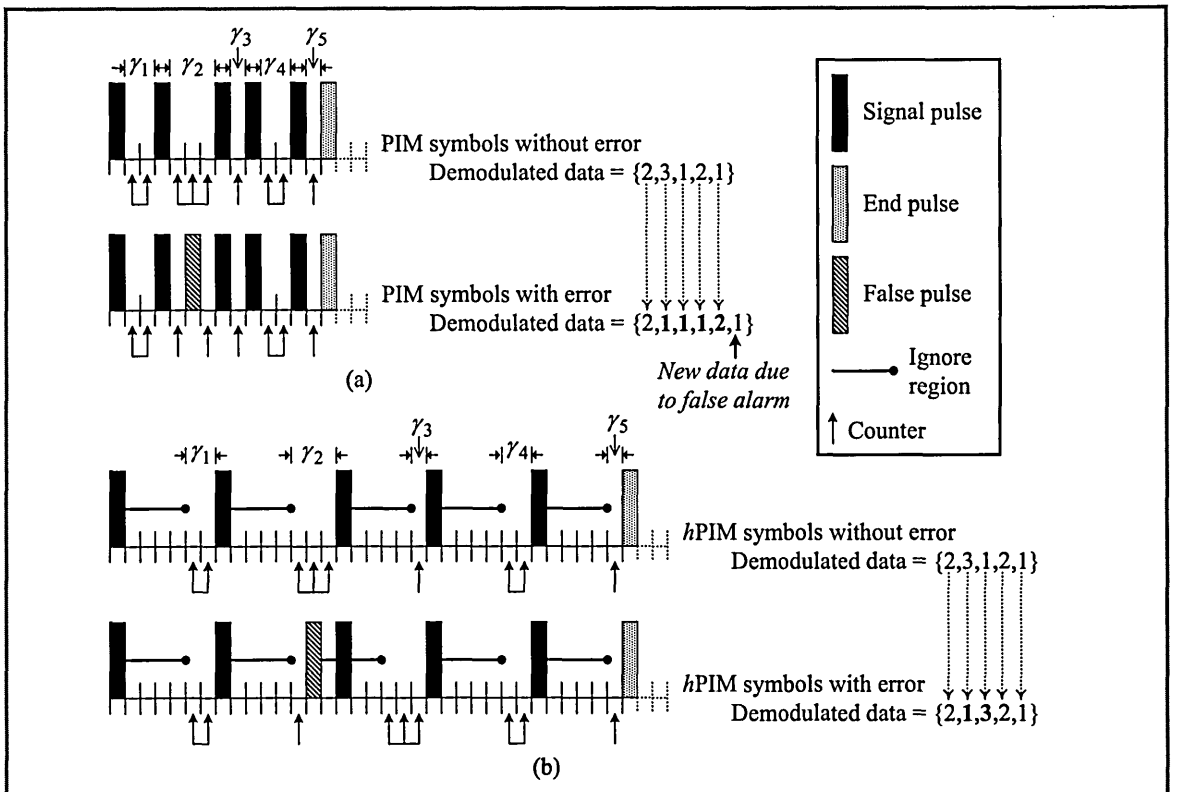

Figure 7.2: Illustration for error occurrence; (a) for PIM (b) for *h*PIM-CDMA.

A symbol is divided into two if the presence of a false alarm pulse does not result in deleting or ignoring the pulse of the next symbol. There are two cases when this will occur. 1.) The *h*PIM-CDMA mapping order L is so high such that $S_k^i > n$. When the demodulator detects a false alarm pulse that occurred within the S_k^i, it is incapable of ignoring the signal pulse of the next symbol when it is ignoring the $n-1$ empty chips, as shown in figure 7.3 (a). 2.) When $P_{SFA|hPIM-CDMA}$ is high such that $S_k^i \leq n$, and there is a high probability of a false alarm pulse occurring in every symbol, see figure 7.3 (b). In this case, a false alarm pulse divides a symbol into two if the following holds:

$$\gamma_1 + n_2 + \gamma_2 + n_3 + \gamma_3 + 1 > n_{f|1} + \gamma_{f|1} + n_{f|2} + \gamma_{f|2} + n_{f|3}. \qquad (7.12)$$

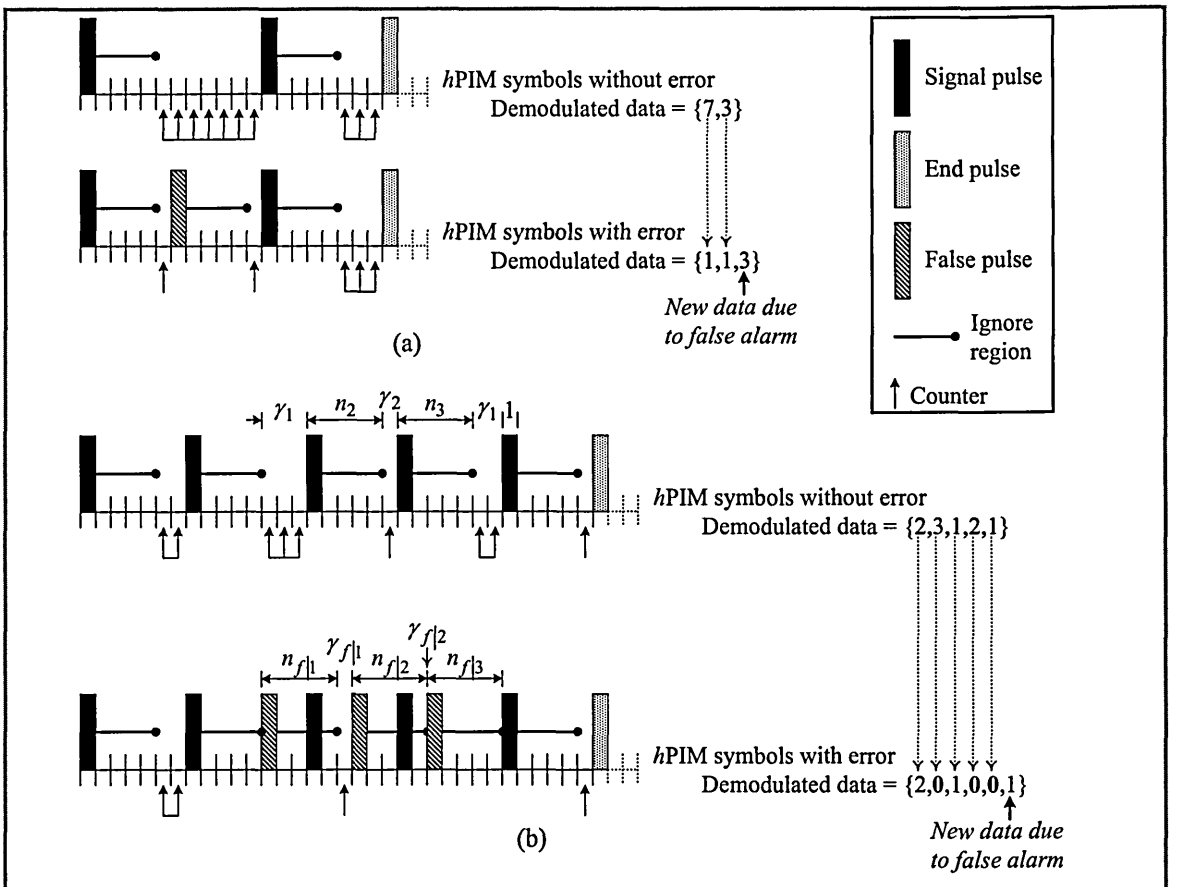

Figure 7.3: Illustration of the probability a *h*PIM-CDMA symbol being divided into two; (a) $n=5$ and $M=3$, and (b) $n=5$ and $M=2$.

The limit of the condition, which is the worst case, is when γ's on the left and right hand sides are all maximum and equal to zero, respectively. Rewriting (7.12), the condition can be generalised as:

$$\left(2^M-1\right)+n_2+\left(2^M-1\right)+n_3+\left(2^M-1\right)+1\le n_{f|1}+n_{f|2}+n_{f|3}$$

$$2^M-1\le\frac{n-1}{3}. \tag{7.13}$$

Note that all n's are equal. The division by 3 can easily be seen, as a factor from 3 consecutive false pulses that must occur one after another at a distance of $n-1$ chips away from one another. The condition for z_{NS} consecutive false alarm pulses to occur is given by:

$$2^M-1\le\frac{n-1}{z_{NS}}$$

or

$$z_{NS}=\left\lfloor\frac{n-1}{2^M-1}\right\rfloor. \tag{7.14}$$

The probability that a new symbol will exist due to the worst case scenario where z_{NS} consecutive symbols are at maximum length, and z_{NS} consecutive false alarm pulses are occurring, is given by:

$$P_{NS|hPIM-CDMA} = \left(\frac{P_{CFA|hPIM-CDMA}}{2^M} \right)^{z_{NS}} . \tag{7.15}$$

Using (7.15), the plots of $P_{NS|hPIM-CDMA}$ for various values of F, M and w are shown in figures 7.4, 7.5 and 7.6. The set of $w=2$ will not be considered as the $P_{SFA|hPIM-CDMA}$ is close to 1. Also shown are the plots of z_{NS} (using (7.14)) against F, M and w that is used to verify when $P_{NS|hPIM-CDMA}$ is low and negligible.

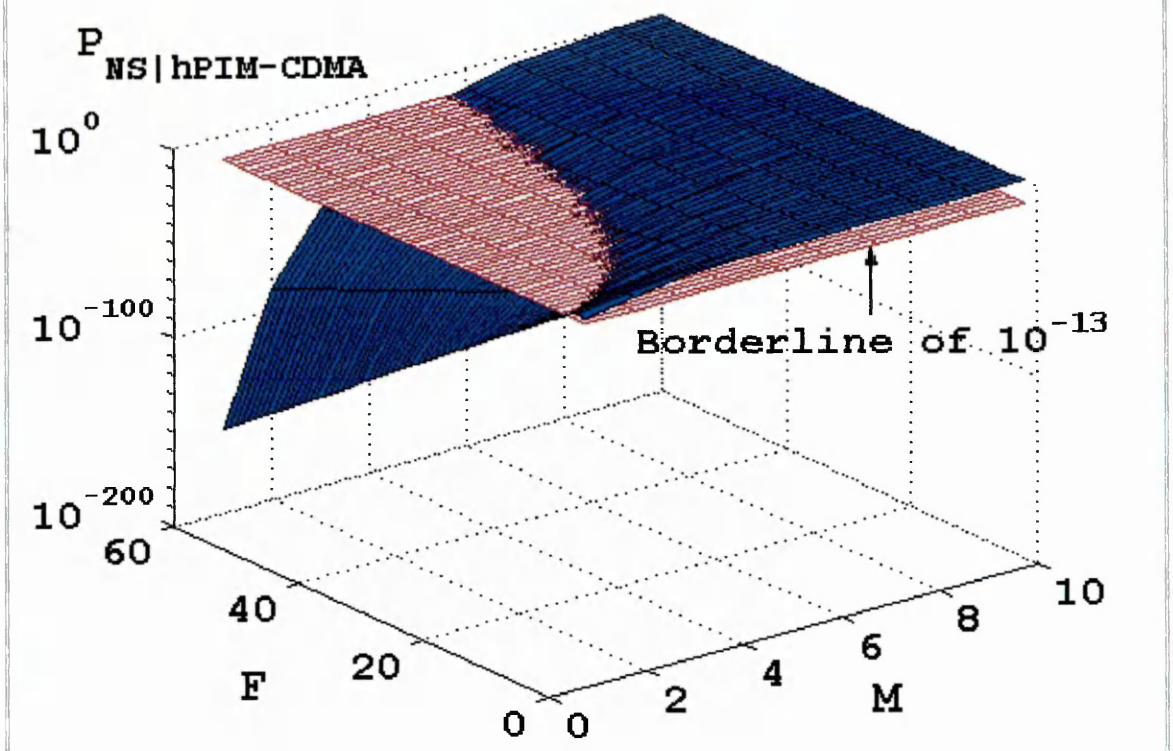

(a)

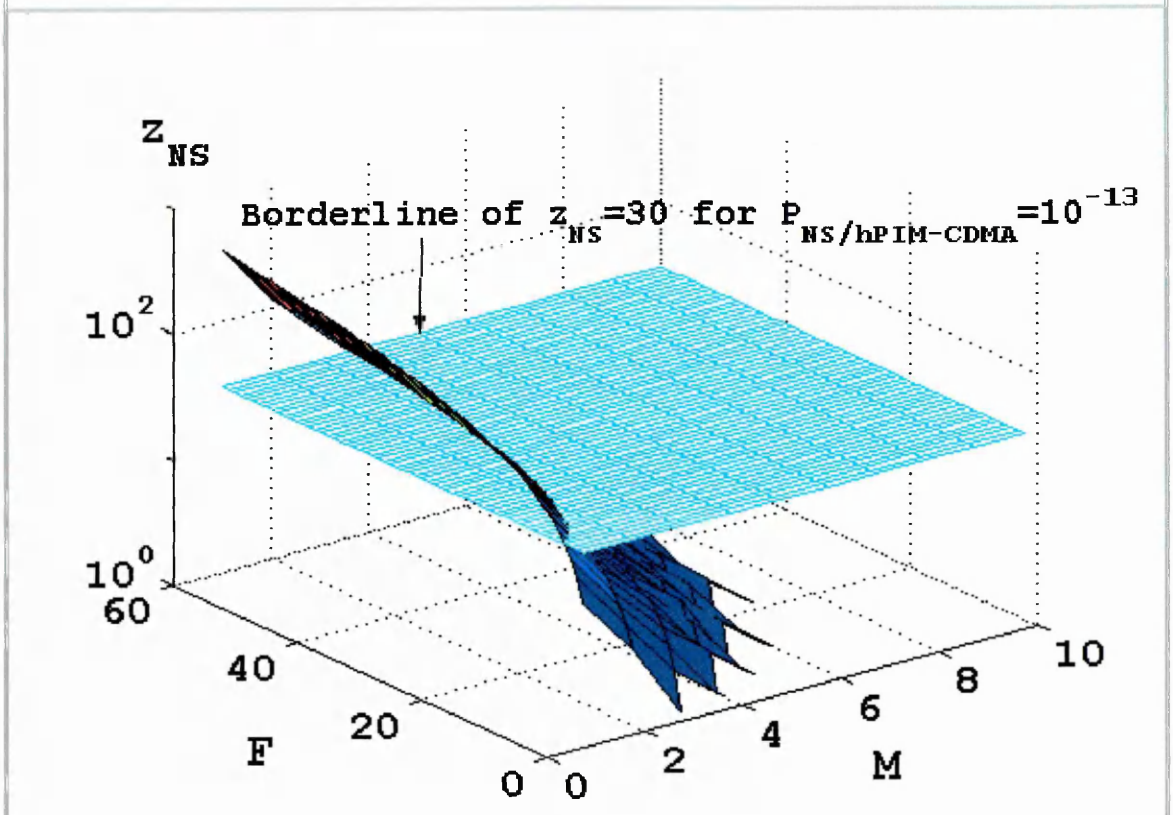

(b)

Figure 7.4: The $P_{NS|hPIM-CDMA}$ for *h*PIM-CDMA employing optimal $(n,3,1,1)$SOOC ; (a) $P_{NS|hPIM-CDMA}$ against F and M , and (b) z_{NS} corresponding to $P_{NS|hPIM-CDMA}$.

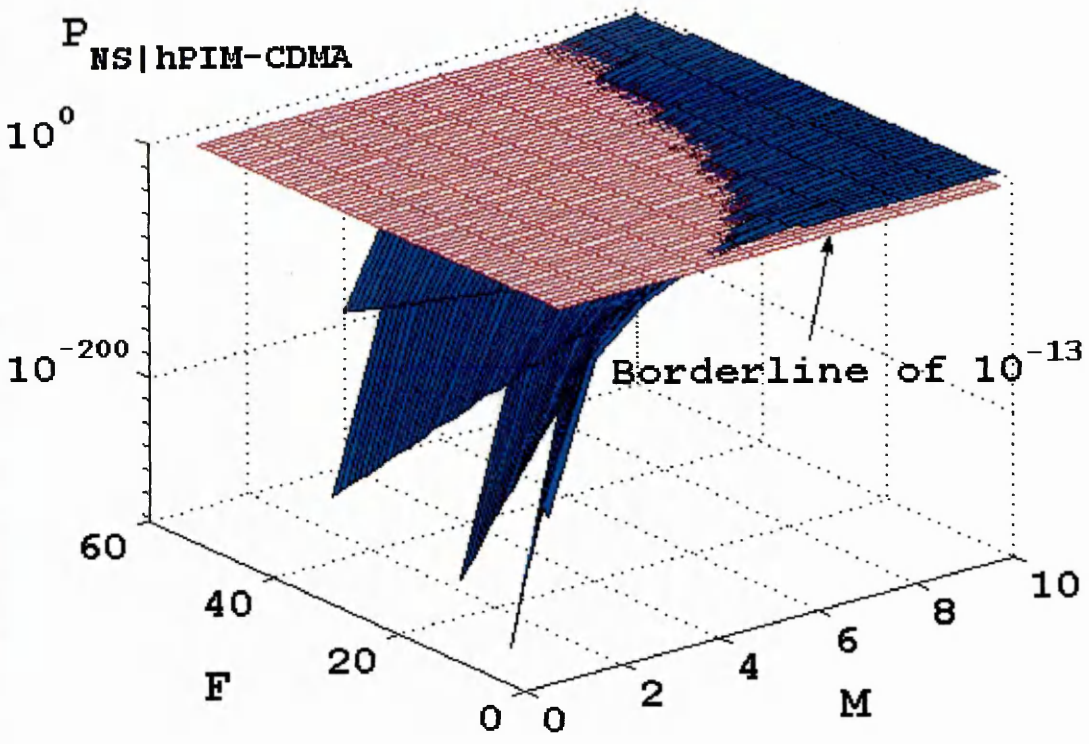

(a)

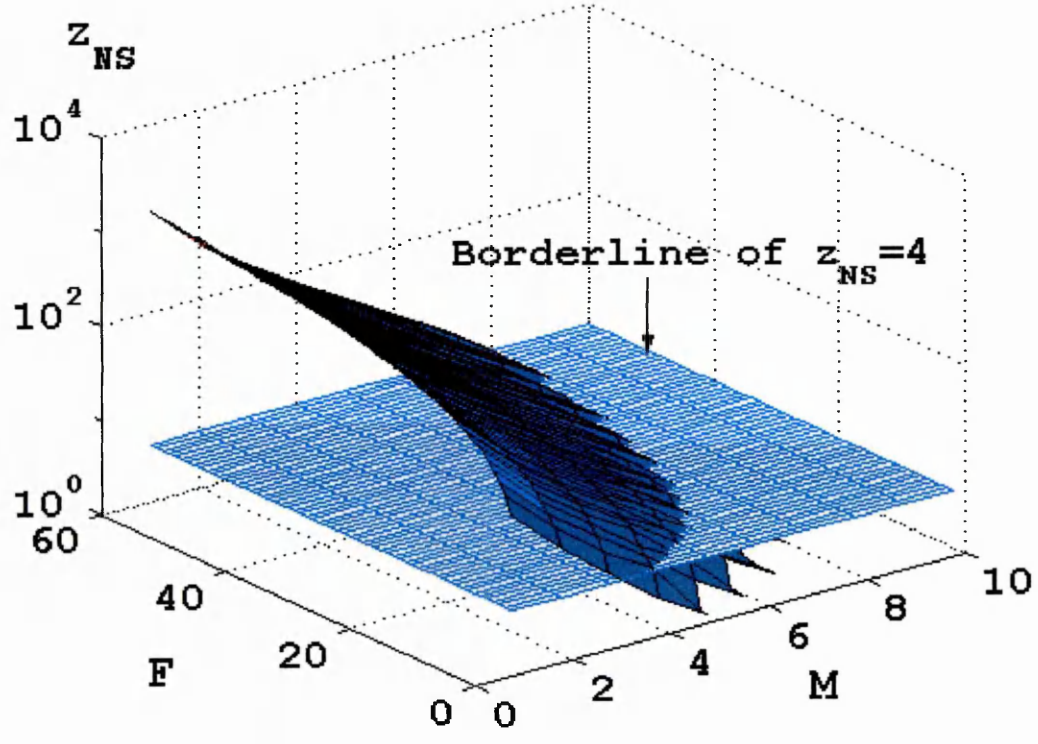

(b)

Figure 7.5: The $P_{NS|hPIM-CDMA}$ for *h*PIM-CDMA employing optimal $(n,5,1,1)$SOOC ; (a) $P_{NS|hPIM-CDMA}$ against F and M , and (b) z_{NS} corresponding to $P_{NS|hPIM-CDMA}$.

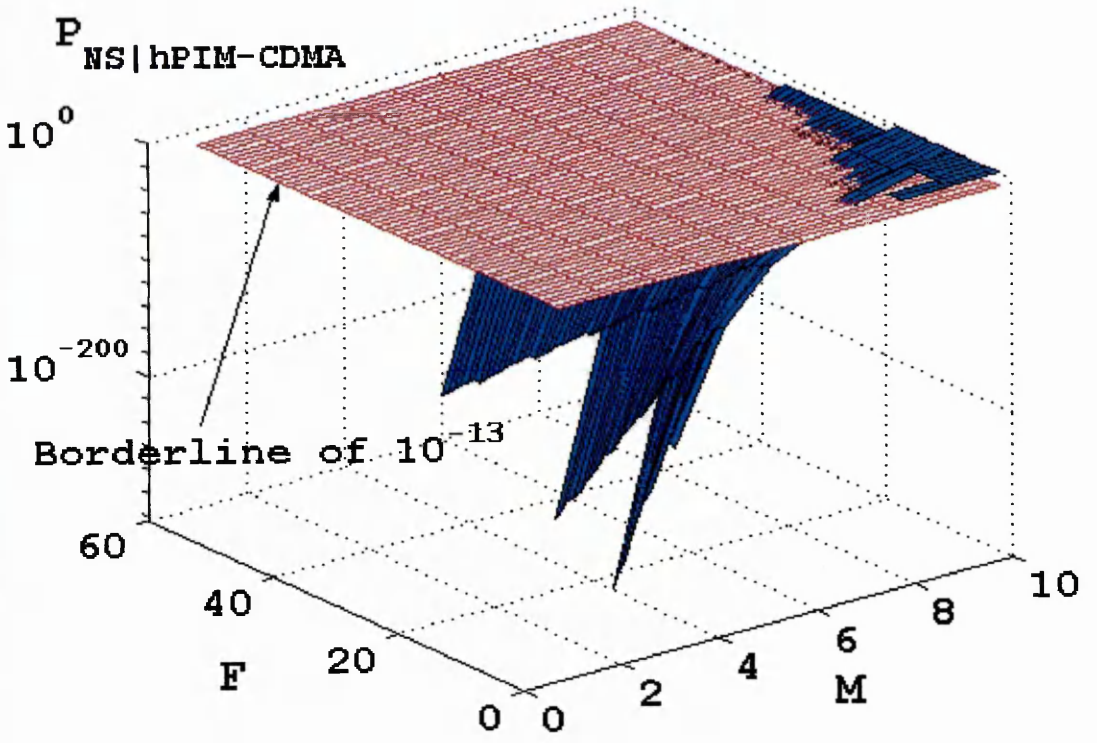

(a)

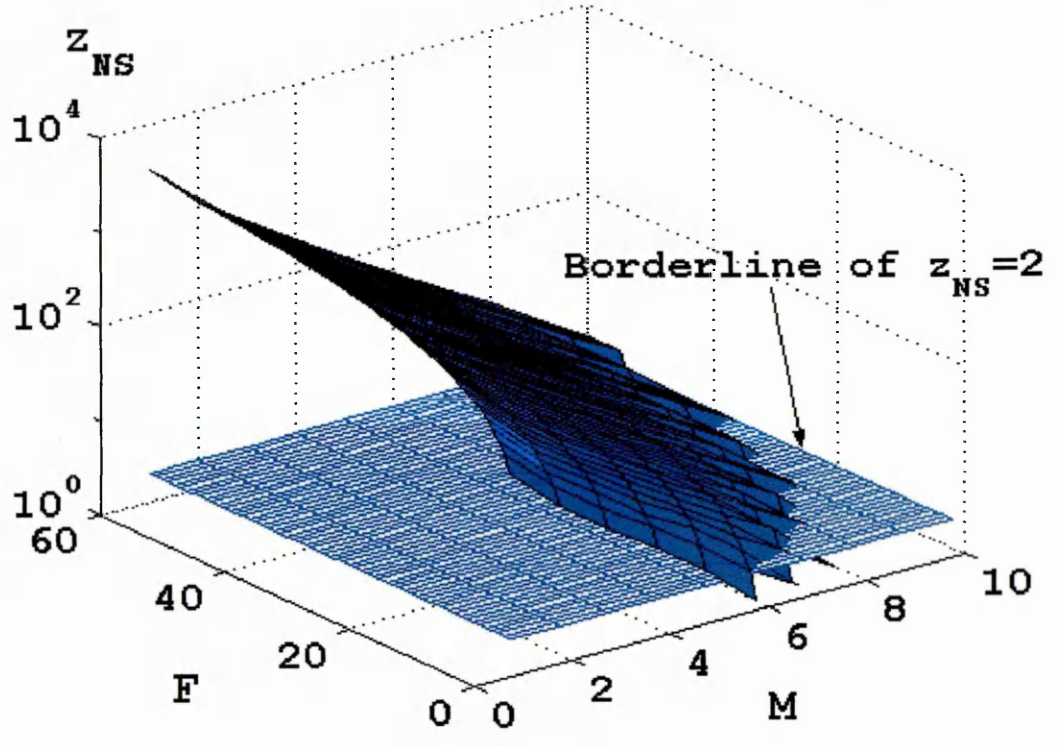

(b)

Figure 7.6: The $P_{NS|hPIM-CDMA}$ for *h*PIM-CDMA employing optimal $(n,8,1,1)$SOOC ; (a) $P_{NS|hPIM-CDMA}$ against F and M , and (b) z_{NS} corresponding to $P_{NS|hPIM-CDMA}$.

As shown in figure 7.4 (a), for a given value of F, as M increases $P_{NS|hPIM-CDMA}$ increases toward 1. This is because for large values of M the average information slot length $\bar{\gamma}$ increases thus resulting in a higher probability of false alarm occurrence, which in turn increases $P_{NS|hPIM-CDMA}$. On the other hand, increasing w reduces $P_{NS|hPIM-CDMA}$ drastically as shown in figures 7.5 (a) and 7.6 (a). This is because increasing w, the code weight that contributes to the auto-correlation peak magnitude, will increase the SIR. In this case, for $P_{NS|hPIM-CDMA} \leq 10^{-13}$ z_{NS} is reduced from 30 for $w=3$ to 2 for $w=8$. Figure 7.4 (b) shows the lower bound for $z_{NS}=30$, any value above this will result in a very low $P_{NS|hPIM-CDMA}$. The lower bound for z_{NS} is therefore given as:

$$z_{NS} \geq \left\lfloor \frac{Fw(w-1)}{2^M - 1} \right\rfloor \geq 30. \tag{7.16}$$

The second condition is that no two or more false alarm pulses will occur in two or more consecutive symbols respectively. This is because when two false alarm pulses occur in two consecutive symbols, then three symbols will be detected in error. Whereas if three false alarm pulses occur in three consecutive symbols, then four symbols will be detected in error, and so on. Hence it is difficult to predict the probability of SER considering all the probability of two or more consecutives symbols being affected by false alarm pulses, over a series of infinite symbols. Nevertheless, the probability of SER can be predicted if the probability of two false alarm pulses each occurring in two consecutives symbols is very unlikely. When one or more false alarm pulse occurs, the length of the current symbol is shortened and the length of the next symbol is lengthened. Thus the probability of false alarm pulse (or pulses) occurring in the next symbol (being in error) will be higher than the probability of them occurring in the current symbol. However, a false alarm pulse (or pulses) occurring in the second consecutive symbol does (or do) not always affect the symbol in error. This is because the next symbol (being in error) length is adjusted back to its original length by a false alarm pulse if it occurs at one specific position. The probability of two consecutive symbols being in error is given as:

$$P_{2SFA|hPIM-CDMA} = \begin{pmatrix}\text{Probability of false alarm occurring in the current symbol}\\ \times \text{Probability of false alarm occurring in the next symbol}\end{pmatrix} - \begin{pmatrix}\text{Probability of false alarm occurring in the current symbol}\\ \times \text{Probability of false alarm occurring in the next symbol}\\ \text{at a position causing no error to the next symbol}\end{pmatrix}$$

$$= \left(\sum_{\gamma_1=1}^{2^M-1}\frac{\gamma_1 P_{CFA|hPIM-CDMA}}{2^M} \times \sum_{\gamma_2=0+\gamma_1}^{2^M-1+\gamma_1}\frac{\gamma_2 P_{CFA|hPIM-CDMA}}{2^M}\right) - \left(\sum_{\gamma_1=1}^{2^M-1}\frac{\gamma_1 P_{CFA|hPIM-CDMA}}{2^M} \times \frac{1}{2^M}\cdot 2^M P_{CFA|hPIM-CDMA}\right)$$

$$= \frac{P_{CFA|hPIM-CDMA}{}^2}{2^{2M}}\sum_{\gamma_1=1}^{2^M-1}\gamma_1\left(\left[\sum_{\gamma_2=\gamma_1}^{2^M-1+\gamma_1}\gamma_2\right]-2^M\right). \quad (7.17)$$

Note that (7.17) is a cumulative probability of one or more false alarm pulses that can occur in each of two consecutives symbols. Hence (7.17) must be redefined according to the condition that if the cumulative probability exceeded one, that is more than one false alarm pulses have occurred, then two symbols are definitely in error and so $P_{2SFA|hPIM-CDMA}$ is set to 1. Else, $P_{2SFA|hPIM-CDMA}$ remains unchanged such as:

$$P_{2SFA|hPIM-CDMA} = \begin{cases}\left\{\dfrac{P_{CFA|hPIM-CDMA}{}^2}{2^{2M}}\displaystyle\sum_{\gamma_1=1}^{2^M-1}\gamma_1\left(\left[\sum_{\gamma_2=\gamma_1}^{2^M-1+\gamma_1}\gamma_2\right]-2^M\right)\right\} & ,\text{if } \{\bullet\}<1.\\ & \\ 1 & ,\text{if } \{\bullet\}\geq 1.\end{cases} \quad (7.18)$$

The SER can be approximated if the probability of two or more consecutive symbols being in error is assumed to be low compared with the probability of one symbol being in error. Knowing that the probability of three or more consecutives symbols being in error is lower than two consecutive symbols, then only the probability of one symbol and two consecutive symbols being in error are compared. Following (7.18), the probability of one symbol being error is expressed as:

$$P_{1SFA|hPIM-CDMA} = \begin{cases} \left\{ \frac{2^M - 1}{2} P_{CFA|hPIM-CDMA} \right\} & ,\text{if } \{\bullet\} < 1. \\ \\ 1 & ,\text{if } \{\bullet\} \geq 1. \end{cases} \tag{7.19}$$

Using (7.18) and (7.19), the probabilities of one and two consecutive symbols being in error against F and w are shown in figure 7.7.

As can be seen in figure 7.7, the probability of one symbol being in error is more likely to happen than the probability of two consecutive symbols being in error when $w > 5$. For $w \leq 5$ and $F > 20$, both probabilities are equal to one. Therefore hPIM-CDMA SER can be approximated based on $P_{1SFA|hPIM-CDMA}$ alone. When one symbol is in error, then two symbols will be detected incorrectly, hence SER is given as:

$$P_{SER|hPIM-CDMA} \approx \begin{cases} \left\{ \left(2^M - 1\right) P_{CFA|hPIM-CDMA} \right\} & ,\text{if } \{\bullet\} < 1. \\ \\ 1 & ,\text{if } \{\bullet\} \geq 1. \end{cases} \tag{7.20}$$

For comparison, the error rate analyses and performances of hPPM-CDMA and OOK-CDMA are also presented. The hPPM-CDMA detection mechanism has some similarity to hPIM-CDMA, where the demodulator will count the empty chip at the start of a symbol until a pulse is detected, as shown in figure 7.8. Any remaining empty chips after a pulse is being detected are not counted and hence any false alarm pulse occurring in these chips are ignored. Symbol is erroneously detected if a false alarm pulse (or pulses) occurs before the pulse. Unlike hPIM-CDMA, the symbol boundary is fixed, thus an error in a symbol does not affect the next symbol. Therefore, in hPPM-CDMA, the false alarm pulse occurring in the information region γ is the only error source.

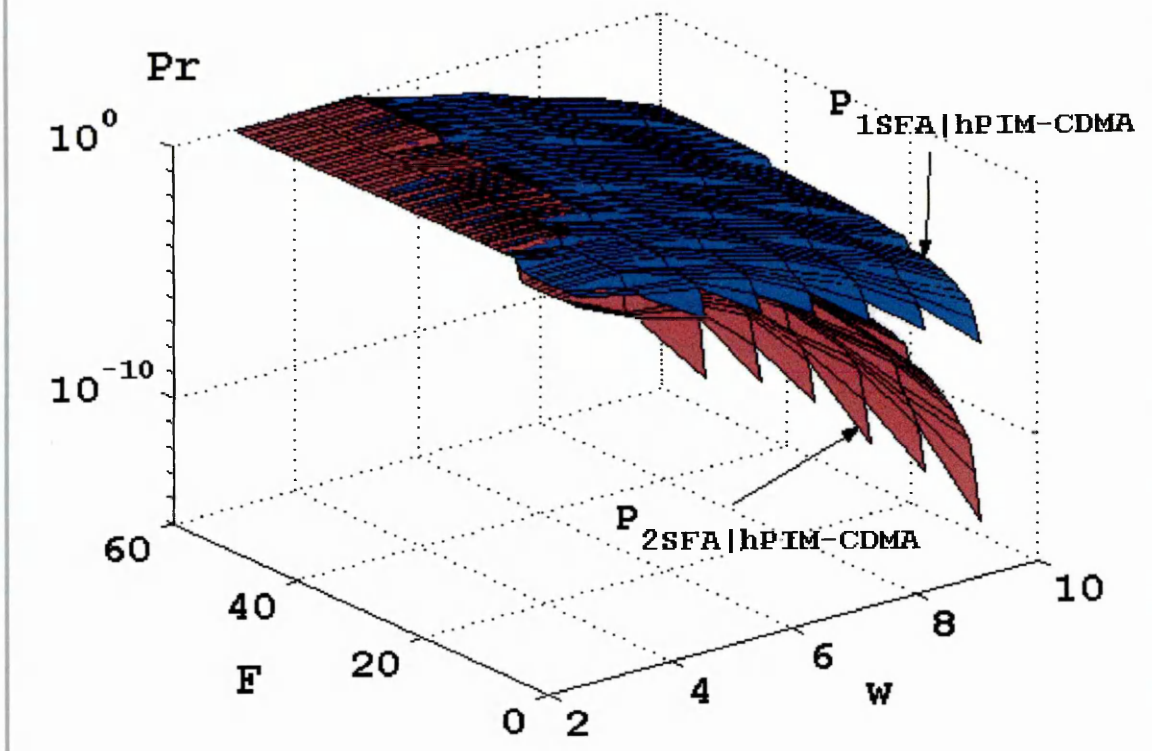

(i): 0° rotation

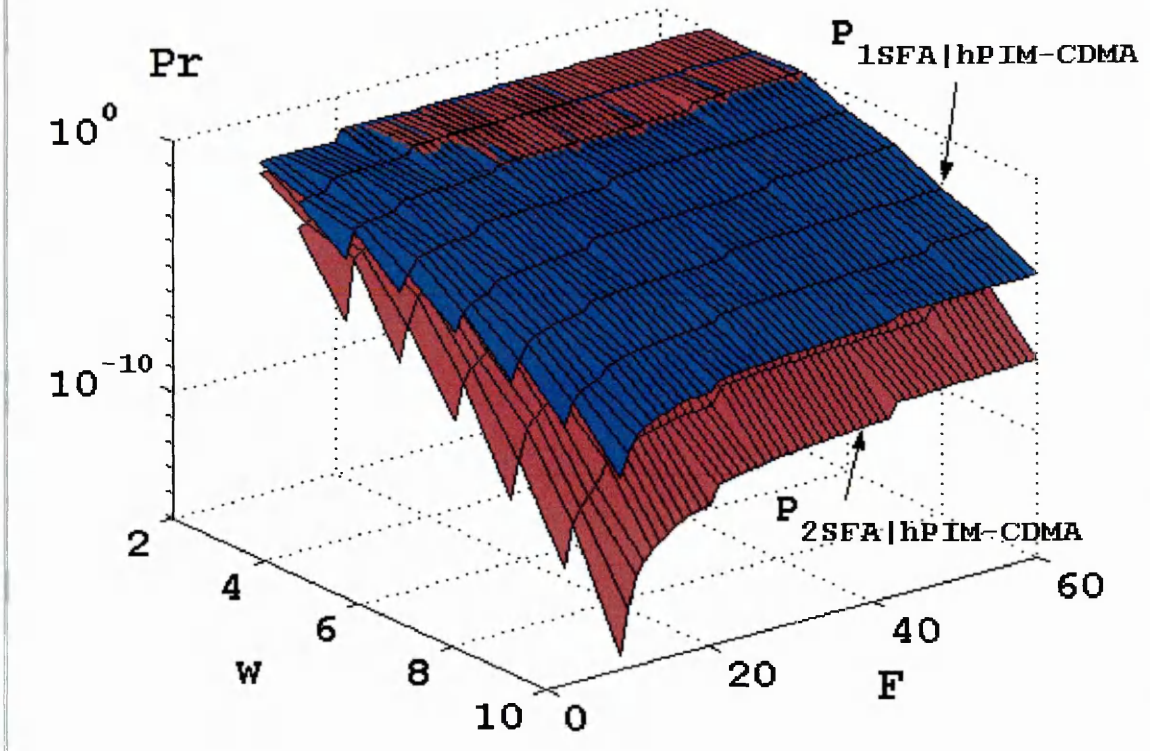

(ii): 90° rotation

Figure 7.7: Probabilities of one symbol and two consecutive symbols being in error, against F and w.

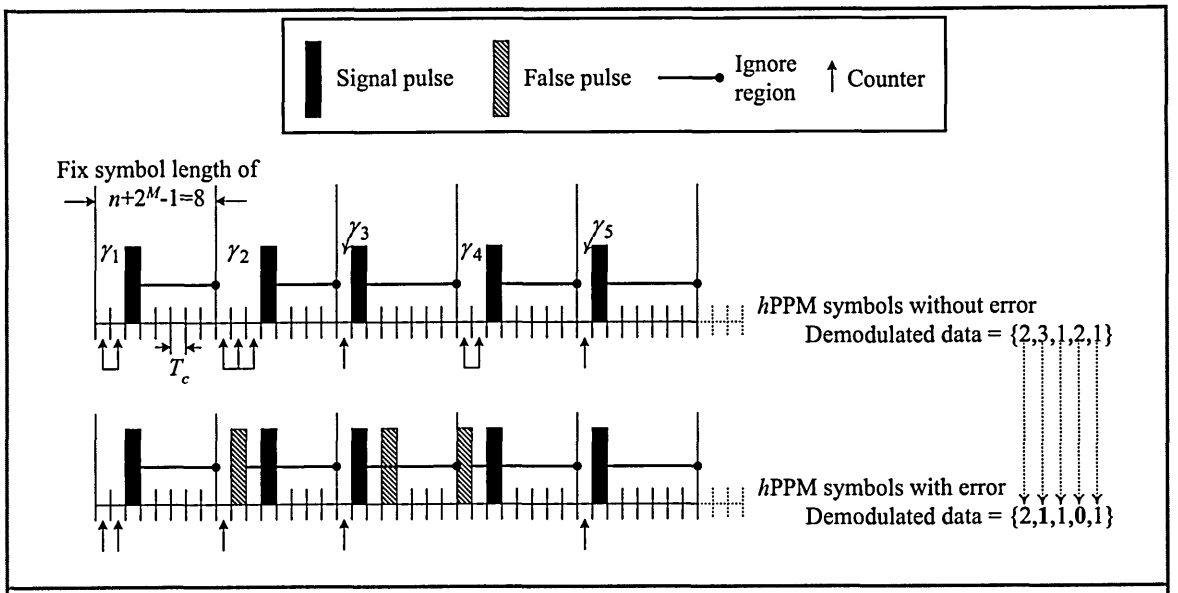

Figure 7.8: Sequence of *h*PPM-CDMA symbols with and without false alarm pulse for $n=5$ and $M=2$.

Following a similar approach to *h*PIM-CDMA error rate analysis, the probability of a false alarm pulse occurring in a single chip in *h*PPM-CDMA is given as:

$$\begin{aligned} P_{CFA|hPPM-CDMA} &= P_{B.Self|hPPM-CDMA} + P_{B.MAI|hPPM-CDMA} \\ &= P_{\lambda_a|hPPM-CDMA} \sum_{i=v_{th}-1}^{F-1} \binom{F}{i+1} \left(P_{\lambda_c|hPPM-CDMA}\right)^i \cdot \left(1-P_{\lambda_c|hPPM-CDMA}\right)^{F-1-i} \\ &\quad + \left(1-P_{\lambda_a|hPPM-CDMA}\right) \sum_{i=v_{th}}^{F-1} \binom{F}{i} \left(P_{\lambda_c|hPPM-CDMA}\right)^i \cdot \left(1-P_{\lambda_c|hPPM-CDMA}\right)^{F-1-i}, \end{aligned} \tag{7.21}$$

where:

$$P_{\lambda_a|hPPM-CDMA} = \frac{w(w-1)}{n+2^M-2}, \tag{7.22}$$

and:

$$P_{\lambda_c|hPPM-CDMA} = \frac{w^2}{n+2^M-1}. \tag{7.23}$$

The SER for *h*PPM-CDMA assuming IID information is expressed as:

$$P_{SER|hPPM-CDMA} = \begin{cases} \left\{ \frac{2^M - 1}{2} P_{CFA|hPPM-CDMA} \right\} & ,\text{if } \{\bullet\} < 1. \\ \\ 1 & ,\text{if } \{\bullet\} \geq 1. \end{cases} \tag{7.24}$$

Conversion from SER to BER for both *h*PIM-CDMA and *h*PPM-CDMA can be carried out using the following relation [Proakis95, Gagliardi95]:

$$P_{B.BER} = \frac{2^M}{2\left(2^M - 1\right)} P_{SER}. \tag{7.25}$$

For OOK-CDMA, SER is the same as BER. This is because one symbol maps only one bit of information. BER of OOK-CDMA, due to false alarm error only, is given as [Salehi89b]:

$$\begin{aligned} P_{B.BER|OOK-CDMA} &= \frac{1}{2} \sum_{i=v_{th}}^{F-1} \binom{F-1}{i} P_{\lambda_c|OOK-CDMA}{}^{i} \left(1 - P_{\lambda_c|OOK-CDMA}\right)^{F-1-i} \\ &= \frac{1}{2} \sum_{i=v_{th}}^{F-1} \binom{F-1}{i} \left(\frac{w^2}{2n}\right)^i \left(1 - \frac{w^2}{2n}\right)^{F-1-i}. \end{aligned} \tag{7.26}$$

In [Elmirghani94], BER expression for *h*PPM-CDMA was given as:

$$P_e' = \frac{2^M}{2\left(2^M - 1\right)} \left(P_r' + P_s'\right) + \frac{2^M}{4} \left(P_f' + P_{cf}'\right), \tag{7.27}$$

where P_r', P_s' and P_f' are the erasure, wrong slot and false alarm errors, respectively. The P_{cf}' is an additional cross-correlation false alarm error defined as:

$$P_{cf}' = \frac{1}{2} \sum_{i=v_{th}}^{F-1} \binom{F-1}{i} \left(\frac{w^2}{2n}\right)^i \left(1 - \frac{w^2}{2n}\right)^{F-1-i}. \tag{7.28}$$

This is false alarm due to MAI for OOK-CDMA and can't be simply adopted for a *h*PPM-CDMA scheme. This is because in *h*PPM-CDMA, a false alarm is due to MAI and self-interference, and the bit resolution M. Increasing M alone will increase the probability of false alarm error rate. Therefore, (7.28) cannot be employed to describe the performance of *h*PPM-CDMA.

7.2.1 Results and discussions

In this section, the BER and BEF performances of *h*PIM-CDMA are presented and compared with OOK-CDMA and *h*PPM-CDMA. All the assumptions outlined in section 7.1 are applied to all the results shown from here onwards.

Using equation (7.20), (7.24), (7.25) and (7.26), the BER performance against F and w for the three schemes are plotted in figure 7.9. The value of M for *h*PIM-CDMA BER is obtained for each value of F and w using (7.16), whereas for *h*PPM-CDMA it is obtained from the optimum BEF shown in figure 5.25. The values of M against F and w for both hybrid schemes are shown in figure 7.10. Referring to figure 7.9, the *h*PIM-CDMA and *h*PPM-CDMA BER profiles are similar to, but of higher amplitude than the OOK-CDMA. The BER decreases linearly as w increases, and increases nonlinearly as F increases. For both hybrid schemes, $\text{BER} \geq 0.5$ for $w = [3,4]$ and all values of F, and for $w = 5$ and $F \geq 25$. This is due to the severity of the MAI, which results in an SER≈1. Note that SER of 1 does not correspond to a BER of 1. In each hybrid scheme, a symbol maps to M number of bits. When one symbol is in error, only some bits are in error. Hence for all possible symbols, the average number of bits being in error is determined by (7.25), which is a function of M. As $w > 5$, the BER for both hybrid schemes decreases linearly. For *h*PIM-CDMA, the BER is forced to 1 for small values of F and w as indicated by the 'invalid values'. This is because these values do not satisfy the condition in (7.16).

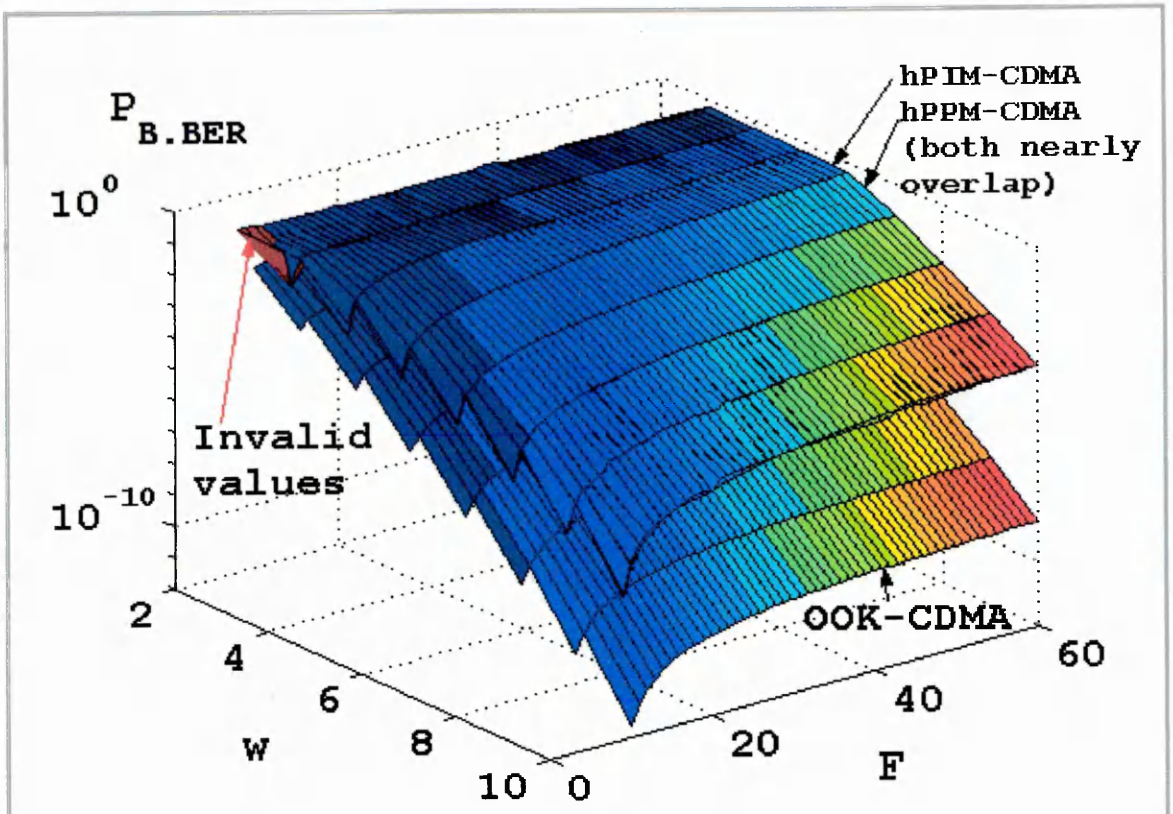

(i): 90° rotation

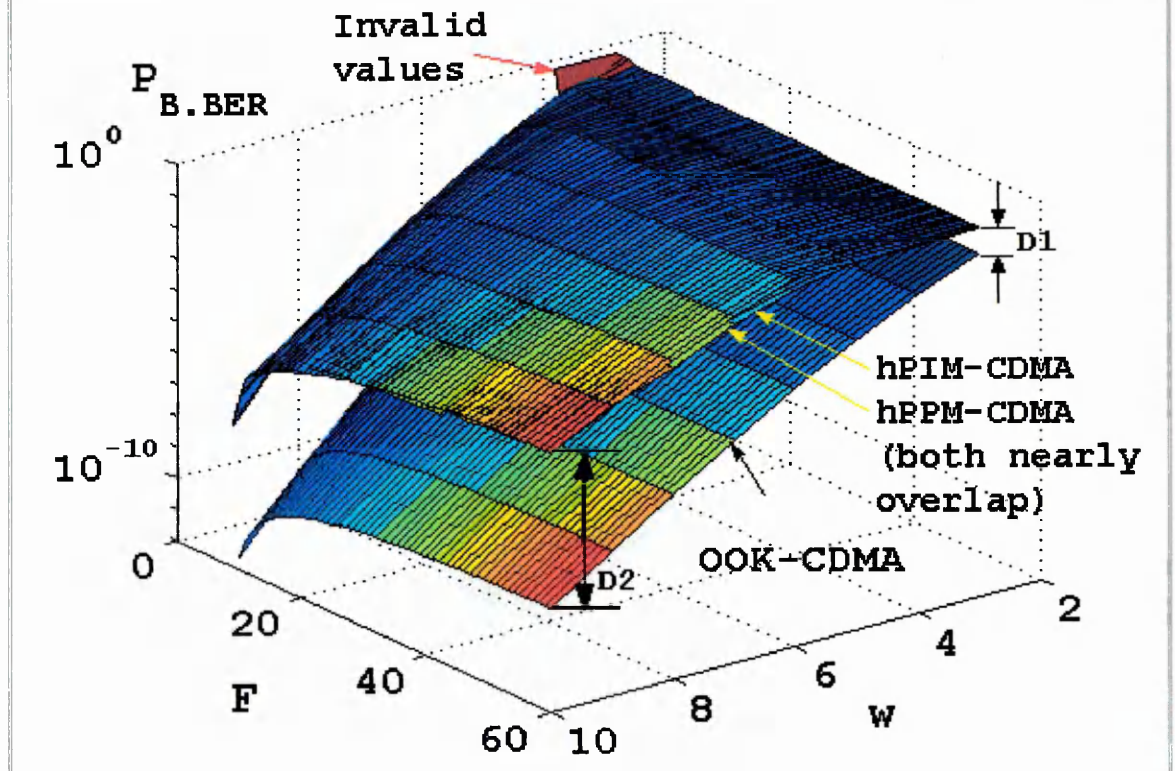

(ii): 180° rotation

Figure 7.9: BER performance of OOK-CDMA, *h*PIM-CDMA and *h*PPM-CDMA, against F and w.

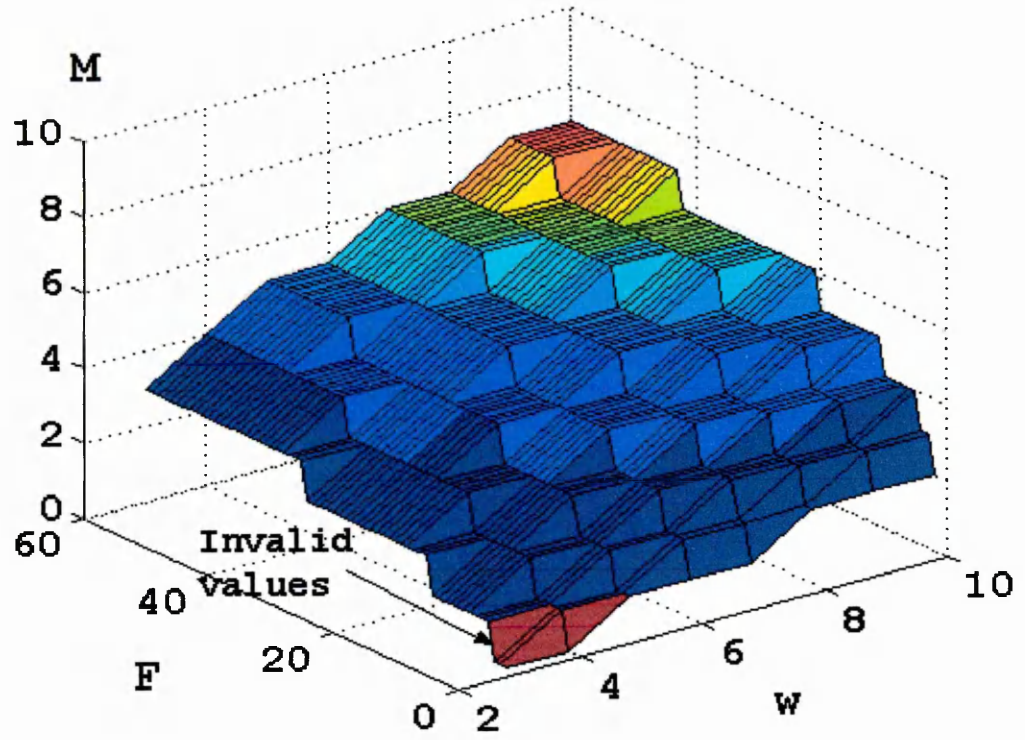

(a)

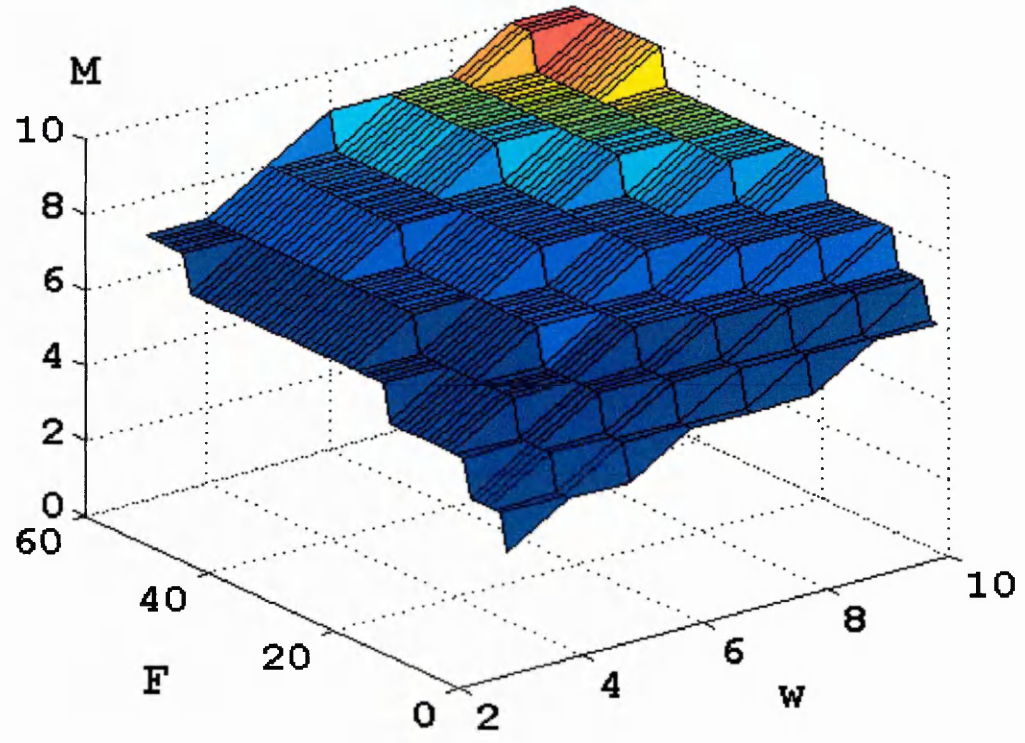

(b)

Figure 7.10: Values of M ; (a) for *h*PIM-CDMA due to condition $z_{NS} = 30$, and (b) for *h*PPM-CDMA when BEF is optimum.

A closer at the BER performance against F and w for the three schemes is shown in figure 7.11. For all values of w, the BER will deteriorate rapidly and consequently will reach a steady state as F increases. Using OOK-CDMA as an example, with $w=3$, the BER reaches steady state at 6.18×10^{-2} for $F\geq7$. For $w=8$, the BER reaches steady state at 3.346×10^{-7} for $F\geq22$. This improvement in BER is due to the increase in SIR as a result of the increase in w.

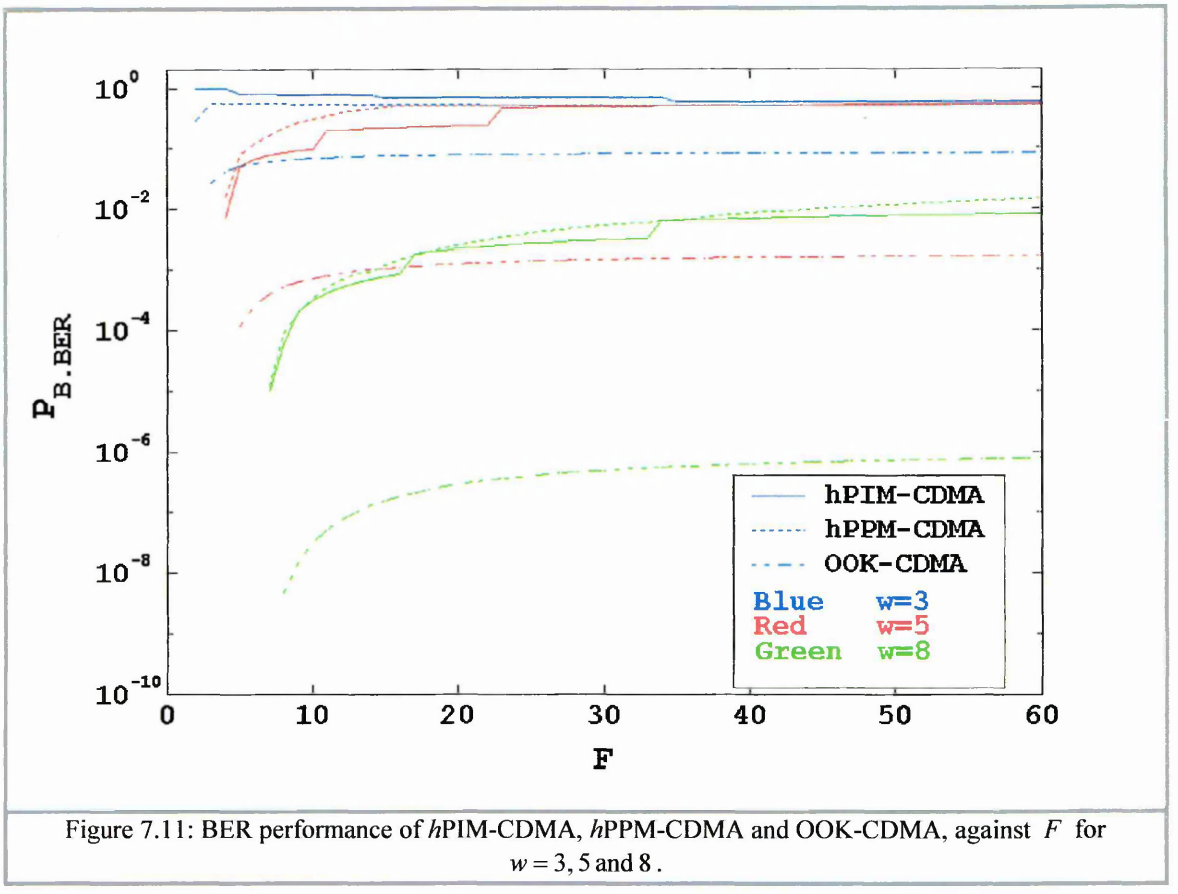

Figure 7.11: BER performance of *h*PIM-CDMA, *h*PPM-CDMA and OOK-CDMA, against F for $w=3,5$ and 8.

The BEF of *h*PIM-CDMA and *h*PPM-CDMA normalised to OOK-CDMA are given, respectively, as:

$$BEF_{\frac{hPIM-CDMA}{OOK-CDMA}}=\frac{2nM}{2n+2^{M}-1}, \tag{7.29}$$

and

$$BEF_{\frac{hPPM-CDMA}{OOK-CDMA}}=\frac{nM}{n+2^{M}-1}. \tag{7.30}$$

Figure 7.12 shows the BEF against F and w for *h*PIM-CDMA and *h*PPM-CDMA. Both BEFs increase with F and w, while *h*PPM-CDMA displays the highest throughput. This is because its bit resolution is higher as shown in figure 7.10. As *h*PIM-CDMA has to conform to the condition given in (7.16), where $z_{NS} \geq 30$, its BEF performance will never give an optimum value. This is because the BEF optimum points for $F \leq 60$ are achieved at $z_{BEF} \leq 4$ as compared with figure 6.11. It is also observed that the *h*PIM-CDMA BEF $= M$, whereas *h*PPM-CDMA BEF $< M$. This implies that if both hybrid schemes use the same value of M, then the *h*PIM-CDMA BEF is higher than the *h*PPM-CDMA.

Note that from figure 7.9, the difference in the BER performance (measured by $P_{B.BER|hPIM-CDMA} / P_{B.BER|OOK-CDMA}$) between *h*PIM-CDMA and OOK-CDMA increases as w increases. For example, the difference indicated by 'D1' is 6.8 and has increased to 8.6×10^4 at 'D2'. This is because as w increases from 3 to 10, M increases from 3 to 7 as shown in figure 7.10. Referring to (7.20), increasing M will increase the average length of the information slots (i.e. $2^M - 1$) of a *h*PIM-CDMA symbol, which will result in increased probability of false alarm pulse occurrence $P_{CFA|hPIM-CDMA}$. This effect is similar to *h*PPM-CDMA. Therefore, it can be deduced that in both hybrid systems the BER performance is lower if low values of M, i.e. $M \leq 4$, are employed instead the values of M that give the optimum BEF. To prove this, further comparisons are made by limiting $M = 2$ and $M = 4$ for all pairs of F and w. It is to be noted that for *h*PIM-CDMA, where the condition in (7.16) should apply, the values of M in figure 7.10 (a) is only the upper bound for $w = 3$ (figure 7.4). For values of $w \geq 4$, the upper bound will be lower, as shown in figures 7.5 and 7.6. If M exceeded the maximum value in figure 7.10 (a), the condition in (7.16) will be void for $w = 3$ only. However, there are only a small number of F and w pairs, at the lowest range, that are invalid. Hence the *h*PIM-CDMA BER obtained for $M = 4$ will not be a close approximation for the F and w pairs at the low range. Since the number of pairs is small, it is assumed that the 'invalid values' will not affect the BER comparison between the two hybrid schemes that will be discussed below. The results for BER and BEF for $M = 2$ are shown in figures 7.13 and 14 respectively.

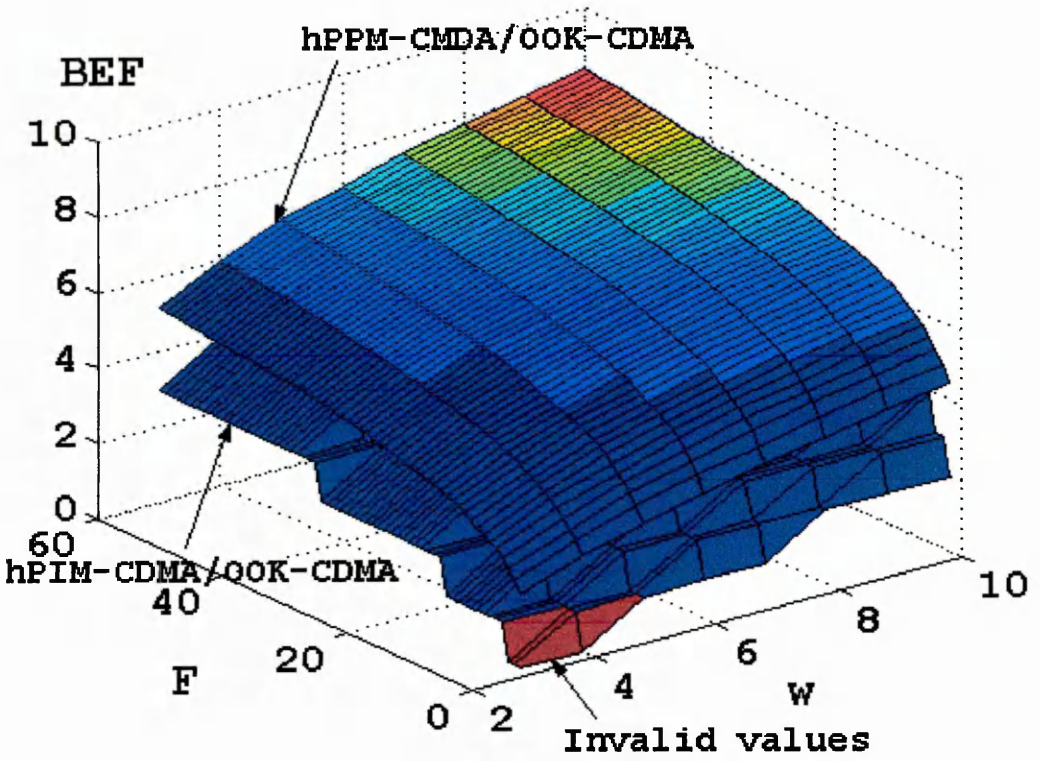

(i): 0° rotation

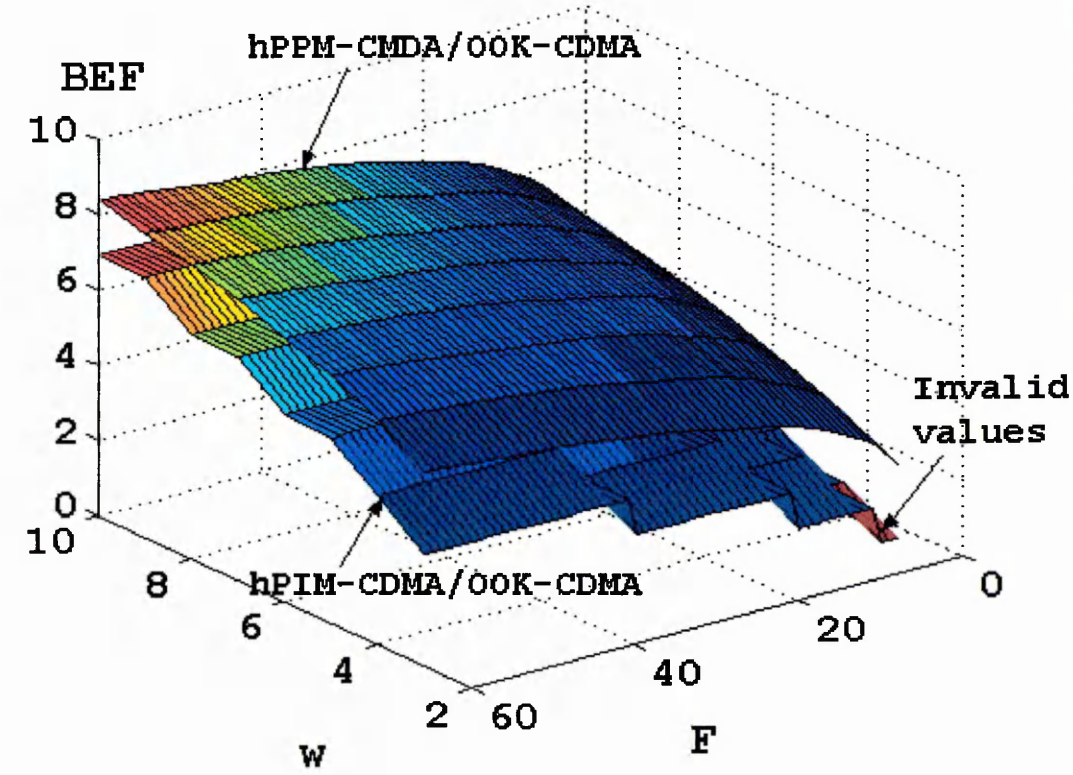

(ii): 270° rotation

Figure 7.12: BEF performance, of *h*PIM-CDMA and *h*PPM-CDMA normalised to OOK-CDMA, against F and w for values of M corresponding to figure 7.10.

As shown in figures 7.13, for $M=2$, the BER performance of both hybrid schemes have improved compared with figures 7.9 (ii) and 7.11. Note that in this case, the *h*PIM-CDMA BER is slightly higher than the *h*PPM-CDMA for all F and w. This is because for the same values of M, *h*PIM-CDMA average symbol duration is shorter than the *h*PPM-CDMA fixed symbol duration (as discussed in section 6.3). As a result, $P_{CFA|hPIM-CDMA}$ is higher than the $P_{CFA|hPPM-CDMA}$. On the other hand, the *h*PIM-CDMA BEF performance is better than *h*PPM-CDMA as shown in figure 7.14. Nevertheless, as F and w increase, the BEF tends to equal M for both hybrid schemes. Increasing M from 2 to 4 will result in further deterioration of BER with an improvement to the BEF for both hybrid schemes as shown in figures 7.15 and 7.16 respectively.

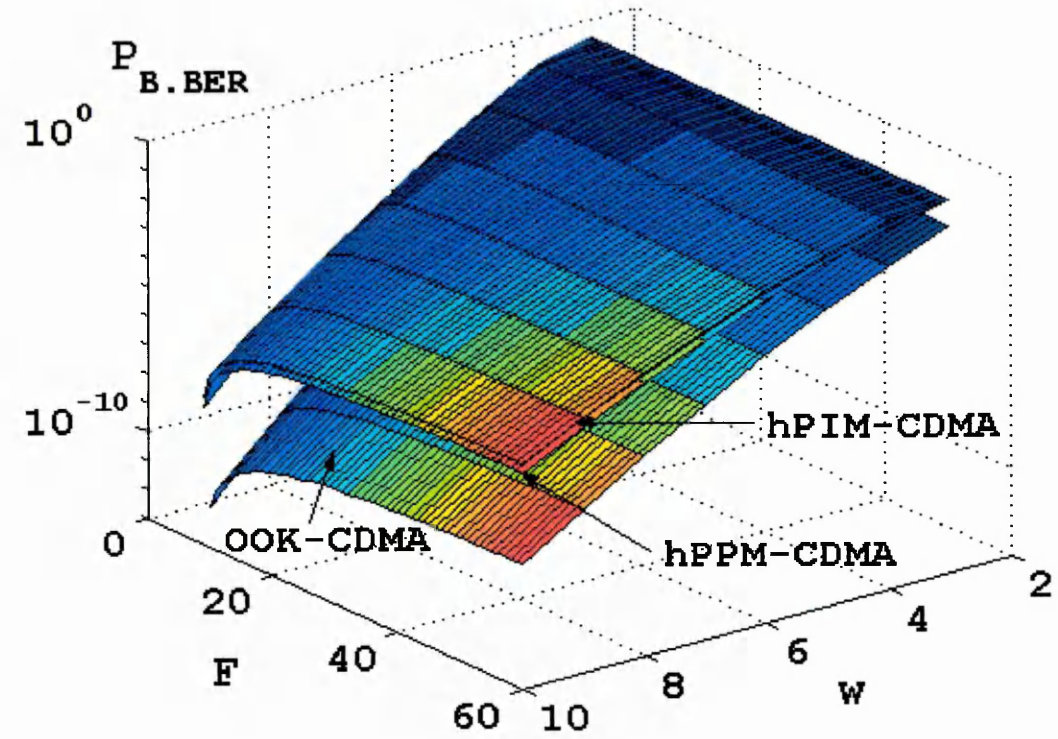

(a): 180° rotation

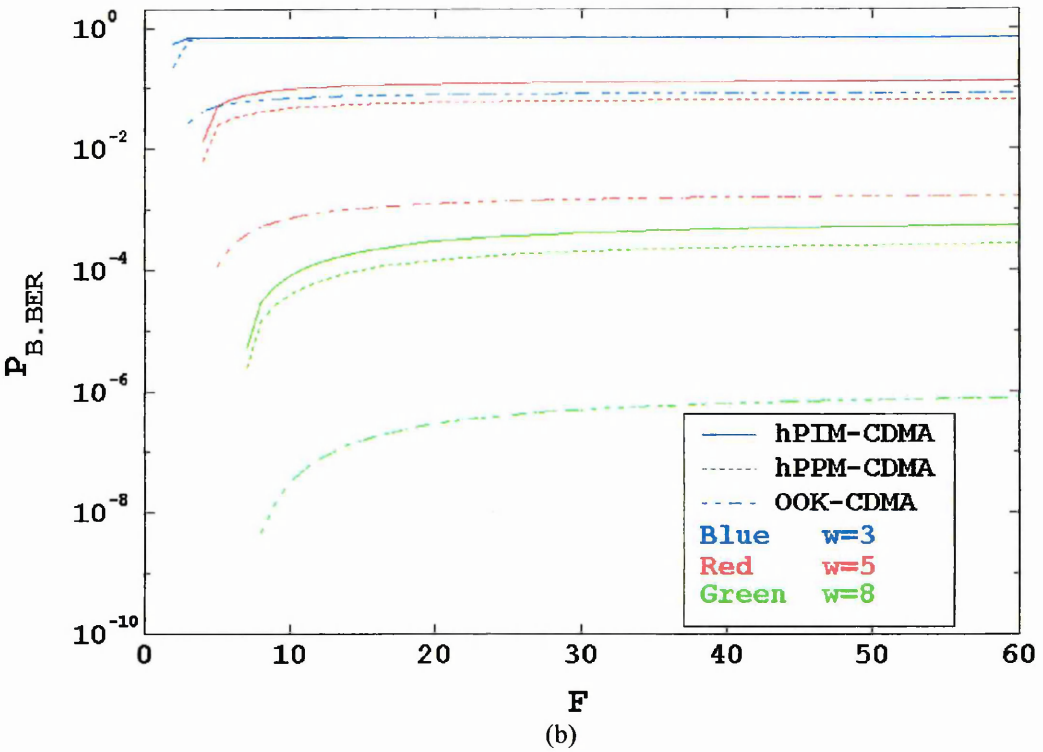

(b)

Figure 7.13: BER performance of *h*PIM-CDMA, *h*PPM-CDMA and OOK-CDMA; (a) against F and w, for $M = 2$, and (b) against F, for $w = 3, 5$ and 8 and $M = 2$.

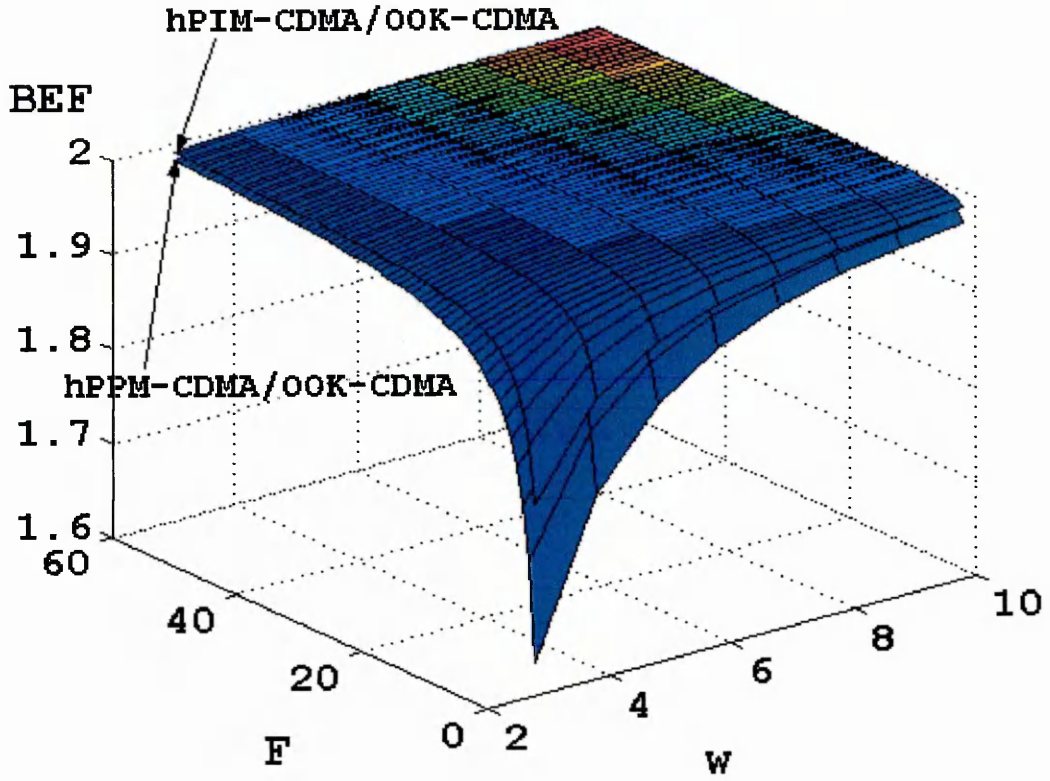

(i): 0° rotation

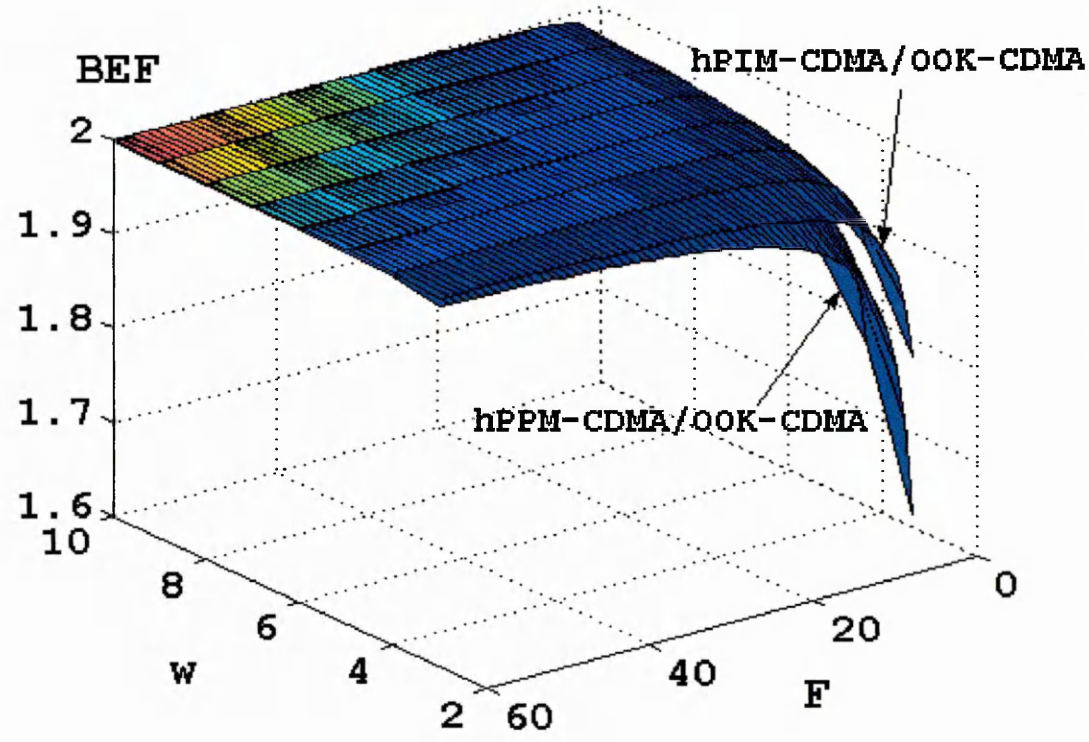

(ii) 270° rotation

Figure 7.14: BEF performance, of *h*PIM-CDMA and *h*PPM-CDMA normalised to OOK-CDMA, against F and w for $M = 2$.

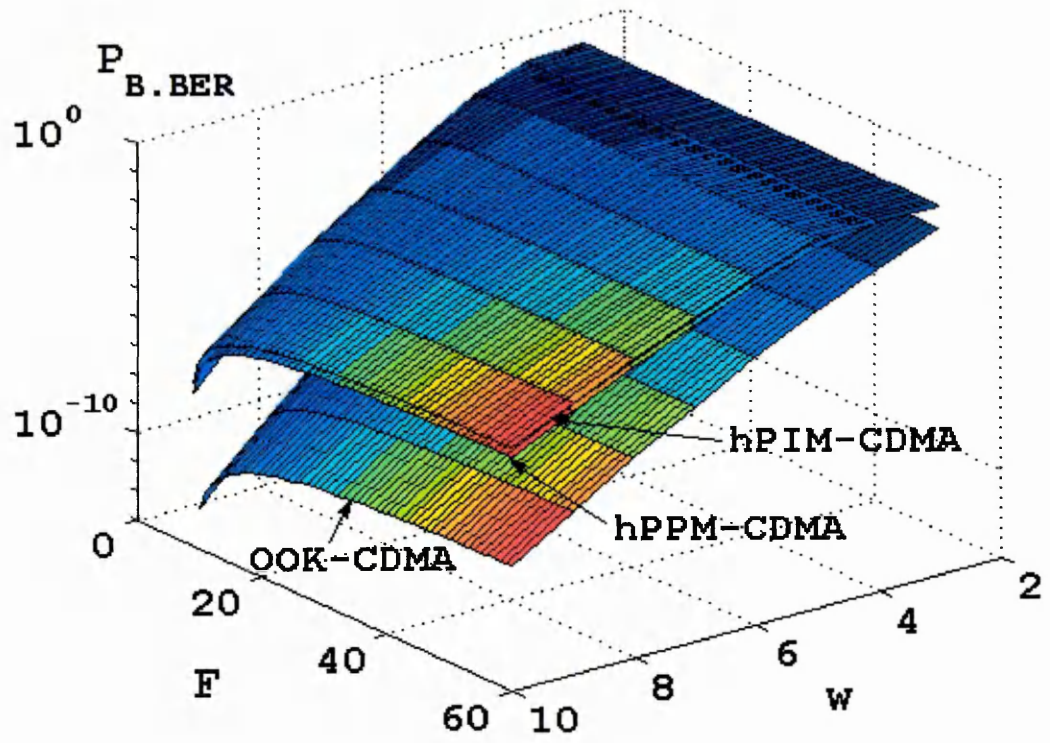

(a): 180° rotation

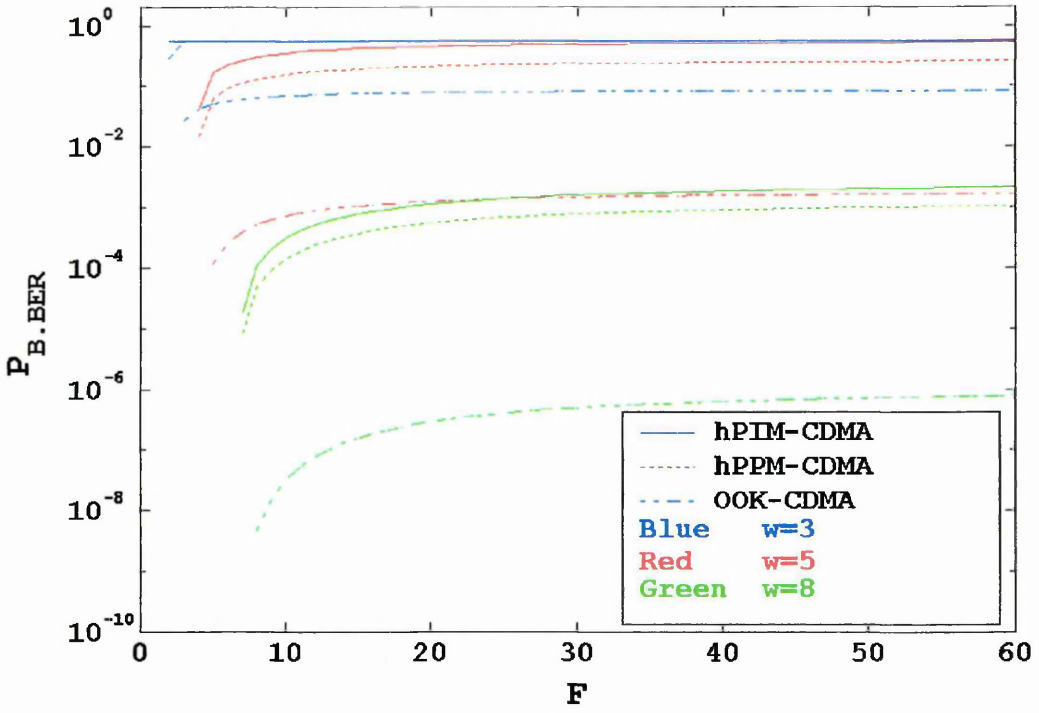

(b)

Figure 7.15: BER performance of *h*PIM-CDMA, *h*PPM-CDMA and OOK-CDMA; (a) against F and w, for $M = 4$, and (b) against F, for $w = 3, 5$ and 8 and $M = 4$.

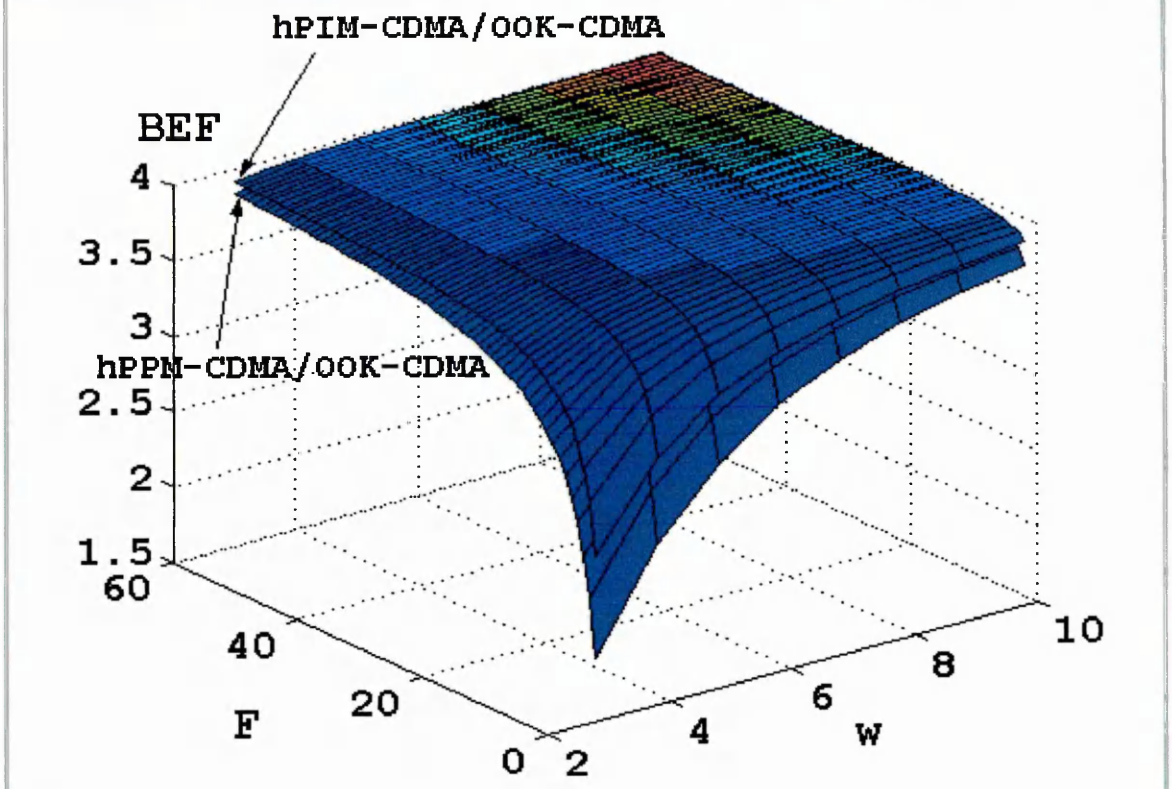

(i): 0° rotation

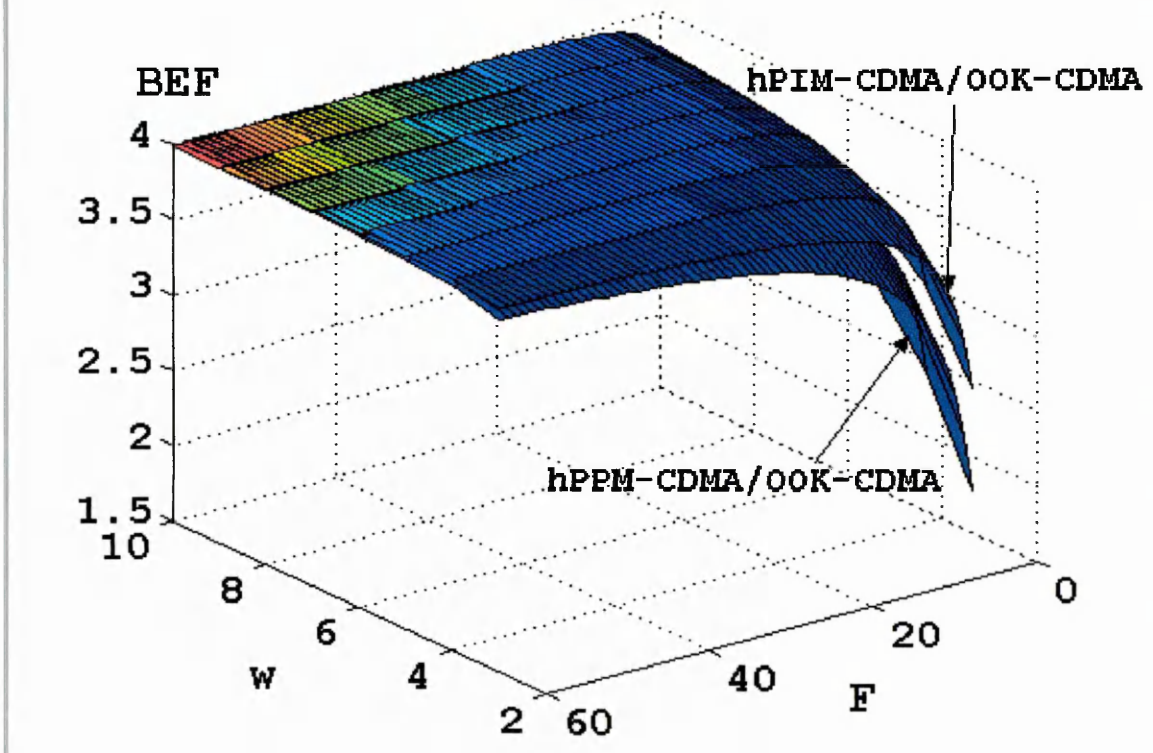

(i): 270° rotation

Figure 7.16: BEF performance, of *h*PIM-CDMA and *h*PPM-CDMA normalised to OOK-CDMA, against F and w for $M = 4$.

7.3 Gaussian Approximation

The Gaussian function has been widely used to approximate most intractable problems of probability errors where the assumption is always made that any naturally occurring random quantities such as noise and measurement errors are Gaussianly distributed [Tranter95]. The probability errors of OOK-CDMA employing different groups of signature sequences will have different probability distribution functions, such as employing a set $(n,w,1,1)$OOC, the probability distribution is Binomial and employing a set $(n,w,\lambda_a>1,\lambda_c>1)$OOC, the probability distribution is multinomial.

The Gaussian function, which is simple and convenient, has been used to approximate, evaluate and compare OOK-CDMA error rates using $(n,w,1,1)$OOC and PS(P) [Marić95, Lee98a]. In this work, the assumption has been made that the MAI distribution, regardless of the group of signature sequences used, will converge to a Gaussian distribution when the number of system users F is large. However in this section, it is shown that this assumption is not true for OOK-CDMA systems employing $(n,w,1,1)$OOC, no matter how large F is. Nevertheless, the probability distribution employing PS(P) is Gaussian distributed [Kwong91]. Results obtained using the Gaussian distribution function and the Binomial distribution function showed that they do not agree. From the results obtained, a method has been proposed to investigate the error rate performance using a Gaussian approximation for both hybrid schemes.

7.3.1 Gaussian approximation to the binomial distribution

There are certain rules for using the Gaussian distribution function to closely approximate Binomial distribution function, where the Binomial distribution must first satisfy both the conditions expressed as [Mendenhall95]:

$$\begin{aligned} \mu - 2\sigma &\geq 0 \\ Xp - 2\sqrt{Xpq} &\geq 0, \end{aligned} \tag{7.31}$$

and

$$\mu + 2\sigma \le X$$
$$Xp + 2\sqrt{Xpq} \le X, \tag{7.32}$$

where μ is the mean, σ is the standard deviation, X is the number of trials, p is the probability of occurrence and q is the compliment of p, which is $q = 1 - p$. The Binomial PDF is represented as:

$$PDF_{B.}(x_B) = \sum_{x_B=0}^{X} \binom{X}{x_B} p^{x_B} q^{X-x_B} \cdot \delta(X - x_B), \tag{7.33}$$

this can be represented equivalently by a Gaussian PDF as:

$$PDF_{G.}(x_G) = \frac{1}{\sigma\sqrt{2\pi}} \exp\left[-\frac{1}{2}\left(\frac{x_G - \mu}{\sigma}\right)^2\right]. \tag{7.34}$$

For (7.33) to display a Gaussian profile, both left and right tails of 2σ away from the mean μ must appear within the valid variable range, 0 and X, as shown in figure 7.17.

It was found that for the condition in (7.31) to be true, the following product:

$$Xp \ge 4 \tag{7.35}$$

must be satisfied. Similarly, for the condition in (7.32) to be true, the product:

$$Xq \ge 4 \tag{7.36}$$

must be satisfied.

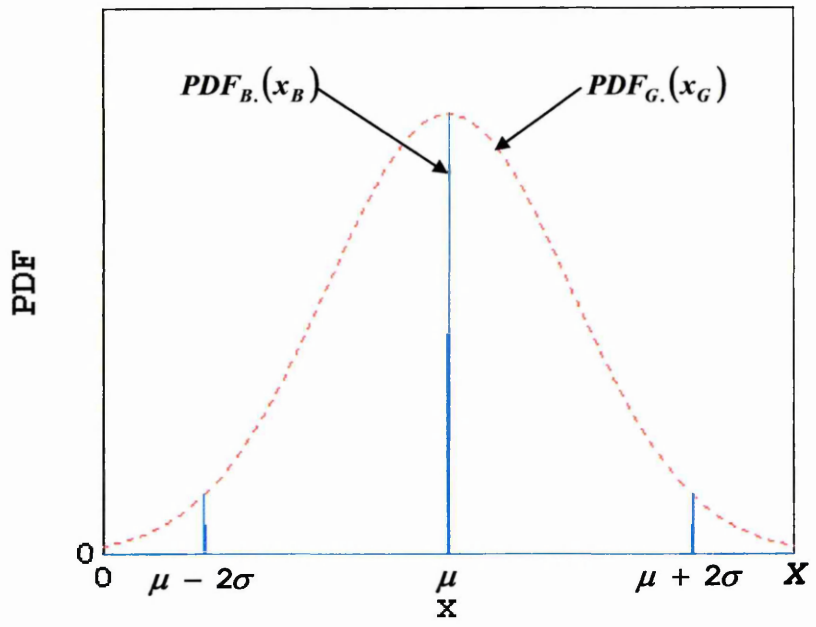

Figure 7.17: Graphical representation conveying the conditions of Binomial distribution to be close approximated by the Gaussian distribution.

The probability of error obtained from the Binomial distribution is:

$$P_{B.E} = \sum_{x_B=x}^{X} \binom{X}{x_B} p^{x_B} q^{X-x_B}, \tag{7.37}$$

which can be represented equivalently by the Gaussian function:

$$P_{G.E} = \frac{1}{\sigma\sqrt{2\pi}} \int_{x_G=x}^{\infty} \exp\left[-\frac{1}{2}\left(\frac{x_G-\mu}{\sigma}\right)^2\right] dx_G . \tag{7.38}$$

Figure 7.18 demonstrates the relationship between the Binomial and the Gaussian distributions based on the conditions given in (7.35) and (7.36). The test values are chosen to be $p = 0.6$, $q = 1 - p = 0.4$ and $1 \le X \le 10$.

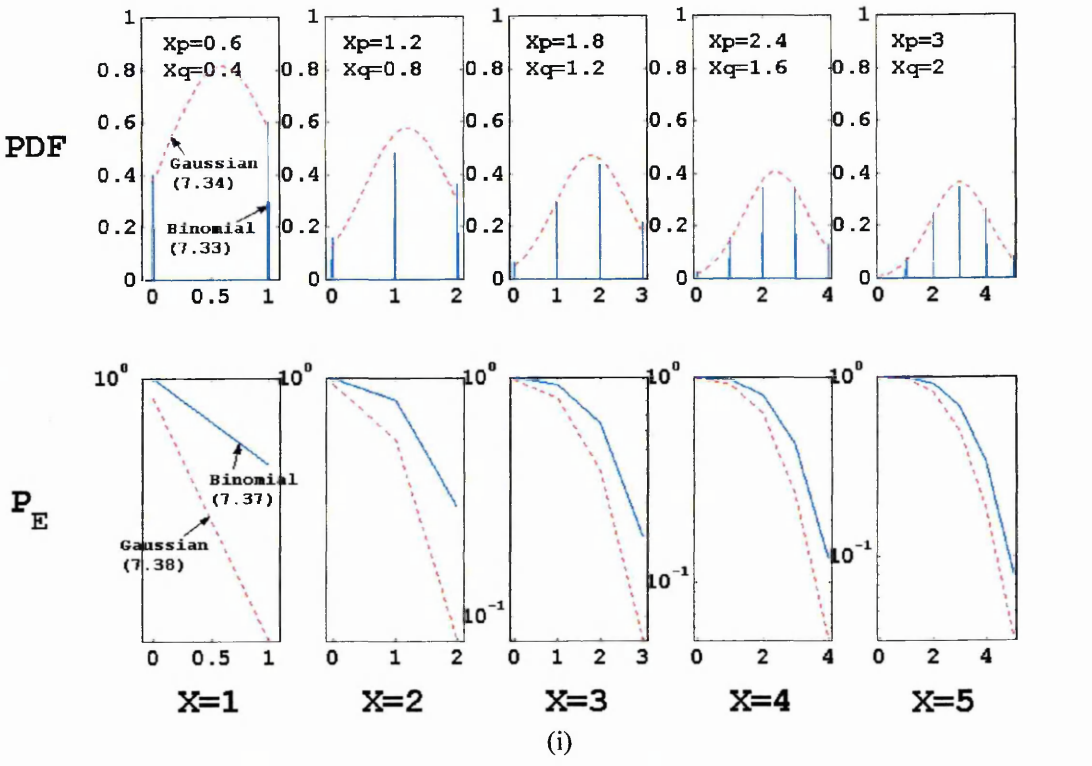

(i)

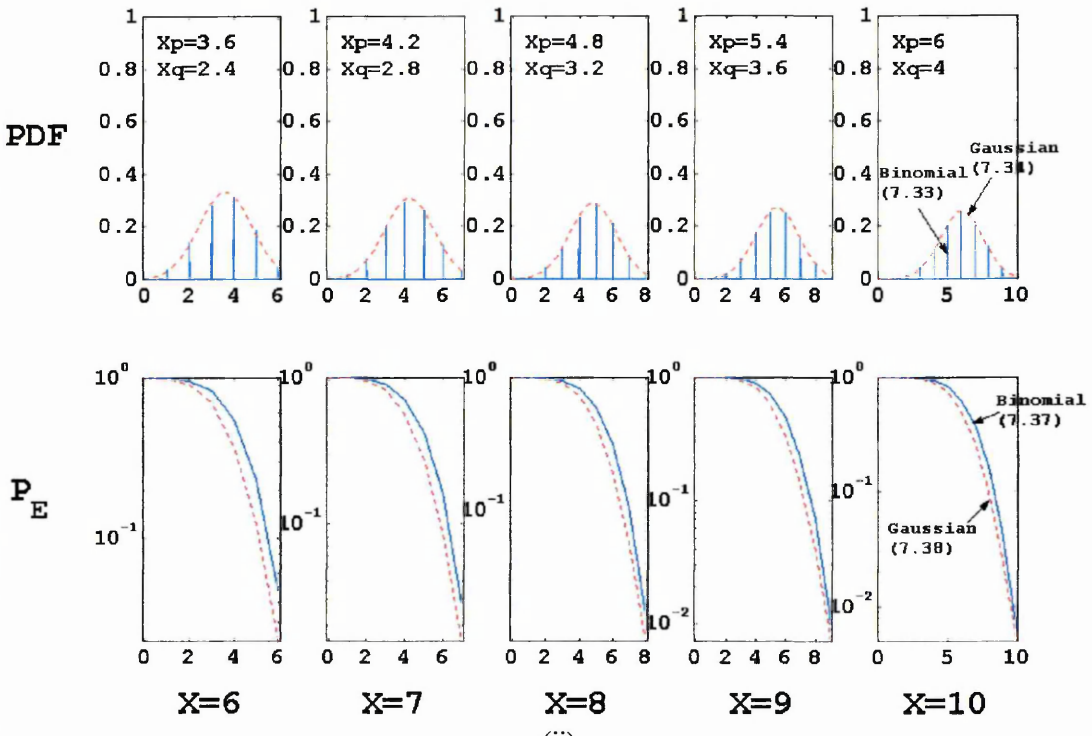

(ii)

Figure 7.18: Graphical demonstration of Binomial distribution in relation to the Gaussian distribution based on the conditions (7.35) and (7.36).

*The top row is PDF and the bottom row is the corresponding P_E.

As shown in figure 7.18 when the conditions are not satisfied, i.e. when $X=1$, the Binomial distribution is not close to the Gaussian distribution. As X increases one by one, the Binomial PDF profile started to form a Gaussian PDF profile, and $P_{G.E}$ moved closer and closer to $P_{B.E}$. As both conditions are then satisfied, it can be seen that the Binomial PDF has formed an entire Gaussian profile with both tails appearing within the variable range, and $P_{G.E}$ almost entirely overlap with $P_{B.E}$ – showing both distributions are almost equal.

7.3.2 OOK-CDMA

The probability of BER of OOK-CDMA $P_{B.BER|OOK-CDMA}$ employing $(n,w,1,1)$OOC has been approximated using the Gaussian function with the assumption that $P_{B.BER|OOK-CDMA}$ will tend to the Gaussian distribution when the number of MAI, $(F-1)$, is large [Yang95a, Lee98a]. The mean and variance for the Gaussian function are respectively defined as [Lee98a]:

$$\mu_{MAI|OOK-CDMA} = (F-1)P_{\lambda_c|OOK-CDMA}, \tag{7.39}$$

and

$$\sigma^2_{MAI|OOK-CDMA} = (F-1)\left(P_{\lambda_c|OOK-CDMA}\right)\left(1-P_{\lambda_c|OOK-CDMA}\right). \tag{7.40}$$

To find out if a $P_{B.BER|OOK-CDMA}$ distribution is Gaussian, the conditions (7.35) and (7.36) for various values of F and w need to be tested. The variables p, q and X in (7.35) and (7.36) are represented as $P_{\lambda_c|OOK-CDMA}$, $\left(1-P_{\lambda_c|OOK-CDMA}\right)$ and $(F-1)$, respectively.

F	$P_{\lambda_c\|OOK-CDMA}$	Condition (7.35) $(F-1)P_{\lambda_c\|OOK-CDMA} = \mu_{MAI\|OOK-CDMA}$	Condition (7.36) $(F-1)\left(1-P_{\lambda_c\|OOK-CDMA}\right)$	$\sigma^2_{MAI\|OOK-CDMA}$
3	≈2.2E-1	≈4.3E-1	≈1.6	≈3.4E-1
5	≈1.3E-1	≈5.2E-1	≈3.5	≈4.6E-1
10	≈6.6E-2	≈6.0E-1	≈8.4	≈5.6E-1
20	≈3.3E-2	≈6.3E-1	≈1.8E+1	≈6.1E-1
100	≈6.7E-3	≈6.6E-1	≈9.8E+1	≈6.6E-1
500	≈1.3E-3	≈6.7E-1	≈5E+2	≈6.6E-1
1E+7	≈6.7E-8	≈6.7E-1	≈1E+7	≈6.7E-1
⋮	⋮	⋮	⋮	⋮
$\to\infty$	$\to 0$	$\to 4/6$	$\to\infty$	$\to 4/6$

(a): $(n,4,1,1)$OOC

F	$P_{\lambda_c\|OOK-CDMA}$	Condition (7.35) $(F-1)P_{\lambda_c\|OOK-CDMA} = \mu_{MAI\|OOK-CDMA}$	Condition (7.36) $(F-1)\left(1-P_{\lambda_c\|OOK-CDMA}\right)$	$\sigma^2_{MAI\|OOK-CDMA}$
3	≈1.9E-1	≈3.8E-1	≈1.6	≈3.1E-1
5	≈1.1E-1	≈4.6E-1	≈3.5	≈4.0E-1
10	≈5.7E-2	≈5.1E-1	≈8.5	≈4.8E-1
20	≈2.9E-2	≈5.4E-1	≈1.8E+1	≈5.3E-1
100	≈5.7E-3	≈5.7E-1	≈9.8E+1	≈5.6E-1
500	≈1.1E-3	≈5.7E-1	≈5E+2	≈5.7E-1
1E+7	≈5.7E-8	≈5.7E-1	≈1E+7	≈5.7E-1
⋮	⋮	⋮	⋮	⋮
$\to\infty$	$\to 0$	$\to 4/7$	$\to\infty$	$\to 4/7$

(b): $(n,8,1,1)$OOC

Table 7.1: Conditions tests for OOK-CDMA employing optimal $(n,w,1,1)$OOC.

The results of condition tests are shown in table 7.1. In table 7.1 (a), for $(n,4,1,1)$OOC, only the condition (7.36) is satisfied when F is large, whereas (7.35) is never satisfied. For $F\to\infty$, both μ and σ^2 approach $4/6$. For a higher value of w, that is $(n,8,1,1)$OOC, the results are shown in table 7.1 (b). Similarly to the previous case, only the condition (7.36) is satisfied. Here as $F\to\infty$, μ and $\sigma^2\to 4/7$. Hence one can deduce that the BER of OOK-CDMA employing $(n,w,1,1)$OOC is not closely approximated by the Gaussian function as only one condition is satisfied when either, or both, of the variables F and w are large. This can also be explained when the condition (7.31), which is related to (7.35), is not satisfied when either F or w is

large. This is because large values of F or w will result in both μ and σ^2 having the same value, that is less than 1. Substituting $\mu = \sigma^2$ into (7.31) will result in the condition being void.

The Binomial PDF for OOK-CDMA MAI is given by [Salehi89b]:

$$PDF_{B.MAI|OOK-CDMA}(i) = \sum_{i=0}^{F-1} \binom{F-1}{i} P_{\lambda_c|OOK-CDMA}{}^{i} \left(1 - P_{\lambda_c|OOK-CDMA}\right)^{F-1-i} \delta(I-i). \qquad (7.41)$$

The equivalent PDF obtained from the Gaussian function is given as:

$$PDF_{G.MAI|OOK-CDMA}(i) = \frac{1}{\sigma_{MAI|OOK-CDMA}\sqrt{2\pi}} \exp\left[-\frac{1}{2}\left(\frac{i-\mu_{MAI|OOK-CDMA}}{\sigma_{MAI|OOK-CDMA}}\right)^2\right]. \qquad (7.42)$$

For the Binomial case the BER is given by (7.26) and for the Gaussian case the BER is defined as [Lee98a]:

$$P_{G.BER|OOK-CDMA} = \frac{1}{2\sigma_{MAI|OOK-CDMA}\sqrt{2\pi}} \int_{i=v_{th}}^{\infty} \exp\left[-\frac{1}{2}\left(\frac{i-\mu_{MAI|OOK-CDMA}}{\sigma_{MAI|OOK-CDMA}}\right)^2\right] di. \qquad (7.43)$$

For a codeword set of $(n,4,1,1)$OOC, the PDF and BER for both the Binomial and Gaussian for $F = 10$ and 100, using (7.41), (7.42), (7.26) and (7.43), are shown in figure 7.19 (a) and (b). For the codeword set $(n,8,1,1)$OOC, the results are shown in figure 7.19 (c) and (d). As can be seen from figures 7.19 (a) and (c), the Binomial distribution do not converge to a Gaussian distribution even though F and w are large, as predicted in table 7.1. As a result, the Gaussian function will give a poor approximation for the BER as shown in figures 7.19 (b) and (d), where the probability approximated by the Gaussian function is much lower than the actual Binomial probability at high v_{th} (in region B). Nevertheless, at low v_{th} (in region A) both the probabilities were shown to be quite close to each other owing that the areas in the region A, under both distributions appeared to be close. As the v_{th} increases beyond $\mu + 2\sigma$ (the upper limit of condition (7.32)), the Gaussian and the Binomial plots depart (see figures 7.19 (b) and (d)) as the Gaussian tail in the region B diverges and falls faster than the Binomial one (see figures 7.19 (a) and (c)).

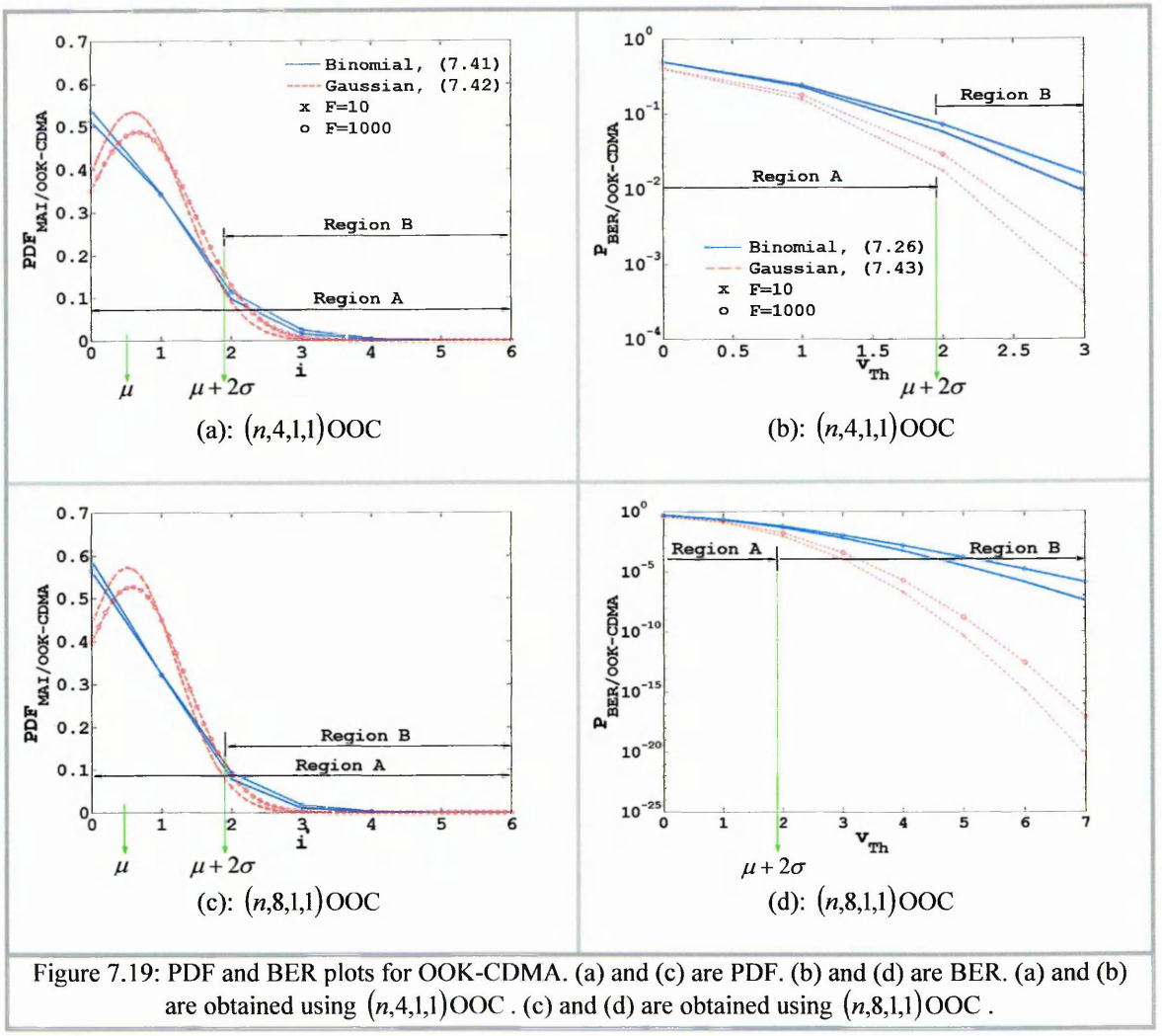

Figure 7.19: PDF and BER plots for OOK-CDMA. (a) and (c) are PDF. (b) and (d) are BER. (a) and (b) are obtained using $(n,4,1,1)$OOC . (c) and (d) are obtained using $(n,8,1,1)$OOC .

In contrast to the assumption that OOK-CDMA MAI will converge to the Gaussian distribution when F is large [Lee98a], the plots in figures 7.19 (a) and (c) show that the MAI distribution, which is a Binomial distribution, actually converges to a semi-triangle shape and stays at the same position. This phenomenon can be best explained by taking a close look at $\mu_{MAI|OOK-CDMA}$ and $\sigma^2_{MAI|OOK-CDMA}$ as outlined below.

The mean is expressed as:

$$\mu_{MAI|OOK-CDMA} = (F-1)P_{\lambda_c|OOK-CDMA}.$$

Substituting for $P_{\lambda_c|OOK-CDMA} = \frac{w^2}{2n}$,

$n = Fw(w-1)+1$, and

as F and $w \to \infty$, the mean is given as:

$$\mu_{MAI|OOK-CDMA} \approx \begin{cases} \frac{w}{2(w-1)} & \text{, for } F \to \infty. \\ \frac{1}{2} & \text{, for } F \;\&\; w \to \infty. \end{cases} \tag{7.44}$$

Similarly for the variance:

$$\sigma^2_{MAI|OOK-CDMA} = (F-1)P_{\lambda_c|OOK-CDMA}\left(1 - P_{\lambda_c|OOK-CDMA}\right)$$

$$\sigma^2_{MAI|OOK-CDMA} \approx \begin{cases} \frac{w}{2(w-1)} & \text{, for } F \to \infty. \\ \frac{1}{2} & \text{, for } F \;\&\; w \to \infty. \end{cases} \tag{7.45}$$

Equation (7.44) proves that the conditions (7.31) and (7.35) will never be satisfied and both (7.44) and (7.45) confirm the fact that the semi-triangle shape remains in the same position, as indicated by the green arrows as shown in figure 7.19, for all F and w. The semi-triangle shape is determined by the PDF of each single-interference defined as [Salehi89a]:

$$PDF^{i}_{SI|OOK-CDMA}(x) = \left(1 - P_{\lambda_c|OOK-CDMA}\right)\delta(x) + P_{\lambda_c|OOK-CDMA}\delta(x-1), \tag{7.46}$$

where i denotes the i^{th} multiple-access-user. Each i^{th} single-interference PDF is identical to the others. From table 7.1, $P_{\lambda_c|OOK-CDMA} \to 0$ as $F \to \infty$, thus $\left(1 - P_{\lambda_c|OOK-CDMA}\right)$ becomes the dominant term in (7.46). The PDF of total MAI, defined in (7.41), is the convolution of all $(F-1)$ single-interference PDF [Salehi89b], defined as:

$$PDF_{MAI|OOK-CDMA}(x) = PDF^{1}_{SI|OOK-CDMA}(x) \otimes PDF^{2}_{SI|OOK-CDMA}(x) \otimes \ldots \\ \ldots \otimes PDF^{F-2}_{SI|OOK-CDMA}(x) \otimes PDF^{F-1}_{SI|OOK-CDMA}(x), \tag{7.47}$$

Since $\left(1-P_{\lambda_c|OOK-CDMA}\right)$ is the dominant term, $PDF_{MAI|OOK-CDMA}(x)$ will skew towards and peak at $x=0$, giving a semi-triangle shape.

The MAI distribution of OOK-CDMA employing PS(P) is Gaussian as shown in figure 7.20 (a). Comparing the BER performance of OOK-CDMA employing $(n,w,1,1)$OOC and PS(P) using the Gaussian function for approximation will not give a fair comparison. Figure 7.20 (b) shows the BER for PS(P) using a Gaussian function (close approximation), $(n,w,1,1)$OOC using the Binomial function (actual) and $(n,w,1,1)$OOC using the Gaussian function (poor approximation). As can be seen the BER of $(n,w,1,1)$OOC using a Gaussian function approaches that of the Binomial function at $v_{th}<2$. As $v_{th}\geq 2$, the BER performance using the Gaussian function is over estimated as compared with the actual BER.

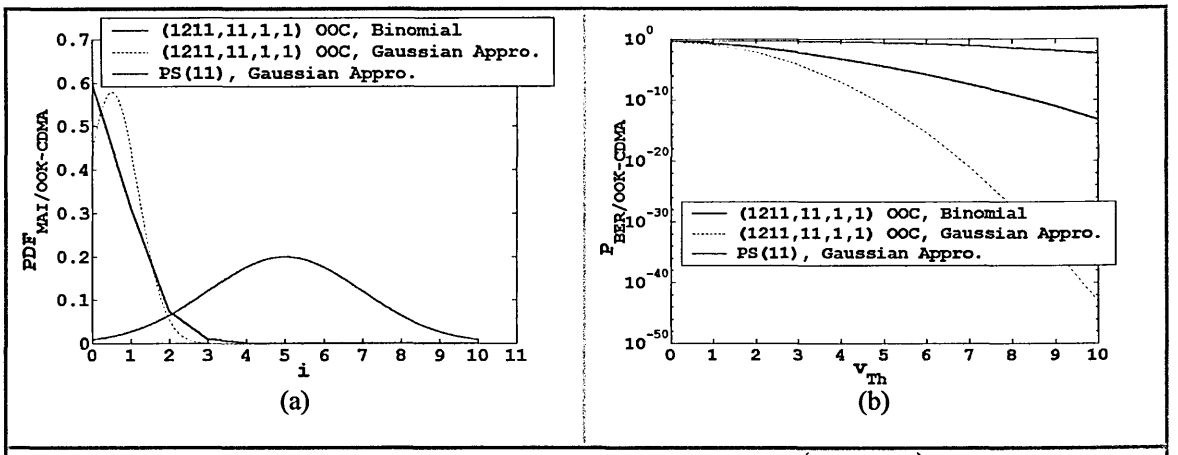

Figure 7.20: PDF and BER plots for OOK-CDMA employing optimal $(1211,11,1,1)$OOC and PS(11).

The PS(P) PDF can be demonstrated to be Gaussianly distributed using the conditions (7.31) and (7.32). The mean and variance for PS(P) are given, respectively, as [Yang95a, Lee98a]:

$$\mu'_{MAI|OOK-CDMA}=(P-1)\frac{P^2}{2P^2}=\frac{(P-1)}{2}$$

and

$$\mu'_{MAI|OOK-CDMA}\approx\frac{P}{2}\quad,\text{as } F\to\infty, \tag{7.48}$$

and

$$\sigma'^{2}_{MAI|OOK-CDMA} = \frac{5P^2 - 2P - 4}{12P^2}$$

and

$$\sigma'^{2}_{MAI|OOK-CDMA} \approx \frac{5P}{12} \quad , \text{as } F \to \infty. \tag{7.49}$$

Note that for PS(P), $w = F = P$. Hence the conditions (7.31) can be tested as:

$$\frac{P}{2} - 2\sqrt{\frac{5P}{12}} > 0, \tag{7.50}$$

and the condition (7.32) as:

$$\frac{P}{2} + 2\sqrt{\frac{5P}{12}} < (P-1). \tag{7.51}$$

It is found that both the conditions (7.50) and (7.51) are always satisfied when $F \geq 11$. Thus confirming that the MAI distribution of OOK-CDMA employing PS(P) is Gaussianly distributed when F is large.

7.3.3 Hybrid cdma systems

In *h*PIM-CDMA and *h*PPM-CDMA, the interferences dependant not only on F and w, but also on M. Here M is assumed fixed and is defined as:

$$M = \log_2\left(\frac{n-1}{30}\right) + 1$$

$$2^M = \frac{n-1}{30} + 1. \tag{7.52}$$

In *h*PIM-CDMA, the mean is composed of the self-interference and as well as the MAI interferences, hence it is expressed as:

$$\mu_{MAI|hPIM-CDMA} = P_{\lambda_a|hPIM-CDMA} + (F-1)P_{\lambda_c|hPIM-CDMA}$$

$$= \frac{2w(w-1)}{2\left[Fw(w-1)+1\right]+\frac{Fw(w-1)}{30}-2} + \frac{2(F-1)w^2}{2\left[Fw(w-1)+1\right]+\frac{Fw(w-1)}{30}},$$

as $F \to \infty$,

$$\frac{2w(w-1)}{2\left[Fw(w-1)+1\right]+\frac{Fw(w-1)}{30}-2} \to \frac{60}{61F} \to 0 \quad \text{and}$$

$$\frac{2(F-1)w^2}{2\left[Fw(w-1)+1\right]+\frac{Fw(w-1)}{30}} \to \frac{60w^2}{61w(w-1)}.$$

$$\therefore \mu_{MAI|hPIM-CDMA} \approx \begin{cases} \frac{60w^2}{61w(w-1)} & \text{, for } F \to \infty. \\ \frac{60}{61} & \text{, for } F \,\&\, w \to \infty. \end{cases} \tag{7.53}$$

The variance is defined as:

$$\sigma^2_{MAI|hPIM-CDMA} = P_{\lambda_a|hPIM-CDMA}\left(1-P_{\lambda_a|hPIM-CDMA}\right) + (F-1)P_{\lambda_c|hPIM-CDMA}\left(1-P_{\lambda_c|hPIM-CDMA}\right)$$

as $F \to \infty$,

$$P_{\lambda_a|hPIM-CDMA}\left(1-P_{\lambda_a|hPIM-CDMA}\right) \to \frac{60}{61F}\left(1-\frac{60}{61F}\right) \to 0 \quad \text{and}$$

$$(F-1)P_{\lambda_c|hPIM-CDMA}\left(1-P_{\lambda_c|hPIM-CDMA}\right) \to \frac{60w^2}{61w(w-1)}\left(1-\frac{60w^2}{61Fw(w-1)}\right) \to \frac{60w^2}{61w(w-1)}.$$

$$\therefore \sigma^2_{MAI|hPIM-CDMA} \approx \begin{cases} \dfrac{60w^2}{61w(w-1)} & \text{, for } F \to \infty. \\ \dfrac{60}{61} & \text{, for } F \,\&\, w \to \infty. \end{cases} \tag{7.54}$$

Similarly, the mean for *h*PPM-CDMA is defined as:

$$\mu_{MAI|hPPM-CDMA} = P_{\lambda_a|hPPM-CDMA} + (F-1)P_{\lambda_c|hPPM-CDMA}$$

$$= \frac{w(w-1)}{2[Fw(w-1)+1]+2^M-2} + \frac{(F-1)w^2}{2[Fw(w-1)+1]+2^M-1},$$

assuming 2^M is small for low BER,

$$\because \mu_{MAI|hPPM-CDMA} \approx \begin{cases} \dfrac{w^2}{2w(w-1)} & \text{, for } F \to \infty. \\ \dfrac{1}{2} & \text{, for } F \,\&\, w \to \infty. \end{cases} \tag{7.55}$$

Using the same approach in (7.55), the variance is found to be:

$$\sigma^2_{MAI|hPPM-CDMA} \approx \begin{cases} \dfrac{w^2}{2w(w-1)} & \text{, for } F \to \infty. \\ \dfrac{1}{2} & \text{, for } F \,\&\, w \to \infty. \end{cases} \tag{7.56}$$

The conditions for the Gaussian distribution for approximating the MAI distribution for the three CDMA systems are tabulated in table 7.2. For all three schemes, the MAI distributions are not close enough to be approximated by a Gaussian function, as the first condition is less than zero. Nevertheless, the second condition is satisfied and the value for OOK-CDMA is similar to *h*PPM-CDMA, and is the lowest. This will mean that *h*PIM-CDMA MAI distribution can be approximated closely to a Gaussian function ranging from 0 to $\mu + 2\sigma = 2.9671$ only. Hence *h*PIM-CDMA employing $(n, w \leq 4,1,1)$SOOC can be approximated by a Gaussian function – as the threshold level for $(n, w = 4,1,1)$SOOC is $v_{Th} = w - 1 = 3$ is within the valid range from 0 to 3 (assuming 2.9671≈3). Similarly for OOK-CDMA and *h*PPM-CDMA, the Gaussian function is a close approximation for the MAI distribution for the system employing $(n, w \leq 3,1,1)$SOOC.

CDMA Systems $(F \,\&\, w \to \infty)$	Conditions	
	$\mu - 2\sigma \geq 0$	$\mu + 2\sigma \leq F - 1$
OOK-CDMA	-0.9142	1.9142
*h*PIM-CDMA	-0.9999	2.9671
*h*PPM-CDMA	-0.9142	1.9142

Table 7.2: Conditions for the Gaussian distribution to approximate MAI distribution of three CDMA systems.

For *h*PPM-CDMA, the value of 2^M in equations (7.55) and (7.56) has been assumed small (e.g. $2 \leq M \leq 4$) for low BER. This has led to the condition $\mu - 2\sigma$ being not satisfied as shown in table 7.2. Consequently, the BER for *h*PPM-CDMA can be approximated closely by a Gaussian function using $(n, w \leq 3,1,1)$SOOC only. On the other hand, if the limit of $2^M \to \infty$, then the denominator of both equations (7.55) and (7.56) will dominates and both the equations will tend toward zero. In that, the BER of *h*PPM-CDMA cannot be approximated by a Gaussian function using any $(n, w,1,1)$SOOC.

7.4 Summary

In this chapter, a BER analyses for *h*PIM-CDMA and *h*PPM-CDMA taking into account MAI, self-interference, and *h*PIM and *h*PPM demodulation schemes was presented. The BER performances of three systems were compared and it was found that OOK-CDMA displays the best performance followed by *h*PPM-CDMA and *h*PIM-CDMA. The BER of the *h*PIM-CDMA is slightly higher than *h*PPM-CDMA for a given M. However, the *h*PIM-CDMA BER performance can only be evaluated if the values of M conform to the condition set in (7.16) so that one symbol being divided into two is unlikely to occur. Otherwise, the probability of BER is indeterminable and high.

The BER performance for both hybrid schemes can be improved with a lower M, however the drawback is a decrease in both BEF performance. It is found that the BEF performance of both hybrid systems is nearly equal to M for large F and w.

It was also found that the three CDMA systems could not be in general approximated closely by a Gaussian distribution function for large sets of $(n,w,1,1)$SOOC (also include $(n,w,1,1)$OOC for OOK-CDMA). The reason was that the MAI and the self-interference PDF always displays an identical semi-triangle shape and on the same location for all sets of $(n,w,1,1)$SOOC. Hence using a Gaussian function distribution for approximation will give incorrect results.

Chapter 8

CONCLUSIONS AND FURTHER WORK

8.1 Conclusions

A novel algorithm for constructing $(n,3,1,1)$OOC has been proposed and implemented using the MATLAB programming language. Compared with other algorithms, this algorithm is well refined with only 5 conditions needed for code construction. The algorithm is systematic, translates easily to program code, and uses low memory. The algorithm is able to obtain a large set of codes (i.e. up to 75) in a short time (approximately 30 minutes) compared with the theoretical determination that can take a number of years. This is achieved by the conditions that instruct the algorithm to only search for the possible arrangements/patterns for the set of codes, avoiding any known unnecessary process. A new set of $(n,3\times \mathrm{K},\mathrm{K},\mathrm{K})$OOC is also proposed, which can be constructed from a $(n,3,1,1)$OOC.

The use of a DS-CDMA system in an optical diffuse wireless link has also been investigated. Analyses prove that an optical DS-CDMA system can achieve quality in message separation when operating with minimum dispersion condition, where the dispersed tail is allowed up to $0.3T_c$, thus limiting the signal bandwidth. With such a condition, it is found that the dispersed tail contributes only 10% of the total signal power, which is small and does not affect the signal quality. In addition the data throughput is reduced. For example, the data throughput of OOK-CDMA is less than the OOK, which can be measured by a $BEF_{\frac{OOK-CDMA}{OOK}} < 1$. Without changing the signal bandwidth, the data throughput can be improved using an efficiency modulation technique such as the *h*PPM-CDMA which achieves data compression.

To achieve even higher throughput, a new modulation technique has been proposed which is *h*PIM-CDMA. It uses a symbol with variable duration, which on average, is shorter than the OOK-CDMA and *h*PPM-CDMA and conveys the same amount of information. However, the *h*PIM-CDMA power efficiency is lower. Nevertheless, it is found that for *h*PIM-CDMA using $(n,w,1,1)$OOC the total transmitted power by all F users simultaneously is no more than the total power of a single OOK transmitted signal.

The *h*PIM-CDMA system is easily implemented compared with OOK-CDMA and *h*PPM-CDMA as the *h*PIM-CDMA symbol is variable and therefore it does not require symbol synchronisation for encoding and decoding. The signature sequence encoding and decoding for *h*PIM-CDMA and *h*PPM-CDMA (whose symbol duration is fixed but has non-periodic signature sequence encoding) can only be carried out using tap-delay lines, which are passive devices.

The BER expression for *h*PIM-CDMA has been developed, taking into account self-interference, MAI and the *h*PIM demodulation technique. The BER expression for *h*PPM-CDMA is also given. For both hybrid systems, the BER will improve when increasing the code weight, w, but deteriorate when increasing either the number of system user, F, or the bit mapping, M. For *h*PIM-CDMA, it is found that the BER can only be evaluated for certain sets of $(n,w,1,1)$OOC and a number of bit mappings, which are related by $Fw(w-1)\geq 30\left(2^M-1\right)$. At low values of M, both hybrid systems BER and BEF are low and it is found that BEF $\approx M$. The BER of OOK-CDMA is the lowest followed by *h*PPM-CDMA and *h*PIM-CDMA. On the contrary, *h*PIM-CDMA has the highest BEF followed by *h*PPM-CMDA and OOK-CDMA.

A Gaussian function has been used extensively for evaluating the BER, in which the MAI PDF displays a Binomial distribution, for an OOK-CDMA system. It is shown here that OOK-CDMA together with *h*PIM-CDMA and *h*PPM-CDMA, employing certain sets of $(n,w,1,1)$OOC cannot be approximated closely by a Gaussian function. This is because there are

two mandatory conditions that must be satisfied in order to use a Gaussian function to close approximate a Binomial distribution. For the three systems, only one condition is satisfied and the MAI PDF never displays a Gaussian distribution but a semi-triangle shape when the MAI is large.

8.2 Further Work

The studies carried out in this thesis only considered asynchronous systems (however the chip is synchronised). As mentioned in section 5.5, the asynchronous systems chip synchronisation (fine synchronisation) can be easily achieved using an external reference to synchronise both the transmitter and receiver. When the chip is synchronised, then the phase/symbol synchronisation can then be easily obtained. In a fully asynchronous system, the synchronisation technique is more challenging, as it needs to perform the phase synchronisation, prior to fine synchronisation, and also has to maintain both synchronisations. A further study is suggested to investigate how optical wireless DS-CDMA can achieve these synchronisations practically.

In optical systems, the addition of simultaneously transmitted signals non-linear as compared with the electrical systems. This is because an optical signal is unipolar (in the positive direction) whereas the electrical signal is bipolar. When multiple optical signals are superimposed, the resultant peaks will grow in one direction only, that is towards positive infinity. On the other hand, when multiple electrical signals are superimposed, the resultant peaks grow in both positive and negative directions with symmetry about zero (which is the DC level). For the optical signal, the DC level is non-zero and is dynamic. The DC level varies with the number of optical signals being superimposed. Therefore, it is deduced here that a DS-CDMA system designed to operate in the electrical domain, with zero threshold level, will not give the same performance when operated in the optical domain. Nevertheless, there have been suggestions to employ the electrical DS-CDMA systems to operate in the optical domain. This is achieved by biasing the electrical signal with a DC level before transmitting to an optical channel and removing the DC at the receiver side before the correlation take place [Almeida98,

Sharma99]. Another method employs a unipolar-bipolar correlator to perform correlation for the PN sequences in the optical domain [O'Farrell95]. Both methods have not taken into account the effect of superposition of the optical signals that is non-linear as indicated above, which may violate the correlation properties of PN sequences. This needs to be investigated.

The BER performance for the asynchronous OOK- and both hybrid CDMA systems has been presented in chapter 7. It was shown that OOK-CDMA offers the best performance followed by *h*PPM-CDMA and *h*PIM-CDMA. Investigation for their fully asynchronous counterparts BER will only provide the same performance but give a lower BER boundary. Hence further work is suggested to investigate the PER performance for the three CDMA systems for the fully asynchronous mode.

An optical hard limiter has been shown to improve the BER performance for OOK-CDMA [Salehi89b, Wu95, Ohtsuki99] and PPM-CDMA [Ohtsuki95, Shalaby99a]. Hence it is worthwhile to investigate the use of optical hard limiter for both hybrid schemes.

Chapter 4 discussions highlighted that $(n, w,1,1)$OOC provides the lowest auto- and cross-correlation constraints, thus it aids phase synchronisation and give the lowest MAI. However, the codeword construction methods available to date are based mainly on recursive algorithms. In section 4.6, it emphasised that a recursive algorithm is time consuming to generate a large set of $(n, w,1,1)$OOC and the waiting time is intolerable. Though one may put more efforts to search for an efficient recursive algorithm, the final result will be same – where the time to generate for a larger set of codeword will become intolerable. It is suggested here that investigations be carried out to modify PC, which can be easily generated, to provide for better correlation properties.

In section 5.6, it was shown that the practical optical DS-CDMA system performance is affected by the locations of the transmitters and receivers, which induce near-far problem. The error-rate performance presented in chapter 7 did not take into account of this. In practice, the near-far

problem is unavoidable. Further investigation can be carried out for the performance of the three DS-CDMA systems and to consider the effect for a more practical channel. A model for a practical channel characteristic obtained by measurement has been proposed [Hashemi94, Pakravan01], that can be considered for investigation.

Appendix

COMPUTER PROGRAMS FOR PROPOSED ALGORITHM

As mentioned in section 4.2.1, the program contains other functions (which have not been discussed) that help to speed up the searching for a valid set of code word. As some of the function are difficult to be integrated into one program (as it would complicate and increase the program size and thus increases searching time), they are written in two separate main function files as GenOOCOptMB10.m and GenOOCOptMB11.m, as shown in figure A.1 below. Each of the main function files has it own two other sub-function files to carry out the initialisation (indicated by the module highlighted in green in figure 4.2) by the function file InitFile.m, and the test conditions (indicated by the module highlighted in yellow in figure 4.2) by the function file SearchTD.m. Both the main function files will share other common sub-function files. Note that the term 'TD' used in the program files is referred to the *ERD* matrix. The other common function file that helps the searching process is the AutoArrange.m, as highlighted in cyan in figure A.1.

The results in the table 4.3 are obtained by running both the main programs concurrently on two separate computers. Each program may use the same amount of time to obtain a same result or one of them may use less time than the other to obtain a result. Hence the results displayed are those obtained in the shortest times.

Both sets of programs (which are written in the MATLAB scripting, or in another word as m-files, formats) can be compiled to machine codes, which are executable, using MATLAB

compiler. Please refer to the comment lines on top of each main program that give the instructions for the compilation. The results can be obtained either by running the programs in the MatLab command prompt using the m-files or in the DOS command prompt using the machine codes. The results in table 4.3 are obtained by the machine codes, which produced the results faster than their uncompiled versions, m-files.

There are switches incoorperated with the main programs, which are used to explore for more conditions to obtaining a valid set of larger codeword in a much shorter time. However, this investigation is still in the progress in the early stage and hence the purpose of each switch will not be discussed further here. Nevertheless, the command lines with the switches used for obtaining the results in table 4.3 are given below:

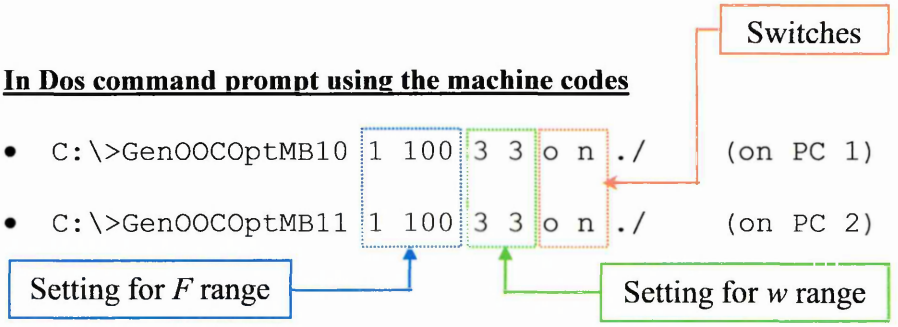

In MatLab command prompt using the m-files

- `>>GenOOCOptMB10(1,100,3,3,'o','n','./')` (on PC 1)
- `>>GenOOCOptMB11(1,100,3,3,'o','n','./')` (on PC 2)

The first parameter in the command line indicates the minimum value for F, and the second parameter indicates the maximum value. The third and fourth parameters are the minimum and maximum vaues for w respectively. For example, the above values are set to instruct the programs to generate sets of codewords for $F=1$ to 100 and for $w=3$. The programs are not capable of generating sets of codeword for $w>3$ yet until further development for their construction algorithm. The last parameter '`./`' is a default setting which indicates current directory.

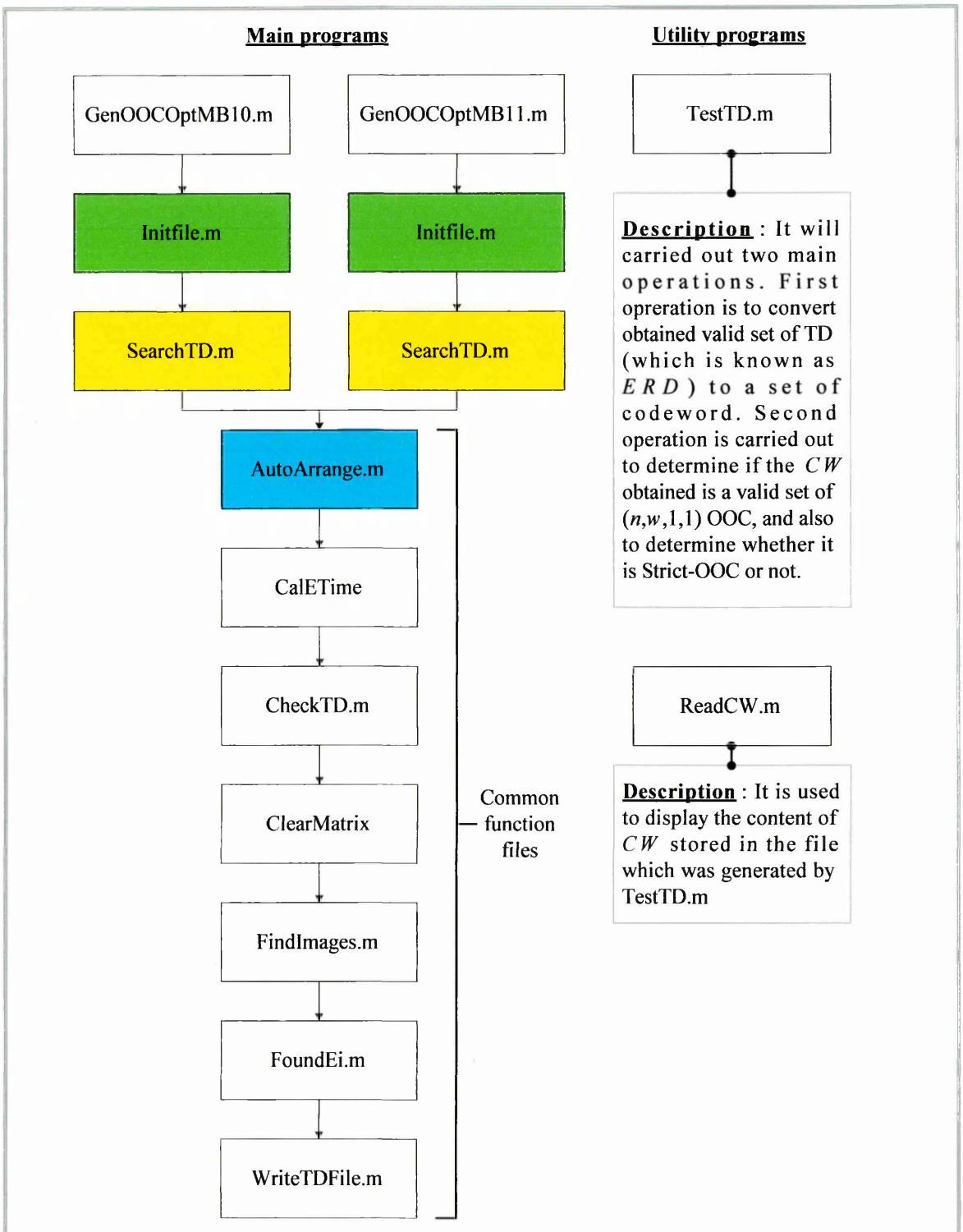

Figure A.1: Program structure of the proposed algorithm and other utilities programs.

REFERENCES

[Al-Ghamdi03]
Al-Ghamdi, A.G. and J. M. H. Elmirghani, "Triangular PFDR Antenna Optimisation Under the Restriction of Background Noise and Multipath Propagation in an Optical Wireless System," IEEE International Conference on Communications v 3 (2003), p2013-2019.

[Almeida98]
Almeida, C. de and S.M. Modenese, "Performance Comparison of Pseudonoise Sequences for Optical CDMA Networks," Microwave and Optical Technology Letters v19 n5 (5 December 1998), p352-354.

[Andonovic99]
Andonovic, I. And W. Huang, "Optical Code Division Multiple Access Networks," Proceedings of SPIE – The International Society for Optical Engineering v3666 (1999), p434-443.

[ARRL91]
Spread Spectrum Source Book, The American Radio Relay League, USA, 1991. ISBN 0 87259 317 7.

[Audeh94]
Audeh, M.D. and J.M. Kahn, "Performance Evaluation of L-Pulse-Position Modulation on Non-Directed Indoor Infrared Channels," International Conference on Communications v2 (1 – 5 May 1994), p660-664.

[Audeh95]
Audeh, M.D. and J.M. Khan, "Performance Evaluation of Baseband OOK for Wireless Indoor Infrared LAN's Operating at 100 Mb/s," IEEE Transactions on Communications v43 n6 (June 1995), p2085-2094.

[Audeh96]
Audeh, M.D., J.M. Khan and J.R. Barry, "Performance of Pulse-Position Modulation on Measured Non-Directed Indoor Infrared Channels," IEEE Transactions on Communications vol44 no6 (June 1996), p654-659.

[Azizoglu92]
Azizoglu, M., J.A. Salehi and Y. Li, "Optical CDMA via Temporal Codes," IEEE Transactions on Communications v40 n7 (July 1992), p1162-1170.

[Barry93]
Barry, J.R., J.M. Kahn, W.J. Krause, E.A. Lee, and D.G. Messerchmitt, "Simulation of multipath impulse response for indoor wireless optical channels," IEEE Journal on Selected Areas in Communications v11 n3 (April 1993), p367-379.

[Barry94]
Barry, J.R., Wireless Infrared Communications, Kluwer Academic Publishers, USA, 1994.

[Carruthers96a]
Carruthers, J.B. and J.M. Kahn, "Modelling of Nondirected Wireless Infrared Channels," IEEE International Conference on Communications v2 (23 – 27 June 1996), p1227-1231.

[Carruthers96b]
Carruthers, J.B. and J.M. Kahn, "Multiple-Subcarrier Modulation for Nondirected Wireless Infrared Communication," IEEE Journal on Selected Areas in Communications v14 n3 (April 1996), p538-546.

[Carruthers97]
Carruthers, J.B. and J.M. Kahn, "Modeling of Nondirected Wireless Infrared Channels," IEEE Transactions on Communications v45 n10 (October 1997), p1260-1268.

[Chan96]
Chan, H.H., J.M.H. Elmirghani and R.A. Cryan, "Performance Analysis of Indoor Infrared Wireless Networks Utilising PPM CDMA," IEEE International Conference on Communications v3 (1996), p1467-1471.

[Chan98]
Chan, H.H., J.M.H. Elmirghani and R.A. Cryan, "Performance Evaluation of PPM-CDMA Under Different Orthogonal Coding Schemes," IEEE International Conference on Communications v3 (1998), p1284-1288.

[Chan99]
Chan, H.H., J.M.H Elmirghani and R.A. Cryan, "Optical Wireless PPM CDMA Networks Employing OC and PC Signature Codes," Journal of Optical Communications v20 (1999), p92-97.

[Chen99]
Chen, H.-H., "Spreading-Code-Dependent Bit Error and Capacity Analysis for Finite Asynchronous CDMA System," International Journal of Communication Systems v12 (1999), p49-64.

[Chung89]
Chung, F.R.K., J.A. Salehi and V.K. Wei, "Optical Orthogonal Codes: Design, Analysis and Applications," IEEE Transactions on Information Theory v35 n3 (May 1989), p595-604.

[Chung90]
Chung, H. and P.V. Kumar, "Optical Orthogonal Codes – New Bounds and an Optimal Construction," IEEE Transactions on Information Theory v36 n4 (July 1990), p866-873.

[Colbourn99]
Colbourn, C.J., J.H. Dinitz and D.R. Stinson, "Application of Combinatorial Designs to Communications, Cryptography, and Networking," downloadable from http://citeseer.nj.nec.com/colbourn99applications.html (1999).

[Cooper86]
Cooper, R.C. and C.D. McGillem, (1986). Modern Communications and Spread Spectrum, McGraw-Hill.

[Elmirghani94]
Elmirghani, J.M.H. and R.A. Cryan, "Indoor Infrared Wireless Networks Utilising PPM CDMA," Singapore ICCS – Conference Proceedings v1 (1994), p334-337.

[Fathallah97]
Fathallah, H., L.A. Rusch, and S. LaRochelle, "Analysis of an Optical Frequency-Hop Encoder with Strain-Tuned Bragg Gratings," Bragg Gratings, Photosensitivity, and Poling in Glass Fibers and Waveguides (October 1997) Williamsburg VA, p200-202.

[Fathallah98]
Fathallah, H., L.A. Rusch, and S. LaRochelle, "Optical Frequency-Hop Multiple Access Communications System," IEEE International Conference on Communications v 3 (1998), p1269-1273.

[Filanowski01]
Filanowski, A., "Optical Code Division Multiple Access," downloadable from http://www.apn.ca/Optical Code Division Multiple Access Networking (Motorola).pdf.

[Gagliardi93]
Gagliardi, R.M., A.J. Mendez, M.R. Dale and E. Park, "Fiber-Optic Digital Video Multiplexing Using Optical CDMA," Journal of Lightwave Technology v11 n1 (January 1993), p20-26.

[Gagliardi95]
R.M. Gagliardi and S. Karp, Optical Communications, 2nd edition, Wiley, New York, (1995).

[Ge01]
Ge, G. and J. Yin, "Constructions for Optimal (v, 4, 1) Optical Orthogonal Codes," IEEE Transactions on Information Theory v47 n7 (November 2001), p2998-3004.

[Gfeller79]
Gfeller, F.R. and U.H. Bapst, "Wireless In-House Data Communication via Diffuse Infrared Radiation," Proceeding of the IEEE v67 n11 (November 1979), p1474-1486.

[Ghassemlooy00]
Ghassemlooy, Z. and A.R. Hayes, "Digital Pulse Interval Modulation for IR Communication Systems – a review," International Journal of Communication Systems v13 n7-8 (Nov 2000), p519-536.

[Ghassemlooy01]
Ghassemlooy, Z., C.K. See, J.M. Holding and C. Lu., "Bit-Error-Rate Analysis for Hybrid PIM-CDMA Optical Wireless Communication Systems," Microwave and Optical Technology Letters v31 n1 (October 2001), p40-44.

[Ghassemlooy98a]
Ghassemlooy, Z., A.R. Hayes, N.L. Seed and E.D. Kaluarachchi, "Digital Pulse Interval Modulation for Optical Communications," IEEE Communications Magazine v36 n12 (Dec 1998), p95-99.

[Ghassemlooy98b]
Ghassemlooy, Z., A.R. Hayes, N.L. Seed and E.D. Kaluarachi, "Digital Pulse Inteval Modulation for Optical Wireless Communications," Proc. 3rd IAA Conf. On Computers and Communications (19 – 20 September 98) NY USA, p198-202.

[Giakos03]
Giakos, G.C., N. Patnekar, S. Sumrain, L. Fraiwan, V. Kumar, and G.B. Mertzios, "A Novel Multipath Dispersion Reduction Technique Based on Controlled-Polarization Optical Wireless Link Set-Up," Conference Record - IEEE Instrumentation and Measurement Technology Conference v2 (2003), p1622-1626.

[Hashemi94]
Hashemi, H., G. Yun, M. Kavehrad, F. Behbahani, and P.A. Galko, "Indoor Propagation Measurements at Infrared Frequencies for Wireless Local Area Networks Applications," IEEE Transactions on Vehicular Technology v43 n3 pt1 (August 1994), p562-576.

[Hayes00]
Hayes, A.R., Z. Ghassemlooy, N.L. Seed and R. McLaughlin, "Baseline-Wander Effects on Systems Employing Digital Pulse-Interval Modulation," IEE Proceedings: Optoelectronics v147 n4 (August 2000), p295-300.

[Hayes02]
Hayes, A.R., Digital Pulse Interval Modulation for Indoor Optical Wireless Communication Systems, Thesis, Sheffield Hallam University, 2002.

[Hayes98]
Hayes, A.R., Z. Ghassemlooy and N.L. Seed, "Optical Wireless Communication using Digital Pulse Interval Modulation", Proceeding of SPIE vol3532 (November 1998), p61-69.

[Ho01]
Ho, C.K., S.W. Lee, and Y.P. Singh, "Optical Orthogonal Code Design Using Genetic Algorithms," Electronics Letters v37 n20 (27 September 2001), p1232-1234.

[Holejko99]
Holejko, K., J. Siuzdak, R. Nowak and A. Marzecki, "Multichannel CDMA Infrared Link for Indoor Application," Proceedings of SPIE - The International Society for Optical Engineering v3731 (1999), p207-214.

[Holmes92]
Holmes, A.S. and R.R.A. Syms, "All-Optical CDMA Using "Quasi-Prime" Codes," Journal of Lightwave Technology v10 n2 (February 1992), p279-286.

[Hui85]
Hui, J.Y., "Pattern Code Modulation and Optical Decoding – A Novel Code-Division Multiplexing Technique for Multifiber Networks," IEEE Journal on Selected Areas in Communications vSac-3 n6 (November 1985), p916-927.

[Hwang97a]
Hwang, S.S., C. Park and J.H. Lee, "Performance of an Indoor Optical Wireless PPM-CDMA System with Interference Cancellation Schemes," IEEE International Symposium on Personal, Indoor and Mobile Radio Communications, PIMRC v3 (1997), p974-978.

[Hwang97b]
Hwang, S.S., C. Park and J.H. Lee, "Asynchronous Multirate Optical Wireless PPM-CDMA in an Indoor Non-Directed Diffuse Channel," Electronics Letters v33 n18 (28 August 1997), p1565-1567.

[IEEE97]
IEEE Standard 802.11-1997, Institute of Electrical and Electronics Engineers (18 November 1997).

[IEEE99]
IEEE Standard 802.11b-1999, Institute of Electrical and Electronics Engineers (20 January 2000).

[Kahn95]
Kahn, J.M., W.J. Krause and J.B. Carruthers, "Experimental Characterization of Non-Directed Indoor Infrared Channels," IEEE Transactions on Communications v43 2-4 pt3 (February – April 1995), p1613-1623.

[Kahn97]
Kahn, J.M. and J.R. Barry, "Wireless Infrared Communications," Proceeding Of The IEEE v85 n2 (February 1997), p265-298.

[Kaluarachi96a]
Kaluarachchi, E.D., Z. Ghassemlooy, and B. Wilson, "Digital Pulse Interval Modulation for Optical Free Space Communication Links", IEE Colloquium Proceedings, IEE Colloquium on Optical Free Space Communication Links, Savoy Place, London (February 1996), p5/1-5/10.

[Kaluarachi96b]
Kaluarachi, E. D., Z. Ghassemlooy and B. Wilson, "Digital Pulse Interval Modulation for Optical Free Space Communication Links," IEE Colloquium (Digest) n032 (1996), p3/1-3/5.

[Kamakura99]
Kamakura, K., T. Ohtsuki and I. Sasase, "Optical Spread Time CDMA Communication Systems with PPM Signaling," IEICE Transactions on Communications vE82-B n7 (July 1999), p1038-1047.

[Kapur80]
Kapur, N., J. Mavor and M.A. Jack, "Convolutional Architecture for Spectrum Analysis Employing CCD programmable Transversal Filters," International Journal of Electronics v49 n2 (August 1980), p131-146.

[Khansefid90]
Khansefid, F., R. Gagliardi and H. Taylor, "Performance Analysis of Code Division Multiple Access Techniques in Fiber Optics with On-Off and PPM Pulsed Signaling," IEEE Military Communications Conference v3 (1990), p909-915.

[Kwong90]
Kwong, W.C. and P.R. Prucnal, "'Synchronous' CDMA Demonstration for Fibre-Optic Networks with Optical Processing," Electronics Letters v26 n24 (22 November 1990), p1990-1992.

[Kwong91]
Kwong, W.C., P.A. Perrier and P.R. Prucnal, "Performance Comparison of Asynchronous and Synchronous Code-Division Multiple-Access Techniques for Fiber-Optic Local Area Networks," IEEE Transactions on Communications v39 n11 (November 1991), p1625-1634.

[Kwong94a]
Kwong, W.C. and G.-C. Yang, "Optical CDMA Coding Architecture with Modified Prime-Sequence Codes," Proceedings of The 28th Annual Conference on Information Sciences and Systems — Princeton, New Jersey (March 1994), p479-484.

[Kwong94b]
Kwong, W.C., J.-G. Zhang and G.-C. Yang, "2n Prime-Sequence Code and Its Optical CDMA Coding Architecture," Electronics Letters v30 n6 (March 1994), p509-510.

[Kwong96]
Kwong, W.C., G.-C. Yang, and J.-G. Zhang, "2n Prime-Sequence Codes and Coding Architecture for Optical Code-Division Multiple-Access," IEEE Transactions on Communications v44 n9 (September 1996), p1152-1162.

[Lam02]
Lam, P.M., "Synchronous Optical Fiber Code-Division Multiple-Access Networks with Bipolar Capacity," Assumption University Journal of Technology (Au J.T.) v5 n3 (January 2002), p129-138.

[Lee98a]
Lee, S.W. and D.H. Green, "Performance Analysis of Optical Orthogonal Codes in CDMA LANs," IEE Proceedings: Communications v145 n4 (August 1998), p265-271.

[Lee98b]
Lee, D.C. and J.M. Kahn, "Coding and Equalization for PPM on Wireless Infrared Channels," Conference Record / IEEE Global Telecommunications Conference v1 (1998), p201-206.

[Lee98c]
Lee, D.C. and J.M. Kahn, "Coding and Equalization for PPM on Wireless Infrared Channels," IEEE Transactions on Communications v47 n2 (1999), p255-260.

[Liu00]
Liu, H., Signal Processing Applications in CDMA Communications, Artech House, (2000).

[Liu01]
Liu, M.-Y. and H.-W. Tsao, "Reduction of Multiple-Access Interference for Optical CDMA Systems," Microwave and Optical Technology Letters v30 n1 (5 July 2001), p1-3.

[Marić93]
Marić, S.V., Z.I. Kostić and E.L. Titlebaum, "A New Family of Optical Code Sequences for Use in Spread-Spectrum Fiber-Optic Local Area Networks," IEEE Transactions on Communications v41 n8 (August 1993), p1217-1221.

[Marić95]
Marić, S.V., M.D. Hahm and E.L. Titlebaum, "Construction and Performance Analysis of a New Family of Optical Orthogonal Codes for CDMA Fiber-Optic Networks," IEEE Transactions on Communications v43 n2/3/4 (February/March/April 1995), p485-489.

[Marsh94]
Marsh, G.W. and J.M. Khan, "50-Mb/s Diffuse Infrared Free-Space Link Using On Off Keying with Decision-Feedback Equalization," IEEE Photonics Technology Letters v6 n10 (October 1994), p1268-1270.

[Marsh96]
Marsh, G.W. and J,M, Kahn, "Performance Evaluation of Experimental 50-Mb/s Diffuse Infrared Wireless Link Using On-Off Keying with Decision-Feedback Equalization," IEEE Transactions on Communications v44 n11 (November 1996), p1496-1504.

[Marsh97]
Marsh, G.W. and J.M. Kahn, "Channel Reuse Strategies for Indoor Infrared Wireless Communications," IEEE Transactions on Communications v45 n10 (10 October 1997), p1280-1290.

[Martirosyan02]
Martirosyan, S. and A.J. Han Vinck, "A Construction for Optical Orthogonal Codes with Correlation 1," IEICE Trans. Fundamentals vE85-A n1 (January 2002), p269-272.

[Matloff01]
Matloff, N., "Channelization of a Communications Medium," download from http://heather.cs.ucdavis.edu/~matloff/Networks/Channel/Channel.pdf.

[McCullagh94]
McCullagh, M.J., D.R. Wisely, P.L. Eardley and P.P. Smyth, "A 50 Mbit/s optical wireless LAN link using novel optical and electronic enabling technologies," International Zurich Seminar on Digital Communications, Zurich (1994), p298-309.

[Mendenhall95]
Mendenhall, W. and T. Sincich, Statistics for Engineering and The Sciences, Fourth Edition, Prentice Hall, USA, (1995). ISBN 0 02 380581 1.

[Nikolajević98a]
Nikolajević, V.S., M.L. Dukić and A. Marinčić, "An Improvement of Synchronous CDMA Techniques for Fiber-Optic Local Area Networks," Proceedings of the Mediterranean Electrotechnical Conference – MELECON v2 (May 1998), p774-778.

[Nikolajević98b]
Nikolajević, V.S., M.L. Dukić and A. Marinčić, "Performance Comparison of Different Receivers of Synchronous CDMA Techniques for Fiber Optic LANs," IEEE International Symposium on Spread Spectrum Techniques and Applications v1 (1998), p67-72.

[O'Farrell95]
O'Farrell, T. and S.I. Lochmann, "Switched Correlator Receiver Architecture for Optical CDMA Networks with Bipolar Capacity," Electronics Letters v31 n11 (25 May 1995), p905-906.

[Ohtsuki95]
Ohtsuki, T., I. Sasase and S. Mori, "Effects of Hard-Limiter and Error Correction Coding on Performance of Direct-Detection Optical CDMA Systems with PPM Signaling," IEICE Transactions on Fundamentals of Electronics, Communications and Computer Sciences vE78-A n9 (September 1995), p1092-1101.

[Ohtsuki99]
Ohtsuki, T., "Performance Analysis of Direct-Detection Optical CDMA Systems with Optical Hard-Limiter Using Equal-Weight Orthogonal Signlaing," IEICE Transactions on Communications vE82-B n3 (March 1999), p512-520.

[Ojanperä01]
Ojanperä, T. and R. Prasad, WCDMA: Towards IP Mobility and Mobile Internet, Artech House, USA, (2001). ISBN 1 58053 180 6.

[Oksa97]
Oksa, J., "S-38.220 Licentiate Course on Signal Processing in Communications, FALL - 97 Optical CDMA Systems," download from http://keskus.hut.fi/opetus/s38220/reports_97/oksa.pdf.

[Ong95]
Ong, C.T. and C. Leung, "Code Diversity Transmission in a Slow-Frequency-Hopped Spread Spectrum Multiple-Access Communication System," IEEE Transactions on Communications v43 n12 (December 1995), p2897-2899.

[Perrier88]
Perrier, P.A. and P.R. Prucnal, "Wavelength-Division Integration of Services in Fibre-Optic Networks," International Journal of Digital & Analog Cabled Systems v1 n3 (July – September 1988), p149-157.

[Petrovic90]
Petrovic, R. and S. Holmes, "Orthogonal Codes for CDMA Optical Fibre LANs with Variable Bit Interval," Electronics Letters v26 n10 (10 May 1990), p662-664.

[Pakravan01]
Pakravan, M.R., M. Kavehrad and H. Hashemi, "Indoor Wireless Infrared Channel Characterization by Measurements," IEEE Transactions on Vehicular Technology v50 n4 (July 2001), p1053-1073.

[Proakis95]
Proakis, J.G., Digital Communications, 3rd edition, McGraw-Hill, (1995).

[Prucnal86]
Prucnal, P.R., M.A. Santoro and T.F. Fan, "Spread Spectrum Fiber-Optic Local Area Network Using Optical Processing," Journal of Lightwave Technology vLT-4 n5 (May 1986), p547-554.

[Punnoose01]
Punnoose, R. J., R.S. Tseng and D.D. Stancil, "Experimental Results for Interference Between Bluetooth and IEEE 802.11b DSSS Systems," IEEE Vehicular Technology Conference v1 n54ND (2001), p67-71.

[Rappaport96]
Rappaport, T.S., Wireless Communications. Principles and Practice, Prentice Hall, USA, (1996). ISBN 0 13 375536 3.

[Salehi89a]
Salehi, J.A., "Code Division Multiple-Access Techniques in Optical Fiber Networks – Part I: Fundamental Principles," IEEE Transactions on Communications v37 n8 (August 1989), p824-833.

[Salehi89b]
Salehi, J.A. and C.A. Brackett, "Code Division Multiple-Access Techniques in Optical Fiber Networks – Part II: Systems Performance Analysis," IEEE Transactions on Communications v37 n8 (August 1989), p834-842.

[Salehi89c]
Salehi, J.A., "Emerging Optical Code-Division Multiple Access Communications Systems," IEEE Network v3 n2 (March 1989), p31-39.

[See00]
See, C.K., Z. Ghassemlooy and J.M. Holding, "Hybrid PIM-CDMA for Optical Wireless Networks," Proceeding of PGNET 2000, 1st Annual PostGraduate Symposium on the Convergence of Telecommunications, Networking and Broadcasting, John Moores University, Liverpool UK (19 – 20 June 2000), p195-200.

[See01]
See, C.K., Z. Ghassemlooy and J.H. Holding, "Bit-Error Rate Analysis for PIM-CDMA Optical Wireless Communication Systems," Proceeding of SPIE v4214 (2001), p153-161.

[Shaar83]
Shaar, A.A. and P.A. Davies, "Prime Sequences: Quasi-Optimal Sequences for or Channel Code Division Multiplexing," Electronics Letters v19 n21 (October, 1983), p888-890.

[Shalaby99a]
Shalaby, H.M.H., "Direct Detection Optical Overlapping PPM-CDMA Communication Systems with Double Optical Hardlimiters," Journal of Lightwave Technology v17 n7 (July 1999), p1158-1165.

[Shalaby99b]
Shalaby, H.M.H., "A Performance Analysis of Optical Overlapping PPM-CDMA Communication Systems," Journal of Lightwave Technology v17 n3 (March 1999), p426-433.

[Sharma99]
Sharma, A.B., P.M. Lam and K. Mäkeläinen, "Hybrid Optical-Electronic Code-Division Multiple-Access Networks Based on the Use of Kronecker Sequences," Proceeding of SPIE v3666 (14 – 18 Dec. 1999), p444-452.

[Shiu98a]
Shiu, D.-S. and J.M. Kahn, "Shaping and Non-Equiprobable Signaling for Intensity-Modulated Signals," Proceeding of the IEEE GLOBECOM 1998 – The Bridge to the Global Integration v1 (8 – 12 November 1998), p213-218.

[Shiu98b]
Shiu, D. and J.M. Kahn, "Differential Pulse Position Modulation for Power-Efficient Wireless Infrared Communication," Conference Record / IEEE Global Telecommunications Conference v1 (1998), p219-224.

[Shiu99]
Shiu, D. and J.M. Kahn, "Differential Pulse-Position Modulation for Power-efficient Optical Communication," IEEE Transactions on Communications v47 n8 (1999), p1201-1210.

[Sidorovich02]
Sidorovich, V.G., "Solar Background Effects in Wireless Optical Communications," Proceedings of SPIE v4873 (2002), p133-142.

[Smyth95]
Smyth, P.P., P.L. Eardley, K.T. Dalton, D.R. Wiseley, P. McKee and D. Wood, "Optical Wireless: A Prognosis," Proceeding of SPIE Conference on Wireless Data Transmission, v2601 (23-25 October 1995), p212-225.

[Stok00]
Stok, A. and E.H. Sargent, "Lighting the Local Area: Optical Code-Division Multiple Access and Quality of Service Provisioning," IEEE Network v14 n6 (November/December 2000), p42-46.

[Street97]
Street, A.M., P.N. Stavrinou, D.C. O'Brien and D.J. Edwards, "Indoor Optical Wireless Systems – A Review," Optical and Quantum Electronics v29 (1997), p349-378.

[Tanaka97]
Tanaka, Y. and M. Nakagawa, "Optical Multi-Wavelength PPM for high data rate transmission on indoor channels," IEEE International Symposium on Personal, Indoor and Mobile Radio Communications, PIMRC v3 (1997), p979-983.

[Tirkel96]
Tirkel, A.Z., "Cross-Correlation of M-Sequences – Some Unusual Coincidences," IEEE International Symposium on Spread Spectrum Techniques & Applications v3 (1996), p969-973.

[Tranter95]
Tranter, Z., Principles of Communications. Systems, Modulation and Noise, Fourth Edition, John Wiley & Sons, USA, (1995). ISBN 0 471 12496 6.

[Vollmer01]
Vollmer, M., M. Haardt and J. Götze, "Comparative Study of Joint-Detection Techniques for TD-CDMA Based Mobile Radio Systems," IEEE Journal on Selected Areas in Communications v19 n8 (August 2001), p1461-1475.

[Weng01]
Weng, C.-S. and J. Wu, "Optical Orthogonal Codes with Nonideal Cross Correlation," Journal of Lightwave Technology v19 n12 (December 2001), p1856-1863.

[Wong00]
Wong, K.K., T. O'Farrell and M. Kiatweerasakul, "The Performance of Optical Wireless OOK, 2-PPM and Spread Spectrum Under the Effects of Multipath Dispersion and Artificial Light Interference," International Journal of Communication Systems v13 n7-8 (November 2000), p551-576.

[Wu95]
Wu, J.-H. and J. Wu, "Synchronous Fiber-Optic CDMA Using Hard-Limiter and BCH Codes," Journal of Lightwave Technology v13 n6 (June 1995), p1169-1176.

[WWW1]
Data Delay Devices, Inc., http://www.datadelay.com/passive.html.

[WWW2]
Lough, D.L., T. K. Blankenship and K.J. Krizman, A Short Tutorial on Wireless LANs and IEEE 802.11, http://www.computer.org/students/looking/summer97/ieee802.htm.

[WWW3]
PhotoCourse.com, http://www.photocourse.com/01/01-04.htm.

[WWW4]
Centre for Wireless Communications, http://www.cwc.oulu.fi/home/iwuwbs/slides/impl_tutorial.pdf.

[Yang95a]
Yang, G.-C. and W.C. Kwong, "Performance Analysis of Optical CDMA with Prime Codes," Electronics Letters v31 n7 (March 1995), p569-570.

[Yang95b]
Yang, G.-C., "Some New Families of Optical Orthogonal Codes for Code-Division Multiple-Access Fibre-Optic Networks," IEE Proceedings: Communications v142 n6 (December 1995), p363-367.

[Yang95c]
Yang, G.-C. and T.E. Fuja, "Optical Orthogonal Codes with Unequal Auto- and Cross-Correlation Constraints," IEEE Transactions on Information Theory v41 n1 (January 1995), p96-106.

[Yang97]
Yang, G.-C. and W.C. Kwong, "Performance Comparison of Multiwavelength CDMA and WDMA+CDMA for Fiber-Optic Networks," IEEE Transactions on Communications v45 n11 (November 1997), p1426-1434.

[Yen85]
Yen, C.S. and R.D. Crawford, "The Use of Directed Optical Beams in Wireless Computer Communications," Proc. Of IEEE Globecom '85 (2 – 5 December 1985) New Orleans, p1181-1184.

[You02]
You, R. and J.M. Kahn, "Upper-Bounding the Capacity of Optical IM/DD Channels With Multiple-Subcarrier Modulation and Fixed Bias Using Trigonometric Moment Space Method," IEEE Transactions on Information Theory v48 n2 (February 2002), p514-523.

[Yu02]
Yu, B., J.M. Kahn and R. You, "Power-Efficient Multiple-Subcarrier Modulation Scheme for Optical Wireless Communications," Proceedings of SPIE v4873 (2002), p41-53.

[Zhang00a]
Zhang, J.-G., G. Picchi and A.B. Sharma, "Design of Efficient All-Optical Code-Division Multiplexing Systems Supporting Multiple-Bit-Rate and Equal-Bit-Rate Transmissions," Applied Optics v39 n14 (10 May 2000), p2264-2277.

[Zhang00b]
Zhang, J.-G., A.B. Sharma and W.C. Kwong, "Cross-Correlation and System Performance of Modified Prime Codes for All-Optical CDMA Applications," Journal of Optics A: Pure and Applied Optics v2 n5 (September 2000), pL25-L29.

[Zhang97a]
Zhang, J.-G., W.C. Kwong and A.B. Sharma, "2n Modified Prime Codes for Use in Fibre Optic CDMA Networks," Electronics Letters v33 n22 (October 1997), p1840-1841.

[Zhang97b]
Zhang, J.-G. and W.C. Kwong, "Design of Optical Code-Division Multiple-Access Networks with Modified Prime Codes," IEEE International Symposium on Information Theory - Proceedings (29 June – 4 July 1997), p480.

[Zhang97c]
Zhang, J.-G. and W.C. Kwong, "Effective Design of Optical Code-Division Multiple Access Networks by Using the Modified Prime Code," Electronics Letters v33 n3 (January 1997), p229-230.

[Zhang97d]
Zhang, J.-G., "Novel Optical Fiber Code-Division Multiple Access Networks Supporting Real-Time Multichannel Variable-Bit-Rate (VBR) Video Distributions," IEEE Transactions on Broadcasting v43 n3 (September 1997), p339-349.

[Zhang98a]
Zhang, J.-G., L.-K. Chen, W.C. Kwong, K.-W. Cheung and A.B. Sharma, "Experiments on High-Speed All-Optical Code-Division Multiplexing (CDM) Systems Using a 2n Prime Code," IEEE International Conference on Communications, v3 (7 – 11 June 1998), p1294-1298.

[Zhang98b]
Zhang, J.-G., W.C. Kwong and S. Mann, "Construction of 2n Extended Prime Codes with Cross-Correlation Constraint of One," IEE Proceedings: Communications v145 n5 (Oct 1998), p297-303.

[Zhang99a]
Zhang, J.-G., L.-K. Chen, W.C. Kwong, K.-W. Cheung and A.B. Sharma, "Experiments on High-Speed All-Optical Code-Division Multiplexing Systems Using All-Serial Encoders and Decoders for 2n Prime Code," IEEE Journal of Selected Topics in Quantum Electronics v5 n2 (March/April 1999), p368-375.

[Zhang99b]
Zhang, J.-G., "Flexible Optical Fiber CDMA Networks Using Strict Optical Orthogonal Codes for Multimedia Broadcasting and Distribution Applications," IEEE Transactions on Broadcasting v45 n1 (March 1999), p106-115.

[Zhang99c]
Zhang, J.-G., "Design of a Spectral Family of Optical CDMA Address Codes for Fully Asynchronous Data Communications," IEEE Transactions on Communications v47 n7 (July 1999), p967-973.

[Zhang99d]
Zhang, J.-G., "Proposed Airborne Optical Fiber Asynchronous CDMA Systems using Fully Optical Orthogonal Codes for Real-Time Avionic Data Distributions and Computer Interconnects," IEEE Aerospace and Electronic Systems Magazine v14 n7 (1999), p35-42.

SOFTWARE (1 CD)